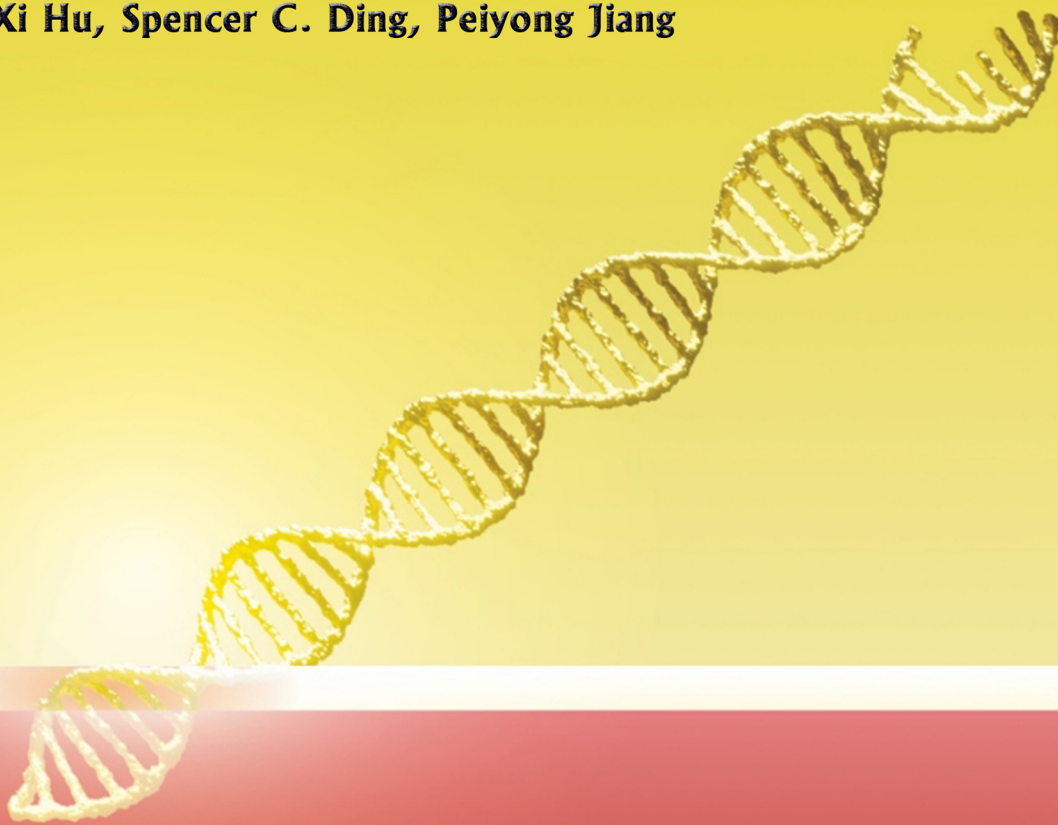


Extracellular Vesicles and Circulating Nucleic Acids

Emerging frontiers of cell-free DNA fragmentomics

Xi Hu, Spencer C. Ding, Peiyong Jiang



EDITORIAL BOARD

Editor-in-Chief

Yoke Peng Loh (USA)

Associate Editors

Shilpa Buch (USA)
Chulhee Choi (South Korea)
Michael Graner (USA)
Michael W. Pfaffl (Germany)
Carlos Salomon (Australia)
Erik A. Sijm (Netherlands)
Weiliang Xia (China)

Editorial Board Members

Benedetta Bussolati (Italy)
Yong Cheng (China)
Wojciech Chrzanowski (Australia)
Carolyn Compton (USA)
William CS Cho (Hong Kong, China)
Navneet Dhillon (USA)
Vincenza Dolo (Italy)
Brian P. Eliceiri (USA)
Georgios Giamas (UK)
Ajay Goel (USA)
Chuan He (USA)
Shannon Holliday (USA)
Guoku Hu (USA)
Peiyong Jiang (China)
Yong Li (Australia)
Guozhen Liu (China)
David M. Lubman (USA)
A. C. Martin (USA)
Janusz W. Rak (Canada)
Rafael Rosell (Spain)
Michel Salzert (France)
Pranav Sharma (USA)
Richard J. Simpson (Australia)
Steven A. Soper (USA)
Frank R.M. Stassen (Netherlands)

Justin Stebbing (UK)
Isaac Kirubakaran Sundar (USA)
Ming-Jer Tang (Taiwan)
Wei Seong Toh (USA)
Hsian-Rong Tseng (USA)
Aijun Wang (USA)
Ju Dong Yang (USA)
Yusuke Yoshioka (Japan)
Janos Zempleni (USA)
Hao Zhang (China)
Long Zhang (China)
Wei Zhang (USA)
Wenwan Zhong (USA)

Junior Editorial Board Members

Leonora Balaj (USA)
Carolina Balbi (Switzerland)
Geneviève Bart (Finland)
Celeste Caruso Bavisotto (Italy)
Sveva Bollini (Italy)
Zhijian Cai (China)
Ilana Chefetz (USA)
Franklin Wang Ngai Chow (Hong Kong, China)
Tomer Cooks (Israel)
Sophie C. Cox (UK)
Xiaolin Cui (China)
Vito G. D'Agostino (Italy)
Fernando De la Cuesta (Spain)
Andrea Del Fattore (Italy)
Haifeng Dong (China)
Suman Dutta (USA)
Orazio Fortunato (Italy)
Susana Garcia-Silva (Spain)
Subhadip Ghatak (USA)
Konstantin Glebov (UK)
André Görgens (Sweden)
Bing Guo (China)
Ramin M. Hakami (USA)

Pingping Han (Australia)
Mario Hiroyuki Hirata (Brazil)
Ayuko Hoshino (Japan)
Shenglin Huang (China)
Zhaohui Huang (China)
Md Nazmul Islam (UK)
Cheng Jiang (China)
Richard J. R. Kelwick (UK)
Dongin Kim (USA)
Arutha Kulasinghe (Australia)
Aurélien Ledreux (USA)
Guoping Li (USA)
Magdalena Lorenowicz (Netherlands)
Yang Luo (China)
David Meckes (USA)
Pietro Parisse (Italy)
Carlos Pedraz (Spain)
Maija Puhka (Finland)
Piul Rabbani (USA)
Enrico Ragni (Italy)
Antonia Reale (Australia)
Ashley E. Russell (USA)
Sharanjot Saini (USA)
Joaquin Seras-Franzoso (Spain)
Susmita Sil (USA)
Jiagan Su (China)
Yaohui Tang (China)
Mujib Ullah (USA)
Pinar Uysal-Onganer (UK)
Yuan Wan (USA)
Shengjun Wang (China)
Takao Yasui (Japan)
Sowmya Yelamanchili Venkata (USA)
Yang You (USA)
Yadong Zheng (China)
Yazhen Zhu (USA)

Media Editors

Federica Anastasi (Italy)
Christian Preußner (Germany)

GENERAL INFORMATION

About the Journal

Extracellular Vesicles and Circulating Nucleic Acids (EVCNA), is an international, peer-reviewed, open access journal. *Extracellular Vesicles and Circulating Nucleic Acids* provides an online platform for the sharing of research data, new methodology, reviews and commentaries in the areas of extracellular vesicles and circulating nucleic acids including DNA, RNA, and miRNA and their therapeutic use. The journal is committed to the rapid publication of original findings that increase our understanding of the molecular and cell biology, biogenesis, and origin of extracellular vesicles and circulating nucleic acids; and their use as biomarkers for the diagnosis, prognostication and surveillance of disease states, and in therapeutics. Manuscripts with clinical relevance are especially encouraged to promote the translation from basic science to clinical applications. The criteria for acceptance are scientific excellence and originality. All works involving the use of animals and human subjects must have been approved by institutional review committees and adhere to accepted international ethical standards.

Information for Authors

Manuscripts should be prepared in accordance with Author Instructions.

Please check www.evcnajournal.com/pages/view/author_instructions for details.

All manuscripts should be submitted online at <https://oaemesas.com/login?JournalId=evcna>.

Copyright

The entire contents of the *EVCNA* are protected under international copyrights. The journal, however, grants to all users a free, irrevocable, worldwide, perpetual right of access to, and a license to copy, use, distribute, perform and display the work publicly and to make and distribute derivative works in any digital medium for any reasonable purpose, subject to proper attribution of authorship and ownership of the rights. The journal also grants the right to make small numbers of printed copies for their personal use under the Creative Commons Attribution 4.0 License.

Copyright is reserved by © The Author(s) 2022.

Permissions

For information on how to request permissions to reproduce articles/information from this journal, please visit www.evcnajournal.com.

Disclaimer

The information and opinions presented in the journal reflect the views of the authors and not of the journal or its Editorial Board or the Publisher. Publication does not constitute endorsement by the journal. Neither the *EVCNA* nor its publishers nor anyone else involved in creating, producing or delivering the *EVCNA* or the materials contained therein, assumes any liability or responsibility for the accuracy, completeness, or usefulness of any information provided in the *EVCNA*, nor shall they be liable for any direct, indirect, incidental, special, consequential or punitive damages arising out of the use of the *EVCNA*. The *EVCNA*, nor its publishers, nor any other party involved in the preparation of material contained in the *EVCNA* represents or warrants that the information contained herein is in every respect accurate or complete, and they are not responsible for any errors or omissions or for the results obtained from the use of such material. Readers are encouraged to confirm the information contained herein with other sources.

Publisher

OAE Publishing Inc.

245 E Main Street st112, Alhambra, CA 91801, USA

Website: www.oaepublish.com

Contacts

E-mail: editorialoffice@evcnajournal.com

Website: www.evcnajournal.com

CONTENTS

Volume 3 / Issue 4 / December 2022

Commentary

- 318 Leveraging biomimetic synthesis strategy for next-generation dendritic cell nanovaccines**

Yutian Xia, Jianzhong Zhang

Review

- 323 Towards extracellular vesicle delivery systems for tissue regeneration: material design at the molecular level**

Ao Chen, Hengli Tian, Nana Yang, Zhijun Zhang, Guo-Yuan Yang, Wenguo Cui, Yaohui Tang

Original Article

- 357 Brain endothelium-derived extracellular vesicles containing amyloid-beta induce mitochondrial alterations in neural progenitor cells**

Olivia M. Osborne, Jennifer M. Kowalczyk, Kelssey D. Pierre Louis, Manav T. Daftari, Brett M. Colbert, Oandy Naranjo, Silvia Torices, Ibolya E. András, Derek M. Dykxhoorn, Michal Toborek

Review

- 380 Emerging frontiers of cell-free DNA fragmentomics**

Xi Hu, Spencer C. Ding, Peiyong Jiang

- 393 A kaleidoscopic view of extracellular vesicles in lysosomal storage disorders**

Charlotte V. Hegeman, Olivier G. de Jong, Magdalena J. Lorenowicz

Editorial

- 422 Year-end reflections of EVCNA - 2022**

Yoke Peng Loh

Commentary

Open Access



Leveraging biomimetic synthesis strategy for next-generation dendritic cell nanovaccines

Yutian Xia, Jianzhong Zhang

State Key Laboratory of Molecular Vaccinology and Molecular Diagnostics, Center for Molecular Imaging and Translational Medicine, School of Public Health, Xiamen University, Xiamen 361102, Fujian, China.

Correspondence to: Jianzhong Zhang, State Key Laboratory of Molecular Vaccinology and Molecular Diagnostics, Center for Molecular Imaging and Translational Medicine, School of Public Health, Xiamen University, Xiamen 361102, Fujian, China. E-mail: jzzhang_xmu@163.com

How to cite this article: Xia Y, Zhang J. Leveraging biomimetic synthesis strategy for next-generation dendritic cell nanovaccines. *Extracell Vesicles Circ Nucleic Acids* 2022;3:318-22. <https://dx.doi.org/10.20517/evcna.2022.35>

Received: 11 Jul 2022 **First Decision:** 30 Aug 2022 **Revised:** 31 Aug 2022 **Accepted:** 26 Sep 2022 **Published:** 8 Oct 2022

Academic Editors: Yoke Peng Loh, Shilpa Buch **Copy Editor:** Pengjuan Wen **Production Editor:** Pengjuan Wen

Abstract

The activation of CD8⁺ cytotoxic T-lymphocytes (CTLs) plays the central role in cancer immunotherapy, which depends on the efficient recognition of peptide-major histocompatibility complex (pMHC) by the T cell receptor (TCR) for the first signal, and B7-CD28 co-stimulating for the second signal. To achieve the potent immune stimulatory effect, a genetically engineered cellular membrane nanovesicles platform that integrates antigen self-presentation and immunosuppression reversal (ASPIRE) for cancer immunotherapy was designed. In preclinical mouse models, ASPIRE could markedly improve antigen delivery to lymphoid organs and generate broad-spectrum T-cell responses that eliminate established tumors. This review highlights that the ASPIRE system represents a novel strategy for personalized cancer immunotherapy.

Keywords: Cancer immunotherapy, extracellular vesicles, bioengineering, nanovaccine

Cancer immunotherapies, including immune checkpoint blockade (ICB), adoptive cell therapy (ACT), and cancer vaccines, have become powerful clinical options for cancer treatment^[1]. Among these, cancer vaccines utilize tumor antigens to induce specific antitumor responses in the body through active immunization, stimulating immune protection mechanisms, and achieving the effect of treating tumors or preventing recurrence, which advances cancer treatment remarkably in recent years. Antitumor immune



© The Author(s) 2022. **Open Access** This article is licensed under a Creative Commons Attribution 4.0 International License (<https://creativecommons.org/licenses/by/4.0/>), which permits unrestricted use, sharing, adaptation, distribution and reproduction in any medium or format, for any purpose, even commercially, as long as you give appropriate credit to the original author(s) and the source, provide a link to the Creative Commons license, and indicate if changes were made.



responses of cancer vaccines are based on the recognition of antigens by professional antigen-presenting cells (APCs) and the activation or initiation of naive antigen-specific T cells, especially CD8⁺ cytotoxic T lymphocytes (CTLs)^[2]. Conventional tumor vaccines rely on random encounters between antigenic epitopes and host APCs, while inappropriate encounters might lead to immune response silencing^[3]. In addition, the delivery of tumor antigens cannot maximize immunogenicity due to the complex and inefficient process of cross-presentation, which extremely limits the activation of CD8⁺ T cells. Although dendritic cell (DC) - based cancer vaccines can provide potent immunostimulatory activity, only a small fraction of activated DCs could migrate to draining lymph nodes (LNs) after injection; this restricts the application of cell-based cancer vaccines^[4]. Furthermore, immune escape caused by tumor evolution, such as immune checkpoints, impairs the functions of antigen-specific CTLs in the fight against tumors^[5]. Therefore, novel strategies are urged to further develop therapeutic cancer vaccines to overcome these challenges and rejuvenate the field of cancer immunology.

Upon harnessing the biomimetic synthesis strategies, protein cargos could be displayed on the cell surface^[6,7]. Liu *et al.* demonstrated a novel nanovaccine platform derived from genetically engineered DCs cytomembrane nanovesicles (DCNVs) integrating antigen self-presentation and immunosuppression reversal (ASPIRE) to induce potent antitumor immunity^[8]. As natural cell membrane-derived vesicles, DCNVs inherit unique biological functions of DCs, due to the presence of membrane-anchored proteins and immunological accessories. Whereas the excellent immune-stimulatory capacity in preclinical mouse models, we highlight that ASPIRE broads the landscape for the next-generation dendritic cell nanovaccines.

As a proof of concept, immature DCs were transduced with recombinant adenoviral vectors expressing chicken ovalbumin (OVA) for endogenous antigen loading by major histocompatibility class-I (MHC-I), during which DCs were activated. Following multistep density gradient ultracentrifugation, DCNVs were obtained. Mass spectrometry analysis revealed that the expression levels of a large number of co-stimulatory molecules (e.g., CD80, CD86, CD40) and chemokines (e.g., CCR2, CCR5, CCR7) were up-regulated in DCNVs, which contributed to the migration of DCNVs to LNs. By co-culturing DCNVs and CD8⁺ T cells, the authors found that DCNVs possess the complete surface functional proteins of mature DCs and could directly present antigens to naive T cells *in vitro*. Benefiting from the nanoscale size and expressed lymphatic homing molecules, DCNVs could be efficiently enriched in LNs, which facilitated adequate contact with T cells. Furthermore, the authors observed that DCNVs significantly elicited robust antigen-specific CTLs expansion and cytokine expression and effectively inhibited the growth of OVA-expressing tumors. It is worth noting that DCNVs also showed strong antitumor ability in mice with incapacitated antigen presentation, which indicated that DCNVs could present antigen directly to T cells without the participation of endogenous APCs.

To explore the utility of the DCNVs platform for neoantigen vaccination, the authors employed DCNVs transduced with three melanoma antigens to elicit broad-spectrum T-cell immune responses. Since such tumors tend to be highly aggressive and low immunogenic, tumor rejection cannot be observed despite DCNVs vaccination showing a significant delay in tumor growth. Further studies showed that this difference was mediated by an immunosuppressive tumor microenvironment in which both CD8⁺ T cells and tumor cells had high expression of PD-1 and its ligand PD-L1 in the draining LNs of tumor-bearing mice. In order to activate the immune response while reversing PD-1/PD-L1-mediated immunosuppression, the authors pre-expressed single-chain antibody fragment (scFv) against PD-1 on the surface of DCs and transferred three melanoma antigens, and the obtained DCNVs were called ASPIRE [Figure 1A]. ASPIRE treatment resulted in complete tumor regression in mice, while the tumor regression rate of DCNVs combined with the same amount of free PD-1 treatment was only about 40%. Interestingly,

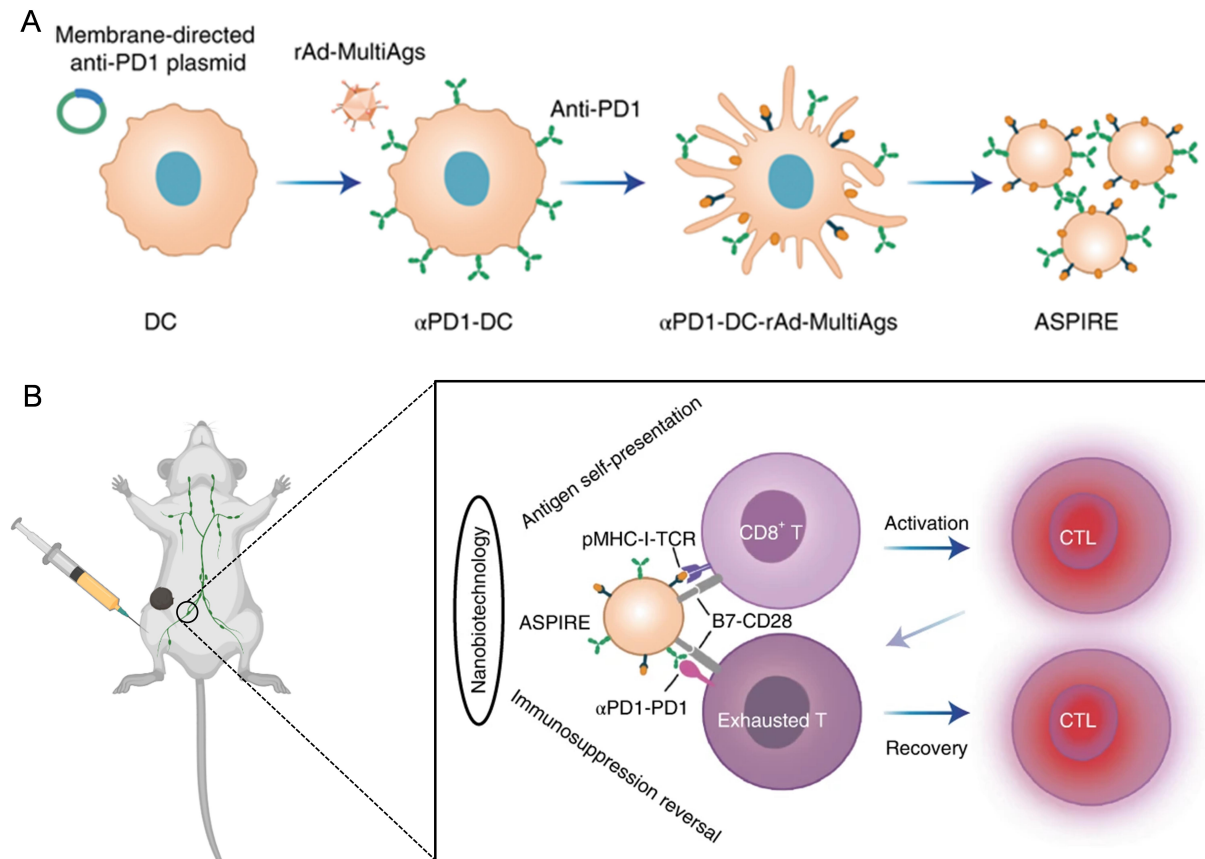


Figure 1. (A) Illustration of the process for preparing ASPIRE from DCs. DCNVs have nanoscale size, good stability, and a homing effect, thus enabling ASPIRE to be rapidly enriched in the lymphatic system. (B) Schematic describing ASPIRE for antigen self-presentation and immunosuppression blockade. ASPIRE: Antigen self-presentation and immunosuppression reversal; DCs: dendritic cells. Reproduced with permission. Copyright 2022, Springer Nature.

when B16F10 cells were injected into the tail vein of mice two months after the third vaccination, no tumor growth was observed in the ASPIRE-treated group, suggesting that ASPIRE induced a strong immune memory. CD28 is a key target of PD-1 blockade, and the co-stimulatory signal B7 molecule binds to the co-activating receptor CD28 on the surface of T cells to regulate T cell activation^[9]. The authors used a Lewis lung cancer model sensitive to anti-PD1 therapy to study the important role of B7 molecules in the antitumor process of α PD1-DCNVs. B7 knockout α PD1-DCNVs did not inhibit tumor growth, and there was no significant difference in tumor progression and mouse survival compared with the free anti-PD1 treated group. This result suggested that B7 molecular co-stimulation is particularly important for enhancing anti-PD1 therapy of α PD1-DCNVs. Interestingly, the authors observed that ASPIRE could significantly decrease PD-1⁺CD38^{high} dysfunctional CTLs in tumor-bearing mice. They found that the responses of infiltrating T cells in the tumor immune microenvironment to anti-PD1 antibody and antigen stimulation differed in spatiotemporal order, and that ASPIRE could reverse immunosuppression [Figure 1B].

The potent tumor treatment effect elicited by ASPIRE in preclinical study promises an enhanced cancer immunotherapy strategy. To encourage the clinical translational, there are a few issues that still need to be considered. For dense solid tumors, it is difficult for circulating CTLs to be transported into the tumor

microenvironment^[2], and without other immunotherapeutic interventions supporting T cell infiltration, DCNVs might be difficult to achieve the desired therapeutic effect. Although the development and innovation of sequencing technology and neoepitope prediction technology are beneficial to the clinical development of DCNVs, the heterogeneity and mutation of the tumor cells might increase the complexity of vaccine design^[10]. At the same time, ASPIRE relies on relatively expensive sequencing and multiple transfections of DCs, so how to achieve cost-effectiveness and reduce the turnaround time (TAT) of patients is also worth consideration. More importantly, exploring the development of human allogeneic DCs-derived ASPIRE will be a more economical and feasible strategy to alleviate the suffering of patients and standardize the production on a large scale. Furthermore, some paralleled strategies, including bacteria-derived outer-membrane vaccines (OMVs) and whole-cell components nanovaccines, *etc.*, are other potential candidates for cancer immunotherapy^[11,12]. We postulate that combining ASPIRE with OMVs may provide a rational combination for enhanced immunostimulatory and antitumor effects, whereas the large amounts of pathogen-associated molecular patterns (PAMPs) are anchored on OMVs.

In summary, this study revealed the mechanism by which co-stimulatory signaling reverses immune suppression and first described a novel nanovaccine formulation to activate the immune response and break immune tolerance simultaneously, which provides a new paradigm for personalized cancer immunotherapy.

DECLARATIONS

Authors' contributions

Drafted the paper: Xia Y

Reviewed and edited the manuscript: Zhang J

Availability of data and materials

Not applicable.

Financial support and sponsorship

None.

Conflict of interest

The authors declare that they have no conflict of interest.

Ethical approval and consent to participate

Not applicable.

Consent for publication

Not applicable.

Copyright

© The Author(s) 2022.

REFERENCES

1. Waldman AD, Fritz JM, Lenardo MJ. A guide to cancer immunotherapy: from T cell basic science to clinical practice. *Nat Rev Immunol* 2020;20:651-68. DOI PubMed PMC
2. Saxena M, van der Burg SH, Melief CJM, Bhardwaj N. Therapeutic cancer vaccines. *Nat Rev Cancer* 2021;21:360-78. DOI PubMed
3. Makkouk A, Weiner GJ. Cancer immunotherapy and breaking immune tolerance: new approaches to an old challenge. *Cancer Res* 2015;75:5-10. DOI PubMed PMC
4. Sabado RL, Balan S, Bhardwaj N. Dendritic cell-based immunotherapy. *Cell Res* 2017;27:74-95. DOI PubMed PMC

5. Sanmamed MF, Chen L. A paradigm shift in cancer immunotherapy: from enhancement to normalization. *Cell* 2018;175:313-26. DOI PubMed PMC
6. Zhang P, Chen Y, Zeng Y, et al. Virus-mimetic nanovesicles as a versatile antigen-delivery system. *Proc Natl Acad Sci U S A* 2015;112:E6129-38. DOI PubMed PMC
7. Squadrito ML, Cianciaruso C, Hansen SK, De Palma M. EVIR: chimeric receptors that enhance dendritic cell cross-dressing with tumor antigens. *Nat Methods* 2018;15:183-6. DOI PubMed PMC
8. Liu C, Liu X, Xiang X, et al. A nanovaccine for antigen self-presentation and immunosuppression reversal as a personalized cancer immunotherapy strategy. *Nat Nanotechnol* 2022;17:531-40. DOI PubMed
9. Kamphorst AO, Wieland A, Nasti T, et al. Rescue of exhausted CD8 T cells by PD-1-targeted therapies is CD28-dependent. *Science* 2017;355:1423-7. DOI PubMed PMC
10. Dagher-Jack I, Shaw AT. Tumour heterogeneity and resistance to cancer therapies. *Nat Rev Clin Oncol* 2018;15:81-94. DOI PubMed
11. Zhao X, Zhao R, Nie G. Nanocarriers based on bacterial membrane materials for cancer vaccine delivery. *Nat Protoc* 2022. DOI PubMed
12. Ma L, Diao L, Peng Z, et al. Immunotherapy and prevention of cancer by nanovaccines loaded with whole-cell components of tumor tissues or cells. *Adv Mater* 2021;33:e2104849. DOI PubMed

Review

Open Access



Towards extracellular vesicle delivery systems for tissue regeneration: material design at the molecular level

Ao Chen¹, Hengli Tian¹, Nana Yang², Zhijun Zhang¹, Guo-Yuan Yang¹, Wenguo Cui³, Yaohui Tang¹

¹Shanghai Jiao Tong Affiliated Sixth People's Hospital, School of Biomedical Engineering, Shanghai Jiao Tong University, Shanghai 200030, China.

²School of Bioscience and Technology, Weifang Medical University, Weifang 261053, Shandong, China.

³Department of Orthopaedics, Shanghai Key Laboratory for Prevention and Treatment of Bone and Joint Diseases, Shanghai Institute of Traumatology and Orthopaedics, Ruijin Hospital, Shanghai Jiao Tong University School of Medicine, Shanghai 200025, China.

Correspondence to: Dr. Yaohui Tang, Shanghai Jiao Tong Affiliated Sixth People's Hospital, School of Biomedical Engineering, Shanghai Jiao Tong University, 1954 Hua Shan Rd., Shanghai 200030, China. E-mail: yaohuitang@sjtu.edu.cn; Prof. Wenguo Cui, Department of Orthopaedics, Shanghai Key Laboratory for Prevention and Treatment of Bone and Joint Diseases, Shanghai Institute of Traumatology and Orthopaedics, Ruijin Hospital, Shanghai Jiao Tong University School of Medicine, 197 Ruijin 2nd Rd., Shanghai 200025, China. E-mail: wgcui80@hotmail.com

How to cite this article: Chen A, Tian H, Yang N, Zhang Z, Yang GY, Cui W, Tang Y. Towards extracellular vesicle delivery systems for tissue regeneration: material design at the molecular level. *Extracell Vesicles Circ Nucleic Acids* 2022;3:323-56. <https://dx.doi.org/10.20517/evcna.2022.37>

Received: 6 Aug 2022 **First Decision:** 4 Sep 2022 **Revised:** 19 Sep 2022 **Accepted:** 26 Sep 2022 **Published:** 14 Oct 2022

Academic Editor: Yoke Peng Loh **Copy Editor:** Pengjuan Wen **Production Editor:** Pengjuan Wen

Abstract

The discovery and development of extracellular vesicles in tissue engineering have shown great potential for tissue regenerative therapies. However, their vesicle nature requires dosage-dependent administration and efficient interactions with recipient cells. Researchers have resorted to biomaterials for localized and sustained delivery of extracellular vesicles to the targeted cells, but not much emphasis has been paid on the design of the materials, which deeply impacts their molecular interactions with the loaded extracellular vesicles and subsequent delivery. Therefore, we present in this review a comprehensive survey of extracellular vesicle delivery systems from the viewpoint of material design at the molecular level. We start with general requirements of the materials and delve into different properties of delivery systems as a result of different designs, from material selections to processing strategies. Based on these differences, we analyzed the performance of extracellular vesicle delivery and tissue regeneration in representative studies. In light of the current missing links within the relationship of material



© The Author(s) 2022. **Open Access** This article is licensed under a Creative Commons Attribution 4.0 International License (<https://creativecommons.org/licenses/by/4.0/>), which permits unrestricted use, sharing, adaptation, distribution and reproduction in any medium or format, for any purpose, even commercially, as long as you give appropriate credit to the original author(s) and the source, provide a link to the Creative Commons license, and indicate if changes were made.



structures, physicochemical properties and delivery performances, we provide perspectives on the interactions of materials and extracellular vesicles and the possible extension of materials. This review aims to be a strategic enlightenment for the future design of extracellular vesicle delivery systems to facilitate their translation from basic science to clinical applications.

Keywords: Biomaterials, material design, extracellular vesicle delivery, tissue regeneration

INTRODUCTION

Tissue regeneration is key to wound healing. Different conditions of tissue regeneration can lead to extremes from full necrosis to near-full recovery, during which regenerative therapies are highly critical, especially for severe injuries. For example, biomolecules, such as growth factors, cytokines^[1] and microRNAs (miRNAs)^[2], have been extensively explored. These signaling molecules direct intrinsic cells to attach, proliferate and differentiate into objective phenotypes. However, the administration of free biomolecules suffers from the shortcomings of fast degradation and consequent deactivation. Despite the use of delivery systems to ease the degradation problem, the paucity of biomolecules can lead to incomplete progression towards near-full recovery, unless complicated recombinant biomolecules are used^[3]. Meanwhile, stem cell therapy by direct administration of exogenous stem cells into the injured tissue has also gained much attention. The full functions of the stem cells are expected to differentiate and replace the damaged tissue. However, the transplantation of stem cells alone cannot meet regenerative purposes due to the poor viability and diminished regenerative activity of the cells^[4]. Such therapy can also induce immunogenicity of the body and is associated with possible ethical problems^[5]. The discovery of extracellular vesicles (EVs) in 1967^[6] and further investigations in 1981^[7] revealed a new understanding of the communication mechanisms between cells. The EVs secreted by stem cells can act as their functional replicates and aid in the repair and protection of damaged tissue. These advances in understanding have generated research interest in using stem cell-derived EVs as intercellular vectors for regenerative therapy^[8]. The use of EVs, therefore, takes the frontier in the development of tissue engineering, covering the regeneration of injured osteopathic^[9], neural^[10], craniofacial^[11], and myocardial tissues^[12]. Nevertheless, EVs are still essentially assemblies surrounded by cellular membranes and thus have to be endocytosed or contacted by the target cells to function. With this concern, four challenges exist in the use of EVs in regenerative therapies:

- 1) Successful delivery of EVs to the injured tissue and interactions with the target cells;
- 2) Long retention of EVs in the injured tissue and protection from fast clearance by organisms;
- 3) The dosage of the delivered EVs above a desired threshold;
- 4) Preservation of the bioactivity of the EVs before delivery.

The exploitation of advanced materials in tissue engineering for the delivery of drugs, biomolecules and stem cells enlightened the solution to the above challenges, which led to the rapid advancement and high effectiveness of EV delivery systems. This is reflected by many recent representative reviews of the investigations. Akbari *et al.* surveyed some successful cases of hydrogel-associated EV delivery and pointed out the critical role of the hydrogels in keeping the EVs and the cargoes within stable^[13]. They also discerned the existing problems for the optimal approach of quantitative loading of EVs and the suitable selection of materials. Huang and coauthors focused on the procedures of the preparation of a diverse library of EV-

laden scaffolds, and listed the challenges to optimally loading EVs and determining the release profile of EVs, especially *in vivo*^[14]. Riau and colleagues provided detailed information on the approaches to loading EVs into materials and the duration of release from different delivery systems^[15]. The dosage of delivery, application of artificial materials and smartness of the delivery systems were stated by the authors as perspectives. Holkar *et al.* provided an overview of EV-laden materials for the recovery of bone repair and presented a library of different delivery systems so far^[16]. Tsintou and coauthors reviewed the cases of injectable hydrogels for prolonged delivery of EVs to achieve maximized regeneration of motor function after ischemic stroke^[17]. The authors gave high remarks on EV delivery systems and urged for a translation of such material in the future. Recently, Murali and Holmes provided detailed lists of the latest EV delivery systems, their corresponding *in vitro* release behaviors and their regenerative performances on specific disease models^[18]. The authors also pointed out issues to be addressed for the clinical translation of the delivery systems, including optimization of material designs for specific diseases, in-depth understanding of *in vivo* release performances, detecting possible sources affecting EVs, and resolving EV manufacturing and storage problems. In their final comments, the authors suggested a better understanding of mechanisms of action and exploration of possible optimization approaches for future EV delivery systems.

From the above excellent reviews, it can be seen that most reviews are based on the viewpoint of the therapeutic performance of EV delivery systems. In fact, the determinants of EV delivery systems are the physicochemical characteristics and structures of the materials, which govern the overall delivery performance. Therefore, we present in this review a comprehensive survey of EV delivery systems from the viewpoint of material design at the molecular level by focusing on the relationship between material structures, physicochemical properties and the performance of EV delivery. Here, “the material” is used to denote the state without EVs, and “the delivery system” stands for the state with EVs loaded. We proceeded from general to specific with the characteristics of different delivery systems as a result of material designs based on various selections of molecules and processing strategies. The materials are further classified into bulk materials and scaffolds based on the modes of loading and delivery of EVs. The according EV loading and delivery behaviors, including the release profiles *in vitro*, retention of EVs *in vivo* and the resulting tissue regeneration, were extracted from representative investigations and analyzed in correlation to the change of materials at the molecular level. From the discussions of these aspects, perspectives were also given in consideration to the current missing links in light of material structures, physicochemical properties and the performance of EV delivery, with possible extensions of materials for future designs of EV delivery systems.

WHAT ARE EXTRACELLULAR VESICLES?

Extracellular vesicles are essentially vesicles with lipid bilayer membrane structures but without functional nuclei, secreted by almost all types of organisms and cell types^[19-25]. Although no consensus was reached for the assignment of EVs to particular biogenesis pathways or subtypes^[19], physical properties such as physical sizes can be used to generally classify the EVs, with diameters < 200 nm as small EVs and > 200 nm all the way to 2000 nm as large ones^[16,19]. EVs carry cargoes from their parental cells^[16], including proteins, RNAs, DNA and cytokines, to direct the behaviors of target cells^[26,27] with promoted stability and lower immunogenicity. The cargoes can also be loaded through various engineering technologies to achieve specific therapeutic purposes^[28]. Thereby, stem cell-derived EVs are a better choice for regenerative therapy compared to the direct use of parental stem cells^[29].

The preparation of EVs from cells is basically composed of three steps. The first is to allow the cells to secrete EVs. The conditions of growth of the cells and the cellular status have strong impacts on EVs^[30-32]. Hence the correct status of the cells must be secured for the production of desired EVs. This step is followed

by the isolation of EVs from the culture media of the cells^[16]. Common approaches are primarily based on physical separation by the distinction in specific physical properties of EVs, including differential ultracentrifugation, density gradient centrifugation, size exclusion chromatography, ultrafiltration, flow field-flow fractionation and microchip-based techniques^[16]. Some chemical or immunological based methods have also been applied, such as polymer-based precipitation, chemical-based precipitation, immunoprecipitation and immunoaffinity capture^[16]. Identifications of morphological properties (electron microscopy), size (dynamic light scattering, nanoparticle tracking analysis or tunable resistive pulse sensing), surface protein markers, and proteomic and RNA cargoes are usually conducted after isolation to confirm the successful harvest of EVs^[33,34]. The isolated EVs are finally cryo-preserved within antifreeze agents or lyophilized with trehalose for storage^[33].

EVs have to interact with the recipient cells to exert functions, either by fusion and releasing the cargoes, initiation of downstream signaling cascade, or endocytosis after binding of EVs with the cells^[8]. The cargoes of the EVs are then transferred to the recipient cells to construct crosstalk from the parental cells at molecular level, including immunomodulation, anti-inflammation, angiogenesis and specific direction of differentiation. This helps the levitation of harsh microenvironment and facilitates the recovery of the injured tissue. Nevertheless, the efficiency of such therapy is still low as simple systemic injections of EVs cannot guarantee the reception of EVs by the targeted cells despite the engineering of targeting function towards EVs. This is reflected by two factors. One is that the EVs fail to reach the recipient cells after systemic administration and are quickly cleared out from body^[35], while the other is the insufficient duration of the supply of EVs, leading to degradation of most EVs by lysosome in a single administration^[36]. A localized and prolonged supply of EVs in the injured tissue can ensure the delivery to the recipient cells at optimal effect. With the introduction of materials for EV delivery, such vesicles can be retained for a longer time and at sustained concentration for localized delivery.

ROLES AND REQUIREMENTS FOR EV DELIVERY SYSTEMS

In order to localize the delivery of EVs to the cells in the injured tissue and extend the whole process, the EV delivery systems are exploited to carry the EVs, transplanted and filled within the injury. Being an agent between the tissue and the EVs, the delivery systems form two interfaces with the EVs and the tissue, taking two roles oriented to each of the interfaces.

Towards the tissue, the material fills the gap created by the injury and provides mechanistic support for cells to attach after their reception of the EVs; it later degrades (if designed to do so) to provide space for further growth of new tissue. The requirements of the EV delivery systems for tissue are as follows:

- 1) Localized delivery of EVs: the material is applied within the gap of injury to ensure delivery of EVs to recipient cells within the local tissue;
- 2) Biocompatibility: the material, including the possible product of degradation, should be non-irritating, non-toxic, non-inflammatory and non-carcinogenic to the local tissue;
- 3) Mechanical support: the material serves as the initial attachment point of cells to migrate, proliferate and differentiate into new tissue;
- 4) Degradability: the material designed to be degradable should degrade either through hydrolysis, responsive decomposition or biodegradation to provide sufficient space for the regeneration of tissue;

5) Other detailed needs: based on the site of application of the material, including but not limited to mechanical strength (for bones), elasticity (blood vessel and muscle), optical properties (cornea), *etc.*

The role towards the EVs is the relay of EVs towards the recipient cells, which is initiated by loading, continued by storage and ended by the delivery of EVs [Figure 1]. The requirements of each step should be met to assure that the EVs reach the target:

- 1) EV loading: EVs should be retained within or immobilized upon the material at a high loading efficiency, with no or low possibility of release before transplantation;
- 2) EV storage: Upon being loaded, EVs should be well protected from possible damages, including physical (primarily mechanical) and chemical (primarily from the residue of chemicals used in fabrication) ones that will cause disruption of the vesicles;
- 3) EV delivery: The delivery should be to the recipient cells at a constant rate and match the kinetics of tissue regeneration. Too fast or too slow of delivery will result in either overflow or insufficient dose, both leading to deficiency of the therapy.

DESIGN STRATEGIES OF MATERIALS FOR EV DELIVERY SYSTEMS

General physicochemical properties of EV delivery systems

As the interface towards the tissue to regenerate, EV delivery systems vary with different choices of materials and functions. The key physicochemical characteristics of materials as the interface for cells are mainly focused on the mechanical and surface properties^[37]. The mechanical strengths of the material can be classified into compression, tension, torsion and shearing moduli according to the directions of force, which are critical mechanical cues towards the proliferation and differentiation of stem cells and further the regeneration of new tissue^[38]. For example, a hydrogel for brain tissue is required to be approximately 180 Pa in shearing modulus, similar to that of brain tissue, for neural stem cells to successfully proliferate and differentiate into neurons^[38], while bone tissue requires hydrogels with compression moduli of 225 kPa to support osteogenesis^[39]. When the attachment of cells occurs, the surface properties of the materials come first for the cells to sense, including the surface tension and the surface charge. Different opinions exist regarding the optimal surface tension for the attachment of cells, but it is considered that both superhydrophilic (water contact angles < 30 °) and superhydrophobic (water contact angles > 150 °) surfaces are improper for cell adhesion^[40]. For surface charge, electrostatic interactions of positively charged surfaces can enhance the sedimentation of negatively charged cells, while the negatively charged surfaces can improve the adsorption of proteins for more binding of the cells^[41]. The use of specific proteins, such as integrin, to modify the surfaces can also promote specific binding of the cells to the surfaces^[40]. All of the above physicochemical properties take different roles in regulating the active changes of the cells in the injured tissue and can be achieved by carefully selecting materials or modifying their structures.

On the other side of the interface, the incorporated EVs have similar membrane structures to their parental stem cells, so the basic surface properties of the material still apply to them. Nevertheless, EVs do not possess cellular entities to actively start an attachment procedure as cells. Therefore, specific attention to the design of the material, especially for molecular sources and processing strategies, must be paid to secure the interactions between materials and EVs for both loading and delivery. As long as the designated biomedical properties are fulfilled, the selection of materials is non-specific to the EVs used.

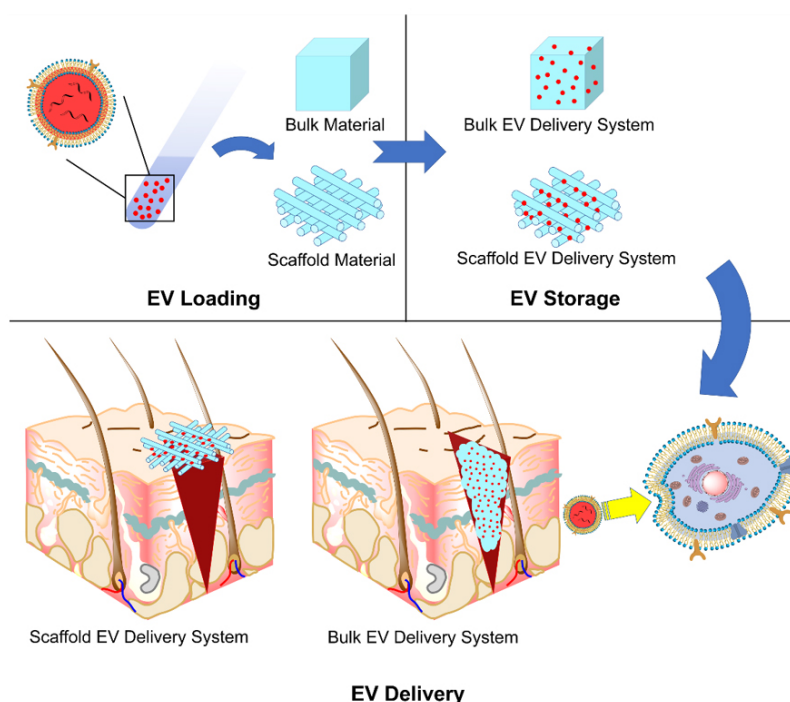


Figure 1. Schematic illustration of the roles of EV delivery systems: EV loading, EV storage and EV delivery. EV: Extracellular vesicle.

EV delivery systems from polymeric sources

Water-soluble polymer-based bulk hydrogels for EV delivery systems

Hydrogels are bulk materials formed by crosslinked water-soluble polymers. Thus crosslinking is the molecular symbol of such materials. The meshes formed by the crosslinked polymer chains act as niches for the encapsulation and retention of biomolecules, as reflected by the vast studies of hydrogels as drug delivery systems^[42] for different parts of body, and this is now extended to the delivery of EVs. The sizes of the meshes are mainly controlled by the density of crosslinking, including not only the number of chemical or physical crosslinking junctions in a unit volume of hydrogel but also the physical entanglement of the polymer chains, which increases with the concentration and the lengths (molecular weights) of the polymer chains. A higher crosslinking density limits the swelling ratio of the hydrogel by reducing the entropy after the swelling process^[43], limiting the sizes of the meshes, increasing the number of meshes and raising the overall mechanical strengths of the hydrogel. By adjusting the crosslinking density from low to high, the mesh size can cover the order of 1 nm to 100 nm^[43], and the elastic moduli range from Pa to MPa levels accordingly. Such easy customizability in both structure and mechanical properties makes hydrogels versatile to be competitive for different types of tissues, especially soft tissues such as neural and cerebral tissues^[44]. The surface property of hydrogels is fundamentally hydrophilic, creating a water-abundant surface resembling that of the tissue surface and therefore improving their compatibility with EVs and coming cells. In addition, most water-soluble polymers for hydrogels can form strong hydrogen bonds with the membrane proteins of cells. In some cases, positively charged hydrogels can promote the attachment of the recipient cells of the EVs. A good example is chitosan hydrogels with protonated ammonium moieties^[45-47].

Most hydrogels exploit natural water-soluble polymers as major components due to their inherent biodegradability. Reported natural water-soluble polymers include pullulan^[48], chitosan^[47,49], silk fibroin^[50], cellulose^[51], alginate^[50], gelatin^[52] and hyaluronic acid^[53,54]. Among them, gelatin and hyaluronic acid are

water-soluble extracts of decellularized extracellular matrices (ECM) and are highly compatible with EVs due to their close nature to ECM. These natural polymers are biodegradable, which is crucial for bulk hydrogels to deliver EVs, and some of them have special intrinsic properties, such as bacteriostatic and hemostatic chitosan. For water-soluble artificial polymers, past studies have mainly focused on relatively limited choices of polymers, such as polyol series [poly(ethylene glycol)(PEG)^[55] and Pluronic F-127^[56,57]], polyethyleneimine (PEI)^[48], vinyl polymer [mostly poly(vinyl alcohol) (PVA)]^[57,58] and artificial peptides^[59]. These polymers have specific functions based on their special structures, but are non-biodegradable except for artificial peptides. Therefore, in many cases, both artificial and natural polymers have been used to provide specific functions and overcome the shortcomings of hydrogels from a single source.

Crosslinking of the above materials is achieved through modification of the polymers or the use of special crosslinkers. Through different crosslinking structures, the hydrogel EV delivery systems can be classified and special properties be endowed. Table 1 lists the crosslinking strategies of hydrogels for EV delivery so far, including the molecular structures of the crosslinking junctions, representative materials and the corresponding properties. In addition to the single crosslinking structures shown in Table 1, some hydrogels incorporate double crosslinking network systems, especially trigger responsive ones, to achieve more controllable crosslinking and other intrinsic functions. The hydrogel developed by Li and colleagues exhibited both thermal and pH responsiveness derived from respectively Pluronic F-127 for and carboxymethyl chitosan-genipin to encapsulate human umbilical cord-mesenchymal stem cells (hUCMSCs)-derived exosomes for skin repair^[73]. The thermal responsiveness leads to *in situ* crosslinking, while the aldehyde-amine crosslinking allows pH-responsive release of EVs to match the weakly acidic microenvironment of injuries. As for Guan and coauthors' hydrogel, GelMA works as the main matrix and aldehyde-functionalized chondroitin mimics ECM in growth plate cartilage to supply ECM environment, promote cartilage healing with the help of bone marrow mesenchymal stem cell-derived EVs, and provide anti-inflammatory functions^[74].

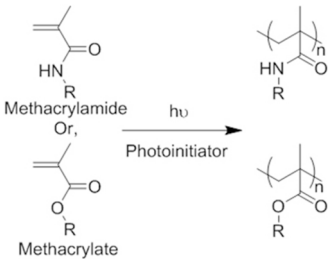
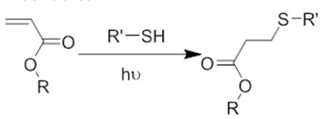
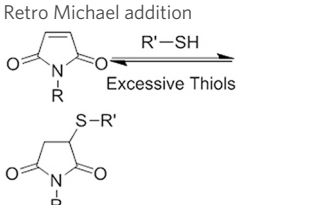
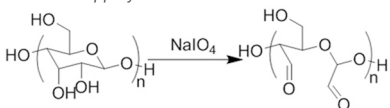
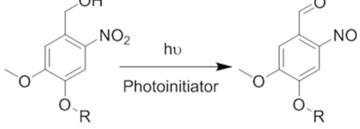
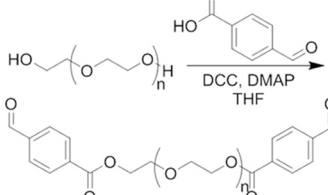
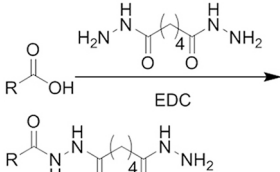
With such a wide selection of polymers and crosslinking strategies, one can easily acquire hydrogels with desired properties. Such versatility makes hydrogel materials suitable for different injuries and desired regenerative therapies.

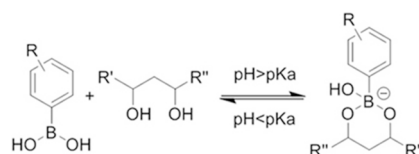
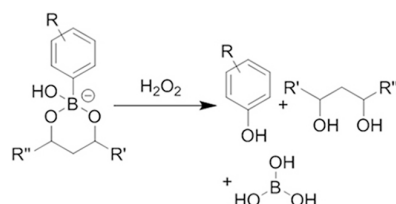
Insoluble polymer-based scaffolds for EV delivery systems

Polymeric scaffolds, in both 2D (membranes) and 3D (scaffolds) forms, serve as microporous matrices for cells to attach, proliferate, differentiate, and finally lead to the regeneration of tissue at the implanting area. The incorporation of EVs into the scaffolds can enhance the regenerative function. However, unlike hydrogels, the polymers for scaffolds are water-insoluble. Therefore, unless emulsion techniques are used (see "ADDITIONAL FUNCTIONS OF EV DELIVERY SYSTEMS")^[75], it is improper for normal-sized scaffolds to encapsulate EVs within, but provide surfaces for EVs to attach and thereafter deliver them to the recipient cells. The water insolubility and high temperature of glass transition (T_g) of the scaffold polymers lead to high elastic moduli easily reaching MPa level for both artificial polymeric scaffolds^[76] and natural polymer-derived scaffolds^[77], making them the choice of tissue engineering in parts requiring high tensile/compression strengths, such as bones^[78], bladders^[79] and dermis^[80].

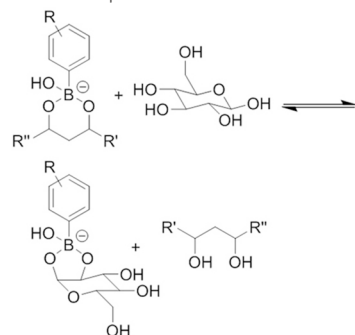
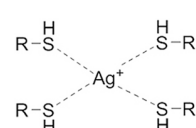
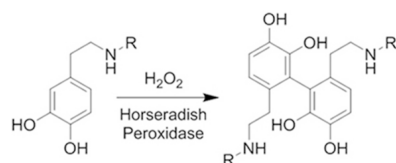
The major difference between hydrogels and scaffolds is the delicate porous structure. Porosity defines the overall available space within the scaffolds. Higher porosity provides more surface area for the loading of EVs. The average pore size is another indicator of the accessibility of the scaffolds. Depending on the source of the material, different porosity-introducing procedures are used. The representative materials and the corresponding processing methods are listed in Table 2. Both the porosity and the pore size can be adjusted

Table 1. Crosslinking strategies, suitable selections of materials and the corresponding properties of hydrogels used as EV delivery systems

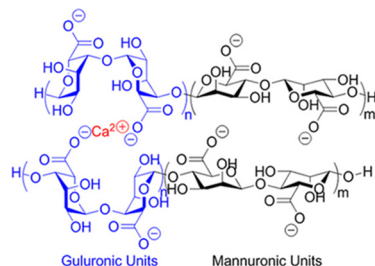
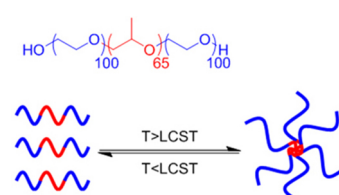
Crosslinking strategies and structures	Representative materials	Properties
(Chemical) Polymerization of methacrylamide or methacrylate 	Gelatin methacrylamide (GelMA) ^[52] Hyaluronic acid methacrylate (HAMA) ^[53,60]	<i>In situ</i> photo-crosslinking
(Chemical) Thiol-ene reaction  	Poly(ethylene glycol) diacrylate/thiolated alginate ^[61] Miktoarm PEG respectively modified with telechelic thiol/maleic acid ^[62]	<i>In situ</i> photo-crosslinking Injectable using double-barrel syringe <i>In situ</i> crosslinking
(Chemical) Amine-aldehyde conjugation (formation of Schiff base) $R-NH_2 + R'-CHO \xrightleftharpoons[\text{Acid or Shear Force}]{} R-N=CH-R'$ <p>Introductions of aldehyde: Oxidation of polysaccharides:</p>  <p>UV radiation over o-nitrobenzyl groups (fast crosslinking):</p>  <p>Modification with 4-formylbenzoic acid:</p>  <p>Introductions of amine: Conjugate with hydrazine:</p> 	Oxidated pullulan and PEI-modified pluronic F-127 ^[48] Oxidated hyaluronic acid and poly-L-lysine ^[63] Oxidated methylcellulose and PEI modified Pluronic F-127 ^[51] o-nitrobenzyl alcohol modified hyaluronic acid and gelatin (UV responsive) ^[64] Chitosan and diformalbenzoic acid-modified PEG ^[65] Hyaluronic acid modified with adipic dihydrazide and oxidated alginate ^[66,67]	Injectable through shear-thinning Self-healing Tissue adhesive Acid responsive degradation (pH < 6)

(Chemical) Phenylboronic acid-diol conjugationH₂O₂ responsiveness:

Glucose responsiveness:

**(Chemical) Silver ion-thiol bonds****(Chemical) Enzyme catalysis of dopamine to form free radicals and chemical conjugation****(Chemical) Enzyme catalysis of water-soluble protein to form insoluble clusters**

Structure varies

(Physical) Electrostatic interactions**(Physical) Temperature raising above LCST, forming hydrophobic clusters**Hyaluronic acid modified with phenylboronic acid and PVA^{#[68]}

Injectable through shear-thinning

Self-healing

Acid responsive degradation

H₂O₂ responsive degradation

Glucose responsive degradation

Silver ion and thiolated miktoarm PEG^[62]

Injectable through shear-thinning

Self-healing

In situ crosslinkingDopamine-modified alginate catalyzed by H₂O₂ and horseradish peroxidase^[50]

Injectable

Tissue adhesive

In situ crosslinkingPartial catalysis of fibrinogen[#] to fibrin by thrombin^{#[69]}

Fast crosslinking, specific reaction

Alginate in aqueous solution of calcium salt^{#[70]}Submersion in Ca²⁺ solution for crosslinkingPluronic F-127[#] above 37 °C^[56]

Injectable

Temperature sensitive *in situ* crosslinking

(Physical) Combination of electrostatic, hydrophobic and hydrogen bonding interactions

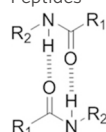
Ionic shielding of electrostatic repulsion, enhancement of hydrophobic interaction, and redistribution of hydrogen bonding with increasing temperature

Chitosan[#] and β -glycerophosphate[#], gelation above 37 °C^[47]

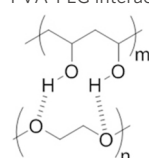
Injectable
Temperature sensitive *in situ* crosslinking

(Physical) Hydrogen bonds

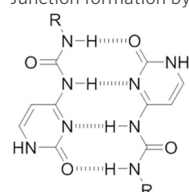
Peptides



PVA-PEG interaction



Junction formation by end groups



Arginine-Glycine-Aspartate (RGD)-Biotin^[59]

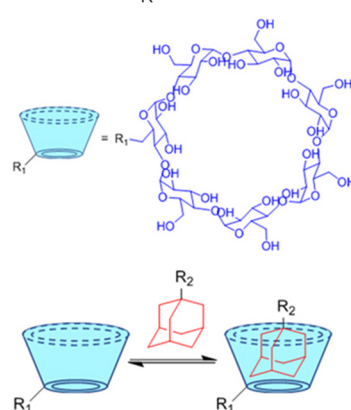
Crosslinking after annealing

PVA[#] and PEG[#] blend hydrogel^[57]

Extrusion of PVA into PEG solution

PEG with telechelic ureidopyrimidinone^[55]

Injectable
pH-responsive *in situ* crosslinking (basic to neutral)

(Physical) Host-guest interactions

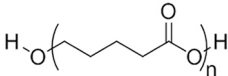
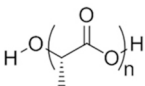
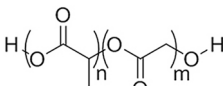
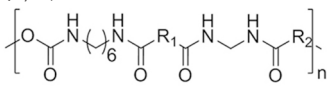
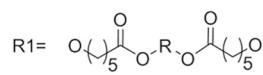
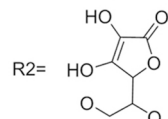
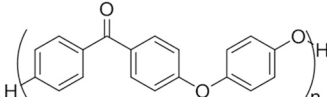
Adamantane- and β -cyclodextrin-modified hyaluronic acid^[71,72]

Injectable through shear-thinning

[#]Commercially available biomaterials. EV: Extracellular vesicle; PEI: polyethylenimine; PEG: poly(ethylene glycol); PVA: poly(vinyl alcohol); LCST: lower critical solution temperature.

by the bottom-up fabrication of the material (through 3D printing) or the sizes of the media to induce porosity (through sacrificial templates). The surface wettability of scaffolds is more crucial than that of hydrogels since their interactions with EVs are mainly at the surface of the material. Due to the explicit hydrophobic functional groups, polymers for the fabrication of scaffolds are mildly hydrophobic on the surface (often with static water contact angles of 60-90 °), which is slightly above the optimal range of surface tension for the adsorption of EVs (with static water contact angles approximately 40-70 ° by referring to the attachment of cells)^[103]. Thus, different surface wettability is tuned depending on the type of EV to reduce excessive hydrophobicity. Generally, the adjustment of surface wettability is through coating hydrophilic materials, especially positively charged polymers, to change the explicit functional groups and thereby promote the adsorption of cells and EVs (for details, see “IMPACT OF DIFFERENT DESIGNS ON THE LOADING AND DELIVERY OF EVs”).

Table 2. Representative water-insoluble polymeric materials used for EV delivery and typical approaches of porosity introduction

Chemical nature	Materials and structures (static water contact angle*)	Approaches of porosity introduction
(Natural) Decellularized ECM	Bovine bone ^[81] (N/A) Porcine cartilage ^[82] (N/A) Dermis of different animals ^[83] (N/A)	Decellularization, followed by decalcification (bones), grinding, crosslinking and lyophilization
(Natural) Protein	Collagen ^{#[84,85]} (-92 °) ^[86] Silk Fibroin ^{#[87]} (-74 °) ^[88]	Electrospinning (in 1,1,1,3,3,3-hexafluoro-2-propanol (HFIP) or acetic acids) Sacrificial templates (cryogel)
(Natural) Polysaccharide	Bacterial cellulose (membrane form only) ^[77] (-33 °) ^[89]	Biofabrication by <i>Komagataeibacter xylinus</i>
(Natural) Mixture of polysaccharide and protein	Chitosan/silk fibroin ^[90,91] (N/A)	Sacrificial templates (cryogel)
(Artificial) Polyester	Polycaprolactone (PCL) ^{#[92,93]} (-75 °) ^[94]  Poly(L-lactide) (PLLA) ^{#[95]} (-80 °) ^[96]  Poly(lactic-co-glycolic acid) (PLGA) ^{#[97]} (57-78 °, from 5:5 to 9:1 LA: GA) ^[98] 	3D printing Sacrificial templates (sugar dissolution or cryogel) Electrospinning (in chloroform and dichloromethane, with polarity adjusted by <i>N,N</i> -dimethylformamide or methanol)
(Artificial) Polyurethane	Diol: ascorbic acid, PCL diol; Diisocyanide: hexamethylene diisocyanide ^[99,100] (N/A)  R1=  R2= 	Sacrificial templates (cryogel)
(Artificial) Others	Polyetheretherketone ^{#[101]} (-85 °) ^[102] 	Strong acid corrosion

*Contact angles of materials without artificial introduction of surface topography. #Commercially available biomaterials. EV: Extracellular vesicle; ECM: extracellular matrices.

The versatility of scaffolds, unlike the wide selection of materials and crosslinking mechanisms for hydrogel, lies in the different porous structures. Changes in pore sizes, pore shapes, and connectivity of the pores, may lead to various EV loading situations and subsequently, different cell attachment, migration and communication. With fine control over the porosity-introducing, different porous structures can be further investigated for optimized regenerative results.

Hydrogel scaffolds for EV delivery systems

Hydrogels are materials encapsulating EVs, serving as bulk materials to fill the space of injuries. They have adjustable crosslinking density to precisely control the mechanical properties in resemblance to tissues, but have low surface areas for the attachment of cells for regeneration. On the other hand, scaffolds have delicate porous structures providing a large surface area for the attachment of EVs and the attachment, migration, proliferation and differentiation of cells, but the high mechanical strength limits their area of application. The combination of hydrogel and scaffold structure into hydrogel scaffolds can merge the advantages while overcoming the shortcomings.

Based on the definition of scaffolds, shear-thinning hydrogels, which self-heal after a certain period of time, are not suitable for the fabrication of hydrogel scaffolds. *In situ* photocrosslinkable hydrogels such as GelMA^[104] and alginate methacrylate (AlgMA)^[105] are the most popular choices. Similar to the fabrication of scaffolds, porosity can also be introduced through sacrificial templates or fine structure building (e.g., 3D printing). Due to the aqueous state of the polymer, ice crystals are the main choice for the templates. The overall procedure follows the route of solution freezing, photocuring and lyophilization^[91]. With the swelling property, lyophilized hydrogel scaffolds exhibit a water-absorbing function when submerged in EV suspensions, providing the potential to suck EVs into the pores distributed on the surface. At the same time, pores become smaller following swelling so that the absorbed EVs are enclosed in the pores. Such behavior gives them the name of “hydrogel sponges” for the loading of EVs through absorption^[91]. Shi *et al.* developed a chitosan (low degree of deacetylation)/silk hydrogel sponge to load EVs from gingival mesenchymal stem cells, with silk fibroin providing mechanical support, and chitosan performing the swelling function and providing cationic charges^[91]. This hydrogel scaffold overcame the excessive swelling of sole chitosan and the brittleness of sole fibroin scaffolds. Similarly, a triple-layer hydrogel scaffold composed of bladder acellular matrix, partially oxidated alginate-grafted gelatin hydrogel (crosslinked by aldehyde-amine and calcium ions) and knitted silk mesh was designed by Xiao and colleagues to provide sufficient waterproofness and stretching resistance^[106]. Such a structure is similar to “steel and concrete”, providing strong mechanical properties in resemblance to those of bladder.

The bottom-up 3D printing of polymer solution with simultaneous printing and crosslinking can build well-defined hydrogel scaffolds. Due to the overall non-damaging process, the EVs can be loaded either after the fabrication of scaffolds as in ordinary fabrication procedure, or can be directly mixed in the polymer solution during the preparation of bulk hydrogels, which is called “bioink”. Chen and colleagues developed a 3D-printable bioink composed of GelMA, mesenchymal stem cell-derived EVs and porcine cartilage ECM powder^[104]. The resulting hydrogel scaffolds, therefore, acquired radially oriented 3D architectures as designed, which facilitated the cell ingrowth for the regeneration of cartilage with the help of mesenchymal stem cell (MSC) derived EVs. Materials of other sources, such as alginate-Ca²⁺ hydrogels, which do not possess *in situ* photo-crosslinking functions but require the addition of specific crosslinking molecules, can undergo monolayer printing-Ca²⁺ solution crosslinking cycles to achieve a multi-layered scaffold, as demonstrated by Sun *et al.* in their macrophage EV-laden alginate scaffolds for osteogenesis and angiogenesis^[107].

The combination of hydrogels and scaffolds brings great diversity to the design and fabrication of EV delivery systems. This endows future EV delivery systems with high tailorability for any injury at any location.

EV delivery systems from inorganic sources

Unlike polymeric materials, inorganic materials are essential minerals with high elastic moduli. For example, hydroxyapatite, with a formula of $\text{Ca}_{10}(\text{PO}_4)_6(\text{OH})_2$, is the major inorganic component of bones, whose elastic modulus can reach ~150 GPa in the form of single crystals under nanoindentation^[108]. In consideration of the type of tissue with high stiffness and with a high abundance of mineral contents, inorganic material EV delivery systems can and have only been applied for bone regeneration. The commonly utilized inorganic materials include β -tricalcium phosphate [β - $\text{Ca}_3(\text{PO}_4)_2$, β -TCP] ceramics^[109], titanium oxide^[110], titanium alloy^[111], bioactive glass (45S5)^[112], hydroxyapatite^[113], and calcium sulfate^[113]. These materials have been used as bone substitutes to exert osteoinductive and osteoconductive functions in tissue engineering for years, especially hydroxyapatite, the major inorganic component of bones. Some of the above materials have to be specifically processed from the raw materials to achieve the desired compounds or structure.

Inorganic materials can be used as bulk materials for the encapsulation of EVs and scaffolds for the attachment of EVs. With their low solubility, a slurry of salts and EVs can set into solid bulk forms after slight evaporation of excessive water. Qayoom and colleagues reported such a bulk salt EV delivery system fabricated by the setting of nanohydroxyapatite, calcium sulfate, human bone morphogenetic protein-2, zoledronate and bone marrow mesenchymal cell-derived EVs^[113]. The slow dissolution of calcium sulfate (~0.26 g/100 g water at 25 °C for $\text{CaSO}_4 \cdot 2\text{H}_2\text{O}$, decrease with temperature^[114]) allows slow creation of pores and release of encapsulated EVs while providing space for the attachment and infiltration of cells. However, compared to the mode of bulk materials, more popularity lies in the mode of scaffolds in the exploitation of inorganic materials. The porosity of the scaffolds can also be introduced, again, using sacrificial templates and 3D printing. Unlike polymeric scaffolds with ice or sugar as sacrificial templates, inorganic scaffolds use polymer beads since a high-temperature sintering process is required to merge the minerals together and mold the shape. The bioglass scaffolds developed by Liu and colleagues used different polymeric templates to introduce hierarchical pores: micelle-forming Pluronic F-127 to form mesopores (7.7 nm), microspheres (0.5-2 μm) to form micropores and polyurethane sponges to form macropores (200-500 μm)^[115]. All materials were mixed with mineral slurry to set and sintered to merge and burn off the polymeric templates to achieve hierarchically porous structures for the attachment of mesenchymal stem cell-derived exosomes. A similar process has been applied to commercially available porous β -TCP scaffolds^[109,116]. 3D printing can combine the steps of sintering and structure-building, as demonstrated by the $\text{Ti}_6\text{Al}_4\text{V}$ alloy and lithium chloride incorporated bioglass scaffolds prepared by Zhai *et al.*^[111] and Liu *et al.*^[112] for the attachment of EVs through incubation. For pure metals with even higher melting points, which cannot be processed by sintering or 3D printing, an even stronger method is needed. Titanium must be processed by electrochemical anodization to fabricate nanotube topography on the surface as a 2D scaffold for further attachment of EVs and bone regeneration^[110]. Again, most inorganic scaffolds are treated with coatings to change the surface chemistry at the molecular level and enhance the interaction with EVs.

Compared to polymeric materials, not many inorganic materials have been tested. The primary difficulties are the relatively harsh processing procedures and the narrow window of selection. It is expected that more inorganic materials with unique properties, such as 2D materials, can be explored in the future.

EV delivery systems complexed of polymeric and inorganic materials

Most inorganic scaffolds have to be fabricated through sintering to achieve a certain volume for implantation, which requires well-controlled high temperatures. Otherwise, the raw materials are in powder form. In addition, the high stiffness of the material may not have a strong affinity for cells to attach and proliferate. Under such circumstances, the combination of polymeric matrix and inorganic material powder into complex material is favored to incorporate the advantages of both types of materials, in a way to take

advantage of the maneuverability, degradability and affinity of polymeric hydrogels or scaffolds and the easy absorption of powder formed minerals by the bones. Such an approach is called “mineral-doping”. Chen *et al.* doped hydroxyapatite in thiolated hyaluronic acid and thiolated heparin hydrogel crosslinked by “ene” modified PEG^[117]. This hydrogel was embedded with miRNA-375-carrying EVs from bone marrow mesenchymal stem cells to treat calvarial defects. Hydroxyapatite was also encapsulated within the hydrogel so that the injured bones could take advantage of the osteoinductive function for regeneration. For non-water-soluble scaffolds, Gandolfi and colleagues mixed finely milled dicalcium phosphate dihydrate and calcium silicate into PLA solution^[95]. Through a phase separation technique, which involves the freezing of a polymer solution and the use of a miscible solvent with an even lower melting point to remove the frozen solvent^[118], a mineral-doped PLA porous scaffold was obtained, with pore diameters ranging from 10 to 200 μm . The minerals, in the form of fine powder, are easier for osteoinduction. This scaffold was later surface-attached with EVs from mesenchymal stem cells to achieve full osteogenic function for bone regeneration. With the development of both polymeric and inorganic materials, more combinations and more functions can be expected for complex EV delivery systems.

IMPACT OF DIFFERENT DESIGNS ON THE LOADING AND DELIVERY OF EVS

For bulk materials: EV-encapsulation and release

For bulk hydrogels (including hydrogel scaffolds fabricated by the 3D printing of EV-encapsulated bioink^[104]) or bulk inorganic materials, the network of materials serves as cages to retain the EVs. The caging process has to be completed before the formation of the meshes, meaning the EVs are mixed directly with the raw material to form a mixture, followed by the curing of hydrogels or the setting of inorganic mineral bulks to establish the meshes. This has been demonstrated by the procedures of preparation in many bulk EV delivery systems^[52,53,61,105].

The major mode for EVs to leave bulk materials is diffusion, which is controlled by the degradation of the bulk material. Diffusion is driven by the concentration (or the chemical potential) of EVs. The initial concentration of EVs, often in the range of 10^9 to 10^{12} particles/mL, is the highest, standing for maximum potential for EVs to diffuse out of the material. This is followed by a sustained release close to a constant rate (zeroth-order), but as time passes, the concentration lowers, so that the rate of diffusion is gradually reduced and ultimately tends to zero.

In addition, the existence of meshes prolongs the diffusion of EVs for bulk materials. The average size of the meshes is generally considered smaller than the diameter of the encapsulated EVs, while a multi-layered mesh structure is also present to increase the number of meshes for EVs to diffuse through. These two structural parameters are the factors in retaining EVs. The enlargement of meshes and the decrease in mesh numbers mark the lifting of the restrictions and the start of the release of EV. Such a change in the mesh is mainly caused by the passive degradation of the material. For water-soluble polymers, degradation occurs through biodegradation by enzymes secreted by the coming cells. Due to the smaller size of cells compared to the meshes, the biodegradation of hydrogel starts from the surface of the hydrogel and then moves inward, which is an accelerating procedure with more availability of enzymes from the increasing number of attached cells and greater infiltration of enzymes into the looser and decomposed hydrogel^[119], until the final remnants of hydrogels with little surface available for enzymatic reaction [Figure 2A]. For inorganic bulks, dissolution (inorganic salts) of the network is the major process limiting the diffusion of EVs [Figure 2B]. However, to the best of our knowledge, there is no reported comparison between the release of EVs versus the dissolution of salt^[113]. It can be speculated that the process takes a similar curve as the biodegradation of the hydrogel. As water gradually breaks the intermolecular or interionic bonds, water molecules infiltrate more easily through the new defects from the dissolved parts until full dissolution of the

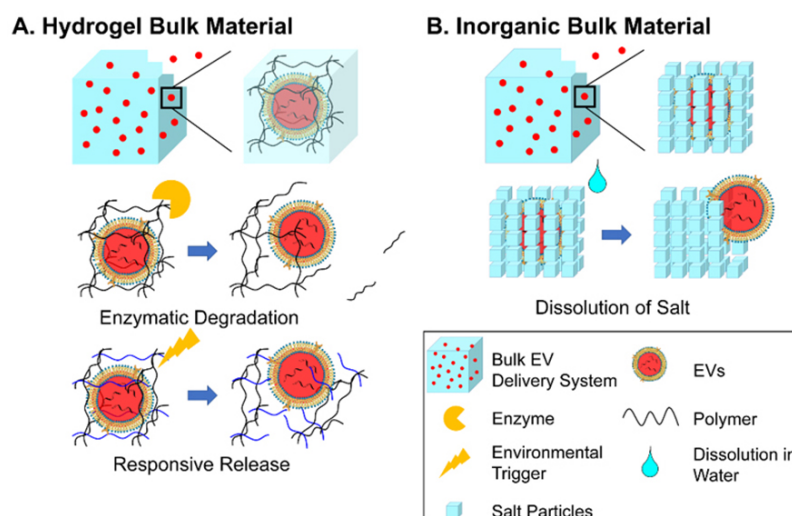


Figure 2. Schematic illustration of the mode of action of bulk EV delivery systems through EV-encapsulation and release by degradation: (A) Enzymatic degradation and responsive release by hydrogels and (B) release by dissolution of inorganic bulk materials. EVs: Extracellular vesicles.

salt.

The relative relationship between the rates of EV diffusion and hydrogel degradation determines the overall release profile *in vitro*, which can be measured by quantification of specific antibodies^[52], particle number^[53] and the intensity of fluorescence labels^[61] of the released EVs after specific lengths of time. At the starting stage (0~30% accumulative release of EVs), the high potential of EVs may cause a burst release of EVs, as observed in some reported delivery systems^[74,120]. As the delivery proceeds into the middle stage (~30%~80% cumulative release of EVs), the reduced potential of EVs and the accelerated degradation cancel out, reaching a close-to-constant release of EVs, which is the key stage of bulk material delivery systems. This stage can cover three^[119] to more than 30 days^[62,121], depending on the material structures and the need for recovery of the injury. A well-tuned hydrogel can even fully match the release profile of EVs with the degradation profile, as illustrated by almost identical curves of material degradation and EV release in Zhang and colleagues' HAMA hydrogel scaffold^[53]. In the final stage, the chemical potential of EVs is too low to overcome the obstacle of diffusion from the remaining hydrogel, leading to non-100% release until the full degradation of the hydrogel.

At the macroscopic level of material, a high crosslinking density can both reduce the mesh size and add the number of meshes in the material, and at the same time slow down the degradation rate. This can effectively extend the retainment of EVs, as demonstrated by the faster release (~90% over 2 h) from 2% AlgMA hydrogel than that (~40% over 2 h) of 4% AlgMA hydrogel in the study by Huang and coauthors [Figure 3A]^[105]. Some hydrogel delivery systems incorporated stimuli-responsive crosslinking. Aldehyde-amine crosslinking is sensitive to an acidic environment. Wang *et al.* showed the difference in EV release under acidic pH of 5.5 compared to that at 7.5 in the injectable hydrogel of oxidized hyaluronic acid and poly- ϵ -L-lysine^[63]. The hydrogel showed slightly faster and more thorough release in an acidic environment (~80% at pH 5.5 compared to ~65% at pH 7.5 on Day 12) [Figure 3B]. Similar results were reported by Jiang *et al.* in their injectable phenylboronic acid-modified hyaluronic acid-PVA hydrogel, which showed faster release of EVs from neural stem cells after treatment with glucose and/or H₂O₂^[68]. Some hydrogels incorporate enzymatically responsive crosslinkers, such as matrix metalloprotease cleavable polypeptide

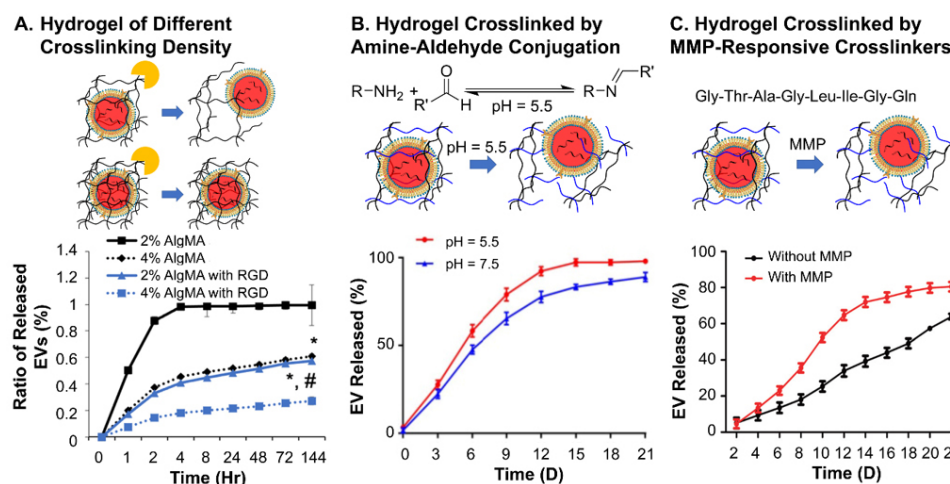


Figure 3. *In vitro* EV release profiles of (A) Hydrogels without responsiveness of different crosslinking densities; (B) acid-responsive hydrogels crosslinked by amine-aldehyde conjugation; (C) enzyme-responsive hydrogels. Figure 3A adapted with permission^[105], Copyright 2021, Elsevier; 3B adapted with permission under terms of the CC-BY NC license^[63], Copyright 2019, the authors, published by Ivyspring International; 3C adapted with permission^[122], Copyright 2019, Royal Society of Chemistry. EV: Extracellular vesicle.

(Gly-Thr-Ala-Gly-Leu-Ile-Gly-Gln), as reported by Han *et al.*^[122]. Due to the relatively high crosslinking density, an obvious accelerated release of EVs has been observed [Figure 3C]. The enzyme-responsive hydrogel released ~70% EVs over 14 days followed by the plateau of release at 80%, while the non-responsive hydrogel followed a relatively linear profile to the delivery of 60% of EVs over 22 days. Microscopically, a homogeneous distribution of crosslinking points within the hydrogel is also crucial^[123], which has not been reported in EV delivery systems but frequently in conventional drug delivery systems. Although considered smaller than that of EVs, the mesh size has a large deviation within a bulk hydrogel, leading to inconsistent degradation, incomplete encapsulation and inconstant release profile of the material, especially for hydrogels crosslinked by reversible crosslinking moieties, which do not possess homogeneously distributed and stable crosslinking structures^[62,120,123,124]. Such a non-uniform crosslinking system also suggests the heterogeneous distribution of EVs within the hydrogel, especially exposed at the surface of the material. These molecular defects all contribute to the possible burst release at the start of the delivery of hydrogel EV delivery systems. Similarly, for bulk inorganic materials, thorough mixing of the salt and EVs is necessary for the constant release of EVs.

In addition to the crosslinking structures and the distribution of EVs in the material, other parameters can also affect the diffusion of EVs from hydrogels. The change of stiffness of physically crosslinked hydrogel (i.e., stress-relaxing hydrogels) is one of such kinds. In their study on the impact of stiffness of hydrogel on the release of EVs, Lenzini and colleagues adjusted the Ca^{2+} concentration to achieve soft (shear modulus ~500 Pa) and stiff (shear modulus ~3 kPa) alginate hydrogel without a dramatic change in mesh size^[70]. It was found that EVs could still diffuse through a stiff Ca^{2+} -crosslinked alginate hydrogel compared to softer or non-stress-relaxing hydrogels. This indicated the possible diffusion by the deformity of EVs under the confinement of stiff stress-relaxing hydrogels. Such a fact also suggests that flexible polymer chains in hydrogel may also affect the diffusion of EVs. A hydrogel of polymers with low T_g , such as polyethyleneglycol (T_g around -63°C ^[125]), is supposedly softer compared to hydrogels of polymers with high T_g , such as hyaluronic acid, given the same crosslinking density. However, no such study has been made to the best of our knowledge.

The tracking of *in vivo* release profiles is a lot more complicated compared to *in vitro* observations, which makes such information highly limited. The major approach to observing the traces of EVs *in vivo* is through qualitative or semiquantitative fluorescence signals of labeled EVs. Han *et al.* tracked the PKH-26 red signal of hUCMSC-EVs released by the enzyme-responsive hydrogels mentioned above in the border region of myocardial infarction^[122]. The retention of EVs matched the *in vitro* release profile with discernable existence at day 21 in the tissue, while no trace of EVs was found for injections with sole EVs [Figure 4A]. Such labeled EVs can also be observed by live and *ex vivo* bioluminescence imaging to locate their distribution after release. Mardpour and colleagues encapsulated MSC-EVs in thiol-maleimide PEG hydrogels to treat chronicle liver failure^[62]. The live and *ex vivo* imaging clearly showed maximum retention of released EVs in liver after seven days and gradual decrease till Day 30, while no trace was found for EV-only groups at the same time spots [Figure 4B]. Similarly, Zhang *et al.* presented the biodistribution of *Gaussia* luciferase labeled MSC-EVs encapsulated in amine-aldehyde chitosan hydrogels for blood vessel regeneration of ischemic hindlimbs [Figure 4C]^[126]. In combination with quantitative analysis results of fluorescence intensity and component (miRNA-126), the hydrogel successfully retained the EVs within the hindlimb for over 72 h.

From the cases above, it can be seen that the bulk materials have been extensively applied to achieve the successful retainment of EVs. Especially for hydrogels, their release profile can be adjusted primarily through the crosslinking strategies and the crosslinking density. However, more structural parameters, such as the intrinsic flexibility of the polymers and the homogeneity of crosslinking density, can be investigated for their impact on the release performance of hydrogels. Moreover, the different delivery performance *in vivo* of responsive crosslinking designs is difficult to reflect in current studies. On the other hand, limited by the rare studies of inorganic bulk material, the correlation of material structure, properties and release performance is still unclear.

For scaffold materials: two different modes

As mentioned in “DESIGN STRATEGIES OF MATERIALS FOR EV DELIVERY SYSTEMS”, most EV delivery scaffolds have EVs attached. Depending on the status of EV attachment, the delivery mechanism can be divided into two modes [Figure 5].

EV-adsorption and release

The first EV attaching mode is through adsorption to scaffolds, and accordingly, the delivery is through the desorption and release. Equation 1 depicts the reversible relationship between adsorption and desorption:



where $EV \cdot Scaffold$ denotes the EV attached state and $EV + Scaffold$ means EVs are released. k_d stands for the coefficient of desorption and k_a for adsorption. The adsorption-desorption is a reversible process. k_d is affected by multiple factors, such as the concentration difference of EVs between the scaffold and the environment and the liquid shear force within the injury, which can be treated as a constant here. k_a is dependent on the interactions of EVs and scaffold surface, and also the concentration difference of EVs.

In the preparation of most EV delivery scaffolds, the incubation of scaffolds with EV suspensions is the basic method to load EVs. A higher concentration of EVs can lead to a higher k_a and thus a larger loading efficiency. However, when transplanted to tissue, k_a significantly decreases due to almost zero presence of

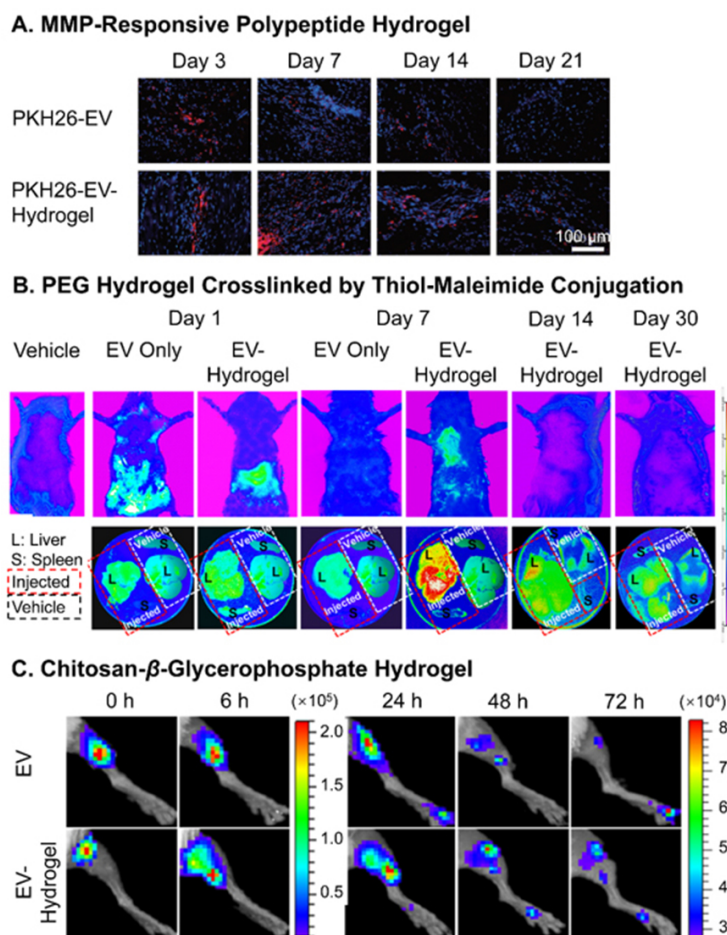


Figure 4. *In vivo* tracking of EVs released from hydrogels. (A) Fluorescence microscopy of PKH-26 red-labeled hUCMSC-EVs released by the MMP-responsive hydrogel in the border region of myocardial infarction; (B) Live and *ex vivo* imaging of PKH-26 red-labeled EV delivery PEG hydrogels crosslinked by thiol-maleimide conjugation in the chronic liver injury model; (C) Live imaging of *Gaussia* luciferase-labeled MSC-EVs encapsulated in chitosan- β -glycerophosphate hydrogel injected in ischemic hindlimb. Figure 4A adapted with permission^[122], Copyright 2019, Royal Society of Chemistry; 4B adapted with permission^[62], Copyright 2019, American Chemical Society; 4C adapted with permission^[126], Copyright 2018, American Chemical Society. EVs: Extracellular vesicles; PEG: poly(ethylene glycol); MSC: mesenchymal stem cell.

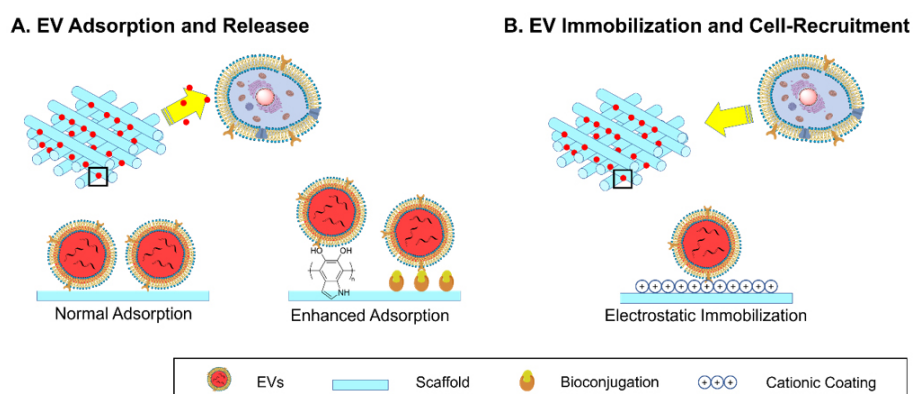


Figure 5. Schematic illustration of two modes of action of EV delivery scaffolds: (A) Surface adsorption and release of EVs and (B) surface immobilization of EVs and cell recruitment. EVs: Extracellular vesicles.

EVs of the same type in injured tissue. Therefore, adsorption alone is unstable and a burst release can be expected from mineral scaffolds or non-treated polymeric scaffolds^[109,127,128]. An increment of k_a by enhancing the EV-surface interaction is necessary for a more controlled release profile. Thus, the adsorption and desorption of EVs to different surfaces of material are crucial to their loading and release. Although previous reports have provided semiquantitative characterizations of the coverage of EVs adsorbed on scaffolds using fluorescence microscopy^[97] or electron microscopy^[129] as a result of adsorption, followed by the release profile of the EVs as a result of desorption, rarely direct investigations have been made, possibly due to the difficulties in the detection of nanosized EVs with sufficient resolution of the whole process^[130]. The only research, to the best of our knowledge, was conducted by Yang and colleagues^[130]. They developed interferometric plasmonic microscopy for imaging and size analysis of the adsorption and desorption of exosomes to negatively charged gold, positively charged gold, PEG-modified gold and CD63 antibody-modified gold surfaces. For the different charges of the surfaces, positive charge exhibited the strongest attraction of EVs from A549 cell lines, i.e., highest k_a , to adsorb to the surfaces, compared to few ($k_a \approx 0$) on negatively charged ones [Figure 6]. On surfaces with different chemical properties, EVs bounced off PEG-modified gold surfaces, as a representative superhydrophilic material with reverse-osmotic properties, while an obvious “adsorb-stay-desorb” procedure was observed for CD63 modified surfaces. This is due to the weak but insufficient interaction, or insufficient k_a , between the antibody and the EVs. The results suggest that in order to promote the loading efficiency and ensure more sustained release, a properly strong interaction and k_a between the EVs and surfaces of scaffolds are required.

EVs have phospholipid bilayer membrane structures with proteins and peptidoglycan attached to or inserted within. The phosphates groups on phospholipids, and amide groups, amine groups, hydroxy groups and carboxylic groups on the proteins and peptidoglycans are able to interact with the scaffolds by hydrogen bonds or van der Waals forces when polar carbonyl groups are present, such as PCL, PLLA and PLGA. This is the case when the surface of the materials is not modified.

One way of enhancing adsorption is to raise the density of hydrogen bonds or van der Waals forces between EVs and scaffold surfaces. Polydopamine coating is the most applied method to increase the k_a . Inspired by the adsorption of mussels on solid surfaces, researchers have applied polydopamines to introduce a high number of hydrogen bond donors (hydroxy on catechol groups) and exert π - π interactions (benzene of catechol groups) between surfaces^[131]. In the report on poly(lactic-co-glycolic acid) (PLGA) EV delivery scaffolds for bone regeneration, Li *et al.* showed that the coating of polydopamine can significantly reduce the burst release of EVs from ~60% to ~20% of the total load, and retention from three days to more than eight days^[97]. Since the membrane of EVs is mainly composed of phospholipids, they are hydrogen bond acceptors as well as negatively charged under physiological conditions, and thus can be adsorbed with polydopamine coating with a higher probability of extending the release [Figure 7A]^[97]. Tannic acid, with a similar catechol structure as polydopamine, has also been used. Under oxidizing and basic conditions, the catechol structures of tannic acid allow it to self-polymerize and become adhesive reminiscent of polydopamine, as demonstrated by the PEEK scaffolds modified by Fan *et al.*^[101]. With the coating of tannic acid, the surface hydrophilicity (i.e., water contact angles ranging from 60 ° to 30 ° after coating) was greatly promoted. Accordingly, an obvious reduction in burst release (50% to 10% release at Day 0 after coating) and more linear release (three days to 14 days to reach 90% release after coating) were both observed [Figure 7B]. Specific bioconjugation has also been exploited to mimic natural EV-ECM complex structures^[132] by applying a coating of ECM involved polymers. Heparin has been used to anchor biomolecules such as growth factors, and was recently also applied as coating of scaffolds by Wei *et al* to treat hyperlipidemia^[93]. A heparin coating on a polycaprolactone (PCL) scaffold for blood vessel graft was implanted on the abdominal aorta. The coating slightly slowed down the release of the vesicles on the

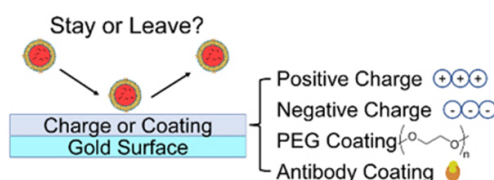
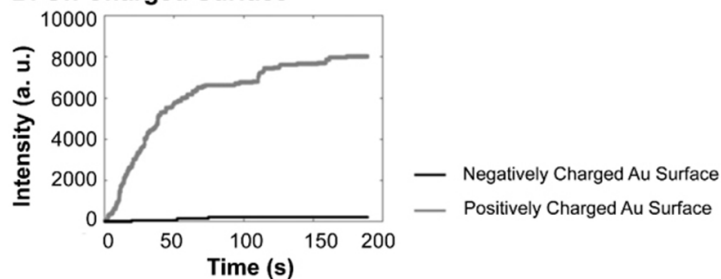
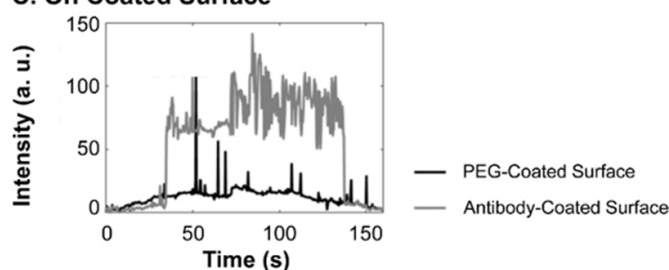
A. Illustration**B. On Charged Surface****C. On Coated Surface**

Figure 6. Interferometric plasmonic microscopy detection of the number of EVs from A549 cell lines binding different surfaces: (A) Illustration of the experiment; (B) EVs binding positive and negatively charged gold surfaces. Positively charged surface shows immobilization effect while negatively charged surface shows bouncing off of EVs; (C) EVs binding PEG and antibody-coated gold Surface. PEG surface shows bouncing off of EVs while antibody-coated surface shows an “adsorb-stay-desorb” procedure. Adaptations with permission^[130], Copyright 2018, National Academy of Sciences. EVs: Extracellular vesicles; PEG: poly(ethylene glycol).

scaffold, as shown by the *in vivo* fluorescence live imaging of luciferase labeled EVs [Figure 8A]^[93]. This is one of the few reported *in vivo* EV release behavior of scaffolds. Similarly, the bioconjugation effect has also been reflected by the prolonged release profiles of scaffolds made from or incorporated with decellularized ECM materials, including collagen (over 14 days release)^[133] and decellularized cartilage (more than 50% compared to blank, 14 days *in vitro* release)^[104]. Another approach for increasing hydrogen bonds is through the modification of the surfaces of scaffolds, exploiting antibodies specific to the antigens on EVs, as was shown by the CD63-A549 cell line-derived EVs in the interferometric plasmonic microscopy test by Yang *et al.*^[130]. Another example is the integrin $\alpha 4 \beta 1$ ligand LLP2A-placenta mesenchymal stem cell-derived EVs on electrospun PLLA-PCL scaffolds by Hao *et al.*, but no information was given on the release profile of the EVs^[134].

Compared to weak hydrogen bonds and van der Waals interaction, electrostatic interactions are much stronger and more effective in retaining EVs. The majority of phosphate groups on the membrane of EVs make them overall negatively charged. Some scaffolds with relatively weak cationic charge can also extend the release of EVs by increasing k_a through electrostatic interactions, such as chitosan (80% in six days *in vitro*)^[90].

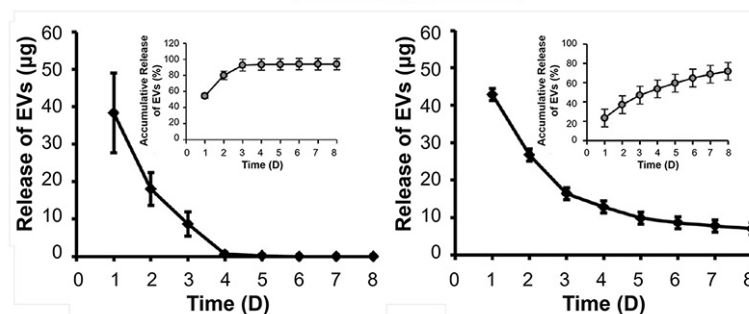
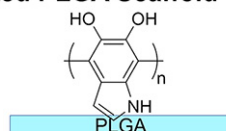
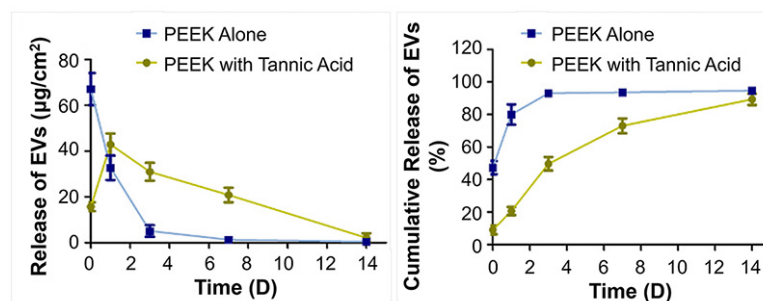
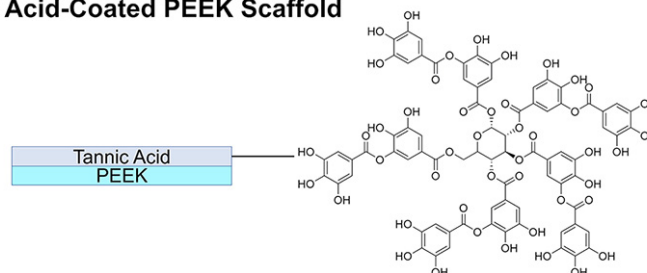
A. Polydopamine-Coated PLGA Scaffold**B. Tannic Acid-Coated PEEK Scaffold**

Figure 7. The *in vitro* release profile of EVs from scaffolds prolonged by coatings: (A) Polydopamine-coated PLGA scaffold and (B) tannic acid-coated PEEK scaffold. Figure 7A adapted with permission^[97], Copyright 2018, American Chemical Society; 7B is adapted with permission^[101], Copyright 2021, the authors, published by KeAi Publishing. EVs: Extracellular vesicles; PLGA: poly(lactic-co-glycolic acid).

EV-immobilization and cell-recruitment

The fixed mode of EV attachment is less frequently utilized compared to the release mode. It involves the full immobilization of EVs on the surfaces of scaffolds for the recruitment of targeted cells instead of releasing them. In this case, k_a is much larger than k_d , so the overall reaction is one way to reach the $EV \cdot Scaffold$ state. As presented by Yang and colleagues, positively charged coatings are ideal for achieving this purpose^[130]. PEI coated upon scaffolds or conjugated to carboxylic moieties to the scaffolds can greatly promote the cationic charge on the material. This can lead to strong electrostatic attraction and subsequent full immobilization of negatively charged EVs. Su and coauthors covalently conjugated PEI to an electrospun PCL scaffold to acquire a high positive charge density^[92]. The material could thus immobilize 75% of the supplied mesenchymal stromal exosomes compared to almost none on the untreated scaffold without further release until consumed by attached cells. The scaffold thus acted as the recruiter and trainer

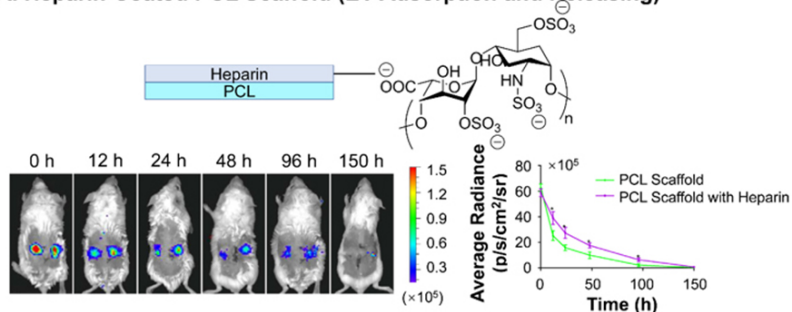
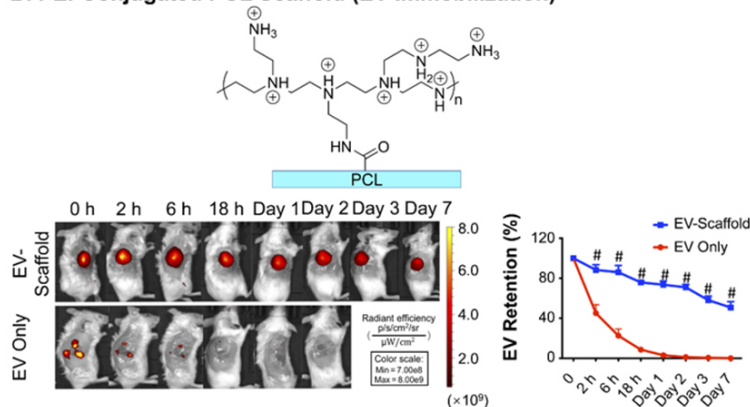
A. Heparin-Coated PCL Scaffold (EV Adsorption and Releasing)**B. PEI-Conjugated PCL Scaffold (EV Immobilization)**

Figure 8. *In vivo* tracking of EVs delivered from scaffolds. (A) Live imaging of the retained delivery of Luciferase-labeled EVs by PCL scaffold coated with heparin at abdominal artery of mice; (B) live imaging of the immobilized EVs on PCL scaffold conjugated with PEI implanted on large skin wound of mice. Figure 8A adapted with permission^[93], Copyright 2019, Elsevier; 8B adapted with permission under terms of the CC-BY NC license^[92], Copyright 2021, the authors, published by American Association for the Advancement of Science. EVs: Extracellular vesicles; PCL: polycaprolactone; PEI: polyethylenimine.

for macrophage and T cells to facilitate skin recovery. Of course, due to the hydrolysis of PCL, the uninternalized EVs were eventually released. The retention rate was 50% after seven days *in vivo* compared to the two-day elimination without material based on the quantitative analysis of fluorescence intensity [Figure 8B].

It follows that surface modifications with specific interactions with EVs have shown to greatly increase the retainment of adsorbed EVs on scaffolds, both *in vitro* and *in vivo*. This has been the mainstream for the preparation of EV delivery systems in scaffold forms. However, a deeper understanding of the intensities of the interaction between the coatings and EVs is necessary for better control of the delivery of EVs. Meanwhile, porosity, the key feature of scaffolds, has not been mentioned in any of the above-discussed studies. This parameter affects the overall loading capacity of EVs and should receive more emphasis in further investigations.

Promotion of tissue regeneration by EV delivery systems

Despite the need for both an in-depth understanding of the interaction between the delivery system and the release of EVs, and more accurate control over stimuli-responsive release, both bulk and scaffold materials have shown good prolonged EV delivery compared to the administration of only EVs and the results are obvious in the regeneration of tissue, as reflected by the many reports of their use in treating various injuries at different sites of the body.

Concerning bulk materials to treat periodontitis, Shen and colleagues injected chitosan- β -sodium glycerophosphate hydrogel encapsulating dental pulp stem cell-derived EVs into the cavity of periodontitis^[47]. Compared to the EV-only group, the groups injected with EV-hydrogel showed an approximately 1.5-time acceleration of the healing of alveolar bone [Figure 9A] and a two-time reduction in the loss of bone, which also matched the reduced amount of cytokine and the increased number of macrophages in anti-inflammatory phenotype for the EV delivery system. In the field of cardiac repair, hUCMSC EVs in functional MMP-responsive polypeptide hydrogels reported by Han and coauthors exhibited an approximately 50% reduction in inflammation, fibrosis and apoptosis, and upregulated angiogenesis for myocardial infarction 28 days after surgery compared to EV-only treatment, as a result of obvious retention of EVs [Figure 4A]^[122]. A similar result was observed in ischemic limbs parallelly treated with MSC-EVs and MSC-EV-chitosan hydrogel, as shown in Figure 4C^[126]. The localized retention of EVs by the material directly led to the reduction of necrotic fibers and inflammatory cells, and improved angiogenesis at both cellular and physiological levels, resulting in optimal muscle recovery after 14-28 days [Figure 9B]. More cases have highlighted the regenerative promise of the administration of EV delivery systems compared to EVs alone^[51,56,74,135].

As for scaffolds, not as many reports compared the results of EV-only and EV-scaffolds groups, since EVs are mostly considered as an enhancement to the functions of scaffolds. Answering the needs for the regeneration of endometrium and fertility, Xin and colleagues loaded hUCMSC-EVs to collagen scaffolds, which could sustain the release over 14 days in an extended burst release manner^[133]. The combination of EVs and scaffolds was found to achieve the results of EV-only group in terms of regenerated endometrium thickness and the number of PR⁺ cells, and have improved effects on the regeneration of glands and reduction of muscular dystrophy after 30 and 60 days of administration [Figure 10A]. Jiang *et al.* exploited acellular ECM scaffolds laden with Wharton's jelly MSC-EVs to induce osteochondral regeneration^[82]. The EV-scaffolds group was assessed to have promoted ~33% of the recovery of cartilage compared to EV-only group three and six months after transplantation. In the representative case of cell-recruiting mode, the PCL scaffolds immobilized with MSC-EVs through conjugated PEI were used to treat square skin excisional wounds with an area of 225 mm²^[92]. After transplantation for two weeks, a lot more newly formed epidermis and the presence of α -smooth muscle actin were found in the tissue using the combinatory material. The EV-scaffolds group exhibited strong function, reaching ~70% of wound closure, while the closure of EV-only group was only 30% and scaffold-only group 20% [Figure 10B].

With greatly promoted regenerative outcomes resulted from EV delivery systems, the followed key question is whether the *in vivo* kinetics of delivery agrees with the physiological patterns of stem cells, which is crucial for the regeneration of tissue and the closing of injuries. The tracking of the internalization of EVs delivered by the bulk materials is thus necessary for the recovery procedure of tissue. This is illustrated by the study conducted by Henriques-Antunes *et al.* on the relationship between the EV release profile and the healing of diabetic chronic wounds^[136]. In order to achieve a fully controlled release of EVs in terms of dose and frequency, a photocleavable crosslinker was synthesized to conjugate EVs and thiolated hyaluronic acid to form a hydrogel, so that the delivery can be proceeded by periodical irradiation. It was found that the matching of the release profile of EVs and the dynamics of the regeneration of skin can promote more than 40% healing effect compared to scaffold alone and single administration of EVs [Figure 11]. This single study calls for more investigations based on different kinetics of EV release and the interaction with cells from different tissues.

ADDITIONAL FUNCTIONS OF EV DELIVERY SYSTEMS

In order to enhance the EV delivery systems to be more suitable for specific conditions in diseases or

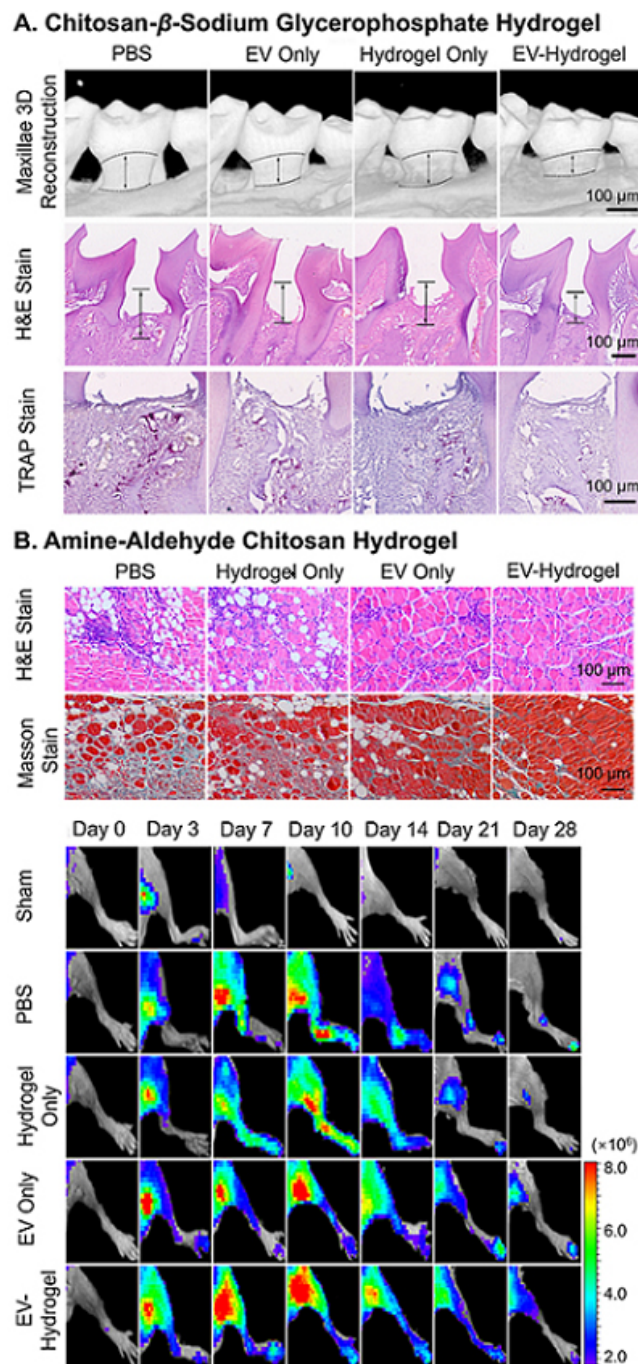


Figure 9. Recovery results of EV delivery hydrogels. (A) Accelerated healing of alveolar bone by dental pulp stem cell-EV chitosan- β -sodium glycerophosphate hydrogels injected within the cavity of periodontitis; (B) reduction of necrotic fibers and inflammatory cells (staining), and improved angiogenesis (live imaging) by MSC-EV-encapsulated amine-aldehyde chitosan hydrogel in hindlimb. Figure 9A adapted with permission^[47], Copyright 2020, the authors, published by KeAi Publishing; 9B adapted with permission^[126], Copyright 2018, American Chemical Society. EV: Extracellular vesicle; MSC: mesenchymal stem cell.

requirements of surgeries, extra functions have been incorporated into the materials through special processing strategies based on the intrinsic properties of the materials or the introduction of specific functional groups/substances to change the property of the material at the molecular level.

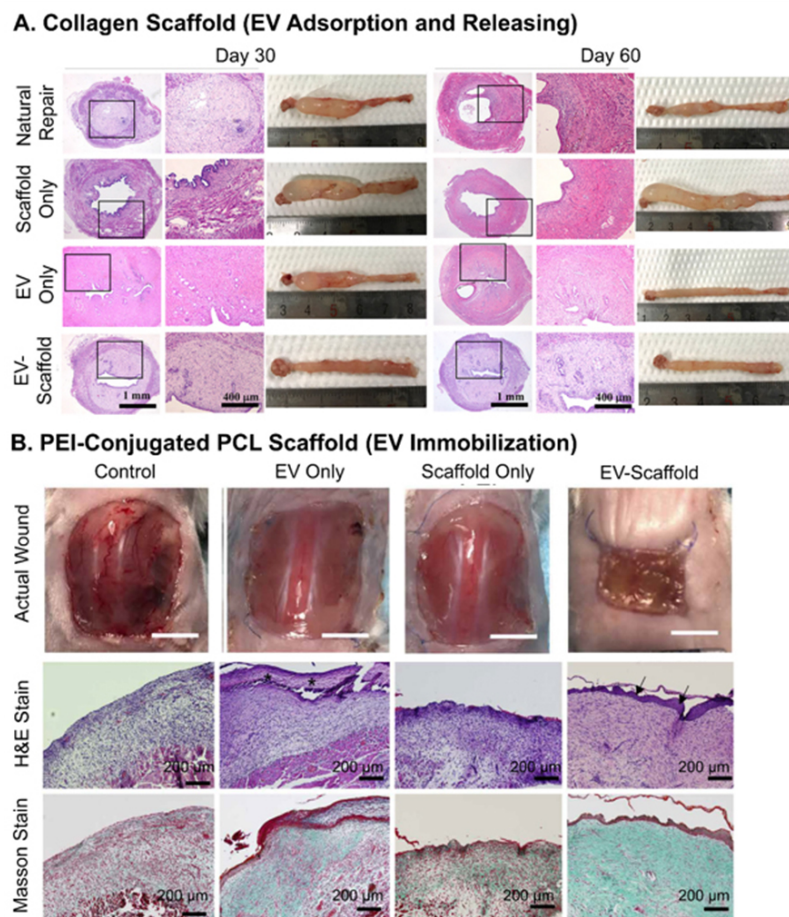


Figure 10. Recovery results of EV delivery scaffolds. (A) Promoted regeneration of glands and reduction of muscular dystrophy by hUCMSC-EVs laden collagen scaffolds for endometrium injury; (B) faster wound closing (picture) and more formation of new epidermis (staining) by MSC-EVs immobilized on PEI-conjugated PCL scaffolds treating large skin wound. Figure 10A adapted with permission^[133], Copyright 2020, Elsevier; 10B adapted with permission under terms of the CC-BY NC license^[92], Copyright 2021, the authors, published by American Association for the Advancement of Science. EV: Extracellular vesicle; MSC: mesenchymal stem cell.

In many cases, minimally invasive surgery is required to reduce the suffering of patients. Injectable hydrogels have met such requirements through shear-thinning properties or mixing with double-barrel syringes, but for materials such as scaffolds and photocrosslinkable hydrogels, transplantation is still needed. To compensate for this, the size of these delivery systems must be sufficiently small, i.e., in micrometer class, for direct injection. So far, the primary approach to miniaturizing EV delivery systems is through the formation of emulsion. To fabricate hydrogel microspheres, water-in-oil emulsion is used. This is demonstrated by Liu *et al.*, who developed chitosan microspheres after high-speed homogenization of acidified chitosan-liquid paraffin/petroleum ether/SPAN80 emulsion system^[137]. With a diameter of 5 μm , the cationic charged spheres were incubated with anionic rabies virus glycoprotein peptide-modified EVs loaded with reactive oxygen species-responsive curcumin nanoparticles. Although the microspheres were prepared only for better observation of EVs, it suggests the possibility of using microspheres as EV carriers through adsorption and such a concept can be extended in future exploration of EV-based therapies. As for the fabrication of non-water-soluble scaffolds, reverse phase emulsion or double emulsion systems can be applied. Hollow PLGA spheres with a diameter of 50 μm were prepared using water-in-oil-in-water double emulsion systems with the help of sonication. The spheres were eventually surface modified with polydopamine for the attachment of serum-derived EVs^[138]. The EV-loaded microspheres were shown to be

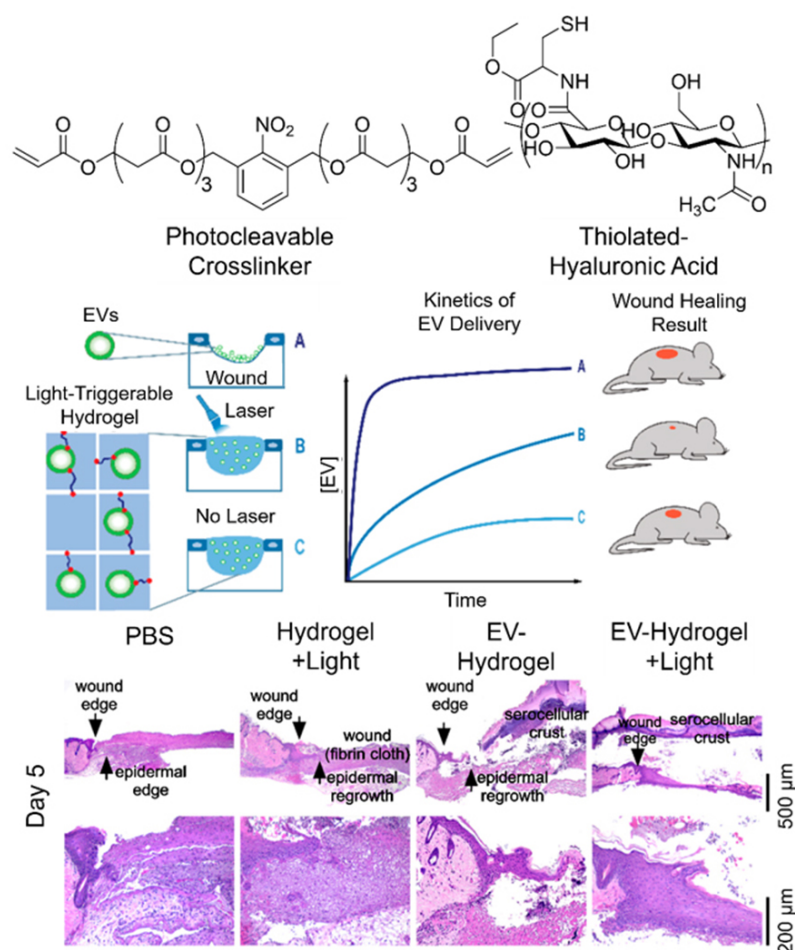


Figure 11. Schematic illustration of the promoted wound-healing effect of controlled release of EVs from photocleavable hydrogel and the according staining of wounds treated with different approaches at Day five. Adaptations with permission^[136], Copyright 2019, American Chemical Society. EVs: Extracellular vesicles.

internalized by DC2.4 and RAW264.7 cells, with the internalization promoted by higher EV loading rates. Such a double emulsion system also allows the use of microfluidic devices for the fabrication of microspheres with more uniform sizes. Through a well-designed PDMS microfluidic chip, Swanson and colleagues were able to fabricate human DPSC-derived EV-encapsulated microspheres with a diameter of around 5 μm , which were later physically adsorbed to poly(L-lactide) (PLLA) scaffolds and transplanted to treat defected calvary of mice^[127]. Such a double scaffold system utilized a two-step release, i.e., desorption of microspheres from scaffold and hydrolysis of microsphere to release EVs. The system was found to make the delivery of EVs more linear. It has to be noted that in order not to disrupt the encapsulated EVs by organic solvent, the oil phases of the above-reported spheres were volatile for thorough evaporation and easy collection. Accordingly, dichloromethane and ethyl acetate were used in the above-mentioned two studies. However, the remnant organic solvent is still potentially harmful to tissue and EVs. A replacement of oil phase with air and *in situ* crosslinking can allow the direct formation of hydrogel microspheres encapsulating EVs within the injured tissue, without the need to remove the organic solvent, as demonstrated by Yao and colleagues^[139]. They filled a double-barrel syringe with fibrinogen/EVs mixture as the polymer solution and thrombin solution as the crosslinker, and equipped the tip of the syringe with a spray needle. By spraying out the combined solution, the droplets crosslinked *in situ* and were sent directly at the myocardial infarction area of a pig model to achieve the purpose of minimum invasive surgery.

Oxidative stress is another frequent problem for tissue regeneration due to a lack of oxygen. Localized supply of oxygen combined with the removal of reactive oxygen species can enhance the result of treatment in addition to the delivery of EVs, especially for chronic diabetic patients. Shiekh and coauthors designed a special polyurethane scaffold for this purpose^[99]. The polyurethane was specifically designed to be an antioxidant with vitamin C as one of the monomers to act as a scavenger of reactive oxygen species [Table 2], while the authors also doped calcium peroxide, which can decompose and produce oxygen when in contact with water, into the polyurethane scaffold for localized delivery of oxygen. The sustained supply of oxygen was confirmed to enhance wound healing of diabetic mice, along with the EVs to stimulate angiogenesis. On Day 14, the antioxidant polyurethane itself could lead to ~98% wound closure, with the non-diabetic wound closure at 90% and diabetic wound closure at only ~80%. With both the oxygen release and EV delivery functions, the wound closing function of the scaffold could reach ~100% after 14 days for both non-diabetic and diabetic mice.

In the field of bone tissue regeneration, specific elements can improve the angiogenesis function of the material so as to stimulate the recovery of injured bones. Li^+ has been proven to promote proliferation and osteogenesis. Liu and colleagues doped LiCl in bioglass ceramics to carry BMSC-EVs^[112]. The investigation showed that the existence of Li^+ in the bioglass could significantly improve angiogenesis through the proliferation of HUVECs both *in vitro* and *in vivo* compared to Li^+ -free bioglass by stimulating the activation of Wnt/ β -catenin, AKT and NF- κ B signaling pathways. The addition of proangiogenic miRNA-130a in EVs further activated the PTEN/AKT signaling pathway to enhance the proangiogenic capacity of endothelial cells. The synergic effect brought promise to the material for the vascularization of injured bone tissue.

Despite the above designs, however, the incorporation of extra functions has not been applied extensively in the overall studies of EV delivery systems. Along with EVs, the combinatorial and multimodal benefits towards injuries are to be expected in future experiments.

CONCLUSION AND PERSPECTIVES FOR FUTURE DESIGN OF EV DELIVERY SYSTEMS

In this review, we surveyed the EV delivery systems from the viewpoint of the material design at the molecular level, focusing on the relationship of material structures, the corresponding physicochemical properties and the performance of EV delivery. Based on the loading and delivery of EVs, the systems were classified into bulk materials, with crosslinking as the crucial structural parameter, and scaffolds, with porosity as the symbolic structure and surface property as the key parameter to interact with EVs. From the analyses of the according delivery behavior *in vitro* and *in vivo*, it can be seen that the delivery can be adjusted in correlation to the changes of material at the molecular level to a certain extent. These all guarantee that the EV delivery systems fill the two “gaps” in the field: one is the successful, localized and sustained release of EVs in the injured tissue; the other is how the material designs can direct the delivery of EVs. From the stand of patients, the use of EV delivery systems can greatly reduce the pain patients receive from otherwise multiple times of systemic, large-dose administration of EVs. This can further lead to cost reduction due to higher efficiency of EV delivery, and better regenerative results due to the various functions different materials can bring about. Therefore, the use of EV delivery systems has shown much promise in promoting EVs as a potential therapeutic approach for tissue regeneration. However, still at its initial stage, the EV delivery systems have missing links within the relationship of material structures, physicochemical properties and the performance of delivery. In order to achieve on-demand control over the delivery behavior through fine-tuning of the materials at the molecular level, we propose and emphasize that EV delivery systems can be further studied in the following directions:

(1) More studies necessary for a better understanding of the impacts of molecular designs on EV delivery

As mentioned in the introduction section, we extracted related information from representative investigations to analyze the relationship between the release profiles *in vitro*, retention of EVs *in vivo* and the resulting tissue regeneration. More systematic studies should be conducted on various types of EV delivery systems for the validation of results, as mentioned above. New reports on the behavior of EV delivery systems should be tracked to build a larger and more complete platform for EV delivery systems;

(2) The interaction between the materials and EVs during the EV storage period

The storage period is one of the three periods of EVs in material delivery systems, but is a missing link compared to the loading and delivery of EVs. Although the results of the delivery systems suggest no obvious change in the function of EVs after a short period of storage, no investigation has been made on how the material affects the encapsulated or carried EVs in the long run. For bulk materials, the distribution of crosslinking junctions/salt crystals and of EVs, as mentioned in “IMPACT OF DIFFERENT DESIGNS ON THE LOADING AND DELIVERY OF EVs”, are critical to the release profile of the EVs and the kinetics of interaction with the recipient cells. Similarly, for scaffold materials, the different surface properties, including mechanical properties, hydrophilicity/hydrophobicity, surface charge, and uninvestigated surface topographies, can also affect the loading and delivery performance of the systems. Meanwhile, previous studies^[140,141] have shown that surface properties can affect the attached stem cells to secrete EVs with different cargoes. It can be inferred that as the functional replicates of the parental stem cells, different properties of materials, including both bulk ones and scaffolds, may also affect the behavior of EVs encapsulated or attached. On the basis of the understanding of the influence of materials on the EVs, better selection of materials and processing strategies can be made for future development of the delivery systems;

(3) The kinetics of EV delivery and the internalization of cells by the adjustments of material designs

As was shown by Henriques-Antunes *et al.* on the relationship between the EV release profiles and the healing of diabetic chronic wounds using photo-cleavable crosslinkers in EV delivery hydrogel, the kinetics of EV delivery is crucial to their interactions with cells and wound healing^[136]. In order to optimize the delivery behavior of the material, careful detection of the relationship between the rates of delivery and the dosage being internalized is necessary. This can be realized, in resemblance to and more controllable than the photo-cleavable crosslinker, by a smart delivery system to finely adjust the interaction between the material and the EVs for release;

(4) Extension to materials previously investigated in tissue engineering

The current exploitation of materials for EV delivery systems accounts for only a small portion of materials in tissue engineering. Many different materials, especially for drug delivery systems, have been developed and extensively investigated. The EV delivery systems can be adapted from these material systems, which will provide a more diverse choice and functions. Furthermore, the scope of material can be extended to fully synthetic materials. Synthetic free radical polymers, for example, have fine structures and can be accurately controlled with living/controlled polymerization techniques. Through the applications such as ring-opening single unit monomer insertion techniques^[142] and anionic ring-opening polymerization (polycarbonate series)^[143], the non-degradability of free radical polymers has also been solved for the dynamic building of bioactive polymers. The incorporation of these well-defined polymers into EV delivery

systems can be of great promise.

DECLARATIONS

Authors' contributions

Conceptualization, writing-original draft: Chen A

Writing - review & editing: Tian H, Yang N, Zhang Z, Yang GY, Cui W

Conceptualization, supervision, writing - review & editing: Tang Y

Availability of data and materials

Not applicable.

Financial support and sponsorship

This study is supported by grants from the National Key R&D Program of China #2019YFA0112000 (Tang Y), the National Natural Science Foundation of China (NSFC) projects 82071284 (Tang Y), 81930051 (Cui W), 81771244 (Zhang Z), 81974179 (Zhang Z), the Scientific Research and Innovation Program of Shanghai Education Commission 2019-01-07-00-02-E00064 (Yang GY), Scientific and Technological Innovation Act Program of Shanghai Science and Technology Commission, 20JC1411900 (Yang GY), and GuangCi Professorship Program of Ruijin Hospital Shanghai Jiao Tong University School of Medicine. The International Postdoctoral Exchange Fellowship Program (Talent-Introduction Program) of Ministry of Human Resources and Social Security of the People's Republic of China is gratefully acknowledged for partial support of this study (Chen A).

Conflicts of interest

All authors declared that there are no conflicts of interest.

Ethical approval and consent to participate

Not applicable.

Consent for publication

Not applicable.

Copyright

© The Author(s) 2022.

REFERENCES

1. Barrientos S, Stojadinovic O, Golinko MS, Brem H, Tomic-Canic M. Growth factors and cytokines in wound healing. *Wound Repair Regen* 2008;16:585-601. DOI PubMed
2. Mulholland EJ, Dunne N, McCarthy HO. MicroRNA as therapeutic targets for chronic wound healing. *Mol Ther Nucleic Acids* 2017;8:46-55. DOI PubMed PMC
3. Robson MC, Mustoe TA, Hunt TK. The future of recombinant growth factors in wound healing. *Am J Surg* 1998;176:80S-2S. DOI PubMed
4. Kwon SG, Kwon YW, Lee TW, Park GT, Kim JH. Recent advances in stem cell therapeutics and tissue engineering strategies. *Biomater Res* 2018;22:36. DOI PubMed PMC
5. Lo B, Parham L. Ethical issues in stem cell research. *Endocr Rev* 2009;30:204-13. DOI PubMed PMC
6. Wolf P. The nature and significance of platelet products in human plasma. *Br J Haematol* 1967;13:269-88. DOI PubMed
7. Trams EG, Lauter CJ, Norman Salem J, Heine U. Exfoliation of membrane ecto-enzymes in the form of micro-vesicles. *Biochimica et Biophysica Acta (BBA) - Biomembranes* 1981;645:63-70. DOI PubMed
8. Newton WC, Kim JW, Luo JZQ, Luo L. Stem cell-derived exosomes: a novel vector for tissue repair and diabetic therapy. *J Mol Endocrinol* 2017;59:R155-65. DOI PubMed
9. Al-Sowayan B, Alammari F, Alshareeda A. Preparing the bone tissue regeneration ground by exosomes: from diagnosis to therapy. *Molecules* 2020;25:4205. DOI PubMed PMC

10. Ching RC, Kingham PJ. The role of exosomes in peripheral nerve regeneration. *Neural Regen Res* 2015;10:743-7. DOI PubMed PMC
11. Cooper LF, Ravindran S, Huang CC, Kang M. A role for exosomes in craniofacial tissue engineering and regeneration. *Front Physiol* 2019;10:1569. DOI PubMed PMC
12. Adamiak M, Sahoo S. Exosomes in myocardial repair: advances and challenges in the development of next-generation therapeutics. *Mol Ther* 2018;26:1635-43. DOI PubMed PMC
13. Akbari A, Jabbari N, Sharifi R, et al. Free and hydrogel encapsulated exosome-based therapies in regenerative medicine. *Life Sci* 2020;249:117447. DOI PubMed
14. Huang J, Xiong J, Yang L, Zhang J, Sun S, Liang Y. Cell-free exosome-laden scaffolds for tissue repair. *Nanoscale* 2021;13:8740-50. DOI PubMed
15. Riau AK, Ong HS, Yam GHF, Mehta JS. Sustained delivery system for stem cell-derived exosomes. *Front Pharmacol* 2019;10:1368. DOI PubMed PMC
16. Holkar K, Vaidya A, Pethe P, Kale V, Ingavle G. Biomaterials and extracellular vesicles in cell-free therapy for bone repair and regeneration: Future line of treatment in regenerative medicine. *Materialia* 2020;12:100736. DOI
17. Tsintou M, Dalamagkas K, Moore TL, et al. The use of hydrogel-delivered extracellular vesicles in recovery of motor function in stroke: a testable experimental hypothesis for clinical translation including behavioral and neuroimaging assessment approaches. *Neural Regen Res* 2021;16:605-13. DOI PubMed PMC
18. Murali VP, Holmes CA. Biomaterial-based extracellular vesicle delivery for therapeutic applications. *Acta Biomater* 2021;124:88-107. DOI PubMed
19. Théry C, Witwer KW, Aikawa E, et al. Minimal information for studies of extracellular vesicles 2018 (MISEV2018): a position statement of the International Society for Extracellular Vesicles and update of the MISEV2014 guidelines. *J Extracell Vesicles* 2018;7:1535750. DOI PubMed PMC
20. Zitvogel L, Regnault A, Lozier A, et al. Eradication of established murine tumors using a novel cell-free vaccine: dendritic cell-derived exosomes. *Nat Med* 1998;4:594-600. DOI PubMed
21. Raposo G, Tenza D, Mecheri S, Peronet R, Bonnerot C, Desaymard C. Accumulation of major histocompatibility complex class II molecules in mast cell secretory granules and their release upon degranulation. *Mol Biol Cell* 1997;8:2631-45. DOI PubMed PMC
22. Peters PJ, Geuze HJ, Van der Donk HA, et al. Molecules relevant for T cell-target cell interaction are present in cytolytic granules of human T lymphocytes. *Eur J Immunol* 1989;19:1469-75. DOI PubMed
23. Heijnen HF, Schiel AE, Fijnheer R, Geuze HJ, Sixma JJ. Activated platelets release two types of membrane vesicles: microvesicles by surface shedding and exosomes derived from exocytosis of multivesicular bodies and alpha-granules. *Blood* 1999;94:3791-9. PubMed
24. Fevrier B, Vilette D, Archer F, et al. Cells release prions in association with exosomes. *Proc Natl Acad Sci U S A* 2004;101:9683-8. DOI PubMed PMC
25. Wolfers J, Lozier A, Raposo G, et al. Tumor-derived exosomes are a source of shared tumor rejection antigens for CTL cross-priming. *Nat Med* 2001;7:297-303. DOI PubMed
26. Crivelli B, Chlapanidas T, Perteghella S, et al; Italian Mesenchymal Stem Cell Group (GISM). Mesenchymal stem/stromal cell extracellular vesicles: from active principle to next generation drug delivery system. *J Control Release* 2017;262:104-17. DOI PubMed
27. Lou G, Chen Z, Zheng M, Liu Y. Mesenchymal stem cell-derived exosomes as a new therapeutic strategy for liver diseases. *Exp Mol Med* 2017;49:e346. DOI PubMed PMC
28. Kim J, Song Y, Park CH, Choi C. Platform technologies and human cell lines for the production of therapeutic exosomes. *EVCNA* 2021. DOI
29. Liu M, Sun Y, Zhang Q. Emerging role of extracellular vesicles in bone remodeling. *J Dent Res* 2018;97:859-68. DOI PubMed
30. Yang M, Chen J, Su F, et al. Microvesicles secreted by macrophages shuttle invasion-potentiating microRNAs into breast cancer cells. *Mol Cancer* 2011;10:117. DOI PubMed PMC
31. Park JE, Tan HS, Datta A, et al. Hypoxic tumor cell modulates its microenvironment to enhance angiogenic and metastatic potential by secretion of proteins and exosomes. *Mol Cell Proteomics* 2010;9:1085-99. DOI PubMed PMC
32. Biasutto L, Chiechi A, Couch R, Liotta LA, Espina V. Retinal pigment epithelium (RPE) exosomes contain signaling phosphoproteins affected by oxidative stress. *Exp Cell Res* 2013;319:2113-23. DOI PubMed PMC
33. Zhang Y, Bi J, Huang J, Tang Y, Du S, Li P. Exosome: a review of its classification, isolation techniques, storage, diagnostic and targeted therapy applications. *Int J Nanomedicine* 2020;15:6917-34. DOI PubMed PMC
34. la Torre Gomez C, Goreham RV, Bech Serra JJ, Nann T, Kussmann M. "Exosomics"-a review of biophysics, biology and biochemistry of exosomes with a focus on human breast milk. *Front Genet* 2018;9:92. DOI PubMed PMC
35. Lai CP, Mardini O, Ericsson M, et al. Dynamic biodistribution of extracellular vesicles in vivo using a multimodal imaging reporter. *ACS Nano* 2014;8:483-94. DOI PubMed PMC
36. Heusermann W, Hean J, Trojer D, et al. Exosomes surf on filopodia to enter cells at endocytic hot spots, traffic within endosomes, and are targeted to the ER. *J Cell Biol* 2016;213:173-84. DOI PubMed PMC
37. Ma Z, Mao Z, Gao C. Surface modification and property analysis of biomedical polymers used for tissue engineering. *Colloids Surf B Biointerfaces* 2007;60:137-57. DOI PubMed

38. Banerjee A, Arha M, Choudhary S, et al. The influence of hydrogel modulus on the proliferation and differentiation of encapsulated neural stem cells. *Biomaterials* 2009;30:4695-9. DOI PubMed PMC
39. Chatterjee K, Lin-Gibson S, Wallace WE, et al. The effect of 3D hydrogel scaffold modulus on osteoblast differentiation and mineralization revealed by combinatorial screening. *Biomaterials* 2010;31:5051-62. DOI PubMed PMC
40. Cai S, Wu C, Yang W, Liang W, Yu H, Liu L. Recent advance in surface modification for regulating cell adhesion and behaviors. *Nanotechnology Reviews* 2020;9:971-89. DOI
41. Metwally S, Stachewicz U. Surface potential and charges impact on cell responses on biomaterials interfaces for medical applications. *Mater Sci Eng C Mater Biol Appl* 2019;104:109883. DOI PubMed
42. Sivashanmugam A, Arun Kumar R, Vishnu Priya M, Nair SV, Jayakumar R. An overview of injectable polymeric hydrogels for tissue engineering. *European Polymer Journal* 2015;72:543-65. DOI
43. Vernerey FJ, Lalitha Sridhar S, Muralidharan A, Bryant SJ. Mechanics of 3D cell-hydrogel interactions: experiments, models, and mechanisms. *Chem Rev* 2021;121:11085-148. DOI PubMed
44. Vedadghavami A, Minooei F, Mohammadi MH, et al. Manufacturing of hydrogel biomaterials with controlled mechanical properties for tissue engineering applications. *Acta Biomater* 2017;62:42-63. DOI PubMed
45. Johns MA, Bae Y, Guimarães FEG, et al. Predicting ligand-free cell attachment on next-generation cellulose-chitosan hydrogels. *ACS Omega* 2018;3:937-45. DOI PubMed PMC
46. Kazi GAS, Yamanaka T, Osamu Y. Chitosan coating an efficient approach to improve the substrate surface for in vitro culture system. *J Electrochem Soc* 2019;166:B3025-30. DOI
47. Shen Z, Kuang S, Zhang Y, et al. Chitosan hydrogel incorporated with dental pulp stem cell-derived exosomes alleviates periodontitis in mice via a macrophage-dependent mechanism. *Bioact Mater* 2020;5:1113-26. DOI PubMed PMC
48. Wang M, Wang C, Chen M, et al. Efficient angiogenesis-based diabetic wound healing/skin reconstruction through bioactive antibacterial adhesive ultraviolet shielding nanodressing with exosome release. *ACS Nano* 2019;13:10279-93. DOI PubMed
49. Zhao X, Liu Y, Jia P, et al. Chitosan hydrogel-loaded MSC-derived extracellular vesicles promote skin rejuvenation by ameliorating the senescence of dermal fibroblasts. *Stem Cell Res Ther* 2021;12:196. DOI PubMed PMC
50. Zhang FX, Liu P, Ding W, et al. Injectable mussel-inspired highly adhesive hydrogel with exosomes for endogenous cell recruitment and cartilage defect regeneration. *Biomaterials* 2021;278:121169. DOI PubMed
51. Wang C, Liang C, Wang R, et al. The fabrication of a highly efficient self-healing hydrogel from natural biopolymers loaded with exosomes for the synergistic promotion of severe wound healing. *Biomater Sci* 2019;8:313-24. DOI PubMed
52. Zhao D, Yu Z, Li Y, Wang Y, Li Q, Han D. GelMA combined with sustained release of HUVECs derived exosomes for promoting cutaneous wound healing and facilitating skin regeneration. *J Mol Histol* 2020;51:251-63. DOI PubMed
53. Zhang Y, Xie Y, Hao Z, et al. Umbilical mesenchymal stem cell-derived exosome-encapsulated hydrogels accelerate bone repair by enhancing angiogenesis. *ACS Appl Mater Interfaces* 2021;13:18472-87. DOI PubMed
54. Xin L, Wei C, Tong X, et al. In situ delivery of apoptotic bodies derived from mesenchymal stem cells via a hyaluronic acid hydrogel: a therapy for intrauterine adhesions. *Bioact Mater* 2022;12:107-19. DOI PubMed PMC
55. Mol EA, Lei Z, Roefs MT, et al. Injectable supramolecular ureidopyrimidinone hydrogels provide sustained release of extracellular vesicle therapeutics. *Adv Healthc Mater* 2019;8:e1900847. DOI PubMed
56. Yang J, Chen P, Pan D, Li H, Shen J. Umbilical cord-derived mesenchymal stem cell-derived exosomes combined pluronic F127 hydrogel promote chronic diabetic wound healing and complete skin regeneration. *Int J Nanomedicine* 2020;15:5911-26. DOI PubMed PMC
57. Fuhrmann G, Chandrawati R, Parmar PA, et al. Engineering extracellular vesicles with the tools of enzyme prodrug therapy. *Adv Mater* 2018;30:e1706616. DOI PubMed PMC
58. Zhang Y, Zhang P, Gao X, Chang L, Chen Z, Mei X. Preparation of exosomes encapsulated nanohydrogel for accelerating wound healing of diabetic rats by promoting angiogenesis. *Mater Sci Eng C Mater Biol Appl* 2021;120:111671. DOI PubMed
59. Zhang C, Shang Y, Chen X, et al. Supramolecular nanofibers containing arginine-glycine-aspartate (RGD) peptides boost therapeutic efficacy of extracellular vesicles in kidney repair. *ACS Nano* 2020;14:12133-47. DOI PubMed
60. Zhu D, Li Z, Huang K, Caranasos TG, Rossi JS, Cheng K. Minimally invasive delivery of therapeutic agents by hydrogel injection into the pericardial cavity for cardiac repair. *Nat Commun* 2021;12:1412. DOI PubMed PMC
61. Shen Y, Xu G, Huang H, et al. Sequential release of small extracellular vesicles from bilayered thiolated alginate/polyethylene glycol diacrylate hydrogels for scarless wound healing. *ACS Nano* 2021;15:6352-68. DOI PubMed
62. Mardpour S, Ghanian MH, Sadeghi-Abandansari H, et al. Hydrogel-mediated sustained systemic delivery of mesenchymal stem cell-derived extracellular vesicles improves hepatic regeneration in chronic liver failure. *ACS Appl Mater Interfaces* 2019;11:37421-33. DOI PubMed
63. Wang C, Wang M, Xu T, et al. Engineering bioactive self-healing antibacterial exosomes hydrogel for promoting chronic diabetic wound healing and complete skin regeneration. *Theranostics* 2019;9:65-76. DOI PubMed PMC
64. Liu X, Yang Y, Li Y, et al. Integration of stem cell-derived exosomes with in situ hydrogel glue as a promising tissue patch for articular cartilage regeneration. *Nanoscale* 2017;9:4430-8. DOI PubMed
65. Wang L, Wang J, Zhou X, et al. A new self-healing hydrogel containing hucMSC-derived exosomes promotes bone regeneration. *Front Bioeng Biotechnol* 2020;8:564731. DOI PubMed PMC
66. Yang S, Zhu B, Yin P, et al. Integration of human umbilical cord mesenchymal stem cells-derived exosomes with hydroxyapatite-

- embedded hyaluronic acid-alginate hydrogel for bone regeneration. *ACS Biomater Sci Eng* 2020;6:1590-602. DOI PubMed
67. Yan HC, Yu TT, Li J, et al. The delivery of extracellular vesicles loaded in biomaterial scaffolds for bone regeneration. *Front Bioeng Biotechnol* 2020;8:1015. DOI PubMed PMC
68. Jiang Y, Wang R, Wang C, et al. Brain microenvironment responsive and pro-angiogenic extracellular vesicle-hydrogel for promoting neurobehavioral recovery in type 2 diabetic mice after stroke. *Adv Healthc Mater* 2022:e2201150. DOI PubMed
69. Yu H, Cheng J, Shi W, et al. Bone marrow mesenchymal stem cell-derived exosomes promote tendon regeneration by facilitating the proliferation and migration of endogenous tendon stem/progenitor cells. *Acta Biomater* 2020;106:328-41. DOI PubMed
70. Lenzini S, Bargi R, Chung G, Shin JW. Matrix mechanics and water permeation regulate extracellular vesicle transport. *Nat Nanotechnol* 2020;15:217-23. DOI PubMed PMC
71. Rodell CB, Kaminski AL, Burdick JA. Rational design of network properties in guest-host assembled and shear-thinning hyaluronic acid hydrogels. *Biomacromolecules* 2013;14:4125-34. DOI PubMed PMC
72. Chen CW, Wang LL, Zaman S, et al. Sustained release of endothelial progenitor cell-derived extracellular vesicles from shear-thinning hydrogels improves angiogenesis and promotes function after myocardial infarction. *Cardiovasc Res* 2018;114:1029-40. DOI PubMed PMC
73. Li Q, Gong S, Yao W, et al. Exosome loaded genipin crosslinked hydrogel facilitates full thickness cutaneous wound healing in rat animal model. *Drug Deliv* 2021;28:884-93. DOI PubMed PMC
74. Guan P, Liu C, Xie D, et al. Exosome-loaded extracellular matrix-mimic hydrogel with anti-inflammatory property Facilitates/promotes growth plate injury repair. *Bioact Mater* 2022;10:145-58. DOI PubMed PMC
75. Swanson WB, Gong T, Zhang Z, et al. Controlled release of odontogenic exosomes from a biodegradable vehicle mediates dentinogenesis as a novel biomimetic pulp capping therapy. *J Control Release* 2020;324:679-94. DOI PubMed PMC
76. Boffito M, Bernardi E, Sartori S, Ciardelli G, Sassi MP. A mechanical characterization of polymer scaffolds and films at the macroscale and nanoscale. *J Biomed Mater Res A* 2015;103:162-9. DOI PubMed
77. Wang B, Li P, Shangguan L, et al. A novel bacterial cellulose membrane immobilized with human umbilical cord mesenchymal stem cells-derived exosome prevents epidural fibrosis. *Int J Nanomedicine* 2018;13:5257-73. DOI PubMed PMC
78. Prasadh S, Wong RCW. Unraveling the mechanical strength of biomaterials used as a bone scaffold in oral and maxillofacial defects. *Oral Science International* 2018;15:48-55. DOI
79. Baker SC, Rohman G, Southgate J, Cameron NR. The relationship between the mechanical properties and cell behaviour on PLGA and PCL scaffolds for bladder tissue engineering. *Biomaterials* 2009;30:1321-8. DOI PubMed
80. Zhu X, Cui W, Li X, Jin Y. Electrospun fibrous mats with high porosity as potential scaffolds for skin tissue engineering. *Biomacromolecules* 2008;9:1795-801. DOI PubMed
81. Xie H, Wang Z, Zhang L, et al. Extracellular vesicle-functionalized decalcified bone matrix scaffolds with enhanced pro-angiogenic and pro-bone regeneration activities. *Sci Rep* 2017;7:45622. DOI PubMed PMC
82. Jiang S, Tian G, Yang Z, et al. Enhancement of acellular cartilage matrix scaffold by Wharton's jelly mesenchymal stem cell-derived exosomes to promote osteochondral regeneration. *Bioact Mater* 2021;6:2711-28. DOI PubMed PMC
83. Iorio ML, Shuck J, Attinger CE. Wound healing in the upper and lower extremities: a systematic review on the use of acellular dermal matrices. *Plast Reconstr Surg* 2012;130:232S-41S. DOI PubMed
84. Zhang L, Fan C, Hao W, et al. NSCs Migration promoted and drug delivered exosomes-collagen scaffold via a bio-specific peptide for one-step spinal cord injury repair. *Adv Healthc Mater* 2021;10:e2001896. DOI PubMed
85. Chew JRJ, Chuah SJ, Teo KYW, et al. Mesenchymal stem cell exosomes enhance periodontal ligament cell functions and promote periodontal regeneration. *Acta Biomater* 2019;89:252-64. DOI PubMed
86. Baier RE. Applied chemistry at protein interfaces. ACS Publication; 1975. p. 155-74. DOI
87. Kim D, Lee S, Kim M, Jeong Y, Lee S. Exosome-coated silk fibroin 3D-scaffold for inducing osteogenic differentiation of bone marrow derived mesenchymal stem cells. *Chem Eng J* 2021;406:127080. DOI
88. Galeotti F, Andicsova A, Bertini F, et al. A versatile click-grafting approach to surface modification of silk fibroin films. *J Mater Sci* 2013;48:7004-10. DOI
89. Ybañez MG, Camacho DH. Designing hydrophobic bacterial cellulose film composites assisted by sound waves. *RSC Advances* 2021;11:32873-83. DOI PubMed PMC
90. Tao SC, Guo SC, Li M, Ke QF, Guo YP, Zhang CQ. Chitosan wound dressings incorporating exosomes derived from microRNA-126-overexpressing synovium mesenchymal stem cells provide sustained release of exosomes and heal full-thickness skin defects in a diabetic rat model. *Stem Cells Transl Med* 2017;6:736-47. DOI PubMed PMC
91. Shi Q, Qian Z, Liu D, et al. GMSC-derived exosomes combined with a chitosan/silk hydrogel sponge accelerates wound healing in a diabetic rat skin defect model. *Front Physiol* 2017;8:904. DOI PubMed PMC
92. Su N, Hao Y, Wang F, Hou W, Chen H, Luo Y. Mesenchymal stromal exosome-functionalized scaffolds induce innate and adaptive immunomodulatory responses toward tissue repair. *Sci Adv* 2021;7:eabf7207. DOI PubMed PMC
93. Wei Y, Wu Y, Zhao R, et al. MSC-derived sEVs enhance patency and inhibit calcification of synthetic vascular grafts by immunomodulation in a rat model of hyperlipidemia. *Biomaterials* 2019;204:13-24. DOI PubMed
94. Wurth JJ, Blumenthal NR, Shastri VP. Hydrophilization of poly(caprolactone) copolymers through introduction of oligo(ethylene glycol) moieties. *PLoS ONE* 2014;9:e99157. DOI PubMed PMC
95. Gandolfi MG, Gardin C, Zamparini F, et al. Mineral-doped poly(L-Lactide) acid scaffolds enriched with exosomes improve

- osteogenic commitment of human adipose-derived mesenchymal stem cells. *Nanomaterials* 2020;10:432. DOI PubMed PMC
96. Hendrick E, Frey M. Increasing surface hydrophilicity in poly(lactic acid) electrospun fibers by addition of Pla-B-Peg co-polymers. *J Eng Fiber Fabr* 2014;9:155892501400900219. DOI
97. Li W, Liu Y, Zhang P, et al. Tissue-engineered bone immobilized with human adipose stem cells-derived exosomes promotes bone regeneration. *ACS Appl Mater Interfaces* 2018;10:5240-54. DOI PubMed
98. Zhang Z, Wang X, Zhu R, et al. Synthesis and characterization of serial random and block-copolymers based on lactide and glycolide. *Polymer Science Series B* 2016;58:720-29. DOI
99. Shiekh PA, Singh A, Kumar A. Exosome laden oxygen releasing antioxidant and antibacterial cryogel wound dressing OxOBand alleviate diabetic and infectious wound healing. *Biomaterials* 2020;249:120020. DOI PubMed
100. Shiekh PA, Singh A, Kumar A. Data supporting exosome laden oxygen releasing antioxidant and antibacterial cryogel wound dressing OxOBand alleviate diabetic and infectious wound healing. *Data Brief* 2020;31:105671. DOI PubMed PMC
101. Fan L, Guan P, Xiao C, et al. Exosome-functionalized polyetheretherketone-based implant with immunomodulatory property for enhancing osseointegration. *Bioact Mater* 2021;6:2754-66. DOI PubMed PMC
102. Ha SW, Kirch M, Birchler F, et al. Surface activation of polyetheretherketone (peek) and formation of calcium phosphate coatings by precipitation. *J Mater Sci Mater Med* 1997;8:683-90. DOI PubMed
103. Lee JH, Khang G, Lee JW, Lee HB. Interaction of different types of cells on polymer surfaces with wettability gradient. *J Colloid Interface Sci* 1998;205:323-30. DOI PubMed
104. Chen P, Zheng L, Wang Y, et al. Desktop-stereolithography 3D printing of a radially oriented extracellular matrix/mesenchymal stem cell exosome bioink for osteochondral defect regeneration. *Theranostics* 2019;9:2439-59. DOI PubMed PMC
105. Huang CC, Kang M, Shirazi S, et al. 3D Encapsulation and tethering of functionally engineered extracellular vesicles to hydrogels. *Acta Biomater* 2021;126:199-210. DOI PubMed PMC
106. Xiao D, Yang M, Zhang M, et al. MicroRNA-126 from stem cell extracellular vesicles encapsulated in a tri-layer hydrogel scaffold promotes bladder angiogenesis by activating CXCR4/SDF-1 α pathway. *Chem Eng J* 2021;425:131624. DOI
107. Sun Y, Zhang B, Zhai D, Wu C. Three-dimensional printing of bioceramic-induced macrophage exosomes: immunomodulation and osteogenesis/angiogenesis. *NPG Asia Mater* 2021;13. DOI
108. Zamiri A, De S. Mechanical properties of hydroxyapatite single crystals from nanoindentation data. *J Mech Behav Biomed Mater* 2011;4:146-52. DOI PubMed PMC
109. Zhang J, Liu X, Li H, et al. Exosomes/tricalcium phosphate combination scaffolds can enhance bone regeneration by activating the PI3K/Akt signaling pathway. *Stem Cell Res Ther* 2016;7:136. DOI PubMed PMC
110. Wei F, Li M, Crawford R, Zhou Y, Xiao Y. Exosome-integrated titanium oxide nanotubes for targeted bone regeneration. *Acta Biomater* 2019;86:480-92. DOI PubMed
111. Zhai M, Zhu Y, Yang M, Mao C. Human mesenchymal stem cell derived exosomes enhance cell-free bone regeneration by altering their miRNAs profiles. *Adv Sci (Weinh)* 2020;7:2001334. DOI PubMed PMC
112. Liu L, Liu Y, Feng C, et al. Lithium-containing biomaterials stimulate bone marrow stromal cell-derived exosomal miR-130a secretion to promote angiogenesis. *Biomaterials* 2019;192:523-36. DOI PubMed
113. Qayoom I, Teotia AK, Kumar A. Nanohydroxyapatite based ceramic carrier promotes bone formation in a femoral neck canal defect in osteoporotic rats. *Biomacromolecules* 2020;21:328-37. DOI PubMed
114. Lebedev AL, Kosorukov VL. Gypsum solubility in water at 25 °C. *Geochem Int* 2017;55:205-10. DOI
115. Liu A, Lin D, Zhao H, et al. Optimized BMSC-derived osteoinductive exosomes immobilized in hierarchical scaffold via lyophilization for bone repair through Bmpr2/Acvr2b competitive receptor-activated Smad pathway. *Biomaterials* 2021;272:120718. DOI PubMed
116. Liu L, Yu F, Li L, et al. Bone marrow stromal cells stimulated by strontium-substituted calcium silicate ceramics: release of exosomal miR-146a regulates osteogenesis and angiogenesis. *Acta Biomater* 2021;119:444-57. DOI PubMed
117. Chen S, Tang Y, Liu Y, et al. Exosomes derived from miR-375-overexpressing human adipose mesenchymal stem cells promote bone regeneration. *Cell Prolif* 2019;52:e12669. DOI PubMed PMC
118. Gandolfi MG, Zamparini F, Degli Esposti M, et al. Polylactic acid-based porous scaffolds doped with calcium silicate and dicalcium phosphate dihydrate designed for biomedical application. *Mater Sci Eng C Mater Biol Appl* 2018;82:163-81. DOI PubMed
119. Shafei S, Khanmohammadi M, Heidari R, et al. Exosome loaded alginate hydrogel promotes tissue regeneration in full-thickness skin wounds: an in vivo study. *J Biomed Mater Res A* 2020;108:545-56. DOI PubMed
120. Li L, Zhang Y, Mu J, et al. Transplantation of human mesenchymal stem-cell-derived exosomes immobilized in an adhesive hydrogel for effective treatment of spinal cord injury. *Nano Lett* 2020;20:4298-305. DOI PubMed
121. Han C, Zhou J, Liu B, et al. Delivery of miR-675 by stem cell-derived exosomes encapsulated in silk fibroin hydrogel prevents aging-induced vascular dysfunction in mouse hindlimb. *Mater Sci Eng C Mater Biol Appl* 2019;99:322-32. DOI PubMed
122. Han C, Zhou J, Liang C, et al. Human umbilical cord mesenchymal stem cell derived exosomes encapsulated in functional peptide hydrogels promote cardiac repair. *Biomater Sci* 2019;7:2920-33. DOI PubMed
123. Huang X, Brazel CS. On the importance and mechanisms of burst release in matrix-controlled drug delivery systems. *J Control Release* 2001;73:121-36. DOI PubMed
124. Lin J, Wang Z, Huang J, et al. Microenvironment-protected exosome-hydrogel for facilitating endometrial regeneration, fertility restoration, and live birth of offspring. *Small* 2021;17:e2007235. DOI PubMed

125. Brandrup J, Immergut EH, Grulke EA. Polymer handbook, 4th ed. John Wiley & Sons Inc.; 2003. DOI
126. Zhang K, Zhao X, Chen X, et al. Enhanced therapeutic effects of mesenchymal stem cell-derived exosomes with an injectable hydrogel for hindlimb ischemia treatment. *ACS Appl Mater Interfaces* 2018;10:30081-91. DOI PubMed
127. Swanson WB, Zhang Z, Xiu K, et al. Scaffolds with controlled release of pro-mineralization exosomes to promote craniofacial bone healing without cell transplantation. *Acta Biomater* 2020;118:215-32. DOI PubMed PMC
128. Wu J, Chen L, Wang R, et al. Exosomes secreted by stem cells from human exfoliated deciduous teeth promote alveolar bone defect repair through the regulation of angiogenesis and osteogenesis. *ACS Biomater Sci Eng* 2019;5:3561-71. DOI PubMed
129. Saravanan S, Vimalraj S, Thanikaivelan P, Banudevi S, Manivasagam G. A review on injectable chitosan/beta glycerophosphate hydrogels for bone tissue regeneration. *Int J Biol Macromol* 2019;121:38-54. DOI PubMed
130. Yang Y, Shen G, Wang H, et al. Interferometric plasmonic imaging and detection of single exosomes. *Proc Natl Acad Sci U S A* 2018;115:10275-80. DOI PubMed PMC
131. Wan Y, Liu X, Liu P, Zhao L, Zou W. Optimization adsorption of norfloxacin onto polydopamine microspheres from aqueous solution: Kinetic, equilibrium and adsorption mechanism studies. *Sci Total Environ* 2018;639:428-37. DOI PubMed
132. Lazar S, Mor S, Chen J, Hao D, Wang A. Bioengineered extracellular vesicle-loaded bioscaffolds for therapeutic applications in regenerative medicine. *Extracell Vesicles Circ Nucl Acids* 2021;2:175-8. DOI PubMed PMC
133. Xin L, Lin X, Zhou F, et al. A scaffold laden with mesenchymal stem cell-derived exosomes for promoting endometrium regeneration and fertility restoration through macrophage immunomodulation. *Acta Biomater* 2020;113:252-66. DOI PubMed
134. Hao D, Swindell HS, Ramasubramanian L, et al. Extracellular matrix mimicking nanofibrous scaffolds modified with mesenchymal stem cell-derived extracellular vesicles for improved vascularization. *Front Bioeng Biotechnol* 2020;8:633. DOI PubMed PMC
135. Xu N, Wang L, Guan J, et al. Wound healing effects of a Curcuma zedoaria polysaccharide with platelet-rich plasma exosomes assembled on chitosan/silk hydrogel sponge in a diabetic rat model. *Int J Biol Macromol* 2018;117:102-7. DOI PubMed
136. Henriques-Antunes H, Cardoso RMS, Zonari A, et al. The kinetics of small extracellular vesicle delivery impacts skin tissue regeneration. *ACS Nano* 2019;13:8694-707. DOI PubMed
137. Liu L, Li Y, Peng H, et al. Targeted exosome coating gene-chem nanocomplex as “nanoscavenger” for clearing α -synuclein and immune activation of Parkinson’s disease. *Sci Adv* 2020;6:eaba3967. DOI PubMed PMC
138. You G, Kim Y, Lee JH, Song J, Mok H. Exosome-modified PLGA microspheres for improved internalization into dendritic cells and macrophages. *Biotechnol Bioproc E* 2020;25:521-7. DOI
139. Yao J, Huang K, Zhu D, et al. A minimally invasive exosome spray repairs heart after myocardial infarction. *ACS Nano* ;2021:11099-111. DOI PubMed
140. Liu M, Wang D, Gu S, et al. Micro/nano materials regulate cell morphology and intercellular communication by extracellular vesicles. *Acta Biomater* 2021;124:130-8. DOI PubMed
141. Liang J, Gu S, Mao X, et al. Endothelial cell morphology regulates inflammatory cells through microRNA transferred by extracellular vesicles. *Front Bioeng Biotechnol* 2020;8:369. DOI PubMed PMC
142. Yang Y, Yu K, Liu S, et al. Radical ring-opening single unit monomer insertion: an approach to degradable and biocompatible sequence-defined oligomers. *Macromolecules* 2021;54:10923-30. DOI
143. Chan JMW, Zhang X, Brennan MK, et al. Organocatalytic ring-opening polymerization of trimethylene carbonate to yield a biodegradable polycarbonate. *J Chem Educ* 2015;92:708-13. DOI

Original Article

Open Access



Brain endothelium-derived extracellular vesicles containing amyloid-beta induce mitochondrial alterations in neural progenitor cells

Olivia M. Osborne^{1,2}, Jennifer M. Kowalczyk¹, Kelssey D. Pierre Louis¹, Manav T. Daftari¹, Brett M. Colbert^{1,3}, Oandy Naranjo^{1,2}, Silvia Torices^{1,2}, Ibolya E. András¹, Derek M. Dykxhoorn⁴, Michal Toborek^{1,2}

¹Department of Biochemistry and Molecular Biology, University of Miami Miller School of Medicine, Miami, FL 33136, USA.

²Dr. JT Macdonald Foundation Biomedical Nanotechnology Institute of the University of Miami, University of Miami Miller School of Medicine, Miami, FL 33136, USA.

³Medical Scientist Training Program, University of Miami Miller School of Medicine, Miami, FL 33136, USA.

⁴Dr. John T. Macdonald Foundation Department of Human Genetics, John P. Hussman Institute for Human Genomics, University of Miami Miller School of Medicine, Miami, FL 33136, USA.

Correspondence to: Olivia M. Osborne, Department of Biochemistry and Molecular Biology, University of Miami Miller School of Medicine, Gautier Building Room 528, 1011 NW 15th Street, Miami, FL 33136, USA. E-mail:

oliviaoosborne@med.miami.edu; Prof. Michal Toborek, Department of Biochemistry and Molecular Biology, University of Miami Miller School of Medicine, Gautier Building Room 528, 1011 NW 15th Street, Miami, FL 33136, USA. E-mail: mtoborek@med.miami.edu

How to cite this article: Osborne OM, Kowalczyk JM, Pierre Louis KD, Daftari MT, Colbert BM, Naranjo O, Torices S, András IE, Dykxhoorn DM, Toborek M. Brain endothelium-derived extracellular vesicles containing amyloid-beta induce mitochondrial alterations in neural progenitor cells. *Extracell Vesicles Circ Nucleic Acids* 2022;3:357-79. <https://dx.doi.org/10.20517/evcna.2022.22>

Received: 2 May 2022 **First Decision:** 8 Jun 2022 **Revised:** 26 Aug 2022 **Accepted:** 11 Nov 2022 **Published:** 1 Dec 2022

Academic Editors: Lynn Pulliam, Shilpa Buch, Yoke Peng Loh **Copy Editor:** Pengjuan Wen **Production Editor:** Pengjuan Wen

Abstract

Aim: Elevated brain deposits of amyloid beta ($A\beta_{40}$) contribute to neuropathology and cognitive dysfunction in Alzheimer's disease (AD). However, the role of the blood-brain barrier (BBB) as an interface for the transfer of $A\beta_{40}$ from the periphery into the brain is not well characterized. In addition, a substantial population of neural progenitor cells (NPCs) resides in close proximity to brain capillaries that form the BBB. The aim of this study is to understand the impact of brain endothelium-derived extracellular vesicles (EV) containing $A\beta_{40}$ on metabolic functions and differentiation of NPCs.



© The Author(s) 2022. **Open Access** This article is licensed under a Creative Commons Attribution 4.0 International License (<https://creativecommons.org/licenses/by/4.0/>), which permits unrestricted use, sharing, adaptation, distribution and reproduction in any medium or format, for any purpose, even commercially, as long as you give appropriate credit to the original author(s) and the source, provide a link to the Creative Commons license, and indicate if changes were made.



Methods: Endothelial EVs were derived from an *in vitro* model of the brain endothelium treated with 100 nM A β_{40} or PBS. We then analyzed the impact of these EVs on mitochondrial morphology and bioenergetic disruption of NPCs. In addition, NPCs were differentiated and neurite development upon exposure to EVs was assessed using the IncuCyte Zoom live cell imaging system.

Results: We demonstrate that physiological concentrations of A β_{40} can be transferred to accumulate in NPCs via endothelial EVs. This transfer results in mitochondrial dysfunction, disrupting crista morphology, metabolic rates, fusion and fission dynamics of NPCs, as well as their neurite development.

Conclusion: Inter cellular transfer of A β_{40} is carried out by brain endothelium-derived EVs, which can affect NPC differentiation and induce mitochondrial dysfunction, leading to aberrant neurogenesis. This has pathological implications because NPCs growing into neurons are incorporated into cerebral structures involved in learning and memory, two common phenotypes affected in AD and related dementias.

Keywords: Blood-brain barrier, mitochondrial bioenergetics, extracellular vesicle, neurogenesis, Alzheimer's disease, Seahorse, neural progenitor cell

INTRODUCTION

Alzheimer's disease (AD) is the most common neurodegenerative disease, affecting one in every eight people over the age of 65 and around half of the individuals over the age of 85^[1]. Elevated brain deposits of beta-amyloid (A β) are now accepted to contribute to the neuropathology and cognitive dysfunction seen in AD^[2]. The levels of A β in the central nervous system (CNS) result from an equilibrium between production in the brain, influx from plasma, and efflux via blood-brain barrier (BBB) efflux transporters^[3]. Although these processes contribute to the formation of A β deposits and plaques in AD, emerging evidence indicates that the BBB is a critical interface in the transfer of A β from the periphery into the brain^[4,5]. However, the mechanisms underlying this process remain unclear. Recent evidence indicates that it is important to consider the role of the BBB in the transfer of A β when analyzing neuropathologies associated with AD^[6-9]. We previously demonstrated that exposure to EVs carrying A β_{40} (EV-A β_{40}) negatively affects the differentiation of NPCs into mature neurons; however, the mechanisms behind these effects are poorly understood^[10,11]. In the present study, we hypothesize that an underlying cause of altered neurogenesis, which is a prominent feature of AD, may be mitochondrial dysfunction that results from EV-mediated A β_{40} exposure. The effect of exposing NPCs to A β_{40} that may be trafficked across the BBB, compounded with endogenous production of A β_{40} in the brain, may exacerbate the mitochondrial dysfunction observed in progenitor cells, leading to aberrant neurogenesis.

The BBB provides a physiological, immunological, and structural interface between the brain parenchyma and the peripheral circulation. It also represents a crucial interface between the circulatory system and brain tissue, helping to maintain the overall homeostasis of the CNS. The brain endothelium, formed by cerebral endothelial cells, is the crucial element of the BBB that is responsible for its structural and metabolic properties. These endothelial cells produce EVs that can travel and interact with other cell types in the brain to deliver various biologically active cargo materials, such as A β_{40} ^[10,11]. A β_{40} is produced by the cleavage of amyloid precursor protein (APP), which is ubiquitously expressed on the membrane of neurons as well as endothelial cells that make up the BBB^[12,13]. CNS levels of A β_{40} result from an equilibrium established between production in the brain, influx from plasma, and efflux by BBB transporters. We here study the involvement of A β_{40} because it is the main isoform produced by the cleavage of APP, making up 90% of all A β_{40} produced in the brain. Increased A β_{40} deposition is also associated with vascular dysfunction and is likely to compromise the integrity of the BBB during AD^[14,15]. Therefore, our studies focus on this

amyloidogenic species along with its ability to cross the BBB and impair neurogenesis via EV-mediated transfer.

EVs have recently been postulated to be significantly involved in various neurodegenerative diseases, including A β_{40} pathology^[16,17]. It was demonstrated that A β_{40} could be packaged into EVs and shed into the microenvironment and that human amyloid plaques are enriched with EV proteins^[9]. Additionally, we previously showed that exposure of brain endothelial cells to A β_{40} results in effective packaging of A β_{40} in EVs, leading to the transfer of A β_{40} into neighboring cells, including NPCs. EVs are heterogeneous in their shape, size, origin, and content. They include exosomes with a size of approximately 30-100 nm and other larger vesicles^[18,19]. EVs are formed in a stepwise process whereby the vesicles bud from the endosomal membranes generating intra-endosomal vesicles, followed by fusion of the endosome membrane with the plasma membrane and release of the EVs into the extracellular environment. Their content is diverse and includes mRNAs, miRNAs, lipids, and proteins^[20]. EV cargo can be released into the immediate microenvironment or peripheral sites when transported via the circulatory system^[21]. EVs, being of endosomal origin, have been shown to be released from multiple cell types creating a unique cell-to-cell communication system, which may play important physiological and pathological roles in the CNS^[22,23]. However, few studies have focused on EVs derived from brain endothelial cells, or on the effect of their cargo on neurogenesis in the brain. This process is of physiological significance because neurogenic niches are predominantly localized around the brain microvasculature that forms the BBB^[24]. Although A β_{40} accumulation has a detrimental effect on neuronal growth in diseases such as AD, the mechanism of action that leads to aberrant neurogenesis remains largely unknown. Therefore, the objective of the present study is twofold: (1) to determine the mechanistic effect of A β_{40} on NPCs that may lead to aberrant neurogenesis; and (2) to delineate whether vesicle-mediated trafficking of A β_{40} can potentiate the neurogenic deficiency seen in AD patients. Our results demonstrate that brain endothelium-derived EVs can transfer cargo to NPCs and may serve as a vehicle for cell-to-cell communication that regulates mitochondrial metabolic dynamics in NPCs and, ultimately, decreases their neurogenic potential.

METHODS

Cell cultures

hCMEC/D3

The human cerebral microvascular endothelial cells (hCMEC/D3) used in this study represent a robust, well-characterized, and stable human brain endothelial cell line. hCMEC/D3 cells were cultured on rat tail collagen type I (Thermo Fisher Scientific, Cat# CB-40236)-coated 100 mm dishes in EBM-2 medium (Lonza, Cat# CC-3156) supplemented with VEGF, IGF-1, EGF, bFGF, hydrocortisone, ascorbate, gentamycin, and 0.5% exosome-depleted FBS (Exo-FBS, Systems Bioscience) at 37 °C and 5% CO₂.

iPSC

Human peripheral blood mononuclear cells (PBMCs) derived from an individual with no familial history of AD or amyloidosis were reprogrammed to iPSCs using the CytoTune iPSC 2.0 Sendai Reprogramming Kit (Thermo Fisher Scientific). This iPSC line (CW50038 line) was obtained from Coriell Institute and was derived from a cognitively intact, elderly (86 years old), non-Hispanic white female participant with the APOE 3/3 genotype. The iPSC line was differentiated into NPCs in accordance with our previously reported approach^[25]. Cells were plated on day in vitro (DIV) 20 on poly-L-ornithine/laminin plates in D/NPEN medium [Supplementary Table 1] enriched with 20 ng/mL b-NGF, 20 ng/mL NT-3, 20 ng/mL BDNF, and 2 mg/mL DAPT (only from DIV 30 to 34). NPC expansion was transitioned into terminal differentiation of glutamatergic neurons by dissociating with accutase and plating onto six-well plates coated with 100 μ g/mL poly-D-lysine (PDL), 20 μ g/mL laminin, and 10 μ g/mL fibronectin and grown in D/NPEN lacking heparin,

and the following small molecules: 20 ng/mL NT3 and 20 ng/mL BDNF. The medium was changed every 2 days or as needed. Duplicate cultures of the cell line were analyzed using IncuCyte Zoom (Sartorius). EVs were used to treat neurons for 24 h to characterize neurite extensions on DIV 51/52.

ReN cells

ReNcell CX Human Neural Progenitor Cells were purchased from Millipore (Cat# SCC007). This immortalized human NPC line can be differentiated into neuronal and glial cell lineages. ReN cells were grown on 20 mg/mL purified mouse laminin (Millipore, Cat# CC095)-coated tissue culture plates in ReNcell NSC Maintenance Medium (Millipore, Cat# SCM005) supplemented with 20 ng/mL basic fibroblast growth factor-1 (Millipore, Cat# GF003) and 20 ng/mL epidermal growth factor (Millipore, Cat# GF001) at 37 °C and 5% CO₂. Cells were used in experiments when they reached 80% confluence, typically 3-4 days after plating. For differentiation experiments, ReN cells were plated in complete medium. The following day, the medium was replaced with fresh medium lacking growth factors. The cells were allowed to differentiate into neurons for 14 days.

Transfection of hCMEC/D3

hCMEC/D3 were transfected with the CD9 Cyto-Tracker constructs to label EVs. EVs were labeled with RFP through the expression of pCT-CD9-RFP Cyto-Tracker vector (pCMV, Exosome/Secretory, CD9 Tetraspanin Tag). The cells were transduced using a transfection kit (System Biosciences, Cat# CYTO123-PA-1) and PureFection Transfection Reagent (System Biosciences, Cat# LV750A-1), in accordance with the manufacturer's protocol. Twenty-four hours after transfection, hCMEC were exposed to 100 nM fluorescent A β ₄₀ HiLyte and the EV-containing supernatant was harvested 48 h later. EVs were isolated from the tissue culture supernatant as outlined below. Once isolated, EVs were pipetted onto glass slides, heat-fixed at 95 °C for 10 min, and fixed again with 100% ethanol for 30 min at 4 °C. Slides were washed three times with PBS and mounted using ProLong Gold Antifade reagent with DAPI (Invitrogen). Specimens were covered with coverslips and fluorescent images [green fluorescence (A β HiLyte Alexa Fluor488) and red fluorescence (CD9-RFP)] were acquired using a Nikon Eclipse Ti-U inverted fluorescent microscope. The settings for fluorescence intensity and contrast were optimized and the same settings were used for the analysis of EVs. Intensity plot images were acquired using Nikon-Elements imaging software (NIS).

A β ₄₀-loaded EVs

EVs were loaded with A β ₄₀ as described earlier. Briefly, hCMEC/D3 cells were grown as a monolayer and split when greater than 90% confluent in exosome-depleted complete medium incubated at 37 °C and 5% CO₂. Freshly solubilized A β ₄₀ (Anaspec, Cat# AS-20698) or A β ₄₀ HiLyte (Anaspec, Cat# AS-60491-01) was used in the following experiments because this species has been shown to induce proinflammatory reactions in brain microvessels and endothelial cells and is the most abundant of the proamyloidogenic species produced from APP^[26,27]. A β ₄₀ was dissolved in 0.1 M NH₄OH basic buffer (Anaspec, Cat# AS-61322) and further diluted in PBS, in accordance with the manufacturer's instructions. Then, hCMEC/D3 were treated with fresh EBM-2 medium supplemented with growth factors and 100 nM A β ₄₀ for 48 h. This dosage of A β ₄₀ was chosen since the A β ₄₀ levels in AD patients' CSF are in the nanomolar range. This concentration has also been shown to result in maximal EV loading^[28]. Control cultures received fresh medium supplemented with PBS as a vehicle control treatment. Treatment was terminated by removal of the medium and EVs were isolated from $\sim 1.7 \times 10^7$ cells using the ExoQuick-TC kit (System Biosciences, Cat# EXOTC50A-1). Briefly, 10 mL of hCMEC/D3 culture supernatant was mixed with 2 mL of ExoQuick Exosome precipitation solution. This mixture was incubated overnight at 4 °C to facilitate even coating of the EVs. The next day, the samples were centrifuged at 1500 \times g for 30 min, the supernatants were removed, and the pellets were centrifuged further at 1500 \times g for 5 min. The resulting EV pellets were resuspended in PBS for characterization or use in our experiments. The whole fraction of isolated EVs was used in our experiments

to account for both small EVs (exosomes) as well as larger particles, both of which can contain A β ₄₀.

Nanoparticle tracking analysis

EVs isolated from the supernatant of hCMEC/D3 cells were characterized and analyzed by nanoparticle tracking analysis (NTA) on the Nanosight NS300 (Malvern Instruments Company, Malvern, UK). Optimal detection settings were acquired with the screen gain set to 11 and a detection threshold level of 5 using Nanosight NTA 2.3 Analytical Software (Malvern Instruments Company). This allowed us to track the EV particles in suspension with minimal background [Supplementary Video 1 and Supplementary Video 2]. EV pellets were diluted 100-fold in sterile-filtered PBS and five 15-s frame captures were recorded for each sample. An average of three batches from each group was used to determine the total number of vesicles. EV-A β ₄₀ vesicle number was normalized to the total average number of EV-PBS for all treatments.

Enzyme-linked immunosorbent assay

Human Amyloid Beta 40 enzyme-linked immunosorbent assay (ELISA) (Invitrogen, Cat# KHB3481) was used to quantify the levels of A β ₄₀ loaded into EVs. First, EVs were lysed at a 1:1 ratio with RIPA buffer (Thermo Fisher Scientific, Cat# 89900) containing protease inhibitor (Thermo Fisher Scientific, Cat# 78431). The resulting lysate was loaded into a precoated 96-well plate, in accordance with the manufacturer's instructions, and absorbance was measured using the Colorimetric SpectraMax 190 plate reader and normalized to total protein levels as measured by a BCA assay (Thermo Fisher Scientific, Cat #23223).

IncuCyte zoom

iPSC-derived NPCs were seeded at a cell density of 40,000 cells per well in a six-well culture plate coated with poly-L-lysine and allowed to differentiate into neurons. Alternatively, ReN cells were seeded at 60,000 cells per well in a 12-well plate coated with laminin. The IncuCyte Zoom automated cell imaging system (Sartorius) was used to automatically acquire kinetic data every hour for either 24 h (iPSC-derived neurons) or 14 days of NPC differentiation (ReN cells) to assess neurite outgrowth and neurogenesis, respectively. iPSC-derived neurons were treated once with EVs, A β ₄₀, or medium alone. Images were taken every hour for 24 h. ReN cells were treated with EVs or A β ₄₀ every other day along with fresh medium over the course of 14 days of differentiation. Neurotrack software was used to quantify neuron cell-body clusters, neurite branch points, and neurite branch points per cell-body area.

Quantitative PCR

Total RNA was isolated from cell culture lysates using RNeasy mini kit (Qiagen, Cat# 74104), in accordance with the manufacturer's instructions. Total nucleic acid concentrations were quantified using the Nanodrop 2000 (Thermo Fisher Scientific). RT-PCR was performed with a total of 100 ng of RNA using the qScript XLT 1-Step RT-qPCR ToughMix Low ROX (Quantabio, Cat# 89236-676) reaction mix and the Applied Biosystems 7500 system (Applied Biosystems, Foster City, CA, USA). TaqMan Gene Expression Assays and the following primers were used: Hs00208382_m1: Mfn2 primer; Hs00250475_m1: Mfn1 primer; Hs00953477_m1: SIRT3 primer; Hs00697394_g1: Mff primer; Hs01047018_m1: OPA1 primer; Hs00608023_m1: Bcl-2 primer; and DNMI1L-Hs01552605_m1: Drp-1 primer. Human GAPDH (ThermoFisher Scientific, Cat# 4310884E) was used as an endogenous control for sample normalization. PCR product specificity was determined using melting curve assessment and gene expression differences were determined using the $\Delta\Delta C_t$ method.

Transmission electron microscopy

EVs

EV samples from both control and A β_{40} -treated groups were visualized using transmission electron microscopy (TEM). EV suspensions were fixed in 2% paraformaldehyde for 1 h and then loaded on a copper mesh grid and allowed to incubate for 45 min. The grids were allowed to dry overnight. Then, the EV suspension was stained using 1% uranyl acetate. Once the grids were dry, EVs were imaged using a JEOL JEM-1400 transmission electron microscope with images acquired using an AMT BioSprint digital camera.

ReN cells

Cells grown on glass coverslips were fixed overnight at 4 °C in 2% glutaraldehyde in 0.1 M phosphate buffer, before being incubated for 1 h in 2% osmium tetroxide in 0.1 M phosphate buffer, dehydrated through a series of graded ethanol concentrations, and embedded in EM-bed (Electron Microscopy Sciences). The glass coverslips were removed by treatment with hydrofluoric acid. Next, 100 nm sections were cut on a Leica Ultracut EM UC7 ultramicrotome and stained with uranyl acetate and lead citrate. The grids were viewed at 80 kV in a JEOL JEM-1400 transmission electron microscope and images were captured by an AMT BioSprint digital camera. For quantitative analysis, fields were chosen at random, and acquisition and quantification were performed using FIJI (NIH) and GraphPad Prism 9.3.1 software, respectively. Morphometric analyses of the mitochondria and substructures were performed by three investigators in a randomized, double-blind manner, which included taking the images, quantifying the data, and running the statistics separately. Images were obtained at random from three independent experiments^[29].

Western blot

Treated cells were washed with PBS and lysed with radioimmunoprecipitation assay (RIPA) buffer (Thermo Fisher Scientific, Cat# 89900) supplemented with protease inhibitors (Thermo Fisher Scientific, Cat# 78431). Total protein concentration was determined using the BCA protein assay kit (Thermo Fisher Scientific, Cat# 23223). Samples were prepared for immunoblotting with RIPA diluent and sodium dodecyl sulfate (SDS). Then, 15-20 μ g of total protein was loaded per lane on 4%-20% midi-PROTEAN TGX Stain-Free polyacrylamide precast gels (Bio-Rad Laboratories, Cat# 4568096) and transferred to a nitrocellulose membrane using the Trans-Blot Turbo Transfer System (Bio-Rad Laboratories, Cat# 1704159). Membranes were blocked using Intercept TBS Blocking Buffer (LICOR, Cat# 927-60001) for 1 h at room temperature. The next day, blots were incubated overnight at 4 °C with primary antibodies [Supplementary Table 2] diluted in 5% bovine serum albumin (BSA). Blots were washed three times using Tris-buffered saline with 0.1% Tween-20 (TBS-T) before incubation with secondary antibody at room temperature for 1 h. Analysis of GAPDH (Novus Biologicals, Cat# NB600-502FR or Cat# NB600-5021) was performed as an internal control and for sample normalization. Bands were imaged with the Odyssey CLX Imaging System (LICOR) and signal quantification was performed with Image Studio 4.0 software (LICOR).

Seahorse XF analyzer

Oxygen consumption rate (OCR) and extracellular acidification rate (ECAR) were measured on a Seahorse XF24 Analyzer (Agilent Technologies, Inc.) using the Seahorse Mito Stress Test kit (Agilent Technologies, Inc., Cat# 103015-100). ReN cells were seeded at a density of 40,000 cells per well in a 24-well Seahorse tissue culture microplate (Agilent Technologies, Inc., Cat# 100777-004) coated with purified mouse laminin (Millipore, Cat# CC095-5MG). Once cells reached ~80% confluence, they were treated with EV-PBS, EV-A β_{40} , or A β_{40} alone for 24 h. Three basal respiratory measurements were obtained before injections of oligomycin (1.5 mM), FCCP (0.5 mM), and rotenone/antimycin A (0.5 mM). OCR and ECAR measurement results were then recorded, and all data were normalized to total protein levels (mg/mL) per well as measured by a BCA assay. Each data point represents the average measurement from five separate

wells.

Confocal microscopy

NPCs were cultured on laminin-coated eight-well chamber slides (Ibidi, Cat# 80841) and treated with EV-PBS, EV-A β_{40} , or A β_{40} for 24 h. The cells were subsequently fixed with 4% PFA for 10 min, washed with PBS, and permeabilized with PBS containing 0.1% Triton X-100 (Millipore Sigma, Cat# 93443). The fixed and permeabilized cells were incubated with blocking buffer (20% FBS and 0.5% Tween-20 in PBS) for 1 h. Then, samples were incubated overnight at 4 °C with primary antibodies [Supplementary Table 3]. The next day, primary antibody was aspirated, and slides were washed with PBS and incubated with Alexa Fluor-conjugated secondary antibodies for 2 h at room temperature. Slides were mounted with a glass coverslip in Fluoromount-G Mounting Medium with 4',6-diamidino-2-phenylindole (DAPI; Invitrogen, Cat# 00-4959-52) to visualize the nuclei. Immunofluorescent images were captured with a Fluoview 1200 confocal microscope (Olympus, 20 \times dry lens, or 40 \times or 100 \times oil immersion lens).

For the nuclear factor- κ B (NF κ B) measurements, mean fluorescence intensity was measured in the nuclear areas outlined by DAPI staining using FIJI software (v.2.3.0, NIH) and the Isodata algorithm. It was then used to convert the NF κ B image to a binary mask that included all fluorescence data above the background. Nuclear and whole-cell histogram data were calculated and normalized for the total number of nuclei included in each image. A comparison was then made from the difference in staining intensities. NF κ B nuclear translocation is represented by an increase in nuclear:cytoplasmic ratio of signal intensity. For TOM20 measurements, the total area of fluorescence intensity on the acquired images was normalized to the number of nuclei. Confocal microscopy images were analyzed using FIJI software (v.2.3.0, NIH). Images were pre-processed using the Bio-Formats (Available from: <https://github.com/ome/bioformats>) plug-in splitting fluorescent channels: DAPI (408 nm) and TOM20 (488 nm). Mitochondrial network parameters including mitochondrial footprint, mean branch length, total branch length, and mitochondrial network were analyzed using the Stuart Lab Mitochondrial Network Analysis (MiNA) (Available from: <https://github.com/StuartLab>) plug-in^[30].

Statistical analysis

Data are presented as the mean \pm standard error of the mean (SEM). All statistical tests were performed and all graphs were constructed using GraphPad Prism software 9.3.1. Statistical comparisons were conducted using one-way ANOVA with Tukey's multiple comparisons test, or an unpaired t-test where indicated. Levels of significance were set to * $P < 0.05$, ** $P < 0.01$, *** $P < 0.001$, and **** $P < 0.0001$.

RESULTS

Characterization of brain endothelium-derived EVs loaded with A β_{40}

The BBB has been shown to act as a route of entry for A β_{40} to transfer into the brain at concentrations in the nanomolar range. Therefore, our studies examined these physiological concentrations using A β_{40} -loaded EVs. In the initial series of experiments, EVs were isolated from the cell culture medium collected from brain endothelial cells (hCMEC) that had been treated for 48 h with exogenous A β_{40} or PBS as a vehicle control. The isolated EVs were assessed by nanoparticle tracking analysis (NTA) and transmission electron microscopy (TEM) to characterize EV size, morphology, and distribution. These analyses showed that the isolation procedure yielded a heterogeneous range of sizes of EVs isolated from both control [Figure 1A] and A β_{40} -treated [Figure 1B] endothelial cells. Most EVs fell between 100 and 400 nm in size for each group. EVs isolated from control hCMEC had a mean size of 182.2 nm (± 7.3 nm) and a total mean EV concentration of 3.67×10^8 particles/mL. EVs isolated from hCMEC treated with A β_{40} had a mean size of 186.4 (± 7.8 nm) and a total mean EV concentration of 2.73×10^8 particles/mL [Figure 1A and B]. We did not observe any significant change in particle size after treatment with A β_{40} . TEM analysis of the isolated

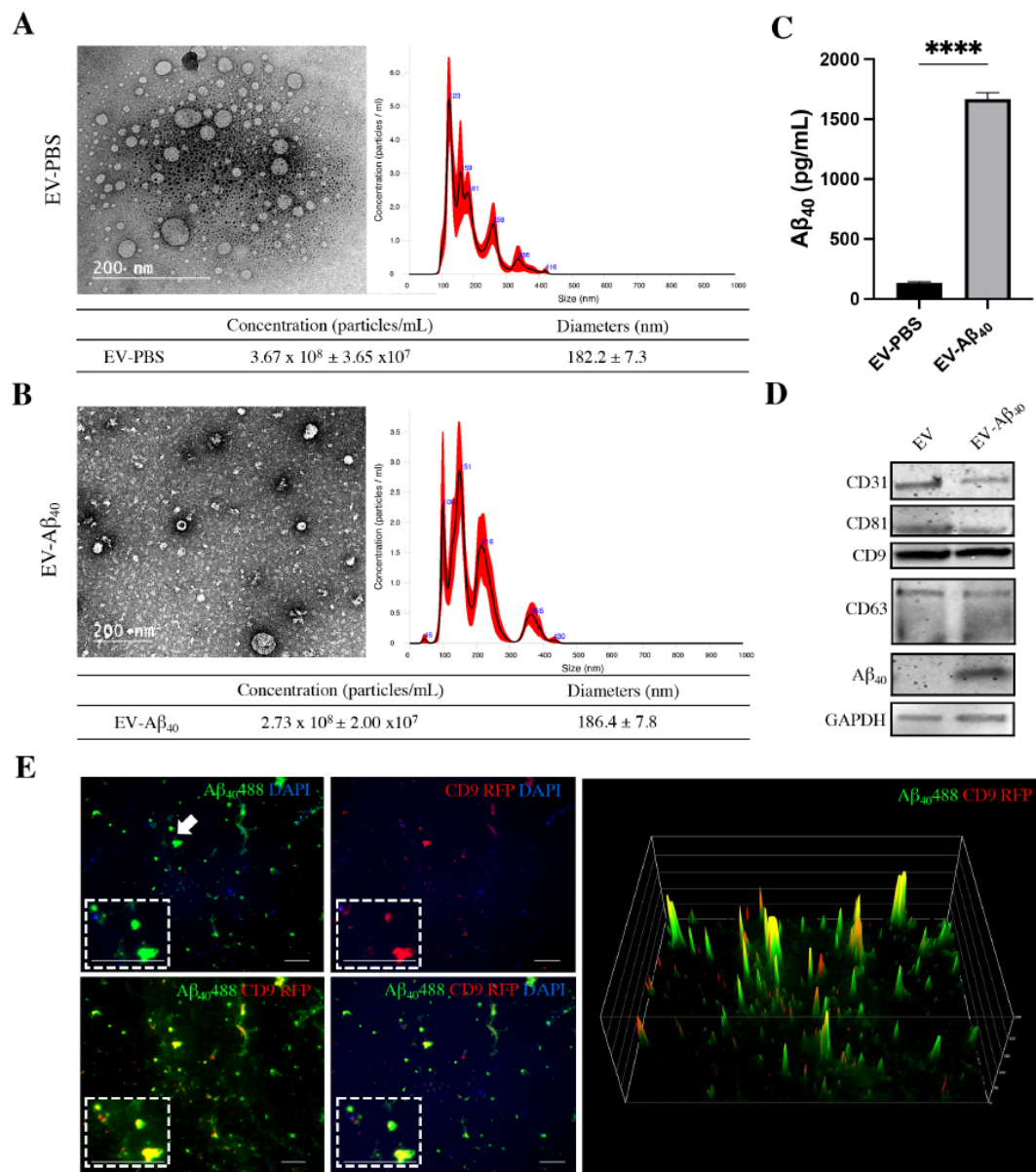


Figure 1. Characterization of brain endothelium-derived extracellular vesicles. Vesicles were isolated from endothelial cell cultures treated with A β_{40} or PBS. TEM demonstrates average size and spherical morphology of (A) control EVs and (B) EV-A β_{40} . NTA of isolated EVs loaded with (A) PBS as a vehicle control and (B) A β_{40} shows variable diameter distribution in the nanometer range. Red outlines indicate error bars (\pm SEM) from five 15-s videos of NTA. (C) ELISA for A β_{40} indicates effective enrichment of EVs isolated from medium of endothelial cells treated with A β_{40} . Student's unpaired *t*-test, *****P* < 0.0001 (isolated vesicle lysates from individual cell culture dishes; *n* = 3). (D) Western blot of lysed EVs for tetraspanin markers CD9, CD63, CD81, and A β_{40} . CD31 expression confirmed that the EVs were secreted from an endothelial cell line. (E) Fluorescent images of EVs isolated from endothelial cells transfected with CD9-RFP (red) and exposed to fluorescent A β_{40} (green). DAPI indicates genetic material (blue). Fluorescent intensity plot shows co-localization of CD9 vesicle marker (red) and A β_{40} (green) in the EV-A β_{40} group. Scale bar for representative images is 10 μ m and zoom inserts are 30 μ m. White arrow indicates the region of interest for the zoom inserts. TEM: Transmission electron microscopy; EV: extracellular vesicles; NTA: nanoparticle tracking analysis; SEM: standard error of the mean; ELISA: enzyme-linked immunosorbent assay.

EVs confirmed the size and morphology of control EVs and EV-A β_{40} (Figure 1A and B, respectively). EVs isolated from hCMEC treated with A β_{40} exhibited effective packaging of A β_{40} comparable to that of those isolated from PBS-treated cells, as measured by ELISA [Figure 1C]. Once the size distribution was

determined, we analyzed EVs for the presence of specific markers, as well as the presence or absence of A β ₄₀ in whole-vesicle lysates. Ubiquitous vesicular markers - CD9, CD63, and CD81 - are tetraspanin proteins present in lipid membrane vesicles of various sizes. All three markers were expressed in isolated EVs, along with A β ₄₀ in EVs isolated from A β ₄₀-treated cells [Figure 1D]. Additionally, we probed for CD31 to confirm that our EVs were derived from endothelial cells making up the BBB. Finally, hCMEC were transfected with CD9-RFP, followed by treatment with green fluorescent A β ₄₀, to visualize co-localization of the EV marker CD9. Uptake of the CD9-RFP and co-localization with the green fluorescence signal from A β ₄₀ HiLyte were assessed by fluorescence microscopy. A surface intensity plot was then created to visualize the intensity peaks of both green (A β ₄₀) and red (CD9) signals and their co-localization. Partial overlap of the two signals demonstrated the diversity of EV species and the efficacy of A β ₄₀ uptake into these vesicles [Figure 1E]. In addition, the EVs stained positive for DAPI, suggesting the uptake of genetic material into them. It is expected that there is a heterogeneous mixture of free A β ₄₀ (partially due to EV rupture during the preparation and the efficacy of A β ₄₀ uptake) as well as EV-associated A β ₄₀ in these isolates.

NPCs are vulnerable to aberrant neurogenesis when treated with brain endothelium-derived EVs containing A β ₄₀

In the next series of experiments, we assessed the impact of EVs on NPC differentiation using ReN cells. The ReN-derived NPCs were allowed to differentiate into neurons through the removal of growth factors from the medium, and images were taken every hour over 14 days. Treatment with EV-A β ₄₀ resulted in lower ratios of neurite extension (traced in pink) to cell body (traced in yellow), compared with those of NPCs exposed to control EVs, which displayed more healthy dendritic extensions and synapse formation between cells [Figure 2A]. Cell-body clusters, outlined in yellow, tended to form dense clusters in the EV-A β ₄₀ and A β ₄₀ groups compared with those in the untreated and EV-PBS NPCs [Figure 2B]. The total number of neurite branch points was calculated as an indicator of proper development and synapse formation. In addition to a higher tendency for cell bodies to cluster together, both A β ₄₀ groups (EV-A β ₄₀ and A β ₄₀ alone) showed reduced numbers of branch points (indicated by pink tracing of the neurites). The number of branch points/cell-body area tended to be higher in control and EV-PBS groups than in EV-A β ₄₀- and A β ₄₀-treated ReN-derived NPCs [Figure 2C]. A decrease in the neurite branch points to cell-body ratio was observed during this differentiation time course following treatment with A β ₄₀. Meanwhile, the control groups displayed a tendency for an elevated growth rate [Figure 2D]. Upon treatment with EVs and fresh medium, it was common to observe elevated rates of growth upon IncuCyte analysis (spikes in plots B-D), with cells returning to a basal state of growth in the time following replacement of the medium.

We also confirmed the impact of EV-A β ₄₀ on decreased neurite growth in an iPSC-derived stem cell model. The experiments were based on a human-derived iPSC line that was sequentially differentiated into NPCs and neurons for *in vitro* neurite extension studies. Cortical neurons were differentiated to 50 DIV and assessed by immunocytochemistry for neuron-specific markers (NeuN and β -tubulin III) [Supplementary Figure 1A]. At DIV 50, neurons were treated with EV-PBS or EV-A β ₄₀ for 24 h. Following this treatment, images were taken on the IncuCyte every hour for 6 h to determine the effect of EV-associated A β ₄₀ on neurite length. Similar to the results seen with the ReN-derived NPCs, the iPSC-derived neurons showed a reduction in the ratio of neurite length to cell-body area [Supplementary Figure 1B and C].

Brain endothelium-derived EVs containing A β ₄₀ alter mitochondrial crista morphology

To investigate the cause of NPC disruption and aberrant neurogenesis upon exposure to EV-A β ₄₀, we sought to understand whether metabolic regulation of NPCs was being affected through alterations in mitochondrial functionality. Mitochondria are essential organelles that mediate cellular function and survival. Organs and tissues that have high energetic requirements, such as the brain, have higher overall levels of mitochondria. The morphology of mitochondria in NPCs was analyzed using TEM following 24 h

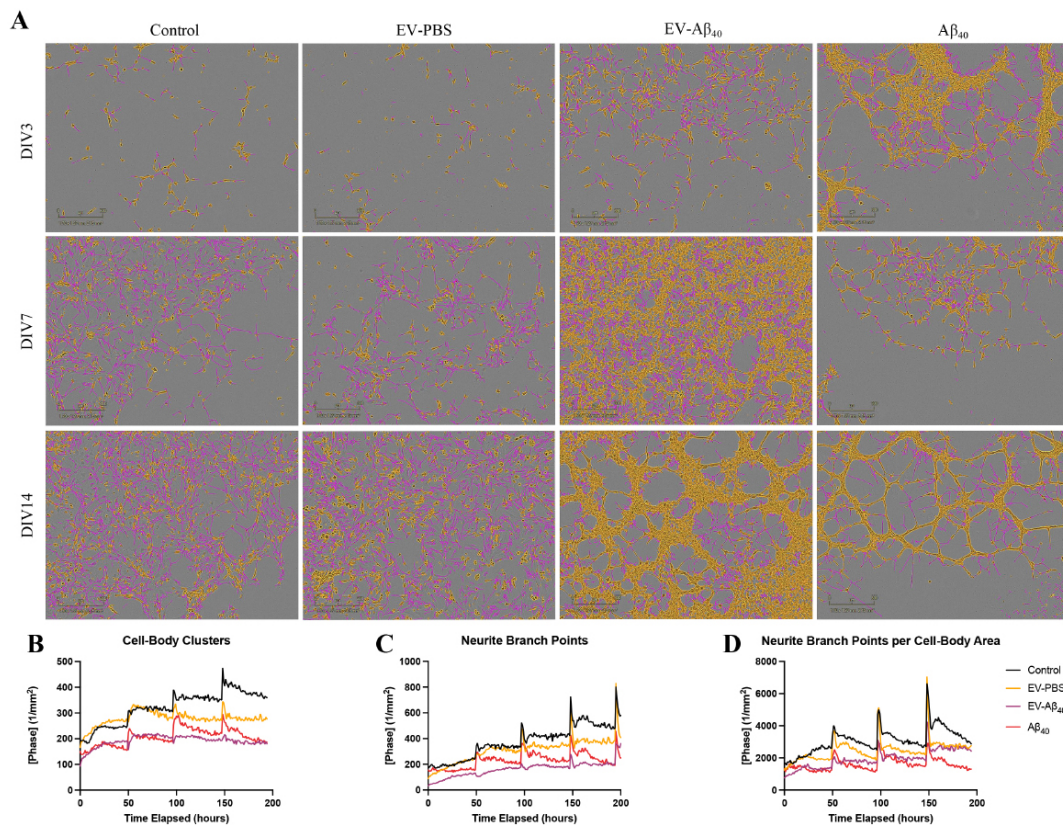


Figure 2. EV-Aβ₄₀ induce aberrant NPC differentiation. (A) IncuCyte Zoom analysis of NPC neurogenesis. ReN cells were exposed to EV-PBS, EV-Aβ₄₀, or Aβ₄₀ every other day for 14 days of differentiation. Representative images from DIV3, DIV7, and DIV14 were taken where pink indicates neurite extensions and yellow represents cell bodies. Quantification of IncuCyte images demonstrates the change in rate of (B) total cell-body cluster area, (C) total neurite branch points, and (D) the ratio of neurite branch points to cell-body area. Graphs represent the average of individual pictures taken in nine image grids over 14 days. Additionally, DIV3 corresponds to timepoint 0 on the graph, the first instance when images were taken of cells after they were plated and treated. EV: Extracellular vesicles; NPC: neural progenitor cell.

of treatment with medium alone (control), EV-A₄₀, control EVs (EV-PBS), or A₄₀ alone. Untreated NPCs and NPCs exposed to EV-PBS exhibited healthy mitochondria with dense, regular, inner mitochondrial membrane formation [Figure 3A and B]. Meanwhile, NPCs exposed to EV-Aβ₄₀ and Aβ₄₀ alone exhibited morphological changes in crista structures [Figure 3C and D]. In addition, the presence of white patches, or crista “voids” (indicated by the arrows), was consistently seen in both EV-Aβ₄₀- and Aβ₄₀-exposed groups, but not in the control groups (control and EV-PBS).

The mitochondrial area and crista structures were analyzed in the perinuclear region of NPCs, as previously described^[29]. Limiting the analysis to this region is crucial to control for the high rate of mitochondrial dynamics normally found in the growth extension regions of differentiating cells. The total perinuclear mitochondrial area was not significantly changed between groups (data not shown). Using TEM analysis, we observed a significant decrease in crista number in both EV-Aβ₄₀- and Aβ₄₀-exposed NPCs compared with the level in untreated or EV-PBS-exposed cells [Figure 3E]. The total crista area was determined from individual mitochondria and the summation of outlined crista surface area was measured. The surface area of perinuclear mitochondrial cristae was significantly decreased between control NPCs compared with that of EV-Aβ₄₀-exposed cells [Figure 3F]. In addition, we measured the density of cristae, which reflects the ratio of crista surface area to the associated mitochondrion area. The relative density of cristae exhibited a

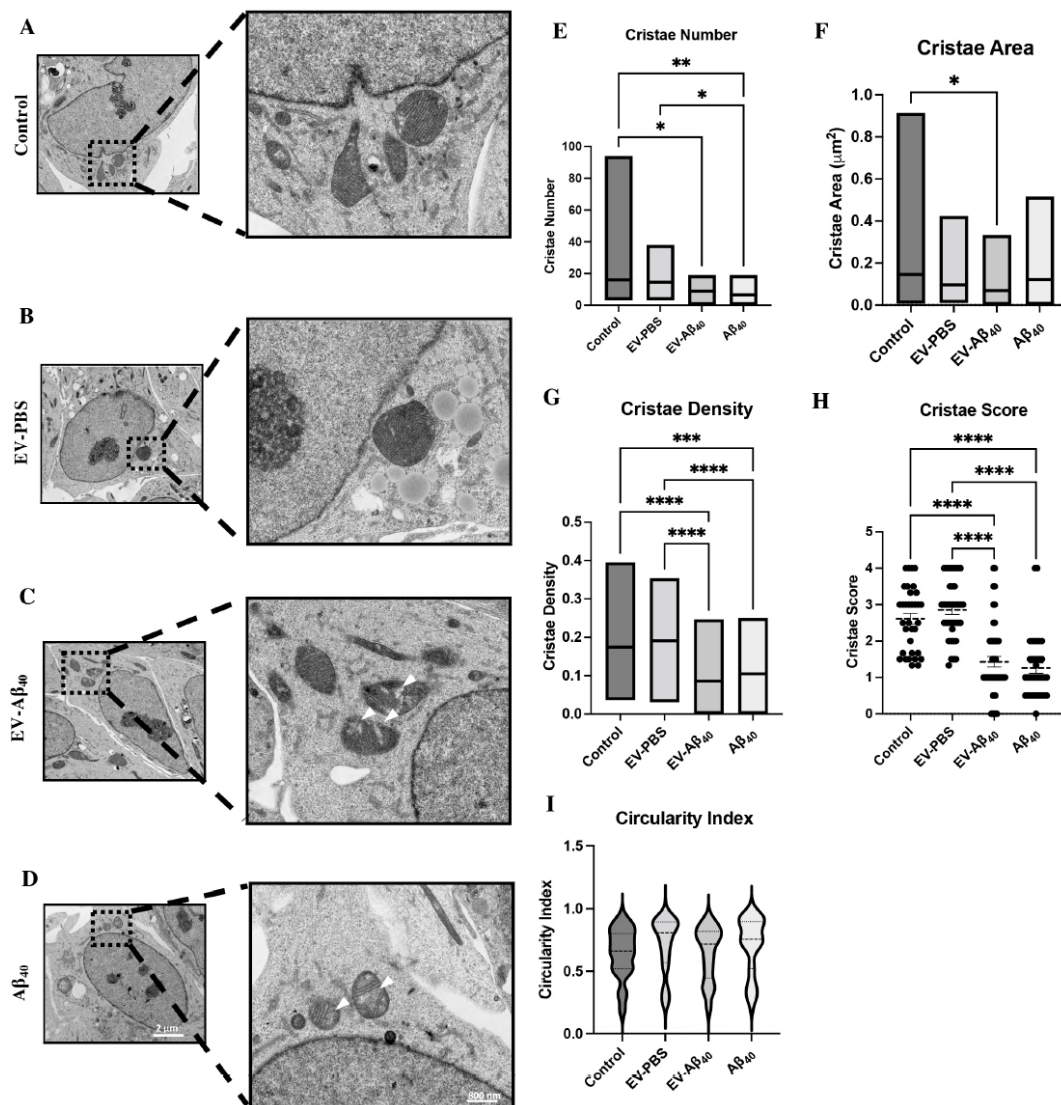


Figure 3. EV-Aβ₄₀ alter the morphology of NPC mitochondrial cristae. Representative TEM images of morphology of perinuclear mitochondria and cristae in (A) untreated NPCs or those treated with (B) EV-PBS, (C) EV-Aβ₄₀, or (D) Aβ₄₀ alone as a positive control for 24 h. Quantification of (E) crista number, (F) crista surface area, (G) crista density, (H) crista score, and (I) circularity index. Scale bar for representative images is 2 μm and zoom inserts are 800 nm. **P* < 0.05, ***P* < 0.01, ****P* < 0.001, and *****P* < 0.0001. *n* = 30 images per group and 38-72 mitochondria per group. EV: Extracellular vesicles; NPC: neural progenitor cell; TEM: transmission electron microscopy.

significant decrease in both Aβ₄₀ treatment groups (EV-Aβ₄₀ and Aβ₄₀ alone) compared with the level in the control groups [Figure 3G]. Similarly, mitochondria in each group were assigned morphometric crista scores to visually assess crista definition. This scale ranges from 0, corresponding to no sharply defined cristae, to 4, corresponding to many regular cristae. Treatment with EV-Aβ₄₀ or Aβ₄₀ alone resulted in a significantly lower crista score than in the control groups. This suggests that exposure to Aβ₄₀ results in the adoption of irregular shapes [Figure 3H]. Circularity index is a relative measure of mitochondrial shape, with 1.0 representing a complete sphere and 0.0 representing an extreme elliptical or elongated shape. NPCs treated with EV-Aβ₄₀ tended to display a greater fluctuation between spherical and elongated extremes than in the control treatments [Figure 3I].

Mitochondrial footprint alterations in NPCs exposed to EVs containing A β_{40}

To further explore the mitochondrial dynamic changes in NPCs exposed to EV-A β_{40} or A β_{40} alone, we next focused on morphological features of mitochondrial networks. TOM20, a translocase protein located on the outer mitochondrial membrane, was used to stain mitochondrial networks within treated NPCs [Figure 4A]. Using MiNA, we quantified the networks using a skeletonized overlay approach. Mitochondrial footprint, which is the total area of the image with a signal, was reduced in both vesicle groups (EV-PBS and EV-A β_{40}) compared with that in untreated cells; however, this impact was more pronounced in NPCs exposed to EV-A β_{40} [Figure 4B]. Interestingly, the overall mitochondrial network number, a measure of networks comprising more than one branch, was unchanged among all groups [Figure 4C]. While networks remained unchanged, network fusion, or the restricted ability of mitochondria to divide, was apparent in A β_{40} -treated NPCs, indicating possible mitochondrial disruption. This was evident by enhanced fragmentation of larger networks in the A β_{40} group, resulting in longer branch lengths, compared with fragmentation of slightly smaller relative networks in control NPCs [Figure 4D]. Additionally, the presence of long branches [Figure 4E] and a larger network size may indicate events leading to the occurrence of hyperfusion and the potential for many of the mitochondria to exhibit an elongated branched network. Hyperfusion can also be induced by stress or mitophagy and can decrease the ability of the cell to divide and differentiate properly. An increase in total overall branch length [Figure 4E] may be related to this phenomenon when fission machinery is disrupted or inhibited as a compensatory mechanism. Overall, our mitochondrial tracking using TOM20 demonstrated that the exposure of NPCs to A β_{40} (either alone or in the form of EV-A β_{40}) results in morphological changes to the mitochondria, as well as alterations in the organelle structure that lead to possible dynamic shifts within the cell.

EV-A β_{40} contribute to the dysregulation of mitochondria by impairing metabolic respiration

After confirming differential regulation in mitochondrial footprint and branch length dynamics, we sought to evaluate whether these effects, combined with changes in the morphology of cristae, altered the respiratory capacity of NPCs. Healthy differentiating NPCs rely mainly on mitochondrial respiration and maintain glycolysis at low levels. Therefore, we analyzed whether EV-A β_{40} treatment could alter mitochondrial respiration and subsequent ATP production using Seahorse technology. First, we assessed oxygen consumption rate (OCR) as an indicator of mitochondrial respiration [Figure 5A and B]. Treatment with A β_{40} , either alone or in the form of EV-A β_{40} , resulted in a decrease in the compensatory rate of respiration compared with that of untreated NPCs or treatment with control EVs. In the subsequent analyses, OCR was measured following injections with oligomycin, to inhibit complex V (ATP synthase) and force the cell into compensatory mechanisms for ATP production; FCCP, to disrupt membrane potential and uncouple the proton gradient across the inner membrane; and rotenone/antimycin A, to block complexes I and III, which eliminates electron transport chain (ETC) mitochondrial respiration. NPCs treated with EV-A β_{40} had significantly lower basal respiration [Figure 5C], maximal respiration [Figure 5D], and spare respiratory capacity [Figure 5E] than untreated NPCs or EV-PBS-treated cells. These parameters measure the capacity of the cells to respond to energy demands and their ability to increase respiration. Proton leakage is indicated by the remaining basal respiration not coupled to ATP production, which showed no statistically significant differences among any of the treatment groups [Figure 5F]. In contrast, both vesicle-treated groups (EV-PBS and EV-A β_{40}) appeared to exhibit an increased ability to respire by non-mitochondrial cellular enzymes that consume oxygen [Figure 5G]. ATP production after treatment with EV-A β_{40} exhibited a tendency to decrease compared with that in the controls [Figure 5H]. We also assessed the extracellular acidification rate (ECAR) as a measure of cellular glycolysis. ECAR values demonstrated a tendency to decrease in NPCs exposed to EV-A β_{40} or A β_{40} alone relative to the levels in control groups [Figure 5I].

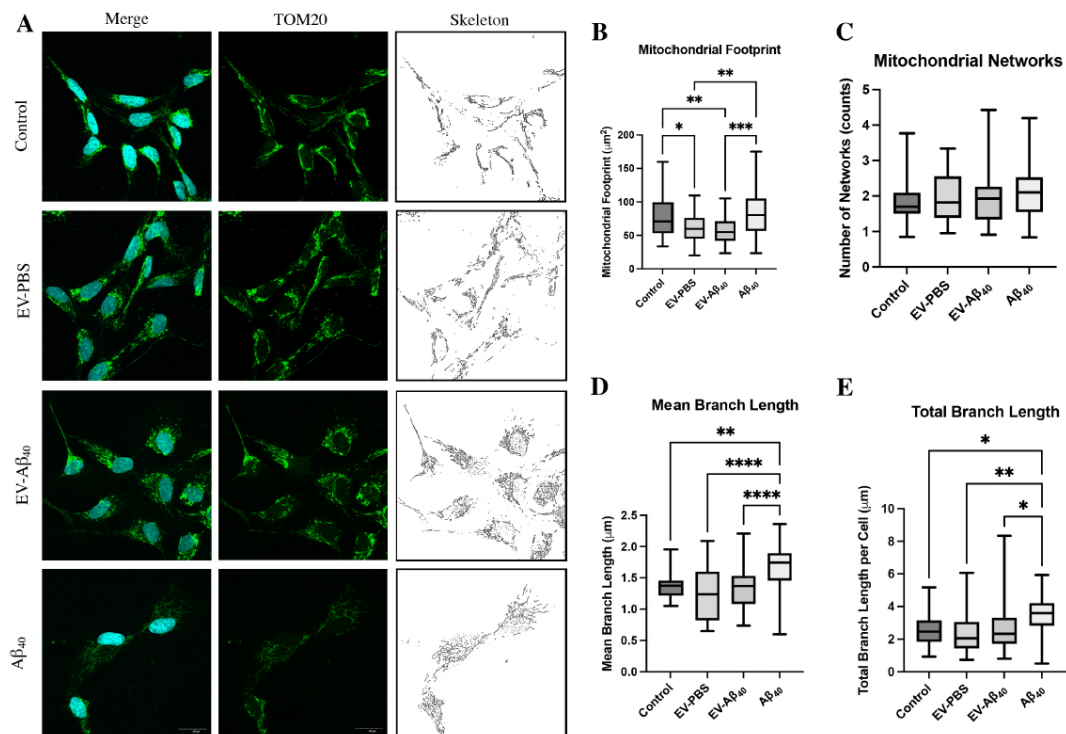


Figure 4. Analysis of the mitochondrial network skeletons in NPCs using MiNA. (A) Confocal images of NPCs stained with DAPI (blue) and TOM20 (green) for tracking the mitochondrial membrane. MiNA plug-in on ImageJ was used to skeletonize the mitochondria. Box and whisker plots quantify the (B) mitochondrial footprint, (C) total mitochondrial networks, (D) mean branch length, and (E) total branch length. Box plots show the mean (horizontal line), first to third quartile (box), and the extreme values within the 95% confidence interval of the interquartile range (whiskers). Scale bar for representative images is 20 μm . * $P < 0.05$, ** $P < 0.01$, *** $P < 0.001$, and **** $P < 0.0001$, using one-way ANOVA. $n = 6-9$ images per group, each image containing 3-12 NPCs. EV: Extracellular vesicles; NPCs: neural progenitor cells; MiNA: mitochondrial network analysis; DAPI: 4',6-diamidino-2-phenylindole.

EV-Aβ₄₀ dysregulate mitochondrial fusion and fission machinery

Mitochondrial morphology is crucial for cellular health and normal metabolic function. To better understand the main functions that regulate mitochondrial morphology, mitochondrial fusion and fission processes were assessed after treatment with EVs or Aβ₄₀. Mitochondrial fusion is mainly regulated by proteins of the outer mitochondrial membrane, mitofusin 1 (Mfn1) and mitofusin 2 (Mfn2), and of the inner mitochondrial membrane, optic atrophy protein (OPA1). We assessed the expression of Mfn1, Mfn2, and OPA1 through mRNA and total protein expression. Although no significant change in total mRNA expression was found among the studied fusion-related genes [Figure 6A], differential protein expression was observed. Specifically, there was a significant decrease in the expression of OPA1 and Mfn2 proteins in NPCs exposed to EV-Aβ₄₀, while Mfn1 showed a modest but not statistically significant increase in the cells treated with Aβ₄₀ alone [Figure 6B-D].

In addition to mitochondrial fusion, fission proteins are essential to mitochondrial maintenance. They include mitochondrial fission factor (Mff), dynamin-related protein 1 (Drp1), and mitochondrial fission protein 1 (Fis1). Similar to the results of the fusion genes, the expression of the fission genes showed no significant differences across the experimental groups [Figure 6E]. Nevertheless, fission proteins were differentially expressed between the treatment groups. Fis1, a common receptor for Drp1 to promote mitochondrial division, was significantly decreased in both Aβ₄₀ groups (EV-Aβ₄₀ and Aβ₄₀ alone) [Figure 6F]. In addition, Drp1 protein expression was found to be decreased in EV-Aβ₄₀-treated NPCs [Figure 6G]. Expression of Mff protein, which is an important regulator in the recruitment of Drp1 to the

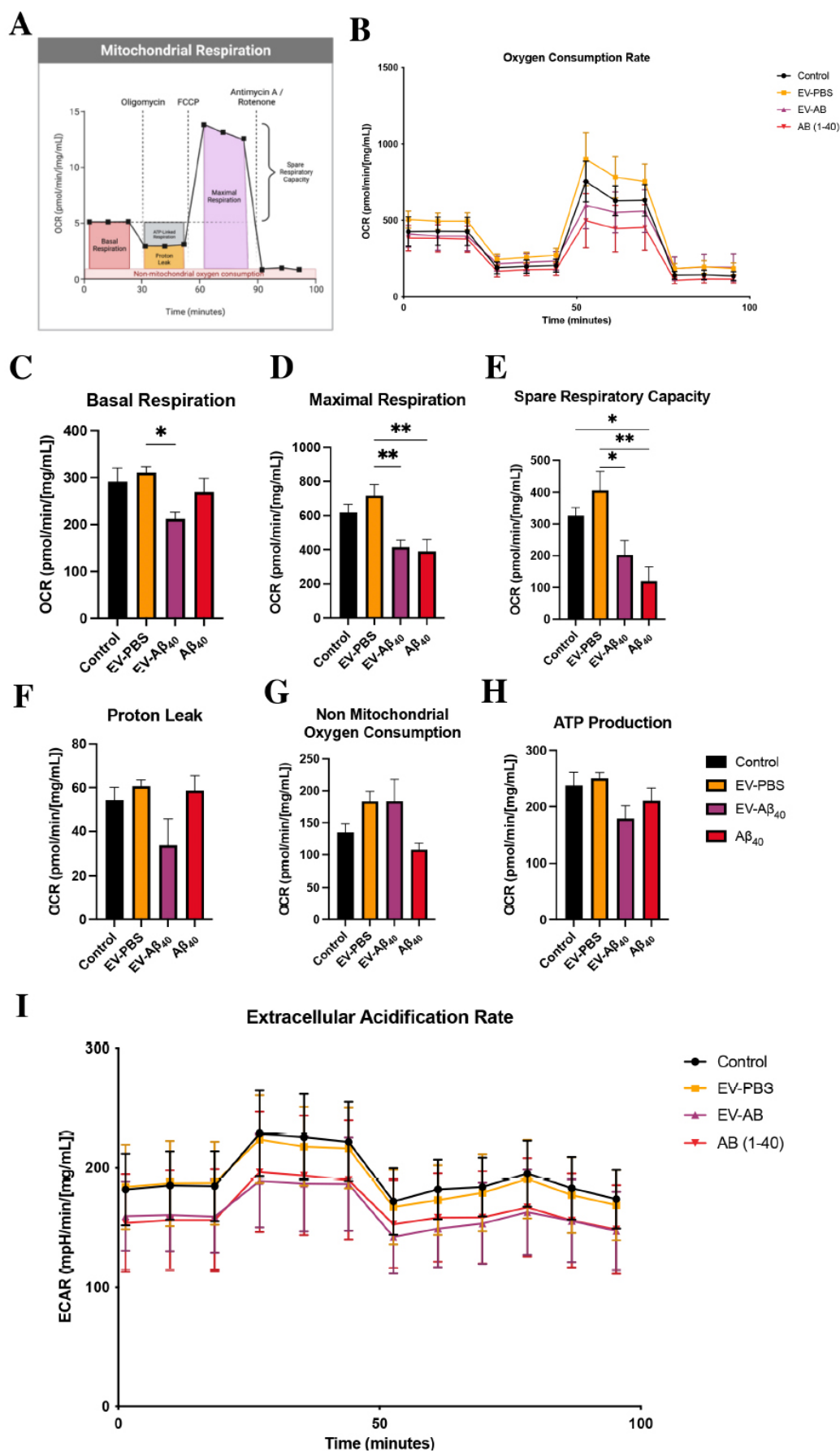


Figure 5. Impact of EV- $A\beta_{40}$ on NPC mitochondrial respiratory function. (A) Schematic of the mitochondrial stress test assay. (B) OCR in untreated NPCs and NPCs exposed to EV-PBS, EV- $A\beta_{40}$, or $A\beta_{40}$ alone for 24 h and normalized to protein levels. Respiratory measurements of OCR associated with (C) basal rate, (D) maximal respiration, (E) spare respiratory capacity, (F) proton leakage, (G) non-mitochondrial oxygen consumption, and (H) ATP production. (I) Glycolysis is measured by ECAR in the same cells as (B-H). All graphs present the mean \pm SEM. Statistical analysis was performed using one-way ANOVA, $*P < 0.05$, $**P < 0.01$, and $***P < 0.001$, $n = 5$ per group. EV: Extracellular vesicles; NPCs: neural progenitor cells; OCR: oxygen consumption rate; ECAR: extracellular acidification rate; SEM: standard error of the mean.

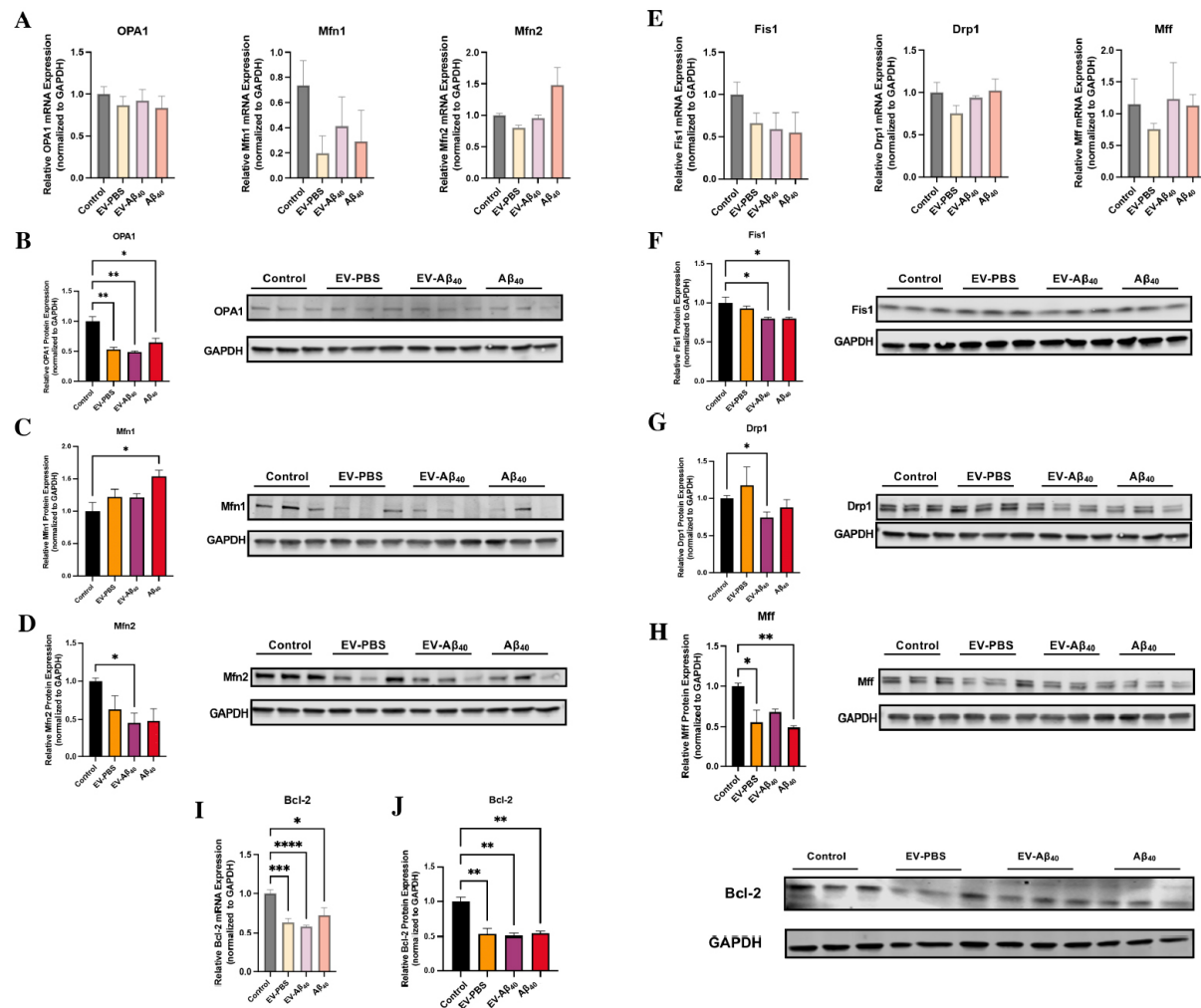


Figure 6. NPC exposure to EV- $A\beta_{40}$ causes dysregulation of mitochondrial fusion and fission machinery. (A) Total mRNA expression was assessed for fusion modulators: *OPA1*, *Mfn1*, and *Mfn2*. The total protein expression levels were assessed along with representative western blots for fusion proteins (B) *OPA1*, (C) *Mfn1*, and (D) *Mfn2*. GAPDH was used as a housekeeping control for all experiments. Additionally, modulators of fission, *Fis1*, *Drp1*, and *Mff*, were assessed via qPCR (E). Total protein expression and representative western blots for mitochondrial fission proteins (F) *Mff*, (G) *Drp1*, and (H) *Fis1* were quantified. Bcl-2 was probed for (I) total mRNA gene expression and (J) total protein expression by western blotting. Bar graphs indicate mean \pm SEM. Statistical analysis was performed using one-way ANOVA, $*P < 0.05$, $**P < 0.01$, $***P < 0.001$, and $****P < 0.0001$, $n = 3-6$ independent experiments per group. EV: Extracellular vesicles; NPC: neural progenitor cell; SEM: standard error of the mean.

mitochondria, was also significantly reduced after treatment with $A\beta_{40}$ and tended to show lower levels in EV- $A\beta_{40}$ [Figure 6H]. This overall decrease in fission regulators supports our findings in mitochondrial morphology that indicated a possible hyperfused state in which mitochondrial division is impaired, leading to a shift in the dynamic balance that results in cell stress and metabolic dysfunction.

Mitochondria are also key regulators of the apoptotic pathway. This involves Bcl-2, a modulator suppressing apoptosis and regulating cell death by mediating mitochondrial membrane permeability. To assess *Bcl-2* levels, total mRNA levels were assessed by qPCR and showed a significant decrease in NPCs exposed to all of the treatments (EV-PBS, EV- $A\beta_{40}$, or $A\beta_{40}$ alone) compared with that of the untreated control [Figure 6I]. Consistent with this, total protein expression for Bcl-2 was significantly lower in all experimental groups than in untreated NPCs [Figure 6J]. Taken together, our data suggest that an imbalance in normal fusion and fission processes occurs in NPCs exposed to EV- $A\beta_{40}$ or $A\beta_{40}$ alone. This imbalance may lead to the remodeling of cristae, as shown in Figure 3, and further apoptosis-associated responses in the mitochondria.

Diminished SIRT3 expression and activation of NF κ B in NPCs exposed to EV- $A\beta_{40}$

To assess the downstream pathways that may alter mitochondrial dynamics in NPCs, we probed for sirtuin 3 (SIRT3) expression, a mitochondrially specific NAD-dependent deacetylase. One of the prominent targets of SIRT3-mediated deacetylation is NF κ B [Figure 7A]. *SIRT3* gene expression was assessed by qPCR, which showed no significant differences across any of the treatment groups [Figure 7B]. However, there was a marked decrease in SIRT3 protein expression in NPCs exposed to EV- $A\beta_{40}$ and $A\beta_{40}$ alone [Figure 7C and D].

We then stained NPCs to examine the expression levels of p65, a subunit of the NF κ B heterodimer that is needed for nuclear translocation [Figure 7E]. We assessed the levels of NF κ B in the nucleus as an indicator of activation and demonstrated that the group treated with EV- $A\beta_{40}$ had increased expression of NF κ B in the nucleus compared with the levels in other treated groups, as quantified by total fluorescence intensity [Figure 7F] and the relative intensity of nuclear staining [Figure 7G]. We also assessed the ratio of p65 fluorescence in the nucleus compared to that in the cytoplasm [Figure 7H]. This analysis indicated that NPCs treated with $A\beta_{40}$ alone exhibited the most significant translocation of NF κ B into the nucleus, while the EV groups showed a trend towards higher nuclear-to-cytoplasmic translocation ratios. It is important to consider that the relative nuclear-to-cytoplasmic ratio in the EV- $A\beta_{40}$ group might be affected by aberrant neurogenesis that also occurs in this group.

DISCUSSION

Unbalanced oxidation and oxidative stress have been widely postulated to be common factors that contribute to pathological aging and aberrant neurogenesis of NPCs. $A\beta_{40}$ has also been shown to possibly impair the viability and differentiation of NPCs by disrupting mitochondrial signaling^[31,32]. The significance of these events is related to the fact that dysfunctional mitochondria are the main inducers of oxidative stress and imbalance of the redox status, which are the critical factors in the stimulation of immune activation, neurotoxicity, and aberrant NPC proliferation^[33-37]. Additionally, EVs have recently been postulated to be significantly involved in various neurodegenerative diseases, including A β pathology^[16,17]. One study has demonstrated that $A\beta_{40}$ can be packaged into EVs and shed into the brain microenvironment, and that human $A\beta_{40}$ plaques are enriched with EV proteins^[9]. The implications of endogenous $A\beta_{40}$ and $A\beta_{40}$ trafficked into the brain may translate into clinical manifestations of AD, such as dementia, and neurodegeneration. Because neurogenesis has been accepted to occur in the adult brain, it is also a crucial modulator of brain plasticity, repair, as well as learning and memory functions^[24,38]. Neurogenesis in the adult brain occurs in distinct zones from NPCs that reside in several parts of the brain, including the subgranular zone (SGZ) and the dentate gyrus (DG) in the hippocampus^[39-41]. Furthermore, the integrity of the brain endothelium is vital for normal self-renewal, proliferation, and differentiation of NPCs^[42]. In this study, we investigated the role of brain endothelium-derived EV biology in the context of $A\beta_{40}$ pathology to understand the mechanistic dysfunction that may induce aberrant neurogenesis in NPCs.

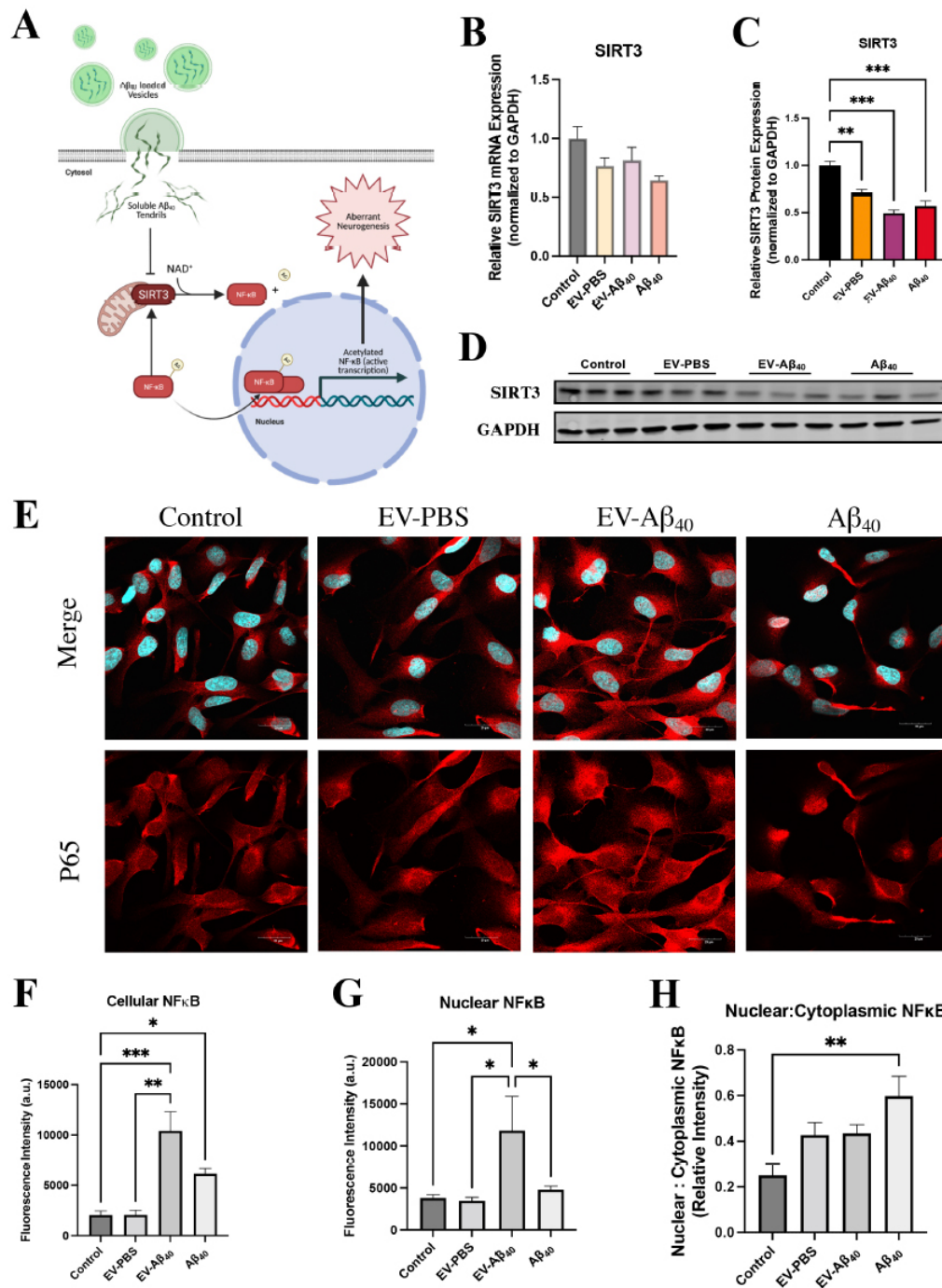


Figure 7. Expression of SIRT3 and NFκB is affected upon exposure to Aβ₄₀. (A) Schematic of mitochondrially dependent SIRT3 function affecting NFκB activation in NPCs. Reduced SIRT3 expression inhibits the deacetylation of NFκB, which allows the acetylated form to translocate into the nucleus and induce downstream inflammatory responses. SIRT3 expression was probed for both (B) total mRNA expression and (C) total protein expression. (D) Representative western blots. (E) Confocal images of NPCs after 24 h of treatment stained for DAPI (blue) and p65 protein (red) indicate translocation of NFκB into the nucleus of cells in the Aβ₄₀ groups. Images were further quantified for (F) total NFκB cell fluorescence, (G) nuclear NFκB, and (H) the nuclear-to-cytoplasmic ratio of NFκB fluorescence. Bar graphs indicate mean ± SEM. Statistical analysis was performed using one-way ANOVA, **P* < 0.05, ***P* < 0.01, ****P* < 0.001, and *****P* < 0.0001, *n* = 3 independent experiments per group. EV: Extracellular vesicles; NPC: neural progenitor cell; DAPI: 4',6-diamidino-2-phenylindole; SEM: standard error of the mean.

The level of $A\beta_{40}$ in the CNS is dependent on the balance achieved between endogenous production in the brain, influx from the plasma, and efflux via BBB efflux transporters^[43]. The relative contributions of these sources to amyloid levels in the brain are difficult to estimate, but they all appear to be critically important. Neurotoxic $A\beta_{40}$ is generated by proteolytic cleavage of the ubiquitously expressed amyloid precursor protein (APP) commonly expressed by neurons^[44]. Amyloidogenic $A\beta$ peptides range from 30 to 42 amino acids in length, with $A\beta_{40}$ and $A\beta_{42}$ being the two main toxic $A\beta$ species. $A\beta_{40}$ is the main amyloidogenic species, accounting for 90% of all amyloid protein produced. The doses of $A\beta_{40}$ used in this study have pathological relevance as the cerebrospinal fluid $A\beta_{40}$ levels in AD brains are in the nanomolar range^[28].

The first goal of the present study was to evaluate whether differentiation of NPCs could be altered after exposure to EVs containing $A\beta_{40}$. We demonstrated that EV- $A\beta_{40}$ had the ability to alter neurite outgrowth and branching in developing NPCs, prompting us to hypothesize that mitochondrial metabolism was being affected. We also observed a similar decrease in neurite length in a human-induced stem cell-derived neuronal model^[45]. Generally, mitochondria have a tightly regulated distribution within the cytoplasm of cells; however, when NPCs are rapidly differentiating and require high energetic turnover, the mitochondria are more commonly found in specific growth cones and extensions of these cells. This has broad implications in aiding ATP and calcium release, presynaptic terminal formation, and overall growth of developing neurite extensions. Therefore, we decided to evaluate the impact of EV-associated $A\beta_{40}$ on the mitochondrial morphology and function of NPCs. While we quantitatively confirmed a decrease in the number and density of cristae, we also noticed structural changes to the integrity of individual mitochondria, with areas showing a lack of crista structure or “voids.” These areas with voids may directly correspond to losses in the number, density, and even score of cristae. This observation is significant because it has recently been demonstrated in many pathological studies revolving around organs with a high-energy demand, such as the brain and heart^[46-49]. This has implications for cell function because it directly corresponds to decreases in mitochondrial membrane permeability, electron transport chain function, and ATP synthesis.

Next, we used mitochondrial network analysis as an alternative method to assess mitochondrial morphology. Interestingly, the mitochondrial footprint was decreased in EV- $A\beta_{40}$ -treated NPCs, while branch length of the networks increased, suggesting a tendency towards a hyperfused state with elongated branches. The presence of a hyperfused state in NPCs is controversial; however, our data suggest that the restricted ability of the organelle to properly divide supports the theory that diseased NPCs have abnormal mitochondria and may exhibit lower ATP production, affecting their potential for self-renewal or differentiation^[50].

The mitochondrial membrane is largely impermeable, and the transfer of molecules across it is mediated by channels, pumps, and transporters. Proper assembly of the inner mitochondrial membrane is crucial for maintaining the electron transport chain and ATP bioenergetic production. While NPCs normally maintain glycolysis at low levels, environmental stressors may cause a switch in cell machinery when metabolic respiration is compromised. Indeed, treatment of NPCs with EV- $A\beta_{40}$ and $A\beta_{40}$ alone resulted in a decrease in metabolic respiration. This led us to hypothesize that the metabolism of NPCs is affected by EVs containing $A\beta_{40}$. With a decrease in metabolic respiration and the inability of $A\beta_{40}$ -exposed NPCs to switch to compensatory glycolysis, as measured by ECAR levels, we confirmed that overall metabolic regulation in the mitochondria was significantly hindered by EV- $A\beta_{40}$.

The circularity index of a mitochondrion is a relative measure of its shape. Typically, more spherical mitochondria are associated with swelling, while elongated ones result from the dynamic fission and fusion

of mitochondria that occur in healthy cells. In our study, NPCs treated with EV- $A\beta_{40}$ showed a tendency for greater fluctuation between spherical and elongated morphology, as well as a decreased respiratory rate. Mitochondrial maintenance is regulated by a balance between fusion and fission^[51,52] and a shift in this balance may lead the mitochondria to induce mitophagy or cellular apoptosis^[53]. The dysregulation of this process can have pathological consequences. This may be particularly important in cells that have high energy demands, such as NPCs, and may have driven the deficits in neurogenesis observed when these cells were exposed to $A\beta_{40}$ ^[54]. In general, mitochondrial fusion acts to ameliorate stressful conditions in cells by substituting damaged mitochondria with healthy ones. Meanwhile, mitochondrial fission is necessary to promote mitochondrial division and growth, but can also be used by the cell as a quality control mechanism under pathological conditions to remove damaged mitochondria^[55]. Fission in the mitochondria is mainly mediated by the GTPase Drp1, which binds to its receptor Fis1 near the endoplasmic reticulum^[56]. In contrast, mitochondrial fusion is mediated by mitofusin proteins, while the integrity of mitochondrial cristae is maintained by OPA1^[57-59]. Our data suggest that mitochondrial fusion machinery is dysregulated in NPCs upon exposure to EV- $A\beta_{40}$ and/or $A\beta_{40}$ alone. Indeed, these treatments decreased the expression of OPA1 and Mfn1, while Mfn2 expression was significantly increased. In contrast, the elements of the fission machinery Drp1 and its receptor, Fis1, were significantly downregulated upon treatment with EV- $A\beta_{40}$, supporting our observation of a hyperfused state. Nevertheless, this could also be a compensatory mechanism achieved by cells due to the loss of the integrity of cristae observed in the TEM and metabolic analyses.

Given the irregular mitochondrial dynamics observed in the $A\beta_{40}$ -treated cells, we assessed the NPCs for potential engagement in the mitochondrial apoptotic pathway with a focus on Bcl-2 levels. The loss in OPA1 protein expression [Figure 6A] suggests a loss in inner mitochondrial membrane (IMM) fusion and crista structure [Figure 3]. OPA1 is a critical protein for IMM fusion and for preserving crista structure and sequestering cytochrome c in the intermembrane space. A loss of this protein may lead to release of cytochrome c and reduced density of mitochondrial cristae, resulting in white patches or voids in TEM^[60]. Our results also reveal that a significant decrease in OPA1 levels was associated with a decreased level of Bcl-2, a mitochondrially specific pro-apoptotic inhibitor [Figure 6I-K], an event that can stimulate the release of cytochrome c, which further triggers apoptotic cascades^[61].

SIRT3 is a mitochondrially specific NAD-dependent deacetylase that is an essential part of mitochondrial maintenance. Targets of SIRT3 include the electron transport chain, enzymes of intermediary metabolism, and antioxidant defense^[62-64]. Although functions of SIRT3 in peripheral metabolic regulation have been studied, its action in the brain is not fully understood. One important function of SIRT3 is the deacetylation of NF κ B. Thus, decreased activity of SIRT3, as seen in Figure 7A-C, may cause activation of NF κ B (acetylated NF κ B is active) and induction of downstream inflammatory reactions. In addition, SIRT3 expression is transcriptionally regulated by NF κ B^[65]. Indeed, our data indicate that a decrease in SIRT3 protein expression was associated with the translocation of NF κ B into the nucleus in the groups with EV- $A\beta_{40}$ and $A\beta_{40}$ alone. This has implications for future studies on inflammatory and signaling pathways that mediate aberrant neurogenesis.

In summary, the results of the present study indicate that EVs derived from brain endothelial cells can effectively transfer $A\beta_{40}$ to NPCs and affect their neurogenesis via alterations of mitochondrial functions. These events have the potential to modulate the dynamics and severity of AD. Therefore, a better understanding of the interactions between $A\beta_{40}$ and the BBB, and the underlying mechanisms that mediate amyloid accumulation in the brain parenchyma may provide targets for pharmacological intervention. Such interventions may facilitate $A\beta$ removal or protect against entry across the BBB and the development of

neurological, neurodevelopmental, and neurocognitive alterations.

DECLARATIONS

Acknowledgments

We acknowledge Vania Almeida and the University of Miami Transmission Electron Microscopy Core for EM sample preparation and assistance with the generation of EM images.

Authors' contributions

Supported the human iPSC development and analysis: Colbert BM, Dykxhoorn DM

Supported the TEM and MiNA analyses: Pierre Louis KD, Daftari MT

Wrote the manuscript: Osborne OM, Kowalczyk JM

Provided funding: Dykxhoorn DM, Toborek M

All authors made substantial contributions to conception and design of the study, performed data analysis and interpretation and approved the manuscript.

Availability of data and materials

Available upon request.

Financial support and sponsorship

This work was supported by the Florida Department of Health grant 8AZ24, the National Institutes of Health (NIH) grants F31NS125905, MH128022, MH122235, MH072567, HL126559, DA044579, DA039576, DA040537, DA050528, and DA047157. Funds from the John P. Hussman Foundation helped support this research in the lab of Derek Dykxhoorn.

Conflicts of interest

All authors declared that there are no conflicts of interest.

Ethical approval and consent to participate

The iPSC line, CW50038, was obtained from the Coriell Institute as a deidentified sample.

Consent for publication

Not applicable.

Copyright

© The Author(s) 2022.

REFERENCES

1. Swerdlow RH. Brain aging, Alzheimer's disease, and mitochondria. *Biochim Biophys Acta* 2011;1812:1630-9. DOI PubMed PMC
2. Musiek ES, Holtzman DM. Three dimensions of the amyloid hypothesis: time, space and "wingmen". *Nat Neurosci* 2015;18:800-6. DOI PubMed PMC
3. Osborne O, Peyravian N, Nair M, Daunert S, Toborek M. The paradox of HIV blood-brain barrier penetrance and antiretroviral drug delivery deficiencies. *Trends Neurosci* 2020;43:695-708. DOI PubMed PMC
4. András IE, Rha G, Huang W, et al. Simvastatin protects against amyloid beta and HIV-1 Tat-induced promoter activities of inflammatory genes in brain endothelial cells. *Mol Pharmacol* 2008;73:1424-33. DOI PubMed PMC
5. Bourassa P, Tremblay C, Schneider JA, Bennett DA, Calon F. Beta-amyloid pathology in human brain microvessel extracts from the parietal cortex: relation with cerebral amyloid angiopathy and Alzheimer's disease. *Acta Neuropathol* 2019;137:801-23. DOI PubMed PMC
6. Xu J, Ikezu T. The comorbidity of HIV-associated neurocognitive disorders and Alzheimer's disease: a foreseeable medical challenge in post-HAART era. *J Neuroimmune Pharmacol* 2009;4:200-12. DOI PubMed PMC

7. Soontornniyomkij V, Moore DJ, Gouaux B, et al. Cerebral β -amyloid deposition predicts HIV-associated neurocognitive disorders in APOE ϵ 4 carriers. *AIDS* 2012;26:2327-35. DOI PubMed PMC
8. András IE, Eum SY, Huang W, Zhong Y, Hennig B, Toborek M. HIV-1-induced amyloid beta accumulation in brain endothelial cells is attenuated by simvastatin. *Mol Cell Neurosci* 2010;43:232-43. DOI PubMed PMC
9. Rajendran L, Honsho M, Zahn TR, et al. Alzheimer's disease beta-amyloid peptides are released in association with exosomes. *Proc Natl Acad Sci USA* 2006;103:11172-7. DOI PubMed PMC
10. András IE, Leda A, Contreras MG, et al. Extracellular vesicles of the blood-brain barrier: role in the HIV-1 associated amyloid beta pathology. *Mol Cell Neurosci* 2017;79:12-22. DOI PubMed PMC
11. András IE, Garcia-Contreras M, Yanick C, et al. Extracellular vesicle-mediated amyloid transfer to neural progenitor cells: implications for RAGE and HIV infection. *Mol Brain* 2020;13:21. DOI PubMed PMC
12. d'Uscio LV, He T, Katusic ZS. Expression and processing of amyloid precursor protein in vascular endothelium. *Physiology* 2017;32:20-32. DOI PubMed PMC
13. Tachida Y, Miura S, Muto Y, et al. Endothelial expression of human amyloid precursor protein leads to amyloid β in the blood and induces cerebral amyloid angiopathy in knock-in mice. *J Biol Chem* 2022;298:101880. DOI PubMed PMC
14. Zenaro E, Piacentino G, Constantin G. The blood-brain barrier in Alzheimer's disease. *Neurobiol Dis* 2017;107:41-56. DOI PubMed PMC
15. Chen L, Choi JJ, Choi YJ, Hennig B, Toborek M. HIV-1 Tat-induced cerebrovascular toxicity is enhanced in mice with amyloid deposits. *Neurobiol Aging* 2012;33:1579-90. DOI PubMed PMC
16. Kalani A, Tyagi A, Tyagi N. Exosomes: mediators of neurodegeneration, neuroprotection and therapeutics. *Mol Neurobiol* 2014;49:590-600. DOI PubMed PMC
17. Joshi P, Benussi L, Furlan R, Ghidoni R, Verderio C. Extracellular vesicles in Alzheimer's disease: friends or foes? *Int J Mol Sci* 2015;16:4800-13. DOI PubMed PMC
18. Mathivanan S, Ji H, Simpson RJ. Exosomes: extracellular organelles important in intercellular communication. *J Proteomics* 2010;73:1907-20. DOI PubMed
19. Théry C, Ostrowski M, Segura E. Membrane vesicles as conveyors of immune responses. *Nat Rev Immunol* 2009;9:581-93. DOI PubMed
20. Luo X, Jean-Toussaint R, Sacan A, Ajit SK. Differential RNA packaging into small extracellular vesicles by neurons and astrocytes. *Cell Commun Signal* 2021;19:75. DOI PubMed PMC
21. Tian T, Wang Y, Wang H, Zhu Z, Xiao Z. Visualizing of the cellular uptake and intracellular trafficking of exosomes by live-cell microscopy. *J Cell Biochem* 2010;111:488-96. DOI PubMed
22. Hornung S, Dutta S, Bitan G. CNS-derived blood exosomes as a promising source of biomarkers: opportunities and challenges. *Front Mol Neurosci* 2020;13:38. DOI PubMed PMC
23. Song Z, Xu Y, Deng W, et al. Brain derived exosomes are a double-edged sword in Alzheimer's disease. *Front Mol Neurosci* 2020;13:79. DOI PubMed PMC
24. Shen Q, Wang Y, Kokovay E, et al. Adult SVZ stem cells lie in a vascular niche: a quantitative analysis of niche cell-cell interactions. *Cell Stem Cell* 2008;3:289-300. DOI PubMed PMC
25. DeRosa BA, Van Baaren JM, Dubey GK, et al. Derivation of autism spectrum disorder-specific induced pluripotent stem cells from peripheral blood mononuclear cells. *Neurosci Lett* 2012;516:9-14. DOI PubMed PMC
26. Paris D, Townsend KP, Obregon DF, Humphrey J, Mullan M. Pro-inflammatory effect of freshly solubilized β -amyloid peptides in the brain. *Prostaglandins Other Lipid Mediat* 2002;70:1-12. DOI PubMed
27. Kanekiyo T, Bu G. The low-density lipoprotein receptor-related protein 1 and amyloid- β clearance in Alzheimer's disease. *Front Aging Neurosci* 2014;6:93. DOI PubMed PMC
28. András IE, Eum SY, Toborek M. Lipid rafts and functional caveolae regulate HIV-induced amyloid beta accumulation in brain endothelial cells. *Biochem Biophys Res Commun* 2012;421:177-83. DOI PubMed PMC
29. Lam J, Katti P, Biete M, et al. A universal approach to analyzing transmission electron microscopy with imageJ. *Cells* 2021;10:2177. DOI PubMed PMC
30. Valente AJ, Maddalena LA, Robb EL, Moradi F, Stuart JA. A simple ImageJ macro tool for analyzing mitochondrial network morphology in mammalian cell culture. *Acta Histochem* 2017;119:315-26. DOI PubMed
31. Kerr JS, Adriaanse BA, Greig NH, et al. Mitophagy and Alzheimer's disease: cellular and molecular mechanisms. *Trends Neurosci* 2017;40:151-66. DOI PubMed PMC
32. Ribeiro MF, Genebra T, Rego AC, Rodrigues CMP, Solá S. Amyloid β peptide compromises neural stem cell fate by irreversibly disturbing mitochondrial oxidative state and blocking mitochondrial biogenesis and dynamics. *Mol Neurobiol* 2019;56:3922-36. DOI PubMed
33. Donato AJ, Morgan RG, Walker AE, Lesniewski LA. Cellular and molecular biology of aging endothelial cells. *J Mol Cell Cardiol* 2015;89:122-35. DOI PubMed PMC
34. Vieira HL, Alves PM, Vercelli A. Modulation of neuronal stem cell differentiation by hypoxia and reactive oxygen species. *Prog Neurobiol* 2011;93:444-55. DOI PubMed
35. Prozorovski T, Schneider R, Berndt C, Hartung HP, Aktas O. Redox-regulated fate of neural stem progenitor cells. *Biochim Biophys Acta* 2015;1850:1543-54. DOI PubMed

36. Batista AF, Rody T, Forny-Germano L, et al. Interleukin-1 β mediates alterations in mitochondrial fusion/fission proteins and memory impairment induced by amyloid- β oligomers. *J Neuroinflammation* 2021;18:54. DOI PubMed PMC
37. Hou Y, Ghosh P, Wan R, et al. Permeability transition pore-mediated mitochondrial superoxide flashes mediate an early inhibitory effect of amyloid beta1-42 on neural progenitor cell proliferation. *Neurobiol Aging* 2014;35:975-89. DOI PubMed PMC
38. Shen Q, Goderie SK, Jin L, et al. Endothelial cells stimulate self-renewal and expand neurogenesis of neural stem cells. *Science* 2004;304:1338-40. DOI PubMed
39. Deng W, Aimone JB, Gage FH. New neurons and new memories: how does adult hippocampal neurogenesis affect learning and memory? *Nat Rev Neurosci* 2010;11:339-50. DOI PubMed PMC
40. Drew LJ, Fusi S, Hen R. Adult neurogenesis in the mammalian hippocampus: why the dentate gyrus? *Learn Mem* 2013;20:710-29. DOI PubMed PMC
41. Mu Y, Gage FH. Adult hippocampal neurogenesis and its role in Alzheimer's disease. *Mol Neurodegener* 2011;6:85. DOI PubMed PMC
42. Kim TA, Chen L, Ge S. The interplay of neurovasculature and adult hippocampal neurogenesis. *Neurosci Lett* 2021;760:136071. DOI PubMed PMC
43. Deane R, Wu Z, Zlokovic BV. RAGE (Yin) versus LRP (Yang) balance regulates Alzheimer amyloid β -peptide clearance through transport across the blood-brain barrier. *Stroke* 2004;35:2628-31. DOI PubMed
44. van der Kant R, Goldstein LS. Cellular functions of the amyloid precursor protein from development to dementia. *Dev Cell* 2015;32:502-15. DOI PubMed
45. Zheng X, Boyer L, Jin M, et al. Metabolic reprogramming during neuronal differentiation from aerobic glycolysis to neuronal oxidative phosphorylation. *Elife* 2016;5:e13374. DOI PubMed PMC
46. Rybka V, Suzuki YJ, Gavriš AS, Dibrova VA, Gychka SG, Shults NV. Transmission electron microscopy study of mitochondria in aging brain synapses. *Antioxidants* 2019;8:171. DOI PubMed PMC
47. Andersen JV, Skotte NH, Christensen SK, Polli FS, Shabani M, et al. Hippocampal disruptions of synaptic and astrocyte metabolism are primary events of early amyloid pathology in the 5xFAD mouse model of Alzheimer's disease. *Cell Death Dis* 2021;12:954. DOI PubMed PMC
48. Takemura G, Onoue K, Kashimura T, Kanamori H, Okada H, et al. Electron microscopic findings are an important aid for diagnosing mitochondrial cardiomyopathy with mitochondrial DNA mutation 3243A>G. *Circ Heart Fail* 2016;9:e003283. DOI PubMed
49. Sabbah HN. Targeting the mitochondria in heart failure: a translational perspective. *JACC Basic Transl Sci* 2020;5:88-106. DOI PubMed PMC
50. Meshrkey F, Cabrera Ayuso A, Rao RR, Iyer S. Quantitative analysis of mitochondrial morphologies in human induced pluripotent stem cells for Leigh syndrome. *Stem Cell Res* 2021;57:102572. DOI PubMed
51. Reddy PH, Yin X, Manczak M, et al. Mutant APP and amyloid beta-induced defective autophagy, mitophagy, mitochondrial structural and functional changes and synaptic damage in hippocampal neurons from Alzheimer's disease. *Hum Mol Genet* 2018;27:2502-16. DOI PubMed PMC
52. Du M, Yu S, Su W, et al. Mitofusin 2 but not mitofusin 1 mediates Bcl-XL-induced mitochondrial aggregation. *J Cell Sci* 2020;133:jcs245001. DOI PubMed
53. Wang X, Su B, Siedlak SL, et al. Amyloid-beta overproduction causes abnormal mitochondrial dynamics via differential modulation of mitochondrial fission/fusion proteins. *Proc Natl Acad Sci USA* 2008;105:19318-23. DOI PubMed PMC
54. Pernas L, Scorrano L. Mito-Morphosis: mitochondrial fusion, fission, and cristae remodeling as key mediators of cellular function. *Annu Rev Physiol* 2016;78:505-31. DOI PubMed
55. Youle RJ, van der Bliek AM. Mitochondrial fission, fusion, and stress. *Science* 2012;337:1062-5. DOI PubMed PMC
56. Valenti D, Rossi L, Marzulli D, et al. Inhibition of Drp1-mediated mitochondrial fission improves mitochondrial dynamics and bioenergetics stimulating neurogenesis in hippocampal progenitor cells from a Down syndrome mouse model. *Biochim Biophys Acta Mol Basis Dis* 2017;1863:3117-27. DOI PubMed
57. Xin Y, Li J, Wu W, Liu X. Mitofusin-2: a new mediator of pathological cell proliferation. *Front Cell Dev Biol* 2021;9:647631. DOI PubMed PMC
58. Frezza C, Cipolat S, Martins de Brito O, et al. OPA1 controls apoptotic cristae remodeling independently from mitochondrial fusion. *Cell* 2006;126:177-89. DOI PubMed
59. Filadi R, Pendin D, Pizzo P. Mitofusin 2: from functions to disease. *Cell Death Dis* 2018;9:330. DOI PubMed PMC
60. Hu C, Shu L, Huang X, et al. OPA1 and MICOS Regulate mitochondrial crista dynamics and formation. *Cell Death Dis* 2020;11:940. DOI PubMed PMC
61. Cozzolino M, Ferraro E, Ferri A, et al. Apoptosome inactivation rescues proneural and neural cells from neurodegeneration. *Cell Death Differ* 2004;11:1179-91. DOI PubMed
62. Wang S, Zhang J, Deng X, Zhao Y, Xu K. Advances in characterization of SIRT3 deacetylation targets in mitochondrial function. *Biochimie* 2020;179:1-13. DOI PubMed
63. Palomer X, Román-Azcona MS, Pizarro-Delgado J, et al. SIRT3-mediated inhibition of FOS through histone H3 deacetylation prevents cardiac fibrosis and inflammation. *Signal Transduct Target Ther* 2020;5:14. DOI PubMed PMC
64. Dikalova AE, Pandey A, Xiao L, et al. Mitochondrial deacetylase Sirt3 reduces vascular dysfunction and hypertension while Sirt3 depletion in essential hypertension is linked to vascular inflammation and oxidative stress. *Circ Res* 2020;126:439-52. DOI PubMed

[PMC](#)

65. Guo X, Yan F, Li J, Zhang C, Su H, Bu P. SIRT3 ablation deteriorates obesity-related cardiac remodeling by modulating ROS-NF- κ B-MCP-1 signaling pathway. *J Cardiovasc Pharmacol* 2020;76:296-304. DOI [PubMed](#)

Review

Open Access



Emerging frontiers of cell-free DNA fragmentomics

Xi Hu^{1,2}, Spencer C. Ding^{1,2}, Peiyong Jiang^{1,2,3}

¹Centre for Novostics, Hong Kong Science Park, Pak Shek Kok, New Territories, Hong Kong, China.

²Li Ka Shing Institute of Health Sciences and Department of Chemical Pathology, The Chinese University of Hong Kong, Prince of Wales Hospital, Shatin, New Territories, Hong Kong, China.

³State Key Laboratory of Translational Oncology, The Chinese University of Hong Kong, Shatin, New Territories, Hong Kong, China.

Correspondence to: Prof. Peiyong Jiang, Centre for Novostics, Hong Kong Science Park, Pak Shek Kok, New Territories, Hong Kong, China. E-mail: jiangpeiyong@cuhk.edu.hk

How to cite this article: Hu X, Ding SC, Jiang P. Emerging frontiers of cell-free DNA fragmentomics. *Extracell Vesicles Circ Nucleic Acids* 2022;3:380-92. <https://dx.doi.org/10.20517/evcna.2022.34>

Received: 8 Jul 2022 **First Decision:** 29 Aug 2022 **Revised:** 10 Nov 2022 **Accepted:** 5 Dec 2022 **Published:** 21 Dec 2022

Academic Editor: Yoke Peng Loh **Copy Editor:** Ying Han **Production Editor:** Ying Han

Abstract

Analysis of cell-free DNA (cfDNA) in the blood has shown promise for monitoring a variety of biological processes. Plasma cfDNA is a mixture comprising DNA molecules released from various bodily tissues, mediated by characteristic DNA fragmentations occurring during cell death. Fragmentation of cfDNA is non-random and contains tissue-of-origin information, which has been demonstrated in circulating fetal, tumoral, and transplanted organ-derived cfDNA molecules. Many studies have elucidated a plurality of fragmentomic markers for noninvasive prenatal, cancer, and organ transplantation assessment, such as fragment sizes, fragment ends, end motifs, and nucleosome footprints. Recently, researchers have further revealed the large population of previously unidentified long cfDNA molecules (kilobases in size) in the plasma DNA pool. This review focuses on the emerging biological properties of cfDNA, together with a discussion on its potential clinical implications.

Keywords: Plasma DNA, urinary DNA, fragmentomics, pregnancy, oncology, transplantation, virology

INTRODUCTION

Liquid biopsy supports numerous approaches that are important for noninvasive prenatal testing (NIPT)^[1-3] and cancer detection^[4-7]. The use of maternal plasma DNA has enabled the rapid global adoption of NIPT for fetal chromosomal abnormalities in clinical practice, profoundly reducing unnecessary invasive tests.



© The Author(s) 2022. **Open Access** This article is licensed under a Creative Commons Attribution 4.0 International License (<https://creativecommons.org/licenses/by/4.0/>), which permits unrestricted use, sharing, adaptation, distribution and reproduction in any medium or format, for any purpose, even commercially, as long as you give appropriate credit to the original author(s) and the source, provide a link to the Creative Commons license, and indicate if changes were made.



Continuous efforts have been extended to noninvasive cancer detection, attempting to create a similar paradigm shift in oncology^[8]. Many studies have focused on deciphering new biological properties of cell-free DNA (cfDNA) molecules, aiming to further improve the performance of NIPT^[9] and achieve cfDNA-based cancer detection at the early stage of a tumor^[6]. This review focuses on several key characteristics of cfDNA that have been recently unveiled, including the properties of short and long cfDNA molecules, fragment ends, nucleosome footprints, and topological shapes, together with discussions on its potential clinical implications.

FRAGMENT SIZES

Short cfDNA molecules

Lo *et al.* deciphered the characteristic fragmentations of fetal and maternal DNA molecules in the maternal plasma DNA of a pregnant woman using massively parallel sequencing technology^[10]. There was a major peak at 166 bp in the respective fetal and maternal size profiles, with a series of 10-bp oscillations in short size ranges^[10], suggesting that the cfDNA molecules are possibly associated with nucleosomal structures. The size distribution of fetal cfDNA molecules displayed a secondary major peak at 143 bp, with enhanced amplitudes across the 10-bp oscillations. This observation suggests that the fetal cfDNA molecules are generally shorter than the maternal DNA molecules. Lo *et al.* speculated that the shortened size of the fetal DNA molecules might be in part attributed to the preferential trimming of approximately 20-bp linkers in the fetal genome as a result of less protection from histones^[10]. Hence, cfDNA fragmentation is non-random and is associated with tissues of origin. Many studies could reproduce similar characteristic size profiles in plasma DNA of healthy control individuals^[6] and patients with organ transplantations^[11], different cancers^[6,12], and autoimmune diseases^[13]. The liver-derived and tumor-derived cfDNA molecules were reported to be generally shorter than background DNA molecules of hematopoietic origin in patients with liver transplantation^[11] and various cancers^[6,12,14,15], respectively.

The discovery of these non-random cfDNA fragmentation patterns has promoted the emergence of novel diagnostic tools. Yu *et al.* used the principle that fetal DNA is shorter than maternal DNA molecules to develop an approach for detecting fetal chromosomal aneuploidies^[16]. The affected chromosome in a trisomic fetus would increase the relative contribution of fetal DNA molecules to the maternal plasma DNA pool, thus further enriching short cfDNA molecules from that chromosome. The affected chromosome in a monosomic fetus, however, would relatively reduce the contribution of short DNA molecules from that chromosome and display a lengthened size. Therefore, measuring cfDNA molecules could provide information on fetal chromosomal trisomy 21 and 18. This approach could achieve 100% sensitivity and specificity, as reported in the study^[16], which was comparable to the count-based approach^[2]. Importantly, the integrated analysis of fragment sizes and counts facilitated the determination of the fetal and/or maternal origin of the copy number aberrations seen in maternal plasma, thus supporting a more accurate interpretation of NIPT results^[9]. Moreover, the researcher attempted to enable the detection of fetal *de novo* mutations in the presence of the overwhelming maternal background DNA. The positive predictive value (PPV) was reported to be extremely low^[17]. In contrast, using the size-based bioinformatic filter together with adjusted read alignment parameters, fetal *de novo* mutations could be detected with a PPV that was two orders of magnitude higher than previously reported^[18].

These developments with fetal cfDNA have also encouraged researchers to actively explore the properties of tumor-derived cfDNA in plasma. Many studies have demonstrated that using size information could help achieve better performance in cancer detection. For example, Jiang *et al.* demonstrated that the PPV of detecting tumor-derived mutations in the plasma of hepatocellular carcinoma (HCC) patients could be improved by up to 85% by taking advantage of how the tumor-derived DNA is shorter than background

DNA^[6]. Using this similar analytical strategy, it was feasible to distinguish clonal hematopoiesis from tumor-derived mutations in plasma DNA^[19]. Additionally, Mouliere reported that an enhanced detection of tumor-derived DNA molecules could be achieved by fragment analysis, for example, by employing the physical size selection of shorter DNA molecules^[12].

Since it became clear that the 166-bp cfDNA molecules were related to the nucleosome core with the linker DNA, while the 143-bp cfDNA molecules represented the nucleosomal core without the linker^[10], “nucleosomal tracks” were constructed *in silico* by maternal plasma DNA data combined from hundreds of cases^[20]. The ratio of fragments starting within 73 bp upstream and downstream of the middle of the nucleosomal core deduced from the “nucleosomal tracks” was able to inform the fetal DNA fraction^[20]. The fetal DNA fraction is a crucial parameter for NIPT. Such nucleosomal tracks could also be reproduced in patients with different cancers, with the use of a metric called window protection score (WPS)^[21]. The WPS was defined as the number of molecules spanning a 120-bp genomic window minus those ending within that window^[21].

Esfahani *et al.* recently demonstrated that using the size variability of the cfDNA fragments surrounding the transcription start sites (TSS) helped predict the expression levels of genes^[22]. The transcriptionally active regions tended to have decreased nucleosome occupancies, conferring more random cleavages and higher DNA fragment length variability. A metric called promoter fragmentation entropy (PFE) was used to quantify such variability in cfDNA fragments originating from promoter regions [Figure 1, Bottom left]. PFE was found to be strongly correlated with RNA expression levels. To further evaluate the clinical utility of PFE, Esfahani *et al.* used targeted deep sequencing of selected biomarker gene promoters that had tumor-specific RNA expression profiles, called “epigenetic expression inference from cell-free DNA-sequencing” (EPIC-seq)^[22]. This method could distinguish lung carcinoma subtypes, with the area under the receiver operating characteristic curve (AUC) values of 0.91 and 0.83 in the training and validation datasets, respectively, for distinguishing individuals with non-small cell lung cancer from controls. The measurement of fragment size variability in gene promoters could provide noninvasive biomarkers for cancer detection. Notably, 90% of the patients were detected at the late stage of cancer (stage III or IV) for PFE-based EPIC-seq data analysis. Moreover, many recent studies have demonstrated that fragmentation patterns could serve as biomarkers for predicting treatment outcomes, such as recurrences of nasopharyngeal carcinoma (NPC)^[23], treatment outcomes of diffuse large B-cell lymphoma (DLBCL)^[24], and response to immunotherapy^[22].

The size characteristics described above were based on double-stranded DNA sequencing library preparation. Interestingly, several recent studies revealed the presence of single-stranded cfDNA molecules in maternal plasma DNA, showing the significant enrichment of short DNA molecules^[25,26]. However, the fetal DNA fraction appeared to be similar between results generated by single-stranded and double-stranded DNA sequencing preparations^[25]. Furthermore, some studies demonstrated that a considerable population of plasma cfDNA fragments centered at ~50 bp was present in the plasma DNA pool using modified single-stranded DNA library preparations. These included combining high-affinity magnetic bead-based DNA extraction with single-stranded DNA sequencing library preparation^[27] and adjusting the concentration of isopropanol to retain the low molecular weight nucleic acids for downstream analysis^[28]. Notably, such ultrashort cfDNA fragments were found to be enriched in the accessible chromatin regions of blood cells, particularly in promoter regions that potentially harbor G-quadruplex (G4) DNA secondary structures [Figure 1, Bottom left]. G4-positive promoter chromatin accessibility was reportedly decreased in cancer patients, potentially providing another type of biomarker for cancer detection^[27].

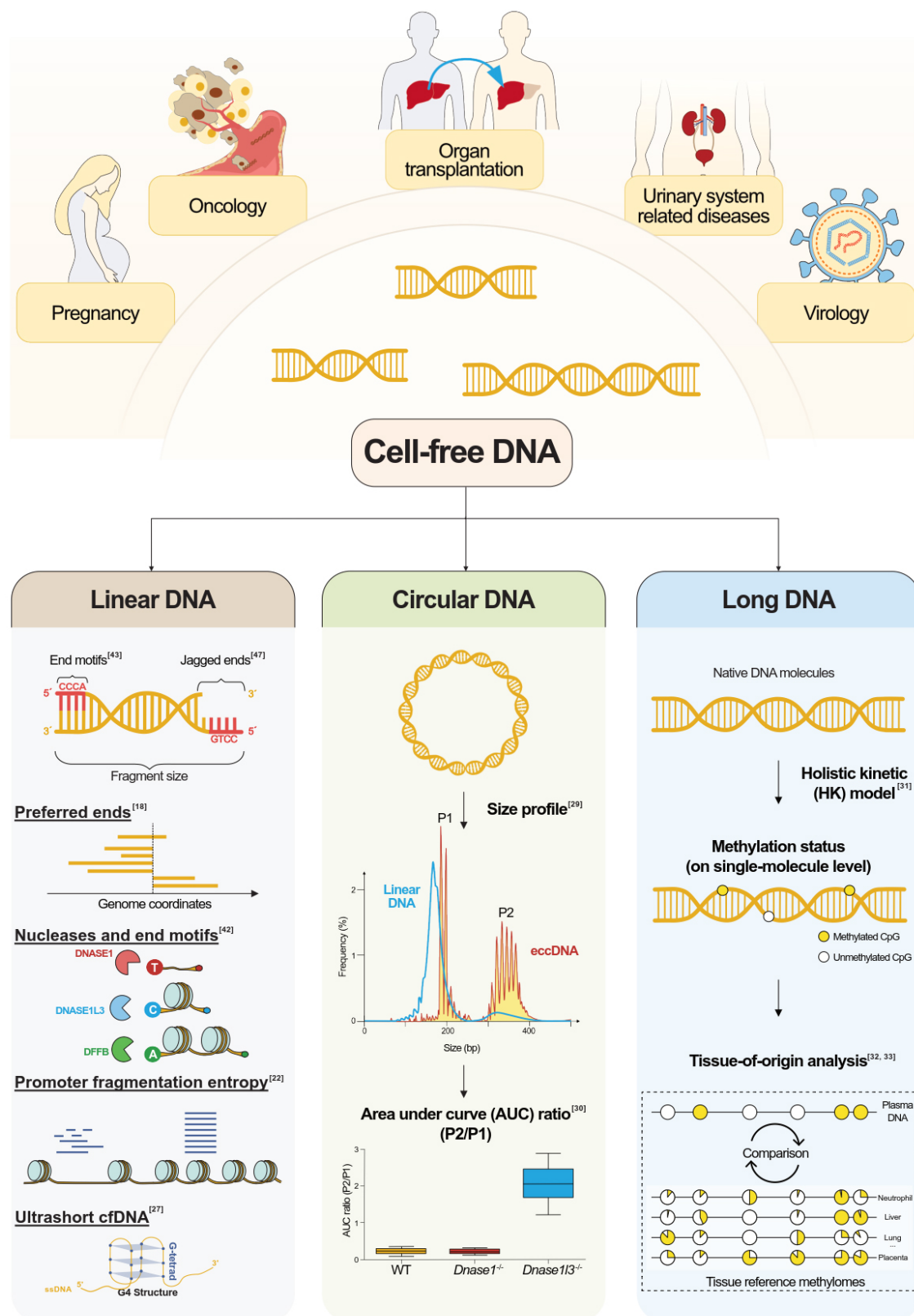


Figure 1. Summary of the emerging frontier of cell-free DNA and potential clinical implications. (Top) Cell-free DNA (cfDNA) is a mixture of fragments released from various healthy and diseased cells in different tissues. The fragmentation of cfDNA is non-random, bearing information directly related to the tissue of origin. In addition, cfDNA methylation can also be used to trace each cfDNA molecule's cellular identity, showing promise for various clinical applications. The fragmentomic and epigenetic analyses of cfDNA offer the opportunity to develop novel diagnostic tools for assessing pregnancy, oncology, organ transplantation, urinary system-related diseases, and virology. (Bottom left) Non-random fragmentation of cfDNA molecules can be reflected by fragment sizes, preferred ends, end motifs, jagged ends, nuclease activities, promoter fragmentation entropy, as well as ultrashort cfDNA. (Bottom middle) Extrachromosomal circular DNA (eccDNA) has a different size profile compared with linear DNA. In human plasma DNA, linear DNA has a pronounced peak at ~166 bp. In contrast, eccDNA has two prominent peaks, the first peak (P1) is at ~200 bp and the second peak (P2) is at ~350 bp^[29]. Interestingly, the area under curve (AUC) ratio of P2 to P1 is significantly increased in *Dnase1/3* knockout mouse (*Dnase1/3*^{-/-}) plasma DNA, whereas *Dnase1*^{-/-} mice do not show an apparent difference from wildtype mice (WT). This suggests that DNASE1L3 possibly prefers to cut long eccDNA^[30]. (Bottom right) A large population of long cfDNA molecules was recently observed in plasma using single-molecule real-time sequencing. The direct methylation detection of native cfDNA molecules enables the determination of tissue of origin for each single cfDNA molecule^[31-33].

Long cfDNA molecules

In contrast to most studies focusing on short DNA molecules (< 500 bp), Yu *et al.* recently revealed the existence of long fetal DNA in maternal plasma by single-molecule real-time (SMRT) sequencing (Pacific Biosciences, PacBio)^[32]. A substantial proportion of long fetal cfDNA molecules was detected in maternal plasma DNA, with 15.5%, 19.8%, and 32.3% in the first, second, and third trimesters of gestation, respectively. The longest fetal cfDNA was more than 23 kb in length. Yu *et al.* further elucidated that the proportion of long cfDNA molecules could serve as a biomarker for preeclampsia. Compared with the short-read sequencing technology (Illumina), the size metric deduced by SMRT sequencing showed a better differentiation between pregnancies with and without preeclampsia^[32]. The previous short-read sequencing technologies (Illumina) were not suited for long cfDNA molecule analysis because bridge amplification on sequencing flow cells does not favor long DNA molecules^[34,35].

The presence of long cfDNA in plasma^[32] could extend the boundary of liquid biopsy from short cfDNA molecules to kilobase-long cfDNA molecules. One important implication of the presence of long cfDNA in plasma is that the use of methylation patterns across a series of CpGs in a long cfDNA molecule theoretically makes it possible to determine the tissue of origin for each plasma DNA molecule [Figure 1, Bottom right]. With the use of an artificial intelligence algorithm, Tse *et al.* demonstrated direct methylation detection of a native DNA molecule using the kinetic signals generated by a DNA polymerase during SMRT sequencing [the holistic kinetic (HK) model]^[31]. Thus, the cell identity of each individual plasma DNA molecule could be traced by the “intrinsic molecular barcode” through the HK model. Yu *et al.* demonstrated such a concept in the maternal plasma of pregnant women, leveraging the abundance of CpG sites on long DNA molecules to identify the fetal-derived DNA molecules with an accuracy of 0.88^[32]. Another independent study illustrated that single-molecule sequencing (PacBio) enabled long cfDNA detection and direct methylation analysis for cancer patients^[36]. Such a proof-of-concept study showed that using long cfDNA molecules could enhance the discriminative power up to an AUC of 0.91, compared with short cfDNA with an AUC of 0.75^[36]. Hence, a previously unidentified long cfDNA population may open many new possibilities for liquid biopsy in NIPT and cancer detection.

FRAGMENT ENDS

Preferred Ends

The characteristic size patterns of cfDNA from various tissues indicate the non-random cleavages occurring across genomes during DNA fragment shedding into blood circulation. From results of ultra-deep sequencing of maternal plasma DNA, it was reported that a subset of genomic coordinates over-represented cfDNA fragment ends, which are referred to as “preferred ends”^[18] [Figure 1, Bottom left]. The plasma DNA molecules terminating at those preferred ends exhibited tissue specificity. For example, those cfDNA

molecules from fetal-preferred ends were shorter in size and correlated with fetal DNA fractions^[18]. Additionally, preferred ends were clustered in line with nucleosomal patterns^[37], pervasively existing in various tissues, such as liver-specific preferred ends in the plasma of patients with liver transplantation and tumor-specific preferred ends in HCC patients^[37]. Using tumor-preferred ends in plasma DNA could facilitate HCC detection, with an AUC of 0.88^[37]. As a large number of preferred ends would be present in plasma DNA, the in-depth analysis of preferred ends potentially paves the way to the sensitive detection of cancer at its early stage^[37,38].

End Motifs

Researchers studied the compositions for several nucleotides (denoted by “k”) proximal to the 5’ end of a cfDNA molecule, namely k-mer end motifs [Figure 1, Bottom left]. Some previous studies showed that the 5’ end motifs of plasma DNA preferentially started with “C” nucleotides^[39,40]. However, the biological mechanism for generating plasma end motifs was still obscure in these studies. The tissue specificity and clinical utility regarding plasma DNA end motifs had not been explored at that time. Recently, Serpas *et al.* used knockout (KO) mice models to reveal that the plasma DNA size and end motifs profile were associated with DNA nucleases^[41]. It was reported that the top six 4-mer end motifs (a total of 256 motifs), which all started with “CC” in WT mouse plasma (7.4%), significantly declined in mice with *Dnase1l3* deletion (4.2%). In contrast, no significant effect was present with *Dnase1* KO in one study^[41]. DNASE1L3 was thus believed to be an important DNA nuclease for generating “CC” ends of plasma DNA molecules.

To determine whether the effect of DNASE1L3 is at a systemic or local tissue level, Serpas *et al.* designed one experiment using a pregnant mouse model in which *Dnase1l3*^{-/-} mice (no functional copy of the *Dnase1l3* gene) were pregnant with *Dnase1l3*^{+/-} fetuses (one functional copy of the *Dnase1l3* gene). A partial normalization of end motifs was observed for both maternal and fetal DNA, with a higher degree of end motif restoration for fetal DNA molecules^[41]. Therefore, DNASE1L3 was believed to act on plasma DNA fragmentation in both a systemic and local manner. The distinct roles of DNASE1, DNASE1L3, and DNA Fragmentation Factor Subunit Beta (DFFB) on cfDNA fragmentation were further demonstrated with the use of different KO mouse models combined with various *in vitro* blood incubations^[42]. Han *et al.* found that the generation of cfDNA molecules might involve a series of DNA nucleases that function in a stepwise manner, including extracellular and intracellular levels. Such a stepwise nuclease-mediated cfDNA fragmentation model suggested that the cfDNA was initially cleaved intracellularly with DFFB, preferentially forming A-end fragments, followed by cleavage events mediated by DNASE1L3 and DNASE1, preferentially producing C-end fragments and T-end fragments, respectively^[42].

Intriguingly, alterations of DNASE1L3-cutting signatures (“CC” end motifs) could be mirrored in the plasma of human subjects with DNASE1L3 deficiency. These included patients with familial monogenic systemic lupus erythematosus (SLE) with DNASE1L3 mutations and many cancers with downregulated DNASE1L3 expression. For example, the most frequently observed end motif in the plasma of healthy human subjects was CCCA, while this end motif was significantly decreased in patients with HCC, colorectal cancer, lung cancer, nasopharyngeal carcinoma, and head and neck squamous cell carcinoma^[43]. Making full use of 256 motifs achieved an AUC value of 0.86 in differentiating patients with and without cancers. Many other groups were used to validate a number of potential clinical applications by employing plasma DNA end motifs^[38,44,45]. Moreover, transducing *Dnase1l3* into *Dnase1l3*-deficient mice could partially restore the altered end motif profiles of *Dnase1l3*-deficient mice to the profiles of WT mice^[46]. Taken together, the analysis of nuclease-associated cutting signatures could provide potential diagnostic tools for detecting and monitoring various diseases associated with DNA nuclease activities.

Jagged ends

Double-stranded plasma DNA was generally subjected to end-repair steps that experimentally altered the ends, but whether single-stranded DNA exists at the ends of a double-stranded cfDNA molecule (referred to as jagged ends) has remained unknown for many years [Figure 1, Bottom left]. To address this research gap in the area of fragmentomics, Jiang *et al.* used the DNA end-repair process to introduce differential methylation signals into the complementary strand of the single-stranded jagged end^[47]. The resulting methylation signal density in the newly generated strand reflected the quantity of jagged ends. Jiang *et al.* found that plasma DNA molecules contained a significantly higher level of jaggedness than the sonicated DNA molecules, with 88% of plasma DNA molecules carrying jagged ends. Interestingly, the property of plasma DNA jagged ends appears to be associated with tissue of origin. For instance, in pregnant women, the fetal DNA was shown to harbor higher jaggedness than background DNA molecules mainly of hematopoietic origin. A similar pattern was observed in tumor-derived DNA molecules in plasma from HCC patients^[47].

Ding *et al.* recently elucidated the relationship between the jagged end length and nucleosomal structures when the DNA nuclease activity of DNASE1, DFFB, or DNASE1L3 is changed^[48]. This study concluded that DNASE1 was responsible for jagged ends across a wide size range, extending from linker DNA to the nucleosomal core. DFFB tended to generate blunt or short jagged ends in linker DNA between two nucleosomes. DNASE1L3 would play different roles in short and long cfDNA molecules. In particular, the deletion of DNASE1L3 would increase the jaggedness in fragments shorter than 150 bp, but decrease the jaggedness in fragments involving multi-nucleosomal structures. The aberration in plasma DNA jaggedness could serve as a biomarker for human subjects with SLE^[48].

FRAGMENT SHAPES

In addition to the linear form of cfDNA molecules, many recent studies focused on another topological form of cfDNA, namely the circular cfDNA. Ma *et al.* revealed the existence of a large proportion of mitochondrial DNA (mtDNA) in its original circular form (~16.5 kb) in plasma after digestion of plasma DNA with a restriction enzyme^[49,50] [Figure 1, Bottom middle]. The main population of mtDNA derived from the liver was in linear form (91%). In contrast, the majority of mtDNA derived from the hematopoietic system was in circular form (88%). Thus, the topological forms of plasma DNA would be related to the tissue of origin. Sin *et al.* extended the members related to topological forms to extrachromosomal circular DNA (eccDNA)^[29]. EccDNA molecules could be found in the maternal plasma DNA of pregnant women, but at a relatively low abundance^[29]. Sin *et al.* further demonstrated that the size distribution of eccDNA molecules is notably different from that of linear cfDNA molecules. EccDNA molecules exhibit two major peaks at 202 bp and 338 bp with a series of sharp 10-bp periodicities^[29] [Figure 1, Bottom middle], suggesting that the generation of eccDNA might also involve nucleosomal structures. The peak at 202 bp might be attributed to one nucleosome core and two linkers, while the 338-bp peak might comprise two nucleosome cores and two linkers^[29,51]. Although there are distinct characteristics between eccDNA and linear plasma DNA, the clearance rates between topological forms did not show a significant difference in the plasma of pregnant women^[51]. Such an observation seems paradoxical to the previous speculation that the structure of eccDNA might be more stable in plasma^[52].

Like linear cfDNA, eccDNA molecules also exhibit tissue-specific properties. Compared with the maternal-derived DNA, the fetal-derived eccDNA appeared to be shorter and hypomethylated. Moreover, eccDNA fragments at the secondary peak cluster (~338 bp) had higher methylation in comparison with the first peak cluster (~202 bp)^[29,51]. Hence, DNA methylation might play a role in forming the biological properties of eccDNA molecules. Cell-free eccDNA in *Dnase1l3*^{-/-} mice were larger in size than those in WT mice^[30].

Therefore, DNASE1L3 was suggested to be one of the nucleases involved in digesting eccDNA. Because there were no observable changes in sizes for those eccDNA molecule identified from cellular DNA between WT and *Dnase1l3*^{-/-} mice, DNASE1L3 might play a role in digesting eccDNA extracellularly rather than intracellularly. This finding provided a biological link between nuclease activities and properties of eccDNA in plasma^[30] [Figure 1, Bottom middle]. However, eccDNA biogenesis has yet to be fully elaborated. A large percentage of eccDNA molecules contained or were proximal to short direct repeats, suggesting that eccDNA generation might in part involve the microhomology-directed repair^[53].

OTHER TYPES OF LIQUID BIOPSIES

In addition to the intensive studies on cfDNA in plasma, there is growing research interest in urinary cell-free DNA (ucfDNA) molecules that comprise a myriad of important molecular information. One advantage of using ucfDNA is that the urine could be readily sampled repeatedly for surveillance after surgery. Similar to plasma cfDNA, ucfDNA is a mixture containing DNA molecules derived from various tissues, including kidneys, bladders, and blood cells. The tissue origin of ucfDNA could be traced by using its methylation patterns. From the data generated from pregnant women^[54] and patients with kidney transplantation^[55], two general pathways related to the generation of ucfDNA were elaborated. The first pathway could be cfDNA in blood circulation passing through the glomerular filtration (referred to as transrenal ucfDNA), while the other might be directly contributed by the urinary system (referred to as postrenal ucfDNA).

Owing to the overwhelming activity of DNASE1^[56] and the weakened interaction between DNA molecules and histones in the presence of urea, fragmentomic patterns of ucfDNA are distinctive from that in plasma. In contrast to the major size peak of 166 bp in plasma cfDNA, ucfDNA molecules are highly enriched in fragments smaller than 100 bp in size and with enhanced 10-bp periodicities^[54,56-58]. Chen *et al.* revealed that the DNASE1L3 cutting signature (“C”-end motifs) was relatively diminished in ucfDNA molecules, whereas the DNASE1 cutting signatures (“T”-end motifs) were greatly overrepresented^[56]. Moreover, a higher jaggedness in ucfDNA molecules was observed when compared with that in plasma cfDNA molecules^[56,59,60]. Of note, the ucfDNA fragmentation appeared to be time-dependent. For example, the *in vitro* incubation of urine at 37 °C resulted in a constant decrease in ucfDNA concentration, an increase in the amplitude of 10-bp oscillations^[57], and an increase in jaggedness^[59].

Compared with traditional invasive cystoscopy^[61,62], bladder cancer could be detected noninvasively using combined fragmentomic patterns in ucfDNA, with a sensitivity of 93.5% and specificity of 95.8%^[58]. One previous study showed that serial monitoring of the ucfDNA in renal transplant patients allowed for assessing the transplant allograft status^[58]. Furthermore, some studies demonstrated that using ucfDNA could more sensitively detect patients with bladder cancer than plasma cfDNA^[63,64]. These promising findings suggested that the use of ucfDNA could be complementary to the existing plasma cfDNA-based approaches, potentially maximizing the overall diagnostic performance.

Moreover, other types of liquid biopsies, such as cerebrospinal fluid (CSF), have also attracted recent research interest. Mouliere *et al.* demonstrated that the analysis of CSF had improved the detection of patients with brain tumors, compared with either the use of urinary or plasma cfDNA^[65]. Wu *et al.* studied non-small cell lung cancer patients with leptomeningeal metastases and revealed that 100% of driver mutations were detected in CSF, whereas only 57.8% were detected in paired plasma cfDNA^[66]. Interestingly, the size shortening of tumor-derived cfDNA was consistently observed in CSF, plasma, and urine samples of glioma patients^[65]. In addition, the short cfDNA (< 150 bp) in CSF was significantly higher than those in plasma cfDNA^[66].

VIRAL CFDNA MOLECULES

Circulating viral cfDNA molecules have also attracted a lot of recent research interest, showing promise in the detection of cancer types driven by viruses. Using real-time quantitative PCR, Lo *et al.* demonstrated that the detection rate of circulating Epstein-Barr virus (EBV) DNA in plasma was 96% in nasopharyngeal carcinoma (NPC) patients, which was much higher than in controls (7%)^[67]. Advanced-stage NPC patients had higher EBV DNA quantity than early-stage patients. The results suggested that the EBV cfDNA could serve as a biomarker for NPC. However, because the NPC incidence is very low, the 7% false positivity would lead to a low PPV. Subsequently, the same group adopted a two-time-point testing approach so that a participant with initially positive EBV DNA in plasma at the first test was required to provide another blood sample for a second EBV DNA test within 4 weeks. Only someone determined to be positive at both time points was confirmed as a positive case. Using a prospective cohort of 20,174 participants, Chan *et al.* elucidated that such an approach provided a promising screening tool for NPC among asymptomatic individuals^[68], improving the PPV from 3.1% to 11.0% (single-time-point testing), making it possible to identify the majority of NPC patients (75%) at an early stage.

Using massively parallel sequencing targeted to the EBV genome, Lam *et al.* revealed the differential size profiles of circulating EBV DNA between patients with and without NPC^[69]. NPC patients generally had a higher amount of circulating EBV DNA, exhibiting higher proportions of longer EBV DNA fragments in plasma than individuals without NPC^[69]. By leveraging the EBV DNA quantity and EBV DNA size characteristics, the PPV for detecting NPC could be improved to 19.6%, with a 100% sensitivity. Another advantage of the massively parallel sequencing-based test is that it only requires a single blood draw.

Furthermore, it was observed that plasma EBV DNA in NPC patients was hypermethylated. By combining such differential methylation signals, the performance of the NPC test could be further improved, achieving a PPV of 35.1%. These studies indicate that the fragmentomic and epigenetic properties of viral cfDNA are important features for developing sensitive tools for virus-driven cancers. Additionally, Linthorst *et al.* found distinct fragmentation patterns for several DNA viruses compared with human cfDNA, such as adeno-associated virus (AAV), herpes simplex virus (HSV), varicella-zoster virus (VZV), cytomegalovirus (CMV), herpesvirus (HHV), torque teno virus (TTV), hepatitis B virus (HBV), and human papillomavirus (HPV), in maternal plasma DNA of pregnant women^[70]. However, the biological and clinical implications for viral DNA in pregnancies remained elusive.

PRE-ANALYTICAL CONSIDERATIONS FOR CFDNA ANALYSIS

Apart from the progress in the field of cfDNA fragmentation, it is still necessary to optimize and standardize the pre-analytical steps during clinical implementation. Plasma DNA was predominantly derived from the hematopoietic system^[71]. The other solid tissues, such as the liver, placenta, lung, and tumor tissues, generally contribute a small amount of DNA to blood circulation^[10,72-74]. The released cellular genomic DNA (gDNA) from blood cells into plasma during the delayed blood processing would dilute the signals of interest, such as fetal DNA and tumoral DNA. To minimize blood coagulation and its associated cell death, the EDTA tube is commonly used for blood collection for plasma DNA analysis. However, a previous study demonstrated that gDNA contamination would be introduced into plasma after the blood was stored for more than 6 h before plasma isolation^[75]. New commercial tube types were developed to control the quality of plasma samples. It was reported that the Streck tube was better than the EDTA tube for preserving plasma samples^[76].

Moreover, the fragmentomic profiling of cfDNA molecules is mainly based on double-stranded DNA library preparation. Compared with double-stranded DNA library preparation in short-read sequencing,

some studies reported that single-stranded DNA library preparation would be biased toward the ultra-short cfDNA molecules^[25,26]. Some recently developed methods for enriching ultra-short single-stranded cfDNA demonstrated the potential for cancer detection^[27,77,78].

In addition to the analysis of long cfDNA molecules using SMRT sequencing (PacBio), nanopore sequencing (Oxford Nanopore technologies, ONT) could also enable direct, real-time analysis of long cfDNA. Yu *et al.* recently published a study comparing PacBio technology and ONT for cfDNA analysis^[33]. Notably, both platforms showed the preference to sequence longer DNA fragments, with a stronger bias for PacBio technology. For example, percentages of cfDNA fragments > 500 bp in PacBio were approximately 6-fold higher than in ONT^[33]. Both PacBio and ONT could generate similar cfDNA end motif profiles, yet displayed platform-dependent patterns. Both platforms achieved a comparable performance of tissue-of-origin analysis based on single-molecule methylation patterns. Although SMRT sequencing generated data with higher percentages of long cfDNA compared with ONT sequencing, a higher absolute number of long cfDNA fragments eligible for the tissue-of-origin analysis were obtained from ONT sequencing because of its much higher sequencing throughput. When analyzing the size and end motif of cfDNA, one should be aware of the analytical characteristics and possible biases of the sequencing platforms being used.

CONCLUSION

Fragmentation patterns of cfDNA molecules contain a wealth of molecular information related to the tissue of origin. The emerging classes of fragmentomic features, such as long cfDNA molecules, eccDNA, and size modalities around TSS, could accelerate the development of high-performance diagnostic tools for NIPT, cancer detection, monitoring of organ transplantation, and the detection of other diseases such as autoimmune diseases. One advantage of using fragmentomic features is potentially a large number of markers available for differentiating the signals derived from tumor and non-tumor cells at the early stage of cancer, with the ability to localize the tumor. In the NIPT field, the detection of fragmentation aberrations in plasma DNA would expand the diagnostic applications beyond the current focus on chromosomal aberrations. For transplant monitoring, the development of fragmentomic markers would provide an alternative to genetic markers for detecting transplant rejection. The mechanistic understanding of the properties of long cfDNA molecules is still in its infancy. The emerging concept that methylation patterns of long cfDNA molecules serve as intrinsic “molecular barcodes” for tracing the tissues of origin at single-molecule resolution needs to be further elucidated in the various diagnostic applications. Of note, the future standardization of experimental procedures would enhance the overall diagnostic performance when implementing those fragmentation-based approaches in clinical settings.

DECLARATIONS

Acknowledgments

The authors would like to thank Dr. Mary-Jane L. Ma for her suggestions in the graphical presentation.

Authors' contributions

Drafted and revised the manuscript: Hu X, Ding SC, Jiang P

Availability of data and materials

Not applicable.

Financial support and sponsorship

This work was supported by the Innovation and Technology Commission (InnoHK Initiative).

Conflicts of interest

Jiang P holds equity in DRA and Grail/Illumina. Jiang P is a consultant to Take2. Jiang P is a Director of DRA and KingMed Future. Other authors declared that there are no conflicts of interest.

Ethical approval and consent to participate

Not applicable.

Consent for publication

Not applicable.

Copyright

© The Author(s) 2022.

REFERENCES

1. Lo YMD, Corbetta N, Chamberlain PF, et al. Presence of fetal DNA in maternal plasma and serum. *Lancet* 1997;350:485-7. DOI PubMed
2. Chiu RWK, Chan KCA, Gao Y, et al. Noninvasive prenatal diagnosis of fetal chromosomal aneuploidy by massively parallel genomic sequencing of DNA in maternal plasma. *Proc Natl Acad Sci USA* 2008;105:20458-63. DOI PubMed PMC
3. van der Meij KR, Sistermans EA, Macville MV, et al. TRIDENT-2: national implementation of genome-wide non-invasive prenatal testing as a first-tier screening test in the Netherlands. *Am J Hum Genet* 2019;105:1091-101. DOI PubMed PMC
4. Chan KCA, Jiang P, Chan CWM, et al. Noninvasive detection of cancer-associated genome-wide hypomethylation and copy number aberrations by plasma DNA bisulfite sequencing. *Proc Natl Acad Sci USA* 2013;110:18761-8. DOI PubMed PMC
5. Chan KA, Jiang P, Zheng YW, et al. Cancer genome scanning in plasma: detection of tumor-associated copy number aberrations, single-nucleotide variants, and tumoral heterogeneity by massively parallel sequencing. *Clin Chem* 2013;59:211-24. DOI PubMed
6. Jiang P, Chan CWM, Chan KCA, et al. Lengthening and shortening of plasma DNA in hepatocellular carcinoma patients. *Proc Natl Acad Sci USA* 2015;112. DOI PubMed PMC
7. Phallen J, Sausen M, Adleff V, et al. Direct detection of early-stage cancers using circulating tumor DNA. *Sci Transl Med* 2017;9:eaan2415. DOI PubMed PMC
8. Lo YMD, Han DSC, Jiang P, Chiu RWK. Epigenetics, fragmentomics, and topology of cell-free DNA in liquid biopsies. *Science* 2021;372:eaaw3616. DOI PubMed
9. Yu SCY, Jiang P, Chan KCA, et al. Combined count- and size-based analysis of maternal plasma DNA for noninvasive prenatal detection of fetal subchromosomal aberrations facilitates elucidation of the fetal and/or maternal origin of the aberrations. *Clin Chem* 2017;63:495-502. DOI PubMed
10. Lo YMD, Chan KCA, Sun H, et al. Maternal plasma DNA sequencing reveals the genome-wide genetic and mutational profile of the fetus. *Sci Transl Med* 2010;2. DOI PubMed
11. Zheng YWL, Chan KCA, Sun H, et al. Nonhematopoietically derived DNA is shorter than hematopoietically derived DNA in plasma: a transplantation model. *Clin Chem* 2012;58:549-58. DOI PubMed
12. Mouliere F, Chandrananda D, Piskorz AM, et al. Enhanced detection of circulating tumor DNA by fragment size analysis. *Sci Transl Med* 2018;10:eaat4921. DOI PubMed PMC
13. Chan RWY, Jiang P, Peng X, et al. Plasma DNA aberrations in systemic lupus erythematosus revealed by genomic and methylomic sequencing. *Proc Natl Acad Sci USA* 2014;111. DOI PubMed PMC
14. Underhill HR, Kitzman JO, Hellwig S, et al. Fragment length of circulating tumor DNA. *PLoS Genet* 2016;12:e1006162. DOI PubMed PMC
15. Diehl F, Li M, Dressman D, et al. Detection and quantification of mutations in the plasma of patients with colorectal tumors. *Proc Natl Acad Sci USA* 2005;102:16368-73. DOI PubMed PMC
16. Yu SCY, Chan KCA, Zheng YWL, et al. Size-based molecular diagnostics using plasma DNA for noninvasive prenatal testing. *Proc Natl Acad Sci USA* 2014;111:8583-8. DOI PubMed PMC
17. Kitzman JO, Snyder MW, Ventura M, et al. Noninvasive whole-genome sequencing of a human fetus. *Sci Transl Med* 2012;4. DOI PubMed PMC
18. Chan KCA, Jiang P, Sun K, et al. Second generation noninvasive fetal genome analysis reveals de novo mutations, single-base parental inheritance, and preferred DNA ends. *Proc Natl Acad Sci USA* 2016;113. DOI PubMed PMC
19. Marass F, Stephens D, Ptashkin R, et al. Fragment size analysis may distinguish clonal hematopoiesis from tumor-derived mutations in cell-free DNA. *Clin Chem* 2020;66:616-8. DOI PubMed PMC
20. Straver R, Oudejans CBM, Sistermans EA, Reinders MJT. Calculating the fetal fraction for noninvasive prenatal testing based on genome-wide nucleosome profiles. *Prenat Diagn* 2016;36:614-21. DOI PubMed PMC
21. Snyder M, Kircher M, Hill A, Daza R, Shendure J. Cell-free DNA comprises an in vivo nucleosome footprint that informs its tissues-

- of-origin. *Cell* 2016;164:57-68. DOI PubMed PMC
22. Esfahani MS, Hamilton EG, Mehrmohamadi M, et al. Inferring gene expression from cell-free DNA fragmentation profiles. *Nat Biotechnol* 2022;40:585-97. DOI PubMed PMC
 23. Chan D, Lam W, Hui E, et al. Improved risk stratification of nasopharyngeal cancer by targeted sequencing of Epstein–Barr virus DNA in post-treatment plasma. *Ann Oncol* 2022;33:794-803. DOI PubMed
 24. Meriranta L, Alkods A, Pasanen A, et al. Molecular features encoded in the ctDNA reveal heterogeneity and predict outcome in high-risk aggressive B-cell lymphoma. *Blood* 2022;139:1863-77. DOI PubMed
 25. Vong JSL, Tsang JCH, Jiang P, et al. Single-Stranded DNA library preparation preferentially enriches short maternal DNA in maternal plasma. *Clin Chem* 2017;63:1031-7. DOI PubMed
 26. Burnham P, Kim MS, Agbor-enoh S, et al. Single-stranded DNA library preparation uncovers the origin and diversity of ultrashort cell-free DNA in plasma. *Sci Rep* 2016;6. DOI PubMed PMC
 27. Hudecova I, Smith CG, Hänsel-hertsch R, et al. Characteristics, origin, and potential for cancer diagnostics of ultrashort plasma cell-free DNA. *Genome Res* 2022;32:215-27. DOI PubMed PMC
 28. Cheng J, Morselli M, Huang W, et al. Plasma contains ultrashort single-stranded DNA in addition to nucleosomal cell-free DNA. *iScience* 2022;25:104554. DOI PubMed PMC
 29. Sin STK, Jiang P, Deng J, et al. Identification and characterization of extrachromosomal circular DNA in maternal plasma. *Proc Natl Acad Sci USA* 2020;117:1658-65. DOI PubMed PMC
 30. Sin ST, Deng J, Ji L, et al. Effects of nucleases on cell-free extrachromosomal circular DNA. *JCI Insight* 2022;7:e156070. DOI PubMed PMC
 31. Tse OYO, Jiang P, Cheng SH, et al. Genome-wide detection of cytosine methylation by single molecule real-time sequencing. *Proc Natl Acad Sci USA* 2021;118. DOI PubMed PMC
 32. Yu SCY, Jiang P, Peng W, et al. Single-molecule sequencing reveals a large population of long cell-free DNA molecules in maternal plasma. *Proc Natl Acad Sci USA* 2021;118. DOI PubMed PMC
 33. Yu SCY, Deng J, Qiao R, et al. Comparison of Single Molecule, Real-Time Sequencing and Nanopore Sequencing for Analysis of the Size, End-Motif, and Tissue-of-Origin of Long Cell-Free DNA In plasma. *Clin Chem* ;2022:hvac180. DOI PubMed
 34. Tan G, Opitz L, Schlappbach R, Rehrauer H. Long fragments achieve lower base quality in Illumina paired-end sequencing. *Sci Rep* 2019;9:2856. DOI PubMed PMC
 35. Head SR, Komori HK, LaMere SA, et al. Library construction for next-generation sequencing: overviews and challenges. *Biotechniques* 2014;56:61-4, 66, 68, passim. DOI PubMed PMC
 36. Choy LYL, Peng W, Jiang P, et al. Single-molecule sequencing enables long cell-free DNA detection and direct methylation analysis for cancer patients. *Clin Chem* 2022;68:1151-63. DOI PubMed
 37. Jiang P, Sun K, Tong YK, et al. Preferred end coordinates and somatic variants as signatures of circulating tumor DNA associated with hepatocellular carcinoma. *Proc Natl Acad Sci USA* 2018;115:E10925-33. DOI PubMed PMC
 38. Bao H, Wang Z, Ma X, et al. Letter to the Editor: an ultra-sensitive assay using cell-free DNA fragmentomics for multi-cancer early detection. *Mol Cancer* 2022;21:129. DOI PubMed PMC
 39. Suzuki N, Kamataki A, Yamaki J, Homma Y. Characterization of circulating DNA in healthy human plasma. *Clin Chim Acta* 2008;387:55-8. DOI PubMed
 40. Chandrananda D, Thorne NP, Bahlo M. High-resolution characterization of sequence signatures due to non-random cleavage of cell-free DNA. *BMC Med Genomics* 2015;8:29. DOI PubMed PMC
 41. Serpas L, Chan RWY, Jiang P, et al. Dnase113 deletion causes aberrations in length and end-motif frequencies in plasma DNA. *Proc Natl Acad Sci USA* 2019;116:641-9. DOI PubMed PMC
 42. Han DSC, Ni M, Chan RWY, et al. The biology of cell-free DNA fragmentation and the roles of DNASE1, DNASE1L3, and DFFB. *Am J Hum Genet* 2020;106:202-14. DOI PubMed PMC
 43. Jiang P, Sun K, Peng W, et al. Plasma DNA end-motif profiling as a fragmentomic marker in cancer, pregnancy, and transplantation. *Cancer Discov* 2020;10:664-73. DOI PubMed
 44. Zhitnyuk YV, Koval AP, Alferov AA, et al. Deep cfDNA fragment end profiling enables cancer detection. *Mol Cancer* 2022;21:26. DOI PubMed PMC
 45. Guo W, Chen X, Liu R, et al. Sensitive detection of stage I lung adenocarcinoma using plasma cell-free DNA breakpoint motif profiling. *EBioMedicine* 2022;81:104131. DOI PubMed PMC
 46. Chan RWY, Serpas L, Ni M, et al. Plasma DNA profile associated with DNASE1L3 gene mutations: clinical observations, relationships to nuclease substrate preference, and in vivo correction. *Am J Hum Genet* 2020;107:882-94. DOI PubMed PMC
 47. Jiang P, Xie T, Ding SC, et al. Detection and characterization of jagged ends of double-stranded DNA in plasma. *Genome Res* 2020;30:1144-53. DOI PubMed PMC
 48. Ding SC, Chan RWY, Peng W, et al. Jagged ends on multinucleosomal cell-free DNA serve as a biomarker for nuclease activity and systemic lupus erythematosus. *Clin Chem* 2022;68:917-26. DOI PubMed
 49. Ma ML, Zhang H, Jiang P, et al. Topologic analysis of plasma mitochondrial DNA reveals the coexistence of both linear and circular molecules. *Clin Chem* 2019;65:1161-70. DOI PubMed
 50. Ma ML, Yakovenko S, Zhang H, et al. Fetal mitochondrial DNA in maternal plasma in surrogate pregnancies: detection and topology. *Prenat Diagn* 2021;41:368-75. DOI PubMed PMC

51. Sin STK, Ji L, Deng J, et al. Characteristics of fetal extrachromosomal circular DNA in maternal plasma: methylation status and clearance. *Clin Chem* 2021;67:788-96. [DOI](#) [PubMed](#)
52. Kumar P, Dillon LW, Shibata Y, Jazaeri AA, Jones DR, Dutta A. Normal and cancerous tissues release extrachromosomal circular DNA (eccDNA) into the circulation. *Mol Cancer Res* 2017;15:1197-205. [DOI](#) [PubMed](#) [PMC](#)
53. Paulsen T, Kumar P, Koseoglu MM, Dutta A. Discoveries of extrachromosomal circles of DNA in normal and tumor cells. *Trends Genet* 2018;34:270-8. [DOI](#) [PubMed](#) [PMC](#)
54. Tsui NB, Jiang P, Chow KC, et al. High resolution size analysis of fetal DNA in the urine of pregnant women by paired-end massively parallel sequencing. *PLoS One* 2012;7:e48319. [DOI](#) [PubMed](#) [PMC](#)
55. Zhang J, Tong KL, Li PK, et al. Presence of donor- and recipient-derived DNA in cell-free urine samples of renal transplantation recipients: urinary DNA chimerism. *Clin Chem* 1999;45:1741-6. [PubMed](#)
56. Chen M, Chan RWY, Cheung PPH, et al. Fragmentomics of urinary cell-free DNA in nuclease knockout mouse models. *PLoS Genet* 2022;18:e1010262. [DOI](#) [PubMed](#) [PMC](#)
57. Cheng THT, Jiang P, Tam JCW, et al. Genomewide bisulfite sequencing reveals the origin and time-dependent fragmentation of urinary cfDNA. *Clin Biochem* 2017;50:496-501. [DOI](#) [PubMed](#)
58. Cheng THT, Jiang P, Teoh JYC, et al. Noninvasive detection of bladder cancer by shallow-depth genome-wide bisulfite sequencing of urinary cell-free DNA for methylation and copy number profiling. *Clin Chem* 2019;65:927-36. [DOI](#) [PubMed](#)
59. Zhou Z, Cheng SH, Ding SC, et al. Jagged ends of urinary cell-free DNA: characterization and feasibility assessment in bladder cancer detection. *Clin Chem* 2021;67:621-30. [DOI](#) [PubMed](#)
60. Xie T, Wang G, Ding SC, et al. High-resolution analysis for urinary DNA jagged ends. *NPJ Genom Med* 2022;7:14. [DOI](#) [PubMed](#) [PMC](#)
61. Burke DM, Shackley DC, O'Reilly PH. The community-based morbidity of flexible cystoscopy. *BJU Int* 2002;89:347-9. [DOI](#) [PubMed](#)
62. Svatek RS, Hollenbeck BK, Holmäng S, et al. The economics of bladder cancer: costs and considerations of caring for this disease. *Eur Urol* 2014;66:253-62. [DOI](#) [PubMed](#)
63. Ou Z, Li K, Yang T, et al. Detection of bladder cancer using urinary cell-free DNA and cellular DNA. *Clin Transl Med* 2020;9:4. [DOI](#) [PubMed](#) [PMC](#)
64. Birkenkamp-Demtröder K, Nordentoft I, Christensen E, et al. Genomic alterations in liquid biopsies from patients with bladder cancer. *Eur Urol* 2016;70:75-82. [DOI](#) [PubMed](#)
65. Mouliere F, Smith CG, Heider K, et al. Fragmentation patterns and personalized sequencing of cell-free DNA in urine and plasma of glioma patients. *EMBO Mol Med* 2021;13:e12881. [DOI](#) [PubMed](#) [PMC](#)
66. Wu X, Xing P, Shi M, et al. Cerebrospinal fluid cell-free DNA-based detection of high level of genomic instability is associated with poor prognosis in NSCLC patients with leptomeningeal metastases. *Front Oncol* 2022;12:664420. [DOI](#) [PubMed](#) [PMC](#)
67. Lo YMD, Chan LY, Lo KW, et al. Quantitative analysis of cell-free Epstein-Barr virus DNA in plasma of patients with nasopharyngeal carcinoma. *Cancer Res* 1999;59:1188-91. [PubMed](#)
68. Chan KCA, Woo JKS, King A, et al. Analysis of plasma Epstein-Barr virus DNA to screen for nasopharyngeal cancer. *N Engl J Med* 2017;377:513-22. [DOI](#) [PubMed](#)
69. Lam WKJ, Jiang P, Chan KCA, et al. Sequencing-based counting and size profiling of plasma Epstein-Barr virus DNA enhance population screening of nasopharyngeal carcinoma. *Proc Natl Acad Sci USA* 2018;115:E5115-24. [DOI](#) [PubMed](#) [PMC](#)
70. Linthorst J, Welkers MRA, Sistermans EA. Distinct fragmentation patterns of circulating viral cell-free DNA in 83,552 non-invasive prenatal testing samples. *Extracell Vesicles Circ Nucleic Acids* 2021. [DOI](#)
71. Lui YY, Chik KW, Chiu RW, et al. Predominant hematopoietic origin of cell-free DNA in plasma and serum after sex-mismatched bone marrow transplantation. *Clin Chem* 2002;48:421-7. [PubMed](#)
72. Sun K, Jiang P, Chan KC, et al. Plasma DNA tissue mapping by genome-wide methylation sequencing for noninvasive prenatal, cancer, and transplantation assessments. *Proc Natl Acad Sci USA* 2015;112:E5503-12. [DOI](#) [PubMed](#) [PMC](#)
73. Moss J, Magenheimer J, Neiman D, et al. Comprehensive human cell-type methylation atlas reveals origins of circulating cell-free DNA in health and disease. *Nat Commun* 2018;9:5068. [DOI](#) [PubMed](#) [PMC](#)
74. Gai W, Zhou Z, Agbor-Enoh S, et al. Applications of genetic-epigenetic tissue mapping for plasma DNA in prenatal testing, transplantation and oncology. *Elife* 2021;10. [DOI](#) [PubMed](#) [PMC](#)
75. Lam NY, Rainer TH, Chiu RW, Lo YM. EDTA is a better anticoagulant than heparin or citrate for delayed blood processing for plasma DNA analysis. *Clin Chem* 2004;50:256-7. [DOI](#) [PubMed](#)
76. Fernando MR, Chen K, Norton S, et al. A new methodology to preserve the original proportion and integrity of cell-free fetal DNA in maternal plasma during sample processing and storage. *Prenat Diagn* 2010;30:418-24. [DOI](#) [PubMed](#)
77. Hisano O, Ito T, Miura F. Short single-stranded DNAs with putative non-canonical structures comprise a new class of plasma cell-free DNA. *BMC Biol* 2021;19:225. [DOI](#) [PubMed](#) [PMC](#)
78. Cheng LY, Dai P, Wu LR, Patel AA, Zhang DY. Direct capture and sequencing reveal ultra-short single-stranded DNA in biofluids. *iScience* 2022;25:105046. [DOI](#) [PubMed](#) [PMC](#)

Review

Open Access



A kaleidoscopic view of extracellular vesicles in lysosomal storage disorders

Charlotte V. Hegeman¹, Olivier G. de Jong^{1, #} , Magdalena J. Lorenowicz^{2,3, #}

¹Department of Pharmaceutics, Utrecht Institute for Pharmaceutical Sciences (UIPS), Utrecht University, Universiteitsweg 99, Utrecht 3584 CG, The Netherlands.

²Regenerative Medicine Center, Uppsalalaan 8, Utrecht 3584 CT, The Netherlands.

³Biomedical Primate Research Centre, Lange Kleinweg 161, Rijswijk 2288 GJ, The Netherlands.

[#]Authors contributed equally.

Correspondence to: Olivier G. de Jong, PhD, Utrecht Institute for Pharmaceutical Sciences, David de Wiedgebouw, Universiteitsweg 99, Utrecht 3584 CG, The Netherlands. E-mail: o.g.dejong@uu.nl; Magdalena J. Lorenowicz, PhD, Biomedical Primate Research Centre, Lange Kleinweg 161, Rijswijk 2288 GJ, The Netherlands. E-mail: lorenowicz@bprc.nl

How to cite this article: Hegeman CV, de Jong OG, Lorenowicz MJ. A kaleidoscopic view of extracellular vesicles in lysosomal storage disorders. *Extracell Vesicles Circ Nucleic Acids* 2022;3:393-421. <https://dx.doi.org/10.20517/evcna.2022.41>

Received: 8 Nov 2022 **First Decision:** 9 Dec 2022 **Revised:** 16 Dec 2022 **Accepted:** 26 Dec 2022 **Published:** 30 Dec 2022

Academic Editor: Yoke Peng Loh **Copy Editor:** Ying Han **Production Editor:** Ying Han

Abstract

Extracellular vesicles (EVs) are a heterogeneous population of stable lipid membrane particles that play a critical role in the regulation of numerous physiological and pathological processes. EV cargo, which includes lipids, proteins, and RNAs including miRNAs, is affected by the metabolic status of the parental cell. Concordantly, abnormalities in the autophagic-endolysosomal pathway, as seen in lysosomal storage disorders (LSDs), can affect EV release as well as EV cargo. LSDs are a group of over 70 inheritable diseases, characterized by lysosomal dysfunction and gradual accumulation of undigested molecules. LSDs are caused by single gene mutations that lead to a deficiency of a lysosomal protein or lipid. Lysosomal dysfunction sets off a cascade of alterations in the endolysosomal pathway that can affect autophagy and alter calcium homeostasis, leading to energy imbalance, oxidative stress, and apoptosis. The pathophysiology of these diseases is very heterogenous, complex, and currently incompletely understood. LSDs lead to progressive multisystemic symptoms that often include neurological deficits. In this review, a kaleidoscopic overview will be given on the roles of EVs in LSDs, from their contribution to pathology and diagnostics to their role as drug delivery vehicles. Furthermore, EV cargo and surface engineering strategies will be discussed to show the potential of EVs in future LSD treatment, both in the context of enzyme replacement therapy, as well as future gene editing strategies like CRISPR/Cas. The use of engineered EVs as drug delivery vehicles may mask therapeutic cargo from the immune system and protect it from degradation, improving circulation time and targeted delivery.



© The Author(s) 2022. **Open Access** This article is licensed under a Creative Commons Attribution 4.0 International License (<https://creativecommons.org/licenses/by/4.0/>), which permits unrestricted use, sharing, adaptation, distribution and reproduction in any medium or format, for any purpose, even commercially, as long as you give appropriate credit to the original author(s) and the source, provide a link to the Creative Commons license, and indicate if changes were made.



Keywords: Lysosomal storage disorders, extracellular vesicles, autophagy, therapeutics, diagnostics

INTRODUCTION

Lysosomal storage disorders (LSDs) include over 70 rare heritable (inborn) errors of metabolism. In LSDs, a single gene mutation causes deficiency of a lysosomal protein or lipid, which leads to gradual accumulation of undigested macromolecules and negatively affects lysosomal function. Because lysosomal hydrolases are involved in the stepwise degradation, primary substrate accumulation in lysosomes gradually leads to secondary accumulation of upstream substrates within the same catabolic pathway. The accumulation leads to enlargement of the organelle and functional inhibition of genetically correct enzymes and proteases which further limits their processing abilities^[1-3]. This sets off a cascade of alterations in the endolysosomal pathway due to impaired fusion that can affect autophagy, but also in other organelles including the endoplasmic reticulum and mitochondria^[4]. This may further lead to altered calcium homeostasis, oxidative stress, energy imbalance, and apoptosis^[5,6]. The degree of the effect on these cellular processes highly depends on the type of LSD and its specific genetic mutation^[7]. The complex interplay of the cellular pathways is shown in [Figure 1](#). The cellular impairments seen in LSDs can lead to cell death and cause progressive multisystemic symptoms that often include visceromegaly, bone abnormalities, cardio-respiratory problems, and neurodegeneration^[8,9].

Around 70% of the LSDs are enzyme deficiencies and can be further subclassified based on their storage material, such as Glycoproteinoses, Mucopolysaccharidoses, and Lipidoses. Other subgroups of LSDs include deficiencies in integral membrane proteins, transporters and proteins involved in trafficking, regulation, or post-translational modification. Despite the classification, LSDs are clinically very heterogeneous, even within the same subtype. The symptoms depend on the specific genetic mutation and to which degree this affects the lysosomal protein or lipid, as well as the spatial and temporal accumulation of macromolecules^[7]. While individual LSDs are rare, collectively, they have an estimated incidence of 1 in 5000-8000^[10-12]. All LSDs that will be described in this review are listed in [Table 1](#).

To date, the most established treatment option for LSDs is enzyme replacement therapy (ERT)^[16]. ERT is available for several enzyme deficiencies, where it can improve clinical symptoms and slow down disease progression. Unfortunately, ERT comes with serious limitations that include the development of neutralizing antibodies against the enzyme, low plasma half-life, inability to cross the blood-brain barrier (BBB), and high costs. Furthermore, patients treated with ERT are left with residual disease due to its poor biodistribution, which fails to effectively target certain organs^[17-19]. Besides ERT, hematopoietic stem cell transplantation (HSCT) is available for a very limited group of LSDs, including MPS-IH, MPS-II, α -Mannosidosis, MLD, and Krabbe Disease. To improve its effects and survival of patients, early diagnosis and early treatment with HSCT are critical. The effect of stem cell transplantation is based on the production of the missing enzyme by the healthy donor cells that will allow cross-correction^[20-25]. However, HSCT is not fully curative and unable to completely halt disease in hard-to-reach tissues. This is often the case for connective tissue, resulting in progression of skeletal malformations, corneal clouding, valvular dysfunction, as well as inconsistent results for joint, tendon, and ligament stiffness^[15]. Several other novel strategies have been developed over the years, including substrate reduction therapy (SRT), pharmacological chaperone therapy (PCT), and gene therapy^[26-28]. For most LSDs, the only solution remains symptomatic treatment and supportive care^[7]. A cure that will be more broadly applicable to treat more LSDs, including those with severely affected neurological manifestations, has yet to be discovered.

Table 1. Described Lysosomal Storage Disorders

Disease (gene) Eponyms and/or types	Primary deficiency	Accumulated molecules	Approved therapies
Sphingolipidoses			
Fabry Disease^a (GLA)	α -Galactosidase A	Globotriaosylceramide	ERT and CT
Farber Lipogranulomatosis^a (ASAH1)	Acid ceramidase	Ceramide	S/S
Gaucher Disease^a (GBA) Type I, II ^b , III ^b , perinatal lethal form ^b and cardiovascular ^{[13]c}	β Glucocerebrosidase/ β -glucosidase	Glucocerebroside/ glucosylsphingosine	ERT and SRT (types I, II and III), none (perinatal lethal form)
GM2 Gangliosidosis Tay-Sachs Disease ^c (HEXA)	β -Hexosaminidase	GM2 ganglioside, glycosphingolipids and oligosaccharides	S/S
Globoid Cell Leukodystrophy^{a,b} (GALC) Krabbe Disease	Galactosylceramidase	Galactocerebroside and psychosine	HSCT (infantile onset) and S/S
Metachromatic Leukodystrophy^{a,b} (ARSA and PSAP) MLD	Arylsulfatase A Sphingolipid activator protein SAP-B	Sulfatides	HSCT
Niemann-Pick Disease^a (SMPD1) Type A ^b and B	Sphingomyelin Phosphodiesterase	Sphingomyelin	S/S
Mucopolysaccharidosis (MPS)			
MPS III^{a,b,d} III-A Sanfilippo A (SGSH) III-C Sanfilippo C (HGSNAT)	N- Sulfoglucosamine sulfohydrolase Heparan- α -glucosaminide- N- acetyltransferase	HS (KS)	S/S
MPS IV^a IV-A Morquio syndrome A (GALNS)	N-acetylgalactosamine- 6-sulfatase	KS, C6S	ERT (IV-A) and S/S (IV-B)
MPS VII^{a,b} (GUSB) Sly Disease	β - Glucuronidase	DS, HS, C4S, C6S (KS)	ERT
Glycogen Storage Disorders (GSD)			
GSD II^a (GAA) Pompe Disease	Lysosomal α - glucosidase/acid maltase	Glycogen	ERT
Glycoproteinoses			
Sialidosis^a (NEU1) Type I, cherry-red spot myoclonus	Neuraminidase-1	Sialylated oligosaccharides and glycopeptides	S/S
Type II ^b , Mucopolidosis I		Sialylated oligosaccharides and glycopeptides, LAMP1 and amyloid precursor protein	
Integral Membrane Protein Disorders			
Cystinosis (CTNS)	Cystinosis	Cystine	SMT
Niemann-Pick Disease C1 (NPC1) C2 ^b (NPC2)	NPC intracellular cholesterol transporter 1 NPC intracellular cholesterol transporter 2	Cholesterol and sphingolipids	SRT
Neuronal Ceroid Lipofuscinoses (NCL or CLN), Batten Disease			
CLN2^b (TPP1) Jansky-Bielschowsky Disease	Tripeptidyl peptidase 1	Subunit c of mitochondrial ATP synthase	ERT

CT: Chaperone therapy; C4S: chondroitin 4-Sulfate; C6S: chondroitin 6-sulfate; DS: dermatan sulfate; ERT: enzyme replacement therapy; HS: heparan sulfate; HSCT: hematopoietic stem cell therapy; KS: keratan sulphate; LAMP1: lysosome-associated membrane glycoprotein 1; SMT: small-molecule therapy; SRT: substrate reduction therapy; S/S: symptomatic and supportive therapy. ^aDenotes enzyme deficiency. ^bDenotes diseases that involve the Central Nervous System (CNS). ^cType depends on specific mutation^[14]. ^dDenotes disorders with severe and attenuated forms that result in a phenotype spectrum^[7,15].

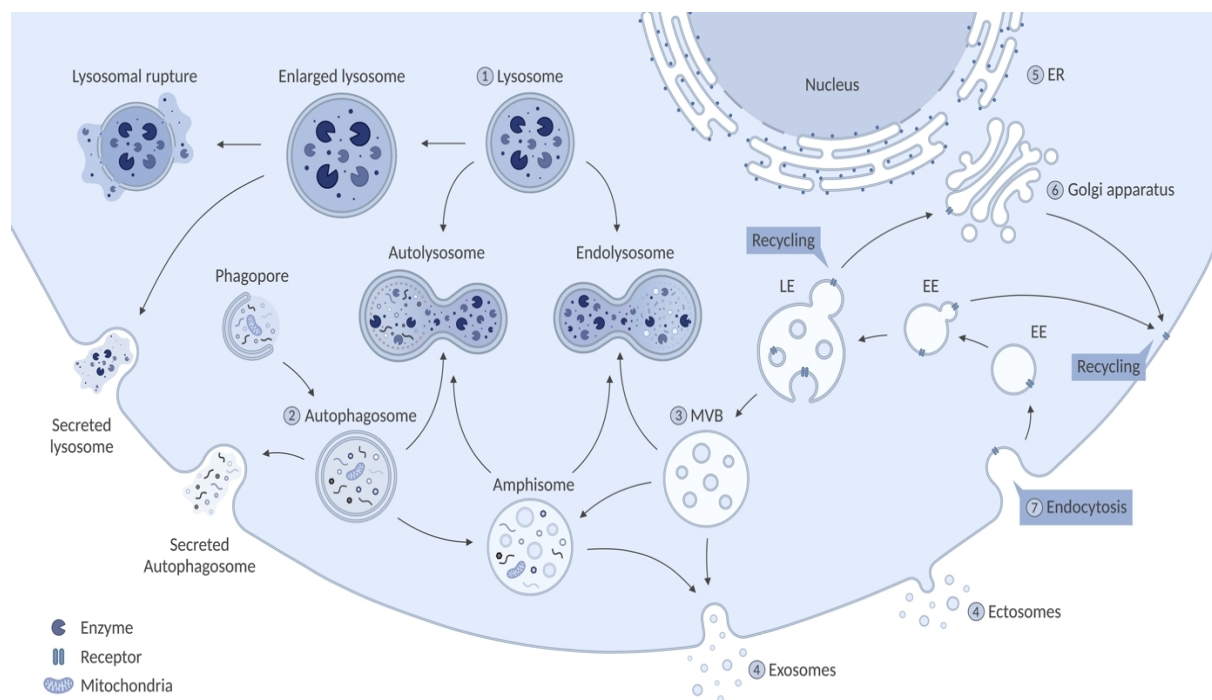


Figure 1. A schematic illustration of different pathways affected in LSDs. (1) In LSDs, a single gene mutation causes the deficiency of a lysosomal protein or lipid. The defect leads to gradual accumulation of macromolecules, inhibition of other lysosomal components, and enlargement of the lysosome which can be followed by lysosomal rupture and secretion. Furthermore, dysfunction of the lysosome and its altered calcium (Ca^{2+}) homeostasis leads to impaired fusion with cellular structures including autophagosomes and endosomes/multivesicular bodies (MVBs). (2) The accumulation of autophagosomes can potentially lead to secretion of the organelle to clear its obstruction. Additionally, autophagy is downregulated by hyperactivation of mTOR in some LSDs (MPS-I, MPS-VI, MPS-VII, and Gaucher Disease). Subsequently, impaired or inhibited autophagy results in mitochondrial dysfunction that can lead to energy imbalance, apoptosis, and inflammation. (3) There is a balance between degradation and EV release, which is highly dependent on the fate of MVBs. (4) Impaired fusion of MVBs with the lysosome can lead to fusion of MVBs with the plasma membrane, which causes increased secretion of EVs (Niemann-Pick type C, Sialidosis, Krabbe and Fabry Disease). Hence, inhibition of autophagy and subsequent increase of EV secretion might be an alternative route for LSD cells to clear obstruction of the accumulating molecules to naturally improve the cellular phenotype. (5) In multiple sphingolipid storage disorders (Gaucher Disease, GM1 and GM2 Gangliosidosis, and Niemann-Pick type A) Endoplasmic reticulum (ER) calcium homeostasis is perturbed, which leads to elevated Ca^{2+} in the cytosol. (6) Dysfunction of the Golgi apparatus has been reported for most lipid storage disorders and MPS IIIB. This includes altered morphology and accumulation of large storage bodies.

Post-treatment residual disease in connective tissues has drawn attention towards multipotent mesenchymal stem cells (MSCs), which have the ability to differentiate into multiple lineages of bone, cartilage, and fat. Moreover, MSCs are characterized by their intrinsic self-renewal capacity and their capability of immunomodulation. Their transplantation is widely tested in clinical trials and considered safe^[29,30]. In comparison to hematopoietic stem cells (HSC), MSCs secrete significantly higher levels of mucopolysaccharidosis (MPS)-related enzymes^[31]. Thus, MSCs might be able to improve skeletal malformations and neurological deficits in LSD patients at an early stage of disease development^[29,32]. Several studies with MSCs derived from various tissue sources have been performed in mice models for different LSDs. In these studies, improvement in motor function, decreased inflammation and apoptosis were reported post-injection of the cells into different parts of the brain^[5]. To date, intravenous injection of MSCs has only been tested on patients with Metachromatic Leukodystrophy (MLD); this showed promising results regarding its safety and improvement of stabilization on neurological manifestations^[33,34]. Currently,

a clinical trial is assessing the safety of human placental-derived MSCs (phase I) in multiple other LSDs (ID: NCT01586455). However, increasing evidence suggests that the therapeutic efficiency of MSC therapy is not dependent on the engraftment of MSCs or their capability to differentiate after transplantation. Most likely, the mode of action of MSCs relies on their paracrine signaling including extracellular vesicles (EVs) to support surrounding tissues^[35].

Over the last two decades, attention has been drawn towards EVs as important mediators of intercellular communication. EVs are a heterogeneous population of stable lipid membrane particles and play a critical role in the regulation of numerous physiological and pathological processes^[36]. EVs capture the metabolic status of the cell^[37], which qualifies them as potential sources of biomarkers for LSDs. Furthermore, EVs are biocompatible, low immunogenic and can traverse multiple biological barriers. For instance, several studies have indicated that EVs are able to cross the BBB^[38,39]. Additionally, bioengineering approaches can modify EVs to load specific cargo or target specific sites^[40]. This makes EVs of high interest as both therapeutic agents and drug delivery vehicles, which could open doors to the development of novel treatments for LSDs including those with neurological deficits. In this review, we will provide an overview of the current knowledge and potential of EVs in unraveling LSDs, their diagnostics, treatment, and potential future drug delivery for gene correction strategies. For an overview of the existing synthetic nanotechnology-based approaches that have been explored as delivery vehicles in the treatment of LSDs, we refer the reader to the reviews of Abasolo *et al.*, Schuh *et al.*, and Del Grosso *et al.*^[41,42,43].

THE BIOGENESIS OF EXTRACELLULAR VESICLES

EVs are a heterogeneous population of small lipid membrane vesicles that are secreted by all cells, and have been observed in all body fluids^[36]. EVs are conventionally classified into subtypes based on their biogenesis: exosomes and ectosomes. Exosomes (40-140 nm) are a part of the endo-lysosomal system and form through intraluminal vesicle (ILV) formation by inward membrane budding in the late endosome. This process involves the endosomal sorting complexes required for transport (ESCRT) machinery, tetraspanins and lipid-dependent interactions, which ultimately leads to the formation of multivesicular bodies (MVBs)^[44]. MVBs can release their intraluminal vesicles upon fusion with the plasma membrane into the extracellular space, after which they are referred to as exosomes. Ectosomes, also referred to as microvesicles (50-1000 nm), directly bud off the plasma membrane^[45]. Clear classification of EVs remains a challenge due to their heterogeneous size, cargo, and lack of specific biomarkers to distinguish the EV subtypes^[46,47].

EVs are known for their contribution to cell-to-cell communication by transferring cargo such as RNA, including mRNA and long noncoding RNAs, lipids, and proteins including lysosomal enzymes^[48-50]. Over the last decade, it has become clear that EV cargo reflects the status of the secreting cell and its tissue origin^[37,51]. Cargo transportation through EVs plays a critical role in the regulation and progression of numerous physiological and pathological processes^[36]. The contribution of EVs to pathology has been shown for several neurological disorders that have been associated with LSDs or other pathologies related to endolysosomal dysfunction, such as Parkinson's Disease (PD)^[52], Alzheimer's Disease^[53], and Huntington's Disease^[54,55]. Since these neurological disorders are currently not classified as classical LSDs, describing the endolysosomal involvement in the pathology of these disorders is beyond the scope of this review. For more in-depth information on these diseases, we refer the readers to the reviews of Navarro-Romero *et al.* and Almeida *et al.*^[56,57]. In these neurological disorders, EVs are thought to contribute to inflammation and seem to sequester and spread the accumulating pathogenic proteins^[53,58]. This suggests that EVs may contribute to the altered physiology in LSDs as well^[59]. This makes EVs a potentially useful source of information to further determine the altered processes in LSDs as biomarkers for diagnostics and disease progression, including their location^[51,60].

As EVs hold the ability to traverse multiple biological barriers and can be modified to avoid uptake by the mononuclear phagocytic system, EVs are potential therapeutic agents and drug delivery vehicles for LSDs, due to their biocompatibility and low immunogenicity^[61-63]. Adaptation of EVs through bioengineering approaches could further optimize their delivery potential and therapeutic value by targeted loading of therapeutic components through fusion proteins, or to target EVs to specific tissues^[40,64]. This strategy could actively load ERT into EVs, which could reduce neutralizing antibodies against the enzyme, improve its plasma half-life, and facilitate delivery towards the nervous system by crossing the BBB^[38]. As such, EVs have the potential to both improve existing treatment and lead to new therapeutic options for LSD patients in the future, including those with severe neurological deficits.

EV RELEASE IN LSDs: A NEW ROUTE IN UNDERSTANDING DISEASE PATHOLOGY

Lysosomes are essential organelles in the degradation of macromolecules delivered by endocytosis or autophagocytosis. The lysosomal characteristic acidic lumen includes over 60 hydrolases that can return molecules to catabolites, thereby allowing recycling of these molecules. These functions allow lysosomes to play a fundamental role in multiple cellular processes including autophagy and its regulation, cellular homeostasis, cell signaling, mitochondrial function and vesicle fusion^[65,66]. Several of these processes are also implicated in EV release and uptake, which are both parts of the endolysosomal pathway. As described before, the fusion of MVBs with the plasma membrane leads to EV release. Alternatively, MVBs can fuse with both lysosomes and autophagosomes, leading to degradation of MVBs. Moreover, both studies on ESCRT proteins and autophagy modulators show a tight relationship between autophagy and MVB biogenesis, thereby determining the fate of its ILVs and, subsequently, of EVs^[44]. The lysosomal dysfunction in LSDs does not make it difficult to envision its effects on both EV release and uptake, which will be discussed in this section.

Autophagy is a multi-step process where damaged organelles and molecular aggregates are degraded and recycled. The process starts with the formation of autophagosomes that can fuse with early and late endosomal vesicles, such as MVBs, to form amphisomes, to eventually fuse with lysosomes^[4,7]. Under homeostatic conditions, cells maintain a constitutive basal level of autophagy; however, the process can be induced in response to cellular and metabolic stress^[67]. In several LSDs, it has been shown that lysosomal dysfunction leads to the accumulation of autophagosomes and autophagic substrates, such as damaged mitochondria^[4,68,69]. However, accumulation of autophagosomes does not necessarily indicate an increased induction of autophagy as this increase could also be caused by blockage of fusion with the lysosome. Nevertheless, the autophagy pathway in LSDs is disrupted, which could either mean activation or inhibition of autophagy, depending on the LSD type. For instance, in MPS-I, MPS-VI, MPS-VII, and Gaucher Disease, hyperactivation of mTOR, a negative regulator of autophagy, has been shown^[69,70]. In this study, mTOR hyperactivation increased phosphorylation of the UVRUG protein, which led to reduced autophagosome maturation and reduced fusion with the lysosome^[69]. Moreover, activated mTOR can phosphorylate transcription factor EB (TFEB), which inhibits its translocation to the nucleus and, with that, lysosomal biogenesis and function^[8]. Thus, there might be a vicious cycle in play where lysosomal accumulation inhibits the induction of autophagy, perhaps to prevent further accumulation-induced damage. The complex interplay of autophagy and the endolysosomal pathways is shown in [Figure 1](#).

There is a balance between autophagy and EV release, which is highly dependent on the fate of MVBs. It has been shown that in hepatic stellate cells, activation of mTOR signaling induced the release of exosomes by inhibiting autophagy. Furthermore, the activation of mTOR can stimulate release of microvesicles through activation of ROCK1 signaling^[71]. The hyperactivation of mTOR in some LSDs could play a vital part in the secretion of EVs by these cells. In a study by Bartolomeo *et al.*, it was shown that mTOR

hyperactivity significantly reduced the formation of Phosphatidylinositol-3-phosphate (PI3P)^[69]. This may influence EV release considering that PI3P is required in vesicle and (auto)phagosome fusion with lysosomes. As PI3P reduction may limit the fusion between MVBs and autophagosomes, this could potentially shift the faith of MVBs towards fusion with the plasma membrane and secretion of EVs instead, to limit accumulation and maintain homeostasis. Furthermore, PI3P is involved in ESCRT protein recruitment and cargo organization, and serves as a substrate for PI(3,5)P₂ formation^[72,73]. Therefore, the diminished presence of PI3P through mTOR hyperactivation could also lead to reduced PIP₂ formation. The absence of PIP₂ has been shown to increase EV secretion^[74]. In addition, reduction of PI3P formation promoted secretion of atypical exosome containing undigested lysosomal components in neuronal disorders with lysosomal dysfunction closely related to Niemann-Pick type C^[73,75]. A study by Strauss *et al.* confirmed increased EV release in Niemann-Pick type C cells^[76]. Table 2 gives an overview of all studies describing the EV release by LSD cells. In Niemann-Pick type C, loss of function of a late endosomal membrane protein leads to accumulation of free cholesterol and sphingolipids. Strauss *et al.* showed a flotillin-dependent pathway of EV secretion as an alternative to secrete free cholesterol to ameliorate its storage within cells^[76,77]. Moreover, increased EV release has been shown in several enzyme deficiencies, including Sialidosis, Krabbe and Fabry Disease^[68,78,79]. Hence, inhibition of autophagy and subsequent increase of EV secretion might be an alternative route for LSD cells to clear obstruction of the accumulating molecules to improve the cellular phenotype.

Therapeutic stimulation of EV release may have the potential as (pre-)treatment for LSDs through the reduction of LSD specific molecule accumulation inside the cell. This could lower the secondary effects on the endolysosomal pathway by ameliorating the accumulation of MVBs. Advantageous effects of autophagy suppression on the secretion of EVs have been shown in Alzheimer's Disease and PD^[85,86]. In these studies, autophagy inhibition by ammonium chloride or bafilomycin A treatment led to the release of EVs containing the accumulated molecules alpha-synuclein and amyloid precursor proteins^[85,86]. A similar effect was observed in Pompe Disease, where ATG7 was inactivated in the mouse muscles. The autophagy suppression alone led to a 50%-60% reduction of the accumulating glycogen, and after ERT delivery, this was restored to normal levels^[87]. Unfortunately, the effects on EV secretion were not tested in this study, and it appeared that the accumulating molecule was digested in the cytosol, which improved the cellular phenotype. Contradictory to these results, other studies on Pompe Disease showed improvements in myotubes and muscle tissue after induction of autophagy through TFEB overexpression^[88,89]. Moreover, induction of autophagy with rapamycin has been shown to lead to higher secretion of lipid particles and CD63+ vesicles in Niemann-Pick type B. This data is in line with studies that predict a way in which autophagy-inducing conditions, mainly rapamycin treatment, have a specific role in unconventional secretion^[90]. It must be noted that in LSDs, there is no problem with the formation of autophagosomes. Autophagy problems are secondary to dysfunctional lysosomes that create a blockage in the autophagic flux and alter this pathway. Therefore, it must carefully be evaluated to what degree each mutation affects the endolysosomal pathway in all LSDs separately. Alongside the effect of TFEB on autophagy, it can increase lysosomal biogenesis and lysosomal exocytosis. Lysosomal exocytosis could be an alternative route to induce cellular clearance and has been implicated as a mechanism used by MLD and mucopolidosis type I cells^[91,92]. Lysosomal exocytosis can also be induced by drugs such as 2-hydroxypropyl- β -cyclodextrin (HPB-CD). HPB-CD is used as excipient to facilitate the transport of molecules across membranes as well as treatment to manipulate cellular cholesterol levels. The drug is approved by the FDA and was already used to alleviate cholesterol accumulation in Niemann Pick Type C patients^[93]. Treatment with HPB-CD can induce calcium-dependent lysosomal exocytosis and EV release^[83].

Table 2. The secretion of extracellular vesicles in lysosomal storage disorder models

LSD	Disease model	EV isolation method	Major results	Reference
Fabry Disease	<i>In vitro</i> CRISPR/Cas9 altered human embryonic stem cells differentiated into cardiomyocytes	Total Exosome Isolation Reagent (Thermo Fisher Scientific)	> Downregulation of proteins related to EV transportation, secretion, and exocytosis (Rab GTPases: Rab-11, GDIIR2, VPS36 and VTI1A) > Impairment of the autophagic flux and protein turnover, which increased reactive oxygen species, apoptosis, and necrosis > Increased production and secretion of exosomes	[68]
Farber Lipogranulomatosis (Partial model)	Asah1 ^{fl/fl} /Smooth Muscle (SM) ^{Cre} mice	Centrifugation (4 °C): 300 g, 10 min Filter 0.22 µm filters to 100,000 g, 90 min <i>Washing step</i> 100,000 g, 90 min	> Acid ceramidase (Ac) contributes to the development of arterial medial calcification (AMC) in the aorta and increases osteogenic markers > Decreased colocalization of MVBs with lysosomes and upregulation of sEV markers was seen in coronary arterial smooth muscle cells (CASMCs) of vitamin D treated Asah1 ^{fl/fl} /SM ^{Cre} mice. The same effect was observed in phosphate (Pi) treated CASMCs <i>in vitro</i> > Untreated Asah1 ^{fl/fl} /SM ^{Cre} CASMCs show increased sEV release, whereas Pi treated Asah1 ^{fl/fl} /SM ^{Cre} CASMCs show even more sEV release and increased MVB formation > Ac gene deletion remarkably decreased ML-SA1 induced Ca ²⁺ release through TRPML1 channels > Psychosine accumulation introduces focal regions of rigidity in the plasma membrane, which affects curvature and facilitates increased budding and shedding of 0.5-4 µm EVs in erythrocytes and oligodendrocytes	[80]
Krabbe Disease	<i>In vitro</i> Primary erythrocytes and oligodendrocytes from Twitcher mice-pups <i>In vivo</i> Twitcher mice (GALC ^{-/-})	Centrifugation: 100 g, 10 min at RT 21,000 g, 20 min at 4 °C Centrifugation: 300 g, 10 min (P1) 2,000 g, 10 min (P2) 10,000 g, 30 min (P3) 100,000 g, 90 min (P4) <i>Sucrose gradient</i> 200,000 g, 16 h <i>Washing step fractions</i> 100,000 g, 90 min	> At early disease stage, an increased number of brain-derived EVs was found, and this was decreased at a late stage > Significant increase in psychosine, myelin proteolipids and myelin basic proteins in brain-derived EVs, which further increased parallel to disease development > Treatment with ceramide production inhibitor GW4869 significantly decreased the number of brain-derived EVs, which accelerated the acquisition of the final disease state	[79]
MLD	<i>In vivo</i> ASA ^{-/-} mice (cortex)	Centrifugation (4 °C): 300 g, 10 min 2000 g, 10 min 10,000 g, 30 min 100,000 g, 70 min <i>Wash step</i> 100,000 g, 70 min <i>Sucrose gradient</i> 200,000 g, 16 h <i>Washing step fractions</i> 100,000 g, 70 min Filtration (0.22 µm) Centrifugation: 100,000 g, 90 min <i>Washing step</i> 100,000 g, 90 min	> ASA ^{-/-} Cells have a defective PDGFRα pathway: Reduced PDGFRα protein levels and failure to phosphorylate AKT > ASA ^{-/-} glia, NP and cortex-derived exosomes contain significantly increased PDGFRα levels > Enzyme correction of ASA ^{-/-} NPs normalized PDGFRα levels, led to re-localization of the receptor in detergent-resistant membrane domains, increased AKT phosphorylation, normalized the production of oligodendrocytes and reduced exosomal shedding > PDGFRα is secreted <i>in vivo</i> through exosomes during the peak of myelination	[82]
Sialidosis (type I and II)	<i>In vitro</i> Neur ^{-/-} mice myofibroblasts	Centrifugation (4 °C): 300 g, 10 min	> In Neur ^{-/-} myofibroblasts, there is excessive lysosomal exocytosis and significantly increased secretion of EVs	[78]

	Human skin fibroblasts	2000 g, 10 min 10,000 g, 30 min 100,000 g, 2 h <i>Washing step</i> 100,000 g, 2 h <i>Sucrose gradient</i> 100,000 g, 2.5 h	> Neu ^{-/-} myofibroblasts-derived EVs contain molecules of the TGF-β and WNT signaling pathways Several molecules were present on the outer membranes of EVs through glypicans > Neu ^{-/-} myofibroblasts and fibroblast EVs induce proliferation and migration/invasion in WT cells through profibrotic signals > Neu ^{-/-} myofibroblasts EVs convert normal fibroblasts into myofibroblasts through significantly upregulating genes encoding members of the TGF-β and WNT signaling pathways
Niemann-Pick Disease type C	<i>In vitro</i> NPC ^{-/-} liver cells from BALB/c mice <i>In vitro</i> Human NPC ^{-/-} skin fibroblasts and CT43 CHO cells; NPC1 siRNA treated oligodendroglia (Olf-neu)	Centrifugation: 100,000 g, 60 min Centrifugation: 3000 g, 10 min 4000 g, 10 min 4000 g, 10 min 10,000 g, 30 min 100,000 g, 60 min <i>Sucrose gradient</i> 200,000 g, 18 h <i>Washing step</i> 100,000 g, 1 h	> 2-hydroxypropyl-β-cyclodextrin (HPB-CD) treatment stimulates lysosomal exocytosis and EV secretion in a calcium-enhanced manner, which ameliorates endolysosomal cholesterol storage > NPC ^{-/-} fibroblasts secrete significantly higher amounts of EVs; > NPC ^{-/-} CHO cells secrete significantly higher amounts of EVs containing cholesterol; > Cholesterol enhances the release of flotillin-2-positive EVs
Niemann-Pick Disease type B	<i>In vitro</i> Human ASMase ^{-/-} B lymphocytes	TEM and Flow Cytometry	> LAMP-3/CD63 accumulation, which points to impairment of endocytic trafficking > Microvesicle/lipid particle release may partially bypass the trafficking blockade caused by lipid accumulation > Rapamycin might regulate autophagy/mitophagy and contribute to the clearance of lipid storage by vesicle secretion and lysosomal exocytosis

While improving the cellular state sounds promising, the secretion of EVs by LSD cells could have negative effects on neighboring cells or tissues. Their cargo could contribute to the progression of the pathological conditions over time, considering that EVs from LSD cells can contain the accumulated metabolites^[76-94]. This could especially have a major impact on neuronal tissue and avascular connective tissue. Both tissue types are hard to reach and treat due to the lack of blood supply or barriers, which results in the progression of symptoms after the first line of treatment^[51]. Increased secretion of the accumulating metabolites could further alter the carefully regulated composition and spatial orientation of the extracellular matrix (ECM). Alterations in the ECM are often seen in LSDs and mostly in MPs, where the primary storage material is a component of the ECM. The specific alterations depend on the type of LSD and may include changes in the size, expression, and arrangement of both fibrous elements and proteoglycans. Furthermore, alterations in the levels of hyaluronic acid (HA) and matrix metalloproteinases (MMPs) are often reported. The ECM modifications in LSDs can have effects on multiple signaling pathways, cell-cell matrix and cell-cell interactions^[95]. The contributions of EVs to these processes were shown by Van de Vlekert *et al.*, who demonstrated that Neu1^{-/-} myofibroblasts derived-EVs were able to convert normal fibroblasts into myofibroblasts propagating fibrosis^[78]. This effect was obtained through upregulation

of genes in the TGF- β and WNT signaling pathways^[78]. This suggests that Neu1^{-/-} myofibroblasts derived-EVs can contribute to and/or cause progression of fibrosis. Furthermore, in Krabbe Disease, accumulation of psychosine results in more rigid myelin fluidity and demyelination which occurs through the shedding of myelin by microvesicles^[79]. This deregulates cell signaling and may introduce focal weak points. In a healthy situation, myelin covers and protects nerve cells to ensure rapid transmission of nerve signals. Consequently, demyelination interrupts signaling of the central and peripheral nervous systems, which contributes to the neurological symptoms seen in Krabbe patients^[96]. In additional Sphingolipidoses Niemann-Pick type A and C^[97,98], changes in the membrane organization and decreased fluidity have been reported. This decrease in membrane fluidity is linked to altered activity of membrane-bound enzymes, carrier-mediated transport, and receptor binding at the cell membrane^[98]. Whether this influences EVs release in these LSDs remains to be determined. To study EV release in Fabry Disease, Song *et al.* used CRISPR/Cas editing to create GLA-null human embryonic stem cells (hESCs)^[68]. This model for hypertrophic cardiomyopathy showed impaired autophagic flux and protein turnover combined with increased EV release^[68]. These studies show the contribution of EVs to the clinical manifestations of LSDs, such as fibrosis, delamination, and hypertrophic cardiomyopathy. More research is needed to investigate the role of the secondary cascade following lysosomal dysfunction in individual LSDs. This will greatly improve our understanding of its pathophysiology inside the cell and its contribution to disease progression. In addition, this could contribute to more targeted and more efficient therapy development. For now, these studies on EVs have demonstrated the potential of vesicles as biomarkers for these symptoms.

THE POTENTIAL OF EVs AS BIOMARKERS FOR LSDs IN DIAGNOSTICS AND DISEASE MONITORING

EVs are able to reflect the metabolic status of the parent cell through alterations in their cargo, including RNAs, lipids, sugars and proteins^[37]. They can be isolated from patient material, such as blood, urine, saliva, tear fluid, cerebrospinal fluid, and amniotic liquid^[99-101]. Moreover, the concentration of EVs in fluids seems to be disease-state dependent as well^[60]. Therefore, EVs are considered a novel and promising tool in diagnostics and their role as biomarkers has been well studied in multiple diseases with similarities to LSDs, including Alzheimer's Disease^[102] and PD^[103]. However, their potential as biomarkers in LSDs has yet to be explored.

Since most LSDs are elusive at birth, the diagnostic process of LSDs often relies on suspicion of the physician based on clinical manifestations. However, early diagnosis of LSDs is of utmost importance to start early treatment and prevent irreversible damage to all organ systems involved^[104]. Current diagnostics of LSDs rely on genetic testing, analyses of undegraded metabolites, and enzymatic activity with dry blood spots (DBSs). Testing on undegraded material is mostly performed on plasma and urine samples; however, this is only available for a limited number of LSDs and lacks specificity. Therefore, confirmation mostly relies on enzymatic testing with DBSs in high-throughput platforms, which is only possible for enzyme deficiencies^[105,106]. Until now, research on the diagnostic potential of EVs in LSDs is limited. Nevertheless, it has been shown that EVs isolated from Niemann-Pick type C cells contain the accumulated metabolite cholesterol and MLD-EVs contain the accumulated sulfatides^[76,94]. This might be the case for EVs in other LSDs as well, as the content of EVs reflects the contents and state of the EV-producing cells. Thus, collection of EVs from different types of body fluids could be a valuable source of biomarkers. Their prediction efficiency as biomarkers could be dependent on the location of specific LSD symptoms. For instance, tear fluid has been shown to contain approximately 100-fold higher EV concentrations than plasma^[101]. Since ocular symptoms such as corneal clouding are often present in LSDs, EVs isolated from tear fluid could be a suitable candidate for biomarker analysis. In other ocular diseases, it has been shown

that isolated EVs contain a distinctive protein pattern compared to healthy controls^[107]. Furthermore, enzyme activity studies can be performed on tear samples as previously shown for MPS I^[108]. These findings warrant EVs to be studied as a potentially valuable biomarker source in diagnostics, monitoring of disease progression and analysis of treatment efficiency in the future.

As stated before, early indication of LSDs is extremely important to start effective treatment and prevent the development of organ damage. Amniotic fluid could be used for the detection of LSDs. However, most LSDs are typically not evaluated for in the initial standard-of-care workup when babies are born. In several states in the US, parent advocacy has led to the expansion of NBS programs that now include newborn screening in dried blood spots (DBS) for Pompe, Krabbe, Gaucher, Fabry, MPS-I, MPS-II, and Niemann-Pick A/B or a subset^[109], while in the Netherlands the screening only includes MPS I^[110]. Firstly, more LSDs and other metabolic disorders could be included in the standard workup^[111]. Secondly, when parents choose to have an amniocentesis, co-collection of an amniotic fluid sample could be performed. Isolation of amniotic EVs from these samples could potentially improve early diagnosis. However, as performing an amniocentesis has several risks, collection of EVs from amniotic fluid could be considered alongside scheduled amniocentesis. Keller *et al.* showed that it is possible to separate EVs derived from the fetus and the mother and that these EVs partly represent the renal system of the fetus^[112]. Even early in development, these EVs could already carry the undegraded material in case of a LSD, as this can normally be detected in urine samples of newborns^[105]. Using EV-based biomarkers in the diagnostic process may hold the potential to improve the speed of diagnosis and clinical risk assessment of LSDs early in development. In general, the use of EVs could increase the sensitivity of biochemical assays by increasing the concentration of test material. If successful, this could improve both maternal and fetal patient management^[113].

Until now, biomarker research in LSDs is limited to the enzyme deficiencies Fabry, Gaucher and MLD. Table 3 shows an overview of all literature related to EVs and their role as biomarkers in these LSDs. EVs could play a role in real-time analysis of disease progression, which could improve personalized treatment protocols. Following this idea, Levstek *et al.* studied urine-derived EVs (uEVs) to evaluate their potential in the prediction of nephropathy progression in Fabry Disease^[114]. In almost all Fabry patients the kidneys are affected. In this study, it was shown that uEVs from Fabry patients with nephropathy contained increased expression of miR-29a-3p and miR-200a-3p. On the other hand, patients who were not affected by renal dysfunction had higher expression levels of miR-30b-5p, which plays a protective role in podocyte injury. This shows that screening of uEVs in these patients could help define the presence and status of nephropathy^[114]. For patients with some residual enzyme activity, this method could be used to assess when to start ERT, while for patients with little or no residual enzyme activity, this could mark the start of dialysis^[115]. Gaucher Disease includes a major genetic risk factor for the development of PD in these patients. Tatiana *et al.* performed proteomic profiling of EV proteins from blood plasma of Gaucher patients to find any association with PD^[116]. While they showed increased EV size in patient material, proteomics did not reveal any PD-associated proteins^[116]. Additional EV cargo, such as lipids, sugars and RNAs, were not tested in this study.

In addition to protein and miRNA content, the lipid composition of EVs could be involved in the reflection of disease pathology. Hence, Pergande *et al.* performed an untargeted lipidomic analysis of brain-derived EVs isolated from MLD mice^[94]. In the sphingolipidosis MLD, deficiency of the aryl-sulfatase A (ARSA) enzyme leads to accumulation of sulfatides, including multiple sulfated glycolipids^[94]. The accumulation of sulfatides causes severe neurological symptoms in MLD patients. Sulfatides have been found in EVs before, for instance, in EVs isolated from plasma and oligodendrocytes^[119,120]. Pergande *et al.* showed that MLD-EVs contained numerous altered lipid species from a broad range of lipid classes^[94]. This included sulfatides and

their ceramide precursors as well as fatty acids (FAs), fatty acid esters of hydroxyl fatty acids (FAHFAs) and acylglycerol lipids. The sulfatides include mostly 18-carbon fatty acid chains, which predominantly accumulate in MLD mice. Furthermore, these lipid alterations in EVs were found to be age-dependent and are proposed as relevant candidates for MLD biomarkers^[94].

Table 3. Extracellular vesicles as biomarkers for LSDs

LSD	Study design	Patient material	EV cargo (biomarker)	Isolation method	Major results	Reference
Fabry Disease	Patient material	Urine	Negative: miR-29a-3p and miR-200a-3p Positive: miR-30b-5p	Centrifugation: 2000 g, 15 min Storage -80 °C Mix urine with PBS and EDTA AMICON Ultra-15 Spin-filter 4000 g, 10 min SEC (70 nm column) AMICON Ultra-4 Spin-Filter 4000 g, 6 min at 4 °C	> uEVs contain increased expression of miR-29a-3p and miR-200a-3p over time in patients with nephrology > Over 10 years, uEVs of patients without renal dysfunction contained increased levels of miR-30b-5p, which has a protective role in podocyte injury	[114]
	Patient material	Plasma	miR-126-3p	Plasma EVs Centrifugation: 1500 g, 10 min 3000 g, 30 min 10,000 g, 30 min 100,000 g, 1 h 45 min at 4 °C	> Circulating miR-126 levels physiologically increase with age > sEVs of Fabry Disease patients contain higher miR-126-3p levels > Glycosphingolipid accumulation induces premature senescence in HUVECs and increases miR-126-3p levels	[117]
	In vitro HUVEC			HUVEC EVs Centrifugation: 300 g, 10 min 2000 g, 20 min 10,000 g, 30 min 110,000 g, 70 min Washing step 110,000 g, 70 min	> Fabry Disease may aggravate the normal aging process	
MLD	In vivo MLD mice (ARSA ^{-/-})	H/n vivo emi sagittal brains		Blade dissociation 100 µm mesh filtration 40 µm mesh filtration Centrifugation: 300 g, 10 min 2000 g, 20 min 10,000 g, 30 min 10,000 g, 30 min 100,000 g, 90 min Sucrose gradient 200,000 g, 16 h 100,000 g, 90 min	> Brain derived-EV concentration increased in parallel with age > MLD brain-EVs are significantly larger at 3 months compared to day 30 or 6 months > There is loading of accumulating sulfatides into MLD-EVs and alterations in the loading of different ceramides > Progressive decrease of FAs and FAHFAs in MLD-EVs	[94]
Gaucher Disease	Patient material	Plasma	Increased size	Centrifugation: 2000 g, 30 min 16,000 g, 30 min 110,000 g, 2 h Washing step Gentle swaying for 1h at 4 °C Filtered (0.45 µm)	> EVs of Gaucher Disease patients are increased in size and have altered morphology > Proteomic profiling of exosomal proteins did not reveal any proteins associated with PD pathogenesis	[116]
	Patient material	Serum	Increased number of MPs	Centrifugation (20 °C): 1550 g, 20 min 18,800 g, 30 min Washing step 18,800 g, 30 min	> Higher levels of MPs from different blood cells in patient samples both before and after ERT compared to controls > After 1 year of ERT, the total MPs in GD were significantly decreased	[118]

FAs: Fatty acids; FAHFAs: fatty acid ester of hydroxyl fatty acids; MPs: microparticles; SEC: size exclusion chromatography.

Further research into specific LSD-related biomarkers could improve our understanding of disease pathology as well as improve patient care. Moreover, unraveling the tissue origin of EVs secreted in different body fluids through specific tissue biomarkers could improve our understanding of disease location and progression and thus improve treatment. We suspect that the use of algorithms in EV research will progress in the upcoming years and will be of great value to analyzing EV data from body fluids in relation to disease^[51,121-123].

IMPROVEMENT OF THERAPEUTIC DELIVERY WITH EXTRACELLULAR VESICLES AS DRUG DELIVERY VEHICLES

EVs are biocompatible and have intrinsic tissue-penetrating abilities^[124]. In addition, EVs show low immunogenicity and are stable in circulation due to their negatively charged surface and their ability to avoid the mononuclear phagocytic system upon modification^[62]. These features qualify EVs as potential new therapeutic drug delivery vehicles. The ability of EVs to cross the BBB could open doors to the development of novel treatment and delivery strategies for LSDs with neurological deficits^[38]. Furthermore, it makes EVs a more desirable delivery tool over existing nanotechnologies such as liposomes, synthetic polymers and gold nanoparticles^[125,126]. EVs naturally contain lysosomal components including heparan-alpha-glucosaminide N-acetyltransferase (HGSNAT)^[50], beta-glucocerebrosidase (GBA), N-acetylgalactosamine-6-sulfate sulfatase (GALNS)^[127], cystinosis (CTNS)^[128], deficient in MPS III, Gaucher, MPS IVA, and Cystinosis respectively. Considering the interplay between the endolysosomal pathway and EV secretion, there could be a broader range of natively loaded LSD deficient proteins into EVs^[128], making them an interesting vehicle for ERT.

EV uptake into recipient cells can take place through a variety of different pathways. EV internalization predominantly occurs through endocytosis, which includes macropinocytosis, receptor-mediated, clathrin-dependent and clathrin-independent mechanisms^[129]. In addition, EVs could also enter the cells through phagocytosis. Additionally, EVs may also exert phenotypical effects on target cells without entry through direct receptor-ligand interactions^[124,130]. Most of the internalization pathways lead EVs to the endolysosomal pathway. Numerous studies have shown strong colocalization of EVs with lysosomes, reaching up to ~50%-60% in fibroblasts^[130]. For most therapies, this will be a disadvantage when (intraluminal) EV cargo needs to be delivered to the cytosol of nucleus. In that case, EVs need to escape the endosome to avoid degradation in the lysosome. It is largely unknown how EVs can naturally induce endosomal escape; however, there is some evidence that fusion between the membranes of EVs and the late endosomal membranes plays a role^[124], potentially under the influence of acidification in the endolysosomal environment^[131]. Nevertheless, EVs being trafficked towards the lysosome could be of substantial benefit for the delivery of therapeutics in the treatment of LSDs. However, whether the same distribution pattern towards the dysfunctional lysosomes in LSD cells will be seen remains to be determined.

Already a decade ago, Coulson-Thomas *et al.* showed that transplantation of human umbilical mesenchymal stem cells improves the corneal defects of MPS-7 mice^[132]. After injections of these MSCs, improvements were hypothesized to be mediated through MSC-derived EVs^[132]. At the time, EVs were gaining more recognition for their potential therapeutic abilities^[133]. To date, several studies have shown that overexpression of lysosomal enzymes in cells leads to passive loading into EVs, including the deficient enzymes of Fabry^[128], MPS IIIA^[128], MPS IVA^[127], and Batten Disease^[134]. An overview of all studies regarding EVs in the treatment of LSDs can be found in [Table 4](#).

While EVs improve drug stability and circulation time^[139], they can be further optimized to improve EV uptake and biodistribution and obtain targeted delivery. All cells release EVs, but the number, composition,

Table 4. Extracellular vesicles as therapeutic carriers for LSD treatment

LSD	Study design	EV cargo	EV concentration	Isolation method	Major results	Reference
Fabry Disease	EVs from stable GLA expressing CHO DG44 cells	GLA	<i>In vitro</i> 2.5 µg EVs/ml (c.a. 125 ng GLA/ml)	Centrifugation (4 °C): 3900 rpm, 15 min (free enzyme) 300 g, 10 min	> Significant amounts of GLA in EV lysates compared to whole cell lysates > Predominant contribution of clathrin-mediated endocytosis and macropinocytosis in EV uptake > EVs protect GLA and increase its enzymatic activity upon delivery compared to commercial GLA and agalsidase alfa used in ERT	[128]
	<i>In vitro</i> HEK293T and NAEC cells		<i>In vivo</i>	10,000 g, 20 min VIVAspin 30,000 KDa	> EVs were well tolerated <i>in vivo</i> and distributed among all main organs, including the brain after i.a. administration	
	<i>In vivo</i> GLA ^{-/-} mice		1 mg/kg GLA	7,000 g, 10 min Precipitation o/n with 'Total Exosome Isolation Reagent' 16,000 g, 1 h		
MPS IIIA	Transient SGSH expressing HEK293 cells	SGSH	2.5 µg EVs/ml	Centrifugation (4 °C): 3900 rpm, 15 min (free enzyme) 300 g, 10 min	> Significant amounts of SGSH in EV lysates compared to whole cell lysates > EVs restore lysosomal function much more efficiently than the recombinant enzyme in clinical use	[128]
	<i>In vitro</i> HEK293T and NAEC cells			2000 g, 10 min 10,000 g, 20 min VIVAspin 30,000 KDa 7000 g, 10 min Precipitation o/n with 'Total Exosome Isolation Reagent' 16,000 g, 1 h	> <i>In vivo</i> , EVs were well tolerated and distributed among all main organs, including the brain	
MPS IVA	hUMSC-derived EVs	GALNS	Co-cultures	<i>Conditioned medium</i> 3000 rpm, 15-20 min at 4 °C	> UMSC-EVs containing functional GALNS enzyme and can deliver it to GALNS deficient cells; > Mannose-6-phosphate inhibition did not affect enzyme delivery after EV treatment; > EVs are a function and novel technique for reducing GAG accumulation in cells of avascular tissues	[127]
	<i>In vitro</i> MPS IVA deficient patient fibroblasts			Centrifugation: 300 g, 10 min 10,000 g, 30 min 0.22-µm filter 100,000 g, 90 min		
Cystinosis	amMSCs and bmMSCs	CTNS	Co-cultures,	Centrifugation (4 °C): 300 g, 5 min 100,000 g, 2 h	> Amniotic fluid or bone marrow derived hMSCs, reduce pathologic cystine accumulation in co-culture with patient CTNS ^{-/-} fibroblasts or proximal tubular cells; > MSC derived EVs contain wildtype cystinosis protein and CTNS mRNA	[135]
	<i>In vitro</i> Patient derived CTNS ^{-/-} skin fibroblast and ciPTEC		1-2 mg microvesicles/mg fibroblast protein	<i>Washing</i> 100,000 g, 1 h <i>Washing</i> 100,000 g, 1 h		
	EVs derived from Spodoptera frugiperda (Sf9) cells infected with Baculovirus	CTNS	-	0.2 µm filter Dialysis to dilution of 1/2500, or 2 (cut-off 3.5 KDa)	> Vesicle addition to CTNS ^{-/-} fibroblast leads to 57% cystine depletion > LC-MS/MS analysis of the vesicles shows three cystinosis peptides with 7.4% coverage of the human cystinosis sequence > Quantitative tandem mass spectrometry showed 0.1 and 1.2 pmol cystinosis per mg of vesicle protein > Both western blot and RT-PCR confirmed the presence of	[136]
	<i>In vitro</i> CTNS ^{-/-} fibroblast			Centrifugation: 140,000 g, 3 h followed filter-sterilization		

EVs derived from Spodoptera frugiperda (Sf9) cells infected with Baculovirus containing the hCTNS-GFP		CTNS	Gas-permeable stoppers containing 50 ml medium with or without the 10^{11} /ml EVs	Freeze-thaw snap freezing medium Thawed Dialyzed into Ham's F12, 48 h at 1:2500 dilution 0.22 μ filter	cystinosis in these vesicles > Baculovirus infected Spodoptera frugiperda cells (Sf9) spontaneously produce EVs that contain cystinosis > EVs are detected in CTNS ^{-/-} fibroblast with perinuclear and cytoplasmic distribution after treatment; > Upon ex vivo ocular EV delivery, GFP signal is detected for 48 h	[137]
<i>In vitro</i> CTNS ^{-/-} fibroblast				Stored at 4 °C		
Rabbit globes						
TPP1-plasmid DNA transfected peritoneal macrophages or sonication and permeabilization of EVs with saponin to load TPP1		TPP1	<i>In vitro</i> 10^{10} /ml <i>In vivo</i> Intraperitoneal administration	Centrifugation: 300 g, 10 min 1000 g, 20 min 10,000 g, 30 min 0.2 μ m syringe filter 100,000 g, 4 h Washing 120,000 g, 70 min Washing 120,000 g, 70 min	> Both transfection with TPP1 plasmid and sonification/permeabilization lead to proficient incorporation of functional TPP1 into macrophage-EVs (EV-TPP1); > EVs significantly increase stability of TPP1 against protease degradation and provide efficient TPP1 delivery to CLIN2 ^{-/-} fibroblasts; > Around 70% of the EV-TPP1 is delivered to lysosomes; > Intraperitoneal administration of EV-TPP1 leads to accumulation in the brain of LINCL mice, which increased lifespan	[134]
<i>In vitro</i> CLIN2 ^{-/-} skin fibroblasts			Bioimaging: 2×10^{11} in 200 μ L saline Brain accumulation: 1×10^{10} in 100 μ L Therapeutic efficiency: 4.3×10^{12} in 150 μ L			
<i>In vivo</i> Intraperitoneal EV administration in late-infantile neuronal ceroid lipofuscinosis (LINCL) mice				Sonification or permeabilization		
EVs derived from mice bone marrow-derived macrophages		TPP1	<i>In vitro</i> 5×10^{11} EVs	Centrifugation: 300 g, 10 min 1000 g, 20 min 10,000 g, 30 min 0.2 μ m syringe filter 100,000 g, 4 h Washing 120,000 g, 70 min Washing 120,000 g, 70 min	> EV-TPP1 treatment through i.t. and i.n. routes lead to accumulation in the brain, decreased neuroinflammation and neurodegeneration and reduced aggregation in CLIN2 ^{-/-} mice; > EV-TPP1 treatment through i.v. and i.p. administration leads delivery to the liver, spleen, kidney, and lungs; > Combined i.t. and i.p. injection significantly prolonged lifespan in CLIN2 ^{-/-} mice	[138]
<i>In vitro</i> CLIN2 ^{-/-} primary cortical neurons			<i>In vivo</i> i.v. 6×10^{11} in 200 μ L i.p. 6×10^{11} in 200 μ L i.t. 1.5×10^{11} in 50 μ L			
<i>In vivo</i> Intrathecal and intranasal routes			i.n. 6×10^{11} in 20 μ L			
CLIN2 ^{-/-} LINCL mice						
Sonification						

cPTEC: Proximal tubular epithelial cells; CTNS: cystinosis; GALNS: acetylgalactosamine-6-sulfate sulfatase; GLA: alpha galactosidase A; i.n.: intranasal; i.p.: intraperitoneal; i.t.: intrathecal; i.v.: intravenous; SGSH: N sulfoglucosamine sulfohydrolase; TPP1: tripeptidyl peptidase-1; UMSC: umbilical mesenchymal stem cells.

functionality and physicochemical characteristics vary between cell sources^[62]. For instance, MSC-derived EVs have immunomodulatory and anti-inflammatory effects. Recently, unmodified MSC-EVs were used to treat osteoarthritis and resulted in amelioration of disease progression through induced polarization of M2-type macrophages among other effects^[140]. These positive effects on disease related to connective tissue could be beneficial to treat residual disease and target the connective tissue in LSD patients. Furthermore, the native characteristics of MSC-EVs could be further exploited through engineering. This might lead to delivery of the loaded protein while also promoting tissue repair and regeneration within the same treatment. Moreover, EV functionality is

dependent on the target as well, considering that some EVs are better taken up by one cell type compared to another^[36]. Therefore, therapy specific selection of the optimal cell source, cell cultivation procedure, EV extraction and purification methods, and storage might be needed.

Recently, Seras-Franzoso *et al.* showed that stabile GLA expressing cell lines were able to produce EVs that protected the enzymes from proteases, and subsequently improved enzymatic delivery directly compared to soluble GLA and clinically approved ERT agalsidase alfa^[128]. In addition, analysis of the GLA biodistribution showed that EVs were able to deliver significantly more active enzymes to the kidneys than non-encapsulated enzymes. It must be noted that agalsidase alfa used in ERT is governed by the presence of the mannose-6-receptor to increase uptake. This receptor is highly expressed in the liver and therefore might interfere with the biodistribution of non-encapsulated enzymes^[141]. Furthermore, they showed the uptake of fluorescent labelled EV-GLA in the brain parenchyma with confocal microscopy an hour post-intra-arterially (i.a.) administration through cannulation of the external carotid artery. This delivery across the BBB could not be detected after intravenous administration through the tail vein^[128]. Likewise, Haney *et al.* showed the loading of tripeptidyl peptidase-1 (TPP1) into EVs, which greatly improved enzyme stability^[134,138]. After showing functional delivery of the TPP1 in EV treated fibroblast, the authors examined intraperitoneal administration of EVs in late-infantile neuronal ceroid lipofuscinosis (LINCL) mice to study EV distribution towards the brain. This type of administration led to accumulation of the enzyme in the brain. However, a clear distribution towards peripheral organs was also seen, including the liver, spleen, kidneys and lungs^[134]. Therefore, they examined different EV administration routes in mice in another study to see the effect on crossing the BBB. Both intranasal and intrathecal administration resulted in accumulation of TPP1 in the brain and spinal cord, which reduced aggregation of lysosomal storage material, neurodegeneration and neuroinflammation. Importantly, these administration routes showed lower distribution of the EVs towards the peripheral organs compared to intraperitoneal and intravenous administration^[138]. The loading of enzymes into EVs and their distribution towards the central nervous system (CNS) shows the potential of EVs as therapeutic carriers to treat the CNS. Thus, EVs could be used to load and protect ERT to improve biodistribution and lower antibody generation in patients.

ENGINEERING OF EXTRACELLULAR VESICLES FOR THERAPEUTIC TREATMENT OF LSDs

While native EVs have multiple features that qualify them as promising drug delivery vehicle, endogenous cargo loading, circulation time and tissue targeting are often inadequate. Biodistribution studies often show accumulation of EVs in the liver, spleen, gastrointestinal tract and lungs. However, the specific pattern of distribution seems to depend on the cell type the EVs are derived from, the route of administration^[142] as well as the injected dose^[64]. Several studies have demonstrated a role for integrins in tissue targeting^[143,144]. Integrins are enriched in EVs through their association with tetraspanins^[145]. For instance, integrin expression patterns in tumor-derived EVs play a role in the uptake of EVs by organ-specific cells and creation of a pre-metastatic niche^[143]. The use of fluorescent labelling and tracking techniques are valuable tools to study and optimize the distribution pattern of (engineered) EVs. For an overview of the currently used labelling and tracking techniques in the EV field, we refer to the review of Kooijmans *et al.*^[129]. To further optimize performance, EVs can be modified and engineered. To date, studies on EV engineering for LSD treatment have solely focused on actively increasing therapeutic cargo loading. These modifications can be obtained through a variety of different exogenous and endogenous methods. In exogenous techniques, EVs are therapeutically loaded post-isolation by simple incubation, electroporation, sonication, extrusion, and freeze-thawing. These techniques have variable degrees of success and can lead to EV or cargo aggregation^[146,147]. Uniquely, EVs can also be endogenously altered by biologically engineering the cells that produce them. This strategy can equip EVs with new moieties while preserving their membrane

integrity, which is an advantage over exogenous loading techniques^[123].

Therapeutic protein loading into EVs is often achieved through parental cell engineering with genes that encode for the therapeutic protein fused to a membrane protein enriched in EVs or a transmembrane domain. These loading strategies may include the use of EV enriched proteins such as tetraspanins (CD9, CD63 and CD81), PTGFRN, and BASP1^[148] or transmembrane domains such as the N-terminal fragment of syntenin^[149]. With this strategy, the therapeutic protein will naturally be incorporated into EVs during biogenesis. This approach allows for both internal and external display of the therapeutic protein^[150]. Successful protein loading and delivery, both *in vitro* and *in vivo*, has been shown in multiple studies^[150-152]. This shows the potential for active enzyme loading and accumulation in EVs to increase functional delivery. When designing active enzyme loading strategies, it must be considered that lysosomal enzymes often require post-translational modification. These modifications need to take place before loading enzymes into EVs to eventually lead to functional delivery upon EV treatment^[153,154].

To date, the only LSD for which active enzyme loading into EVs has been studied is Gaucher Disease. An overview of these studies can be found in Table 5. In patients with Gaucher Disease, the GBA enzyme is deficient, which leads to symptoms that include neurological complications. Do *et al.* showed active GBA loading into EVs with the use of vesicular stomatitis virus glycoprotein (VSV-G)^[153]. In addition to loading and potential uptake through the VLDL receptor on the surface of recipient cells, VSV-G can also induce endosomal escape^[90]. It should be noted that induced endosomal escape could potentially counteract the goal of this EV treatment by enabling the EV cargo escape their route to the lysosome. Despite that, Do *et al.* show significant colocalization of the EVs throughout uptake with the endosome, late-endosome and lysosome in an *in vitro* HEK293 cell model^[153]. However, it is possible that delivery of GBA to these cellular structures would even further increase with the use of a loading strategy that does not additionally induce endosomal escape. Flow cytometry analysis showed a 73%-75% uptake rate based on mean fluorescent intensity of the co-loaded GFP^[153]. Although this study focused on *in vitro* cell culture models, it underlines the potential of active loading strategies into EVs to deliver deficient enzymes as next-generation ERT. In the future, such therapies may lower antibody generation to ERT in patients and deliver functional enzymes to target organs including the central nervous system (CNS), which is severely affected in multiple LSDs.

THE USE OF EVs IN FUTURE THERAPEUTIC TREATMENT OF LSDs

Engineered EVs have already been explored for multiple purposes, including regenerative therapy^[155], immune modulation^[156], delivery of small molecular drugs^[157], vaccines^[158], therapeutic proteins, and nucleic acids^[159]. For instance, cardiac progenitor cell-derived EVs loaded with miR-322 outperformed their unloaded controls in enhancing angiogenesis in mice after ischemic injury^[155]. Furthermore, numerous small molecular drugs have been successfully incorporated into EVs, including curcumin. The loading of curcumin into EVs enhanced its delivery and anti-inflammatory activity^[156]. Drug loading into EVs has been shown to improve accumulation in target cells and enhance drug stability and circulation time^[139]. Currently, multiple groups are exploring the potential of employing EV engineering for the development of therapeutic treatments. The variety and possibilities of this technique could greatly improve therapeutic options for LSDs in the future.

Alongside the mentioned positive effects of using EVs to deliver ERT, delivery of other forms of LSD treatment might also benefit from this camouflage strategy. This may include SRT and PCT, which use small drugs to inhibit the production of the accumulating substrate and stabilize native structures of mutated enzymes, respectively^[26,27]. Loading both SRT and CPT into EVs might improve their distribution and potential delivery to the CNS. Furthermore, newly discovered molecular drugs might benefit from

Table 5. Engineered extracellular vesicles to treat LSDs

LSD	Study design	EV cargo	Readout	EV concentration	Isolation method	Major results	Reference
Gaucher Disease	EVs from HEK293T cells	GBA	<i>In vitro</i> HEK293T, U7 and HepG2	0.3 µg/µl	Centrifugation: 1500 g, 10 min 0.2 µm syringe filter	> HEK cells transfected with VSVG-GFP-GBA constructs secrete EVs that contain significantly more active GBA compared to control EVs;	[153]
	Active loading				Mixed with ExoQuick-TC solution (1:4) o/n at 4 °C	> The uptake of green, fluorescent dye labelled GBA-EVs was 73%–75%;	
	VSVG-GFP-GBA				> Upon treatment, GBA loaded EVs co-localize with lysosomes and lead to the delivery of functional GBA (40%–45%)	> Both transfection with TPP1 plasmid and sonification/permeabilization lead to proficient incorporation of functional TPP1 into macrophage-EVs (EV-TPP1) > EVs significantly increase stability of TPP1 against protease degradation and provide efficient TPP1 delivery to CLIN2 ^{-/-} fibroblasts > Around 70% of the EV-TPP1 is delivered to lysosomes > Intraperitoneal administration of EV-TPP1 leads to accumulation in the brain of LINCL mice, which increased lifespan	[134]
CLIN2	TPP1-plasmid DNA transfected peritoneal macrophages or sonication and permeabilization of EVs with saponin to load TPP1	TPP1	<i>In vitro</i> IC21 cells, neuronal PC12 cells and Human skin CLIN2 ^{-/-} fibroblasts	<i>In vitro</i> 10 ¹⁰ /mL	Centrifugation: 300 g, 10 min 1000 g, 20 min 10,000 g, 30 min 0.2 µm syringe filter 100,000 g, 4 h		
	<i>In vitro</i> CLIN2 ^{-/-} skin fibroblasts		<i>In vivo</i> LINCL mice	<i>In vivo</i> Intraperitoneal administration	Bioimaging: 2 × 10 ¹¹ in 200 µL saline Brain accumulation: 1 × 10 ¹⁰ in 100 µL Therapeutic efficiency: 4.3 × 10 ¹² in 150 µL	Washing 120,000 g, 70 min	
	<i>In vivo</i> Intraperitoneal EV administration in late-infantile neuronal ceroid lipofuscinosis (LINCL) mice				Sonification or permeabilization		
	EVs derived from mice bone marrow-derived macrophages	TPP1	<i>In vitro</i> Primary bone murine marrow-derived macrophages, cortical neurons and IC21 cells	<i>In vitro</i> 5 × 10 ¹¹ EVs	Centrifugation: 300 g, 10 min 1000 g, 20 min 10,000 g, 30 min 0.2 µm syringe filter 100,000 g, 4 h	> EV-TPP1 treatment through i.t. and i.n. routes lead to accumulation in the brain, decreased neuroinflammation and neurodegeneration and reduced aggregation in CLIN2 ^{-/-} mice	[138]
	<i>In vitro</i> CLIN2 ^{-/-} primary cortical neurons			<i>In vivo</i> i.v. 6 × 10 ¹¹ in 200 µL i.p. 6 × 10 ¹¹ in 200 µL i.t. 1.5 × 10 ¹¹ in 50 µL	Washing 120,000 g, 70 min	> EV-TPP1 treatment through i.v. and i.p. administration leads delivery to the liver, spleen, kidney, and lungs. > Combined i.t. and i.p. injection significantly prolonged lifespan in CLIN2 ^{-/-} mice	
	<i>In vivo</i> Intrathecal and intranasal routes CLIN2 ^{-/-} LINCL mice		<i>In vivo</i> LINCL mice	i.n. 6 × 10 ¹¹ in 20 µL	Washing 120,000 g, 70 min		
Sonification							

GBA: β-Glucocerebrosidase/β-glucosidase; GCase: Glucocerebrosidase; VSV-G: Vesicular stomatitis virus G.

being loaded into EVs as well by increased loading efficiency, protection, improved circulation and crossing of biological membranes. As discussed before, in most LSDs, autophagy is altered and affected cells might reduce their accumulation through secretion in the hope of maintaining homeostasis. Curcumin treatment has been shown to alleviate the phenotype of Niemann-Pick type C through the elevation of cytosolic calcium levels^[160]. Additionally, it has been

shown that curcumin promotes EV secretion in cells that represent Niemann-Pick type C, inducing cholesterol shuttling out of the cell^[161]. Loading and delivery of curcumin via EVs may be a therapeutic approach to treat Niemann-Pick type C.

In addition to enzyme deficiencies, there are other subgroups of LSDs that include deficiencies in integral membrane proteins, transporters and proteins involved in the post-translational modification, trafficking, or regulation. For these subgroups, there are limited treatment options available. Gene therapy was evaluated to treat Niemann-Pick type C in which patients are missing or have defective NPC1 transporters. Currently, Evox Therapeutics filed a patent to facilitate the loading of NPC1 fused to syntenin/CD63 into EVs (Patent number: WO2019/092287 AI). The use of EVs to transport NPC1 will stabilize the integral membrane protein through the presence of lipid molecules^[162]. This strategy of EV engineering could potentially be a step forward in designing treatment strategies for currently untreatable LSDs.

Current challenges of EVs that must be addressed to improve their therapeutic efficacy include their rapid clearance and limited targeted delivery. Possible solutions may involve adaptation of administration routes depending on the target tissue. Local administration might be preferred for connective tissues with limited blood supply, whereas intranasal or intrathecal administration might be beneficial to target the CNS^[138]. Moreover, modification of the EV surface may improve EV circulation and tissue targeting^[63,163,164]. Kamerkar *et al.* have reported that the presence of CD47 on EV surface inhibited EV uptake and clearance by macrophages and monocytes, which may lead to increased cargo delivery^[165]. However, considering that LSDs are monogenetic disorders, the monocyte-macrophage system is affected in multiple LSDs as well^[166]. Therefore, the uptake of drug-loaded EVs by these immune cells could also be beneficial. Several bioengineering strategies have been developed to increase the affinity of EVs for specific recipient cells. These approaches include receptor-ligand, enzymatic, and antigen-antibody or a combination of these methods. For instance, EVs containing a LAMP2b-designed ankyrin repeat protein (DARPin) G3 fusion protein are able to specifically target HER-2 positive breast cancers through receptor-ligand interaction. DARPins are a class of synthetic peptides that can bind biological receptors with high specificity and binding affinity and specificity^[167]. An adaptation of the EV membrane that both improved circulation time and cell specificity was shown by the addition of epidermal growth factor receptor (EGFR) nanobodies conjugated to phospholipid (DMPE)-polyethylene glycol (PEG). The shielding properties of PEG compromised cell binding and increased detectability of EVs in the plasma from less than 10 min to over 60 min post-injection. At the same time, the EGFR nanobodies directed the EVs towards tumor cells overexpressing the EGFR^[63]. Surface modification can also be used to evade phagocytosis by the mononuclear phagocyte system (MPS). These strategies will increase circulation time which will improve the chance of EV uptake by the specific recipient cells and can be used to increase EV accumulation and cargo delivery in targeted tissues^[63]. Alongside biological engineering, EVs can externally be altered through chemical or synthetic engineering by using click chemistry or fusion with nanotechnologies^[62,129]. All the different engineering strategies make it possible to optimize EVs to potentially target any tissue and disease.

EV-MEDIATED GENE EDITING: THE POTENTIAL ROUTE TO A PERMANENT CURE FOR LSDs

LSDs are genetic disorders and recent studies have been exploring the possibilities of gene editing to correct their mutations^[168]. CRISPR/Cas technology possesses the ability to selectively target genes and create deletions, insertions, and base pair substitutions. In this technology, the Cas9 protein is guided towards a sequence with the help of single guide RNA (sgRNA). When using the native Cas9 protein, this results in a specific double-stranded break (DSB) in the targeted genomic DNA that can be corrected by the native DNA repair mechanisms of the cell^[169]. The repair of DSBs is associated with non-specific mutations, since

it is typically repaired by the error-prone non-homologous end-joining (NHEJ) pathway, resulting in point mutations, deletions, and frameshifts^[170]. To create precise changes in the DNA, the homology-directed repair (HDR) pathway utilizes a DNA repair template which shows homology in the sequences surrounding the DSB. This template can be delivered as a double-stranded DNA template or a single-stranded DNA oligo, which can contain a desired restorative mutation. However, HDR occurs at a relatively low frequency as compared to NHEJ. Thus, in order to generate base pair substitutions without the presence of NHEJ-mediated non-specific mutations, Base Editing (BE) was developed. Here, enzymatic groups that are able to convert specific nucleotides are attached to dCas9, an adapted form of Cas9 whose endonuclease activity is removed through point mutations in its endonuclease domains. As a result, Cas9 will no longer create DSBs while still interacting with specific genomic sequences through the sgRNAs, and the base editing enzymatic groups are able to generate nucleotide substitutions in the sgRNA target sequence. There are different types of base editors, including cytosine base editors (CBEs) and adenine base editors (ABEs) that can mediate single base changes in the genome. Base editors can induce these alterations without requiring DSBs, HDR processes, or donor DNA templates^[171–173]. The main drawback of these techniques is that the type of substitutions that can be made are currently limited, and since these substitutions could be made throughout the ~20 nt target sequence of the sgRNA, only a limited number of target sequences are suitable for base editing techniques.

Recently, Anzalone *et al.* reported a new versatile and precise genome editing method called prime editing^[174]. Prime editing does not require a separate donor DNA repair template to precisely edit the DNA. Instead, the needed repair template is incorporated into the sgRNA combined with the desired edit, now called prime editing guide RNA (pegRNA). Furthermore, a catalytically impaired Cas9 nickase is fused to an engineered reverse transcriptase, now called the prime editor (PE). As prime editing is based on the use of a Cas9 nickase, which only cuts one strand of the double helix, DSBs and the subsequent error-prone NHEJ repair process are avoided. After the pegRNA guides the PE towards the target sequence, the reverse transcriptase domain of the PE uses the repair sequence added to the pegRNA to template reverse transcription of the desired edit. This leads to direct transcription of the DNA onto the nicked target DNA strand. The edited DNA strand will replace the original DNA strand, which creates a heteroduplex of one edited strand and one unedited strand. The edited strand will be favored due to the inherent preference of the endogenous endonuclease FEN1 to excise 5' flaps. This leads to hybridization of the edited 3' flap being favored copying the edit onto the unedited strand, completing the process. Prime editing can incorporate all the potential 12 modifications; accordingly, prime editing could, in principle, correct up to 89% of known genetic variants associated with human diseases^[174,175]. In addition to efficient gene correction in cell lines, prime editing has already been shown to be as efficient in 3D grown organoids derived from patients with inherited metabolic disorders^[176]. This substantially expands the scope and capabilities of genome editing, but the *in vivo* delivery remains challenging^[174].

The CRISPR/Cas system can be delivered either as plasmid DNA, mRNA or as ribonucleoprotein (RNP) complex. Delivery of the RNP complex has advantages over plasmid and mRNA delivery, including lower off-target effects, and faster and more efficient gene editing^[177]. Nevertheless, there are limitations to *in vivo* RNP complex delivery, including its large size, negative charge, immunogenicity, pre-existing antibodies^[178], and rapid degradation^[179]. Loading of the RNP complex into EVs could potentially overcome most of its limitations, as well as lowering its off-target effects by increased tissue targeting.

Whereas EV trafficking towards the lysosome after uptake by recipient cells is an advantage when using engineered EVs to deliver ERT, for the functional delivery of the RNP complex, endosomal escape is required, as the RNP complex needs to be able to reach the cell nucleus to induce genomic editing.

Incorporation of viral fusogenic proteins into the EV membrane could increase the relatively low efficiency of endosomal escape of unaltered EVs. The viral protein VSV-G is known to incorporate into the EV membrane upon transfection of the cells with VSV-G encoding plasmids^[180]. This protein specifically induces endosomal escape, as it requires the decrease in pH in the late endosome to undergo the conformational transformation that induces the membrane fusion that facilitates cargo release. This will greatly increase endosomal escape and with that the delivery of the EV loaded RNP complexes or other therapeutic components that require delivery to the cytoplasm. Nevertheless, the use of viral proteins can be problematic due to their cytotoxicity and potential immunogenicity^[181]. The substitution of these viral proteins is a hurdle that needs to be overcome. EVs may contain some endogenous capacity to escape the endosome that could be explored. For instance, through the incorporation of endogenous proteins with fusogenic activity like syncytins. Syncytins are incorporated into placenta-derived EVs and mediate uptake by recipient cells^[182]. Their incorporation into the membrane may facilitate EV fusion and subsequently deliver the EV cargo^[129,183]. It is hypothesized that EVs contain additional proteins that facilitate endosomal escape through membrane fusion, as treatment of unmodified EVs with proteinases has been shown to abrogate their capability of membrane fusion^[131]. The use of endogenous proteins with fusogenic activity to induce endosomal escape for the delivery of CRISPR/Cas could increase the safety of these EVs.

Efficient gene editing after EV mediated delivery of RNP complexes has already been demonstrated. Active loading can be obtained through direct or indirect fusion of the Cas9 protein to known EV markers. This was shown by the indirect loading approach of Ye *et al.*, who used CD63-GFP and Cas9-GFP nanobody fusion proteins that sufficiently loaded and delivered the complex^[184]. Furthermore, Wang *et al.* proposed the use of ARRDC1, a protein required in plasma membrane budding together with known EV marker TSG101 to form ectosomes^[152]. ARRDC1 interacts with proteins containing WW domains and recruits them into vesicles. Wang *et al.* fused either two or four WW domains to a Cas9 protein and showed that co-expression with ARRDC1 leads to sufficient loading of the RNP complex into EVs^[152]. They went on to show functional gene editing upon delivery by knocking down GFP expression in their recipient cells using an anti-GFP sgRNA^[152]. Recently, light-induced dimerization loading was shown to be effective. In this approach, Osteikoetxea *et al.* used Cryptochrome 2 combined with either CD9 or a Myristoylation-Palmitoylation-Palmitoylation lipid modification^[185]. This method provides controllable loading and release of the complex upon delivery^[185]. In addition to loading of the complex through the Cas9 protein, RNA binding proteins such as HuR can increase complex loading by the addition of AU rich elements to the sgRNA^[159]. At the same time, this strategy shows the potential of EV engineering in the delivery of other RNAs, including miRNA^[159] and mRNA^[152]. Furthermore, the delivery of Cas9-sgRNA or prime editing complexes with EVs could be a major step towards a permanent cure for LSDs. Figure 2 gives an overview of the general EV engineering strategies and the potential of engineered EVs for future LSD treatment.

CONCLUSION

As with any new class of therapeutic agents, EVs face several hurdles in their advancement into the clinic^[186]. Optimization of loading efficiency, EV production, isolation, functional properties, purity, storage for potential off-the-shelf availability, as well as selection of the optimal cell source, is needed^[47]. In addition, standardization of these processes' clinical and industry-accepted validation must be developed for the regulatory approval of EV- diagnostics and therapeutics. A better understanding of EV biogenesis, uptake, cargo delivery and the normal *in vivo* journey will not only accelerate their therapeutic translation, but also improve their function in understanding LSD pathology and use as biomarkers. The EV field holds great potential and may one day contribute to diagnostics and the design of a new generation of smart vehicles for targeted delivery of drugs, ERT, RNA therapeutics and gene editing to manage or treat multisystemic LSDs.

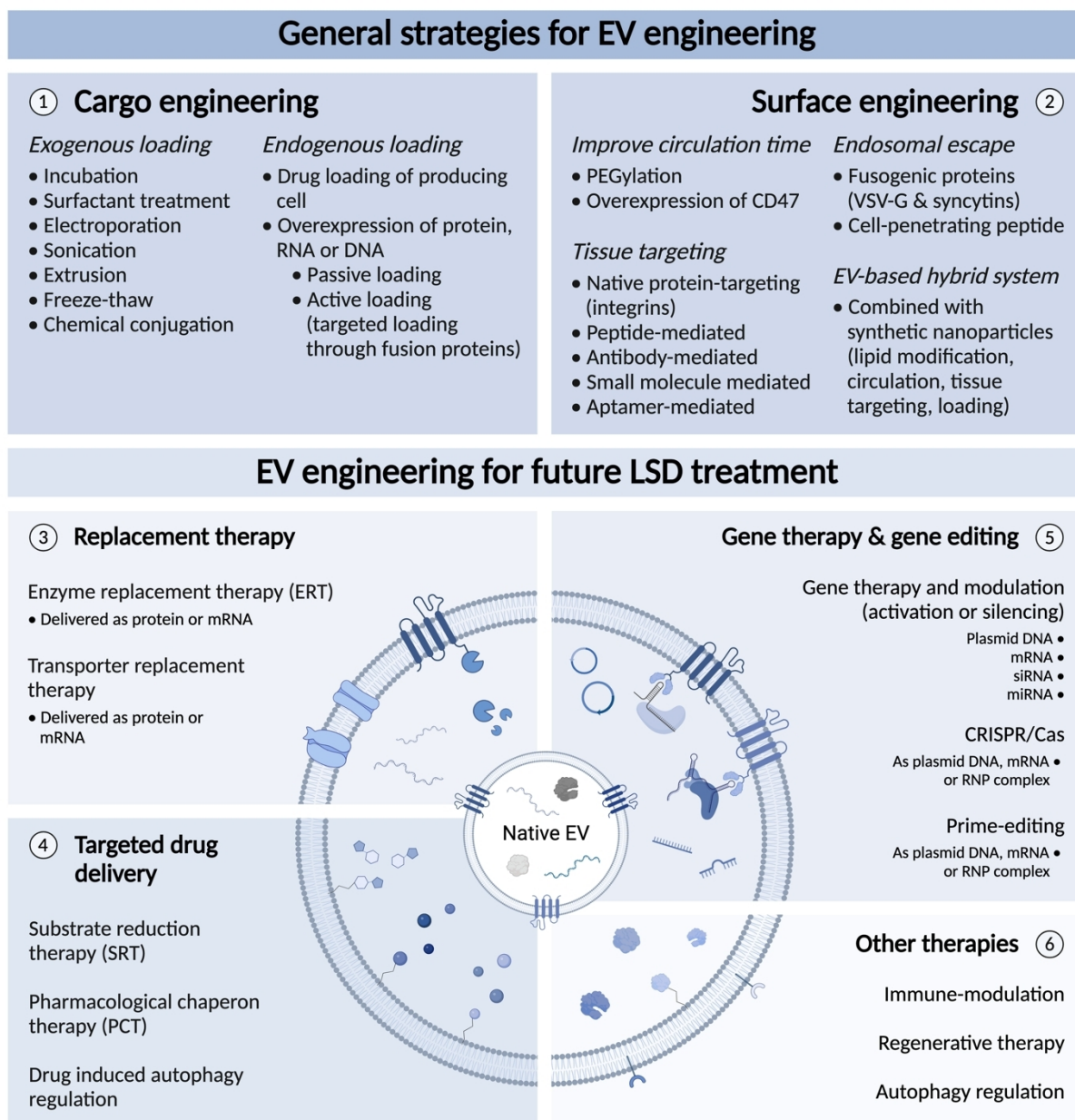


Figure 2. Future EV-based therapeutic options for the treatment of LSDs. Various EV engineering approaches and techniques can be used to optimize the therapeutic potential of EVs, including: (1) Cargo engineering, which can either be accomplished through exogenous loading techniques applied to the EVs post-isolation or endogenous loading techniques. In endogenous loading techniques, loading is accomplished through adaptation of the parental cell. Cargo can either be passively or actively loaded with the use of fusion proteins binding the cargo to EV-enriched proteins or transmembrane domains; (2) Surface engineering, which can improve circulation time of EVs, their tissue targeting potential and endosomal escape, which is needed for efficient intraluminal cargo delivery. Furthermore, EVs can be combined with synthetic nanoparticles. These hybrid systems can modulate the contents and functionality of both the particle surface and cargo. Future EV therapeutic modalities for LSDs potentially include; (3) Replacement therapies, which include enzyme-, and transporter-replacement therapy. These therapies can be loaded into EVs and delivered to target cells as mRNA or directly as protein; (4) Targeted drug delivery, for substrate reduction therapy (SRT), pharmacological chaperon therapy (PCT) and potentially drug induced autophagy regulation; (5) Gene therapy & gene editing, which includes loading of constructs such as plasmid DNA, mRNA, miRNA and siRNA for gene addition or modulation. Moreover, EVs could be engineered to contain CRISPR/Cas or Prime editing constructs in the form of plasmid DNA, mRNA or RNP complexes; and (6) Other therapies, which include unmodified or engineered EVs for adjuvant therapy, including immune-modulatory, regenerative therapy and autophagy regulation.

DECLARATIONS

Acknowledgements

Figures were created with BioRender.com.

Authors' contributions

Wrote and edited the manuscript: Hegeman CV, de Jong OG, Lorenowicz MJ

Availability of data and materials

Not applicable.

Financial support and sponsorship

None.

Conflicts of interest

All authors declared that there are no conflicts of interest.

Ethical approval and consent to participate

Not applicable.

Consent for publication

Not applicable.

Copyright

© The Authors 2022.

REFERENCES

1. Walkley SU, Vanier MT. Secondary lipid accumulation in lysosomal disease. *Biochim Biophys Acta* 2009;1793:726-36. DOI PubMed PMC
2. Lamanna WC, Lawrence R, Sarrazin S, Esko JD. Secondary storage of dermatan sulfate in Sanfilippo disease. *J Biol Chem* 2011;286:6955-62. DOI PubMed PMC
3. Prinetti A, Prioni S, Chiricozzi E, Schuchman EH, Chigorno V, Sonnino S. Secondary alterations of sphingolipid metabolism in lysosomal storage diseases. *Neurochem Res* 2011;36:1654-68. DOI PubMed
4. Lieberman AP, Puertollano R, Raben N, Slaughterhaupt S, Walkley SU, Ballabio A. Autophagy in lysosomal storage disorders. *Autophagy* 2012;8:719-30. DOI PubMed PMC
5. Köse S, Aerts-kaya F, Uçkan Çetinkaya D, Korkusuz P. Stem cell applications in lysosomal storage disorders: progress and ongoing challenges. In: Turksen K, editor. *Cell biology and translational medicine*, Volume 14. Cham: Springer International Publishing; 2021. p. 135-62. DOI PubMed
6. Platt FM, Boland B, van der Spoel AC. The cell biology of disease: lysosomal storage disorders: the cellular impact of lysosomal dysfunction. *J Cell Biol* 2012;199:723-34. DOI PubMed PMC
7. Platt FM, d'Azzo A, Davidson BL, Neufeld EF, Tiffit CJ. Lysosomal storage diseases. *Nat Rev Dis Primers* 2018;4:27. DOI PubMed
8. Marques ARA, Saftig P. Lysosomal storage disorders - challenges, concepts and avenues for therapy: beyond rare diseases. *J Cell Sci* 2019;132:jcs221739. DOI PubMed
9. Parenti G, Andria G, Ballabio A. Lysosomal storage diseases: from pathophysiology to therapy. *Annu Rev Med* 2015;66:471-86. DOI PubMed
10. Meikle PJ, Hopwood JJ, Clague AE, Carey WF. Prevalence of lysosomal storage disorders. *JAMA* 1999;281:249-54. DOI PubMed
11. Fuller M, Meikle PJ, Hopwood JJ. Epidemiology of lysosomal storage diseases: an overview. In: Mehta A, Beck M, Sunder-Plassmann G, editors. *Fabry disease: perspectives from 5 years of FOS*. Oxford: Oxford PharmaGenesis; 2006. Chapter 2. PubMed
12. Mehta A, Beck M, Sunder-Plassmann G. *Fabry disease: perspectives from 5 years of FOS*. Oxford: Oxford PharmaGenesis; 2006. PubMed
13. Stone WL, Basit H, Master SR. *Gaucher disease*. StatPearls. Treasure Island (FL): StatPearls Publishing; 2022. PubMed
14. Grabowski GA, Dinur T, Osiecki KM, Kruse JR, Legler G, Gatt S. Gaucher disease types 1, 2, and 3: differential mutations of the acid beta-glucosidase active site identified with conduritol B epoxide derivatives and sphingosine. *Am J Hum Genet* 1985;37:499-510. PubMed PMC

15. van den Broek BTA, van Doorn J, Hegeman CV, et al. Hurdles in treating Hurler disease: potential routes to achieve a “real” cure. *Blood Adv* 2020;4:2837-49. DOI PubMed PMC
16. Li M. Enzyme replacement therapy: a review and its role in treating lysosomal storage diseases. *Pediatr Ann* 2018;47:e191-7. DOI PubMed
17. Kishnani PS, Dickson PI, Muldowney L, et al. Immune response to enzyme replacement therapies in lysosomal storage diseases and the role of immune tolerance induction. *Mol Genet Metab* 2016;117:66-83. DOI PubMed
18. Safary A, Akbarzadeh Khiavi M, Mousavi R, Barar J, Rafi MA. Enzyme replacement therapies: What is the best option? *Bioimpacts* 2018;8:153-7. DOI PubMed PMC
19. Solomon M, Muro S. Lysosomal enzyme replacement therapies: historical development, clinical outcomes, and future perspectives. *Adv Drug Deliv Rev* 2017;118:109-34. DOI PubMed PMC
20. Aldenhoven M, Jones SA, Bonney D, et al. Hematopoietic cell transplantation for mucopolysaccharidosis patients is safe and effective: results after implementation of international guidelines. *Biol Blood Marrow Transplant* 2015;21:1106-9. DOI PubMed
21. Guffon N, Pettazzoni M, Pangaud N, et al. Long term disease burden post-transplantation: three decades of observations in 25 Hurler patients successfully treated with hematopoietic stem cell transplantation (HSCT). *Orphanet J Rare Dis* 2021;16:60. DOI PubMed PMC
22. Selvanathan A, Ellaway C, Wilson C, Owens P, Shaw PJ, Bhattacharya K. Effectiveness of early hematopoietic stem cell transplantation in preventing neurocognitive decline in mucopolysaccharidosis type II: a case series. In: Morava E, Baumgartner M, Patterson M, Rahman S, Zschocke J, Peters V, editors. JIMD Reports, Volume 41. Berlin: Springer Berlin Heidelberg; 2018. p. 81-9. DOI PubMed PMC
23. Mynarek M, Tolar J, Albert MH, et al. Allogeneic hematopoietic SCT for alpha-mannosidosis: an analysis of 17 patients. *Bone Marrow Transplant* 2012;47:352-9. DOI PubMed
24. Beschle J, Döring M, Kehrer C, et al. Early clinical course after hematopoietic stem cell transplantation in children with juvenile metachromatic leukodystrophy. *Mol Cell Pediatr* 2020;7:12. DOI PubMed PMC
25. Wright MD, Poe MD, DeRenzo A, Haldal S, Escolar ML. Developmental outcomes of cord blood transplantation for Krabbe disease: a 15-year study. *Neurology* 2017;89:1365-72. DOI PubMed PMC
26. Aerts JM, Hollak CE, Boot RG, Groener JE, Maas M. Substrate reduction therapy of glycosphingolipid storage disorders. *J Inherit Metab Dis* 2006;29:449-56. DOI PubMed
27. Hughes DA, Nicholls K, Shankar SP, et al. Oral pharmacological chaperone migalastat compared with enzyme replacement therapy in Fabry disease: 18-month results from the randomised phase III ATTRACT study. *J Med Genet* 2017;54:288-96. DOI PubMed PMC
28. Nagree MS, Scalia S, McKillop WM, Medin JA. An update on gene therapy for lysosomal storage disorders. *Expert Opin Biol Ther* 2019;19:655-70. DOI PubMed
29. Phinney DG, Isakova IA. Mesenchymal stem cells as cellular vectors for pediatric neurological disorders. *Brain Res* 2014;1573:92-107. DOI PubMed PMC
30. Pittenger MF, Discher DE, Péault BM, Phinney DG, Hare JM, Caplan AI. Mesenchymal stem cell perspective: cell biology to clinical progress. *NPJ Regen Med* 2019;4:22. DOI PubMed PMC
31. Jackson M, Derrick Roberts A, Martin E, Rout-Pitt N, Gronthos S, Byers S. Mucopolysaccharidosis enzyme production by bone marrow and dental pulp derived human mesenchymal stem cells. *Mol Genet Metab* 2015;114:584-93. DOI PubMed
32. Hawkins-Salsbury JA, Reddy AS, Sands MS. Combination therapies for lysosomal storage disease: Is the whole greater than the sum of its parts? *Hum Mol Genet* 2011;20:R54-60. DOI PubMed PMC
33. Koç ON, Peters C, Aubourg P, et al. Bone marrow-derived mesenchymal stem cells remain host-derived despite successful hematopoietic engraftment after allogeneic transplantation in patients with lysosomal and peroxisomal storage diseases. *Exp Hematol* 1999;27:1675-81. DOI PubMed
34. Meuleman N, Vanhaelen G, Tondreau T, et al. Reduced intensity conditioning haematopoietic stem cell transplantation with mesenchymal stromal cells infusion for the treatment of metachromatic leukodystrophy: a case report. *Haematologica* 2008;93:e11-3. DOI PubMed
35. de Windt TS, Vonk LA, Slaper-Cortenbach IC, et al. Allogeneic mesenchymal stem cells stimulate cartilage regeneration and are safe for single-stage cartilage repair in humans upon mixture with recycled autologous chondrons. *Stem Cells* 2017;35:256-64. DOI PubMed
36. Yáñez-Mó M, Siljander PR, Andreu Z, et al. Biological properties of extracellular vesicles and their physiological functions. *J Extracell Vesicles* 2015;4:27066. DOI PubMed PMC
37. de Jong OG, Verhaar MC, Chen Y, et al. Cellular stress conditions are reflected in the protein and RNA content of endothelial cell-derived exosomes. *J Extracell Vesicles* 2012;1:18396. DOI PubMed PMC
38. Saint-Pol J, Gosselet F, Duban-Deweer S, Pottiez G, Karamanos Y. Targeting and crossing the blood-brain barrier with extracellular vesicles. *Cells* 2020;9:851. DOI PubMed PMC
39. Banks WA, Sharma P, Bullock KM, Hansen KM, Ludwig N, Whiteside TL. Transport of extracellular vesicles across the blood-brain barrier: brain pharmacokinetics and effects of inflammation. *Int J Mol Sci* 2020;21:4407. DOI PubMed PMC
40. Liu S, Wu X, Chandra S, et al. Extracellular vesicles: emerging tools as therapeutic agent carriers. *Acta Pharm Sin B* 2022;12:3822-42. DOI PubMed PMC

41. Abasolo I, Seras-Franzoso J, Moltó-Abad M, et al. Nanotechnology-based approaches for treating lysosomal storage disorders, a focus on Fabry disease. *Wiley Interdiscip Rev Nanomed Nanobiotechnol* 2021;13:e1684. [DOI](#) [PubMed](#)
42. Schuh RS, Baldo G, Teixeira HF. Nanotechnology applied to treatment of mucopolysaccharidoses. *Expert Opin Drug Deliv* 2016;13:1709-18. [DOI](#) [PubMed](#)
43. Grosso A, Parlanti G, Mezzena R, Cecchini M. Current treatment options and novel nanotechnology-driven enzyme replacement strategies for lysosomal storage disorders. *Adv Drug Deliv Rev* 2022;188:114464. [DOI](#) [PubMed](#)
44. Baixauli F, López-Otín C, Mittelbrunn M. Exosomes and autophagy: coordinated mechanisms for the maintenance of cellular fitness. *Front Immunol* 2014;5:403. [DOI](#) [PubMed](#) [PMC](#)
45. Zaborowski MP, Balaj L, Breakefield XO, Lai CP. Extracellular vesicles: composition, biological relevance, and methods of study. *Bioscience* 2015;65:783-97. [DOI](#) [PubMed](#) [PMC](#)
46. Vardieridou-Minasian S, Lorenowicz MJ. Mesenchymal stromal/stem cell-derived extracellular vesicles in tissue repair: challenges and opportunities. *Theranostics* 2020;10:5979-97. [DOI](#) [PubMed](#) [PMC](#)
47. Théry C, Witwer KW, Aikawa E, et al. Minimal information for studies of extracellular vesicles 2018 (MISEV2018): a position statement of the International Society for Extracellular Vesicles and update of the MISEV2014 guidelines. *J Extracell Vesicles* 2018;7:1535750. [DOI](#) [PubMed](#) [PMC](#)
48. Thakur BK, Zhang H, Becker A, et al. Double-stranded DNA in exosomes: a novel biomarker in cancer detection. *Cell Res* 2014;24:766-9. [DOI](#) [PubMed](#) [PMC](#)
49. Coutinho MF, Prata MJ, Alves S. A shortcut to the lysosome: the mannose-6-phosphate-independent pathway. *Mol Genet Metab* 2012;107:257-66. [DOI](#) [PubMed](#)
50. Fedele AO, Isenmann S, Kamei M, et al. Lysosomal N-acetyltransferase interacts with ALIX and is detected in extracellular vesicles. *Biochim Biophys Acta Mol Cell Res* 2018;1865:1451-64. [DOI](#) [PubMed](#)
51. Li Y, He X, Li Q, et al. EV-origin: Enumerating the tissue-cellular origin of circulating extracellular vesicles using exLR profile. *Comput Struct Biotechnol J* 2020;18:2851-9. [DOI](#) [PubMed](#) [PMC](#)
52. Emmanouilidou E, Melachroinou K, Roumeliotis T, et al. Cell-produced alpha-synuclein is secreted in a calcium-dependent manner by exosomes and impacts neuronal survival. *J Neurosci* 2010;30:6838-51. [DOI](#) [PubMed](#) [PMC](#)
53. Trotta T, Panaro MA, Cianiulli A, Mori G, Di Benedetto A, Porro C. Microglia-derived extracellular vesicles in Alzheimer's Disease: a double-edged sword. *Biochem Pharmacol* 2018;148:184-92. [DOI](#) [PubMed](#)
54. Ananbeh H, Vodicka P, Kupcova Skalnikova H. Emerging roles of exosomes in huntington's disease. *Int J Mol Sci* 2021;22:4085. [DOI](#) [PubMed](#) [PMC](#)
55. Tancini B, Buratta S, Sagini K, et al. Insight into the role of extracellular vesicles in lysosomal storage disorders. *Genes (Basel)* 2019;10:510. [DOI](#) [PubMed](#) [PMC](#)
56. Navarro-Romero A, Montpeyó M, Martinez-Vicente M. The emerging role of the lysosome in parkinson's disease. *Cells* 2020;9:2399. [DOI](#) [PubMed](#) [PMC](#)
57. Almeida MF, Bahr BA, Kinsey ST. Endosomal-lysosomal dysfunction in metabolic diseases and Alzheimer's disease. Metabolic and bioenergetic drivers of neurodegenerative disease: neurodegenerative disease research and commonalities with metabolic diseases. Elsevier; 2020. p. 303-24. [DOI](#) [PubMed](#) [PMC](#)
58. Porro C, Panaro MA, Lofrumento DD, Hasalla E, Trotta T. The multiple roles of exosomes in Parkinson's disease: an overview. *Immunopharmacol Immunotoxicol* 2019;41:469-76. [DOI](#) [PubMed](#)
59. Gassart A, Géminard C, Hoekstra D, Vidal M. Exosome secretion: the art of reutilizing nonrecycled proteins? *Traffic* 2004;5:896-903. [DOI](#) [PubMed](#)
60. Bernardi S, Balbi C. Extracellular vesicles: from biomarkers to therapeutic tools. *Biology (Basel)* 2020;9:258. [DOI](#) [PubMed](#) [PMC](#)
61. Parada N, Romero-Trujillo A, Georges N, Alcayaga-Miranda F. Camouflage strategies for therapeutic exosomes evasion from phagocytosis. *J Adv Res* 2021;31:61-74. [DOI](#) [PubMed](#) [PMC](#)
62. de Jong OG, Kooijmans SAA, Murphy DE, et al. Drug delivery with extracellular vesicles: from imagination to innovation. *Acc Chem Res* 2019;52:1761-70. [DOI](#) [PubMed](#) [PMC](#)
63. Kooijmans SAA, Fliervoet LAL, van der Meel R, et al. PEGylated and targeted extracellular vesicles display enhanced cell specificity and circulation time. *J Control Release* 2016;224:77-85. [DOI](#) [PubMed](#)
64. Wiklander OP, Nordin JZ, O'Loughlin A, et al. Extracellular vesicle in vivo biodistribution is determined by cell source, route of administration and targeting. *J Extracell Vesicles* 2015;4:26316. [DOI](#) [PubMed](#) [PMC](#)
65. Yim WW, Mizushima N. Lysosome biology in autophagy. *Cell Discov* 2020;6:6. [DOI](#) [PubMed](#) [PMC](#)
66. Schröder BA, Wrocklage C, Hasilik A, Saftig P. The proteome of lysosomes. *Proteomics* 2010;10:4053-76. [DOI](#) [PubMed](#)
67. Chang NC. Autophagy and Stem Cells: self-eating for self-renewal. *frontiers in cell and developmental Biology* 2020;8. [DOI](#) [PubMed](#) [PMC](#)
68. Song HY, Chien CS, Yarmishyn AA, et al. Generation of GLA-knockout human embryonic stem cell lines to model autophagic dysfunction and exosome secretion in fabry disease-associated hypertrophic cardiomyopathy. *Cells* 2019;8:327. [DOI](#) [PubMed](#) [PMC](#)
69. Bartolomeo R, Cinque L, De Leonibus C, et al. mTORC1 hyperactivation arrests bone growth in lysosomal storage disorders by suppressing autophagy. *J Clin Invest* 2017;127:3717-29. [DOI](#) [PubMed](#) [PMC](#)
70. Brown RA, Voit A, Srikanth MP, et al. mTOR hyperactivity mediates lysosomal dysfunction in Gaucher's disease iPSC-neuronal cells. *Dis Model Mech* 2019;12. [DOI](#) [PubMed](#) [PMC](#)

71. Gao J, Wei B, de Assuncao TM, et al. Hepatic stellate cell autophagy inhibits extracellular vesicle release to attenuate liver fibrosis. *J Hepatol* 2020;73:1144-54. DOI PubMed PMC
72. Skotland T, Sagini K, Sandvig K, Llorente A. An emerging focus on lipids in extracellular vesicles. *Adv Drug Deliv Rev* 2020;159:308-21. DOI PubMed
73. Gurung S, Perocheau D, Touramanidou L, Baruteau J. The exosome journey: from biogenesis to uptake and intracellular signalling. *Cell Commun Signal* 2021;19:47. DOI PubMed PMC
74. Hessvik NP, Øverbye A, Brech A, et al. PIKfyve inhibition increases exosome release and induces secretory autophagy. *Cell Mol Life Sci* 2016;73:4717-37. DOI PubMed
75. Miranda AM, Lasiecka ZM, Xu Y, et al. Neuronal lysosomal dysfunction releases exosomes harboring APP C-terminal fragments and unique lipid signatures. *Nat Commun* 2018;9:291. DOI PubMed PMC
76. Strauss K, Goebel C, Runz H, et al. Exosome secretion ameliorates lysosomal storage of cholesterol in Niemann-Pick type C disease. *J Biol Chem* 2010;285:26279-88. DOI PubMed PMC
77. Illytska O, Jeziorek M, Lai K, Altan-Bonnet N, Dobrowolski R, Storch J. Lysobisphosphatidic acid (LBPA) enrichment promotes cholesterol egress via exosomes in Niemann Pick type C1 deficient cells. *Biochim Biophys Acta Mol Cell Biol Lipids* 2021;1866:158916. DOI PubMed PMC
78. van de Vlekkert D, Demmers J, Nguyen XX, et al. Excessive exosome release is the pathogenic pathway linking a lysosomal deficiency to generalized fibrosis. *Sci Adv* 2019;5:eaav3270. DOI PubMed PMC
79. D'Auria L, Reiter C, Ward E, et al. Psychosine enhances the shedding of membrane microvesicles: Implications in demyelination in Krabbe's disease. *PLoS One* 2017;12:e0178103. DOI PubMed PMC
80. Bhat OM, Li G, Yuan X, et al. Arterial medial calcification through enhanced small extracellular vesicle release in smooth muscle-specific *asah1* gene knockout mice. *Sci Rep* 2020;10:1645. DOI PubMed PMC
81. Reiter CR, Rebiai R, Kwak A, et al. The pathogenic sphingolipid psychosine is secreted in extracellular vesicles in the brain of a mouse model of krabbe disease. *ASN Neuro* 2022;14:17590914221087817. DOI PubMed PMC
82. Pituch KC, Moyano AL, Lopez-Rosas A, et al. Dysfunction of platelet-derived growth factor receptor α (PDGFR α) represses the production of oligodendrocytes from arylsulfatase a-deficient multipotential neural precursor cells. *J Biol Chem* 2015;290:7040-53. DOI PubMed PMC
83. Chen FW, Li C, Ioannou YA. Cyclodextrin induces calcium-dependent lysosomal exocytosis. *PLoS One* 2010;5:e15054. DOI PubMed PMC
84. Canonico B, Cesarini E, Salucci S, et al. Defective autophagy, mitochondrial clearance and lipophagy in niemann-pick type B lymphocytes. *PLoS One* 2016;11:e0165780. DOI PubMed PMC
85. Alvarez-Erviti L, Seow Y, Schapira AH, et al. Lysosomal dysfunction increases exosome-mediated alpha-synuclein release and transmission. *Neurobiol Dis* 2011;42:360-7. DOI PubMed PMC
86. Vingtdoux V, Hamdane M, Loyens A, et al. Alkalizing drugs induce accumulation of amyloid precursor protein by-products in luminal vesicles of multivesicular bodies. *J Biol Chem* 2007;282:18197-205. DOI PubMed
87. Raben N, Schreiner C, Baum R, et al. Suppression of autophagy permits successful enzyme replacement therapy in a lysosomal storage disorder—murine Pompe disease. *Autophagy* 2010;6:1078-89. DOI PubMed PMC
88. Spanpanato C, Feeney E, Li L, et al. Transcription factor EB (TFEB) is a new therapeutic target for Pompe disease. *EMBO Mol Med* 2013;5:691-706. DOI PubMed PMC
89. Gatto F, Rossi B, Tarallo A, et al. AAV-mediated transcription factor EB (TFEB) gene delivery ameliorates muscle pathology and function in the murine model of Pompe Disease. *Sci Rep* 2017;7:15089. DOI PubMed PMC
90. Manjithaya R, Subramani S. Autophagy: a broad role in unconventional protein secretion? *Trends Cell Biol* 2011;21:67-73. DOI PubMed PMC
91. Klein D, Büsow H, Fewou SN, Gieselmann V. Exocytosis of storage material in a lysosomal disorder. *Biochem Biophys Res Commun* 2005;327:663-7. DOI PubMed
92. Yogalingam G, Bonten EJ, van de Vlekkert D, et al. Neuraminidase 1 is a negative regulator of lysosomal exocytosis. *Dev Cell* 2008;15:74-86. DOI PubMed PMC
93. Hastings C, Vieira C, Liu B, et al. Expanded access with intravenous hydroxypropyl- β -cyclodextrin to treat children and young adults with Niemann-Pick disease type C1: a case report analysis. *Orphanet J Rare Dis* 2019;14:228. DOI PubMed PMC
94. Pergande MR, Kang C, George D, et al. Lipidomic analysis identifies age-disease-related changes and potential new biomarkers in brain-derived extracellular vesicles from metachromatic leukodystrophy mice. *Lipids Health Dis* 2022;21:32. DOI PubMed PMC
95. Batzios SP, Zafeiriou DI, Papakonstantinou E. Extracellular matrix components: an intricate network of possible biomarkers for lysosomal storage disorders? *FEBS Lett* 2013;587:1258-67. DOI PubMed
96. Feltri ML, Weinstock NI, Favret J, Dhimal N, Wrabetz L, Shin D. Mechanisms of demyelination and neurodegeneration in globoid cell leukodystrophy. *Glia* 2021;69:2309-31. DOI PubMed PMC
97. Galvan C, Camoletto PG, Cristofani F, Van Veldhoven PP, Ledesma MD. Anomalous surface distribution of glycosyl phosphatidyl inositol-anchored proteins in neurons lacking acid sphingomyelinase. *Mol Biol Cell* 2008;19:509-22. DOI PubMed PMC
98. Koike T, Ishida G, Taniguchi M, et al. Decreased membrane fluidity and unsaturated fatty acids in Niemann-Pick disease type C fibroblasts. *BBA-Mol Basis Dis* 1998;1406:327-35. DOI PubMed
99. Keller S, Ridinger J, Rupp AK, Janssen JW, Altevogt P. Body fluid derived exosomes as a novel template for clinical diagnostics. *J*

- Transl Med* 2011;9:86. DOI PubMed PMC
100. Lässer C, Alikhani VS, Ekström K, et al. Human saliva, plasma and breast milk exosomes contain RNA: uptake by macrophages. *J Transl Med* 2011;9:9. DOI PubMed PMC
101. Liu H, Yuan W, Pang Q, Xue C, Yan X. Single-particle analysis of tear fluid reveals abundant presence of tissue factor-exposing extracellular vesicles with strong coagulation activity. *Talanta* 2022;239:123089. DOI PubMed
102. Nielsen JE, Honoré B, Vestergård K, et al. Shotgun-based proteomics of extracellular vesicles in Alzheimer's disease reveals biomarkers involved in immunological and coagulation pathways. *Sci Rep* 2021;11:18518. DOI PubMed PMC
103. Upadhy R, Shetty AK. Extracellular vesicles for the diagnosis and treatment of parkinson's disease. *Aging Dis* 2021;12:1438-50. DOI PubMed PMC
104. Zhou H, Fernhoff P, Vogt RF. Newborn bloodspot screening for lysosomal storage disorders. *J Pediatr* 2011;159:7-13.e1. DOI PubMed
105. Wang RY, Bodamer OA, Watson MS, Wilcox WR; ACMG Work Group on Diagnostic confirmation of lysosomal storage diseases. lysosomal storage diseases: diagnostic confirmation and management of presymptomatic individuals. *Genet Med* 2011;13:457-84. DOI PubMed
106. Puentes-Tellez MA, Lerma-Barbosa PA, Garzón-Jaramillo RG, et al. A perspective on research, diagnosis, and management of lysosomal storage disorders in Colombia. *Heliyon* 2020;6:e03635. DOI PubMed PMC
107. Han JS, Kim SE, Jin JQ, et al. Tear-derived exosome proteins are increased in patients with thyroid eye disease. *Int J Mol Sci* 2021;22:1115. DOI PubMed PMC
108. van den Broek BTA, van Egmond-Ebbeling MB, Achterberg JA, et al. Longitudinal analysis of ocular disease in children with mucopolysaccharidosis i after hematopoietic cell transplantation. *Biol Blood Marrow Transplant* 2020;26:928-35. DOI PubMed
109. Gelb MH. Newborn screening for lysosomal storage diseases: methodologies, screen positive rates, normalization of datasets, second-tier tests, and post-analysis tools. *Int J Neonatal Screen* 2018;4:23. DOI PubMed PMC
110. Metakids. Welke ziekten zitten er in de hiepprik? Available from: <https://www.metakids.nl/metabole-ziekten-in-de-hiepprik/> [Last accessed on 28 Dec 2022].
111. Iyer NS, Gimovsky AC, Ferreira CR, Critchlow E, Al-Kouatly HB. Lysosomal storage disorders as an etiology of nonimmune hydrops fetalis: a systematic review. *Clin Genet* 2021;100:493-503. DOI PubMed
112. Keller S, Rupp C, Stoeck A, et al. CD24 is a marker of exosomes secreted into urine and amniotic fluid. *Kidney Int* 2007;72:1095-102. DOI PubMed
113. Ebert B, Rai AJ. Isolation and characterization of amniotic fluid-derived extracellular vesicles for biomarker discovery. In: Levy B, editor. Prenatal Diagnosis. New York: Springer; 2019. p. 287-94. DOI PubMed
114. Levstek T, Mlinšek T, Holcar M, et al. Urinary extracellular vesicles and their mirna cargo in patients with fabry nephropathy. *Genes (Basel)* 2021;12:1057. DOI PubMed PMC
115. Del Pino M, Andrés A, Bernabéu AA, et al. Fabry nephropathy: an evidence-based narrative review. *Kidney Blood Press Res* 2018;43:406-21. DOI PubMed
116. Tatiana S, Stanislav N, Darya K, et al. Altered level of plasma exosomes in patients with Gaucher disease. *Eur J Med Genet* 2020;63:104038. DOI PubMed
117. Lo Curto A, Taverna S, Costa MA, et al. Can Be miR-126-3p a biomarker of premature aging? *Cells* 2021;10:356. DOI PubMed PMC
118. Zahran AM, Elsayh KI, El-Deek SE, El-Baz MA. Oxidative stress, trace elements, and circulating microparticles in patients with Gaucher disease before and after enzyme replacement therapy. *Clin Appl Thromb Hemost* 2015;21:58-65. DOI PubMed
119. Moyano AL, Li G, Boullerne AI, et al. Sulfatides in extracellular vesicles isolated from plasma of multiple sclerosis patients. *J Neurosci Res* 2016;94:1579-87. DOI PubMed
120. Krämer-Albers EM, Bretz N, Tenzer S, et al. Oligodendrocytes secrete exosomes containing major myelin and stress-protective proteins: Trophic support for axons? *Proteomics Clin Appl* 2007;1:1446-61. DOI PubMed
121. Best MG, In 't Veld SGJG, Sol N, Wurdinger T. RNA sequencing and swarm intelligence-enhanced classification algorithm development for blood-based disease diagnostics using spliced blood platelet RNA. *Nat Protoc* 2019;14:1206-34. DOI PubMed
122. Best MG, Sol N, In 't Veld SGJG, et al. Swarm intelligence-enhanced detection of non-small-cell lung cancer using tumor-educated platelets. *Cancer Cell* 2017;32:238-252.e9. DOI PubMed PMC
123. Sol N, Leurs CE, Veld SGI', et al. Blood platelet RNA enables the detection of multiple sclerosis. *Mult Scler J Exp Transl Clin* 2020;6:2055217320946784. DOI PubMed PMC
124. Niel G, Carter DRF, Clayton A, Lambert DW, Raposo G, Vader P. Challenges and directions in studying cell-cell communication by extracellular vesicles. *Nat Rev Mol Cell Biol* 2022;23:369-82. DOI PubMed
125. Kumari A, Yadav SK, Yadav SC. Biodegradable polymeric nanoparticles based drug delivery systems. *Colloids Surf B Biointerfaces* 2010;75:1-18. DOI PubMed
126. Sahay G, Querbes W, Alabi C, et al. Efficiency of siRNA delivery by lipid nanoparticles is limited by endocytic recycling. *Nat Biotechnol* 2013;31:653-8. DOI PubMed PMC
127. Flanagan M, Pathak I, Gan Q, et al. Umbilical mesenchymal stem cell-derived extracellular vesicles as enzyme delivery vehicle to treat Morquio A fibroblasts. *Stem Cell Res Ther* 2021;12:276. DOI PubMed PMC
128. Seras-Franzoso J, Díaz-Riascos ZV, Corchero JL, et al. Extracellular vesicles from recombinant cell factories improve the activity

- and efficacy of enzymes defective in lysosomal storage disorders. *J Extracell Vesicles* 2021;10:e12058. DOI PubMed PMC
129. Kooijmans SAA, de Jong OG, Schiffelers RM. Exploring interactions between extracellular vesicles and cells for innovative drug delivery system design. *Adv Drug Deliv Rev* 2021;173:252-78. DOI PubMed
 130. Heusermann W, Hean J, Trojer D, et al. Exosomes surf on filopodia to enter cells at endocytic hot spots, traffic within endosomes, and are targeted to the ER. *J Cell Biol* 2016;213:173-84. DOI PubMed PMC
 131. Bonsergent E, Lavieu G. Content release of extracellular vesicles in a cell-free extract. *FEBS Lett* 2019;593:1983-92. DOI PubMed
 132. Coulson-Thomas VJ, Caterson B, Kao WW. Transplantation of human umbilical mesenchymal stem cells cures the corneal defects of mucopolysaccharidosis VII mice. *Stem Cells* 2013;31:2116-26. DOI PubMed PMC
 133. Lai RC, Arslan F, Lee MM, et al. Exosome secreted by MSC reduces myocardial ischemia/reperfusion injury. *Stem Cell Res* 2010;4:214-22. DOI PubMed
 134. Haney MJ, Klyachko NL, Harrison EB, Zhao Y, Kabanov AV, Batrakova EV. TPP1 delivery to lysosomes with extracellular vesicles and their enhanced brain distribution in the animal model of batten disease. *Adv Healthc Mater* 2019;8:e1801271. DOI PubMed PMC
 135. Iglesias DM, El-Kares R, Taranta A, et al. Stem cell microvesicles transfer cystinosis to human cystinotic cells and reduce cystine accumulation in vitro. *PLoS One* 2012;7:e42840. DOI PubMed PMC
 136. Thoene J, Goss T, Witcher M, et al. In vitro correction of disorders of lysosomal transport by microvesicles derived from baculovirus-infected Spodoptera cells. *Mol Genet Metab* 2013;109:77-85. DOI PubMed
 137. Thoene JG, DelMonte MA, Mullet J. Microvesicle delivery of a lysosomal transport protein to ex vivo rabbit cornea. *Mol Genet Metab Rep* 2020;23:100587. DOI PubMed PMC
 138. Haney MJ, Zhao Y, Jin YS, Batrakova EV. Extracellular vesicles as drug carriers for enzyme replacement therapy to treat CLN2 batten disease: optimization of drug administration routes. *Cells* 2020;9:1273. DOI PubMed PMC
 139. Luan X, Sansanaphongpricha K, Myers I, Chen H, Yuan H, Sun D. Engineering exosomes as refined biological nanoplateforms for drug delivery. *Acta Pharmacol Sin* 2017;38:754-63. DOI PubMed PMC
 140. Li K, Yan G, Huang H, et al. Anti-inflammatory and immunomodulatory effects of the extracellular vesicles derived from human umbilical cord mesenchymal stem cells on osteoarthritis via M2 macrophages. *J Nanobiotechnology* 2022;20:38. DOI PubMed PMC
 141. Sly WS, Vogler C, Grubb JH, et al. Enzyme therapy in mannose receptor-null mucopolysaccharidosis VII mice defines roles for the mannose 6-phosphate and mannose receptors. *Proc Natl Acad Sci USA* 2006;103:15172-7. DOI PubMed PMC
 142. Roefs MT, Heusermann W, Brans MAD, et al. Evaluation and manipulation of tissue and cellular distribution of cardiac progenitor cell-derived extracellular vesicles DOI PubMed PMC
 143. Hoshino A, Costa-Silva B, Shen TL, et al. Tumour exosome integrins determine organotropic metastasis. *Nature* 2015;527:329-35. DOI PubMed PMC
 144. Park EJ, Prajuabjinda O, Soe ZY, et al. Exosomal regulation of lymphocyte homing to the gut. *Blood Adv* 2019;3:1-11. DOI PubMed PMC
 145. Perez-Hernandez D, Gutiérrez-Vázquez C, Jorge I, et al. The intracellular interactome of tetraspanin-enriched microdomains reveals their function as sorting machineries toward exosomes. *J Biol Chem* 2013;288:11649-61. DOI PubMed PMC
 146. Elsharkasy OM, Nordin JZ, Hagey DW, et al. Extracellular vesicles as drug delivery systems: Why and how? *Adv Drug Deliv Rev* 2020;159:332-43. DOI PubMed
 147. Lennaárd AJ, Mamand DR, Wiklander RJ, El Andaloussi S, Wiklander OPB. Optimised electroporation for loading of extracellular vesicles with doxorubicin. *Pharmaceutics* 2021;14:38. DOI PubMed PMC
 148. Dooley K, McConnell RE, Xu K, et al. A versatile platform for generating engineered extracellular vesicles with defined therapeutic properties. *Mol Ther* 2021;29:1729-43. DOI PubMed PMC
 149. Gupta D, Wiklander OPB, Görgens A, et al. Amelioration of systemic inflammation via the display of two different decoy protein receptors on extracellular vesicles. *Nat Biomed Eng* 2021;5:1084-98. DOI PubMed
 150. Silva AM, Lázaro-Ibáñez E, Gunnarsson A, et al. Quantification of protein cargo loading into engineered extracellular vesicles at single-vesicle and single-molecule resolution. *J Extracell Vesicles* 2021;10:e12130. DOI PubMed PMC
 151. Yim N, Ryu SW, Choi K, et al. Exosome engineering for efficient intracellular delivery of soluble proteins using optically reversible protein-protein interaction module. *Nat Commun* 2016;7:12277. DOI PubMed PMC
 152. Wang Q, Yu J, Kadungure T, Beyene J, Zhang H, Lu Q. ARMMs as a versatile platform for intracellular delivery of macromolecules. *Nat Commun* 2018;9:960. DOI PubMed PMC
 153. Do MA, Levy D, Brown A, Marriott G, Lu B. Targeted delivery of lysosomal enzymes to the endocytic compartment in human cells using engineered extracellular vesicles. *Sci Rep* 2019;9:17274. DOI PubMed PMC
 154. Hasilik A. The early and late processing of lysosomal enzymes: proteolysis and compartmentation. *Experientia* 1992;48:130-51. DOI PubMed
 155. Youn SW, Li Y, Kim YM, et al. Modification of cardiac progenitor cell-derived exosomes by miR-322 provides protection against myocardial infarction through Nox2-dependent angiogenesis. *Antioxidants (Basel)* 2019;8:18. DOI PubMed PMC
 156. Sun D, Zhuang X, Xiang X, et al. A novel nanoparticle drug delivery system: the anti-inflammatory activity of curcumin is enhanced when encapsulated in exosomes. *Mol Ther* 2010;18:1606-14. DOI PubMed PMC
 157. Wei H, Chen J, Wang S, et al. A nanodrug consisting of doxorubicin and exosome derived from mesenchymal stem cells for

- osteosarcoma treatment in vitro. *Int J Nanomedicine* 2019;14:8603-10. DOI PubMed PMC
158. Escudier B, Dorval T, Chaput N, et al. Vaccination of metastatic melanoma patients with autologous dendritic cell (DC) derived-exosomes: results of the first phase I clinical trial. *J Transl Med* 2005;3:10. DOI PubMed PMC
159. Li Z, Zhou X, Wei M, et al. In vitro and in vivo RNA inhibition by CD9-HuR functionalized exosomes encapsulated with miRNA or CRISPR/dCas9. *Nano Lett* 2019;19:19-28. DOI PubMed
160. Lloyd-Evans E, Morgan AJ, He X, et al. Niemann-Pick disease type C1 is a sphingosine storage disease that causes deregulation of lysosomal calcium. *Nat Med* 2008;14:1247-55. DOI PubMed
161. Canfrán-Duque A, Pastor O, Quintana-Portillo R, et al. Curcumin promotes exosomes/microvesicles secretion that attenuates lysosomal cholesterol traffic impairment. *Mol Nutr Food Res* 2014;58:687-97. DOI PubMed
162. Lu B, Ku J, Flojo R, Olson C, Bengford D, Marriott G. Exosome- and extracellular vesicle-based approaches for the treatment of lysosomal storage disorders. *Adv Drug Deliv Rev* 2022;188:114465. DOI PubMed
163. Belhadj Z, He B, Deng H, et al. A combined “eat me/don’t eat me” strategy based on extracellular vesicles for anticancer nanomedicine. *J Extracell Vesicles* 2020;9:1806444. DOI PubMed PMC
164. Komuro H, Kawai-Harada Y, Aminova S, et al. Engineering extracellular vesicles to target pancreatic tissue in vivo. *Nanotheranostics* 2021;5:378-90. DOI PubMed PMC
165. Kamekar S, LeBleu VS, Sugimoto H, et al. Exosomes facilitate therapeutic targeting of oncogenic KRAS in pancreatic cancer. *Nature* 2017;546:498-503. DOI PubMed PMC
166. Kieseier BC, Wisniewski KE, Goebel HH. The monocyte-macrophage system is affected in lysosomal storage diseases: an immunoelectron microscopic study. *Acta Neuropathol* 1997;94:359-62. DOI PubMed
167. Limoni SK, Moghadam MF, Moazzeni SM, Gomari H, Salimi F. Engineered exosomes for targeted transfer of siRNA to HER2 positive breast cancer cells. *Appl Biochem Biotechnol* 2019;187:352-64. DOI PubMed
168. Gomez-Ospina N, Scharenberg SG, Mostrel N, et al. Human genome-edited hematopoietic stem cells phenotypically correct Mucopolysaccharidosis type I. *Nat Commun* 2019;10:4045. DOI PubMed PMC
169. Paquet D, Kwart D, Chen A, et al. Efficient introduction of specific homozygous and heterozygous mutations using CRISPR/Cas9. *Nature* 2016;533:125-9. DOI PubMed
170. Hsu PD, Lander ES, Zhang F. Development and applications of CRISPR-Cas9 for genome engineering. *Cell* 2014;157:1262-78. DOI PubMed PMC
171. Gaudelli NM, Komor AC, Rees HA, et al. Programmable base editing of A•T to G•C in genomic DNA without DNA cleavage. *Nature* 2017;551:464-71. PubMed PMC
172. Komor AC, Kim YB, Packer MS, Zuris JA, Liu DR. Programmable editing of a target base in genomic DNA without double-stranded DNA cleavage. *Nature* 2016;533:420-4. DOI PubMed PMC
173. Kim YB, Komor AC, Levy JM, Packer MS, Zhao KT, Liu DR. Increasing the genome-targeting scope and precision of base editing with engineered Cas9-cytidine deaminase fusions. *Nat Biotechnol* 2017;35:371-6. DOI PubMed PMC
174. Anzalone AV, Randolph PB, Davis JR, et al. Search-and-replace genome editing without double-strand breaks or donor DNA. *Nature* 2019;576:149-57. DOI PubMed PMC
175. Scholefield J, Harrison PT. Prime editing - an update on the field. *Gene Ther* 2021;28:396-401. DOI PubMed PMC
176. Schene IF, Joore IP, Oka R, et al. Prime editing for functional repair in patient-derived disease models. *Nat Commun* 2020;11:5352. DOI PubMed PMC
177. Liang Y, Iqbal Z, Wang J, et al. Cell-derived extracellular vesicles for CRISPR/Cas9 delivery: engineering strategies for cargo packaging and loading. *Biomater Sci* 2022;10:4095-106. DOI PubMed
178. Simhadri VL, McGill J, McMahon S, Wang J, Jiang H, Sauna ZE. Prevalence of pre-existing antibodies to CRISPR-associated nuclease Cas9 in the USA population. *Mol Ther Methods Clin Dev* 2018;10:105-12. DOI PubMed PMC
179. Gee P, Lung MSY, Okuzaki Y, et al. Extracellular nanovesicles for packaging of CRISPR-Cas9 protein and sgRNA to induce therapeutic exon skipping. *Nat Commun* 2020;11:1334. DOI PubMed PMC
180. Meyer C, Losacco J, Stickney Z, Li L, Marriott G, Lu B. Pseudotyping exosomes for enhanced protein delivery in mammalian cells. *Int J Nanomedicine* 2017;12:3153-70. DOI PubMed PMC
181. Tomás HA, Mestre DA, Rodrigues AF, Guerreiro MR, Carrondo MJT, Coroadinha AS. Improved GaLV-TR glycoproteins to pseudotype lentiviral vectors: impact of viral protease activity in the production of LV pseudotypes. *Mol Ther Methods Clin Dev* 2019;15:1-8. DOI PubMed PMC
182. Vargas A, Zhou S, Éthier-Chiasson M, et al. Syncytin proteins incorporated in placenta exosomes are important for cell uptake and show variation in abundance in serum exosomes from patients with preeclampsia. *FASEB J* 2014;28:3703-19. DOI PubMed
183. Prada I, Meldolesi J. Binding and fusion of extracellular vesicles to the plasma membrane of their cell targets. *Int J Mol Sci* 2016;17:1296. DOI PubMed PMC
184. Ye Y, Zhang X, Xie F, et al. An engineered exosome for delivering sgRNA: Cas9 ribonucleoprotein complex and genome editing in recipient cells. *Biomater Sci* 2020;8:2966-76. DOI PubMed
185. Osteikoetxea X, Silva A, Lázaro-Ibáñez E, et al. Engineered Cas9 extracellular vesicles as a novel gene editing tool. *J Extracell Vesicles* 2022;11:e12225. DOI PubMed PMC
186. Lener T, Gimona M, Aigner L, et al. Applying extracellular vesicles based therapeutics in clinical trials - an ISEV position paper. *J Extracell Vesicles* 2015;4:30087. DOI PubMed PMC

Editorial

Open Access



Year-end reflections of *EVCNA* - 2022

Yoke Peng Loh

American Biochemist and Molecular Biologist, Bethesda, MD 20817, USA.

Correspondence to: Dr. Y. Peng Loh, American Biochemist and Molecular Biologist, Bethesda, MD 20817, USA. E-mail: oaepub2019@yahoo.com

How to cite this article: Loh YP. Year-end reflections of *EVCNA* - 2022. *Extracell Vesicles Circ Nucleic Acids* 2022;3:422-3. <https://dx.doi.org/10.20517/evcna.2022.45>

Received: 28 Dec 2022 **Accepted:** 30 Dec 2022 **Published:** 30 Dec 2022

Academic Editor: Yoke Peng Loh **Copy Editor:** Pengjuan Wen **Production Editor:** Pengjuan Wen

Extracellular Vesicles and Circulating Nucleic Acids (EVCNA) has completed another successful year in 2022, the 3rd year since its inception in December 2019. This year we have expanded our Editorial Board of eminent scientists to 46 members from 14 countries/regions with 7 Associate Editors. In addition, we now have an international junior Editorial Board of 59 young scientists who are supporting many aspects of the journal, including participating as reviewers and organizing Roundtable discussions and Academic Talks that we have added this year. In 2022, *EVCNA* published 30 papers with a total of 77,832 views, 14,527 downloads and 107 citations in Web of Science. Manuscript submissions were thoroughly peer-reviewed, and our rejection rate in 2022 was 45.5%. Currently, there are 13 Special Issues in progress covering diverse topics. They include Extracellular Vesicles in Intercellular Communication: A Decade of Achievements (Guest Editors: Randy Schekman and Y. Peng Loh), Extracellular Vesicles and miRNA in the Aging Process (Guest Editors: Consuelo Barras Blasco and Jorge Sanz-Rios), Circulating Nucleic Acids in Bodily Fluids: Noninvasive Prenatal Testing, Oncology, Transplant Monitoring and Beyond (Guest Editors: Eric Stermans and Peiyong Jiang), Extracellular Vesicles and Neuroinflammation: Response to Infection, Injury and Aging Plus Vehicles for Treatment (Guest Editor: Lynn Pulliam), and Extracellular Vesicles in Tissue Remodelling in Health and Disease (Guest Editor: Sigrun Lange). All readers are welcome to submit to any of the Special Issues by contacting the Guest Editors.

The journal is indexed by Dimensions, CNKI Scholar and Google Scholar. Our articles funded by NIH and Europe PMC 37 funders are included in PMC. This year *EVCNA* became a member of COPE. *EVCNA* has



© The Author(s) 2022. **Open Access** This article is licensed under a Creative Commons Attribution 4.0 International License (<https://creativecommons.org/licenses/by/4.0/>), which permits unrestricted use, sharing, adaptation, distribution and reproduction in any medium or format, for any purpose, even commercially, as long as you give appropriate credit to the original author(s) and the source, provide a link to the Creative Commons license, and indicate if changes were made.



several partners and sponsored meetings, including Research Gate, 3rd Liquid Biopsies Congress in Europe and the American Society of Intercellular Communications (ASIC) 2022 Annual Meeting.

Looking forward to 2023, the *EVCNA* editorial office is offering \$600 each for two Best Paper Awards, a Review article and a Research article. We encourage you to submit your papers to *EVCNA*. Readers are invited to listen and participate in the upcoming Academic Talks and Roundtable Discussions announced on our website. If you are interested in organizing a Roundtable Discussion, please contact the Editorial Manager (managingeditor@evcna.com). We hope that scientists in the Extracellular Vesicle and Liquid Biopsy fields will continue to use *EVCNA* as a platform to share their work and opinions, commentaries and discussions with their fellow researchers. For 2023, the APC is still waived, which provides an opportunity for everyone to publish their experimental data or scholarly reviews and commentaries freely.

EVCNA would like to thank the Extracellular Vesicle and Liquid Biopsy research community for their great support of the journal in 2022 and look forward to their continued support and serving you in 2023.

Best Wishes to Everyone for Good Health and Success in 2023.

DECLARATIONS

Author's contributions

Preparing the manuscript draft: Loh YP

Availability of data and materials

Not applicable.

Financial support and sponsorship

None.

Conflicts of interest

The author declared that there are no conflicts of interest.

Ethical approval and consent to participate

Not applicable.

Consent for publication

Not applicable.

Copyright

©The Author 2022.

AUTHOR INSTRUCTIONS

1. Submission Overview

Before you decide to publish with *Extracellular Vesicles and Circulating Nucleic Acids (EVCNA)*, please read the following items carefully and make sure that you are well aware of Editorial Policies and the following requirements.

1.1 Topic Suitability

The topic of the manuscript must fit the scope of the journal. Please refer to Aims and Scope for more information.

1.2 Open Access and Copyright

The journal adopts Gold Open Access publishing model and distributes content under the Creative Commons Attribution 4.0 International License. Copyright is retained by authors. Please make sure that you are well aware of these policies.

1.3 Publication Fees

The publication fee for each submission is \$299. There are no additional charges based on color, length, figures, or other elements. OAE provides expense deduction for authors as appropriate. For more details, please refer to OAE Publication Fees.

1.4 Language Editing

All submissions are required to be presented clearly and cohesively in good English. Authors whose first language is not English are advised to have their manuscripts checked or edited by a native English speaker before submission to ensure the high quality of expression. A well-organized manuscript in good English would make the peer review even the whole editorial handling more smoothly and efficiently.

If needed, authors are recommended to consider the language editing services provided by Charlesworth to ensure that the manuscript is written in correct scientific English before submission. Authors who publish with OAE journals enjoy a special discount for the services of Charlesworth via the following two ways.

Submit your manuscripts directly at <http://www.charlesworthauthorservices.com/~OAE>;

Open the link <http://www.charlesworthauthorservices.com/>, and enter Promotion Code “OAE” when you submit.

1.5 Work Funded by the National Institutes of Health

If an accepted manuscript was funded by National Institutes of Health (NIH), the authors may inform Editors of the NIH funding number. The Editors are able to deposit the paper to the NIH Manuscript Submission System on behalf of the authors.

2. Submission Preparation

2.1 Cover Letter

A cover letter is required to be submitted accompanying each manuscript. It should be concise and explain why the study is significant, why it fits the scope of the journal, and why it would be attractive to readers, *etc.*

Here is a guideline of a cover letter for authors' consideration:

In the first paragraph: include the title and type (e.g., Original Article, Review, Case Report, *etc.*) of the manuscript, a brief on the background of the study, the question the author sought out to answer and why;

In the second paragraph: concisely explain what was done, the main findings and why they are significant;

In the third paragraph: indicate why the manuscript fits the Aims and Scope of the journal, and why it would be attractive to readers;

In the fourth paragraph: confirm that the manuscript has not been published elsewhere and not under consideration of any other journal. All authors have approved the manuscript and agreed on its submission to the journal. Journal's specific requirements have been met if any.

If the manuscript is contributed to a special issue, please also mention it in the cover letter.

If the manuscript was presented partly or entirely in a conference, the author should clearly state the background information of the event, including the conference name, time and place in the cover letter.

2.2 Types of Manuscripts

There is no restriction on the length of manuscripts, number of figures, tables and references, provided that the manuscript is concise and comprehensive. The journal publishes Original Article, Review, Meta-Analysis, Case Report, Commentary, *etc.* For more details about paper type, please refer to the following table.

Manuscript Type	Definition	Abstract	Keywords	Main Text Structure
Original Article	An Original Article describes detailed results from novel research. All findings are extensively discussed.	Structured abstract including Aim, Methods, Results and Conclusion. No more than 250 words.	3-8 keywords	The main content should include four sections: Introduction, Methods, Results and Discussion.
Review	A Review paper summarizes the literature on previous studies. It usually does not present any new information on a subject.	Unstructured abstract. No more than 250 words.	3-8 keywords	The main text may consist of several sections with unfixed section titles. We suggest that the author includes an "Introduction" section at the beginning, several sections with unfixed titles in the middle part, and a "Conclusion" section in the end.
Case Report	A Case Report details symptoms, signs, diagnosis, treatment, and follows up an individual patient. The goal of a Case Report is to make other researchers aware of the possibility that a specific phenomenon might occur.	Unstructured abstract. No more than 150 words.	3-8 keywords	The main text consists of three sections with fixed section titles: Introduction, Case Report, and Discussion.
Meta-Analysis	A Meta-Analysis is a statistical analysis combining the results of multiple scientific studies. It is often an overview of clinical trials.	Structured abstract including Aim, Methods, Results and Conclusion. No more than 250 words.	3-8 keywords	The main content should include four sections: Introduction, Methods, Results and Discussion.
Systematic Review	A Systematic Review collects and critically analyzes multiple research studies, using methods selected before one or more research questions are formulated, and then finding and analyzing related studies and answering those questions in a structured methodology.	Structured abstract including Aim, Methods, Results and Conclusion. No more than 250 words.	3-8 keywords	The main content should include four sections: Introduction, Methods, Results and Discussion.
Technical Note	A Technical Note is a short article giving a brief description of a specific development, technique or procedure, or it may describe a modification of an existing technique, procedure or device applied in research.	Unstructured abstract. No more than 250 words.	3-8 keywords	/
Commentary	A Commentary is to provide comments on a newly published article or an alternative viewpoint on a certain topic.	Unstructured abstract. No more than 250 words.	3-8 keywords	/
Editorial	An Editorial is a short article describing news about the journal or opinions of senior editors or the publisher.	None required	None required	/
Letter to Editor	A Letter to Editor is usually an open post-publication review of a paper from its readers, often critical of some aspect of a published paper. Controversial papers often attract numerous Letters to Editor	Unstructured abstract (optional). No more than 250 words.	3-8 keywords (optional)	/
Opinion	An Opinion usually presents personal thoughts, beliefs, or feelings on a topic.	Unstructured abstract (optional). No more than 250 words.	3-8 keywords	/
Perspective	A Perspective provides personal points of view on the state-of-the-art of a specific area of knowledge and its future prospects. Links to areas of intense current research focus can also be made. The emphasis should be on a personal assessment rather than a comprehensive, critical review. However, comments should be put into the context of existing literature. Perspectives are usually invited by the Editors.	Unstructured abstract. No more than 150 words.	3-8 keywords	/

2.3 Manuscript Structure

2.3.1 Front Matter

2.3.1.1 Title

The title of the manuscript should be concise, specific and relevant, with no more than 16 words if possible. When gene or protein names are included, the abbreviated name rather than full name should be used.

2.3.1.2 Authors and Affiliations

Authors' full names should be listed. The initials of middle names can be provided. Institutional addresses and email addresses for all authors should be listed. At least one author should be designated as corresponding author. In addition, corresponding authors are suggested to provide their Open Researcher and Contributor ID upon submission. Please note that any change to authorship is not allowed after manuscript acceptance.

2.3.1.3 Abstract

The abstract should be a single paragraph with word limitation and specific structure requirements (for more details please refer to Types of Manuscripts). It usually describes the main objective(s) of the study, explains how the study was done, including any model organisms used, without methodological detail, and summarizes the most important results and their significance. The abstract must be an objective representation of the study: it is not allowed to contain results which are not presented and substantiated in the manuscript or exaggerate the main conclusions. Citations should not be included in the abstract.

2.3.1.4 Keywords

Three to eight keywords should be provided, which are specific to the article, yet reasonably common within the subject discipline.

2.3.2 Main Text

Manuscripts of different types are structured with different sections of content. Please refer to Types of Manuscripts to make sure which sections should be included in the manuscripts.

2.3.2.1 Introduction

The introduction should contain background that puts the manuscript into context, allow readers to understand why the study is important, include a brief review of key literature, and conclude with a brief statement of the overall aim of the work and a comment about whether the aim was achieved. Relevant controversies or disagreements in the field should be introduced as well.

2.3.2.2 Methods

Methods should contain sufficient details to allow others to fully replicate the study. New methods and protocols should be described in detail while well-established methods can be briefly described or appropriately cited. Experimental participants selected, the drugs and chemicals used, the statistical methods taken, and the computer software used should be identified precisely. Statistical terms, abbreviations, and all symbols used should be defined clearly. Protocol documents for clinical trials, observational studies, and other non-laboratory investigations may be uploaded as supplementary materials.

2.3.2.3 Results

This section contains the findings of the study. Results of statistical analysis should also be included either as text or as tables or figures if appropriate. Authors should emphasize and summarize only the most important observations. Data on all primary and secondary outcomes identified in the section Methods should also be provided. Extra or supplementary materials and technical details can be placed in supplementary documents.

2.3.2.4 Discussion

This section should discuss the implications of the findings in context of existing research and highlight limitations of the study. Future research directions may also be mentioned.

2.3.2.5 Conclusion

It should state clearly the main conclusions and include the explanation of their relevance or importance to the field.

2.3.3 Back Matter

2.3.3.1 Acknowledgments

Anyone who contributed towards the article but does not meet the criteria for authorship, including those who provided professional writing services or materials, should be acknowledged. Authors should obtain permission to acknowledge from all those mentioned in the Acknowledgments section. This section is not added if the author does not have anyone to acknowledge.

2.3.3.2 Authors' Contributions

Each author is expected to have made substantial contributions to the conception or design of the work, or the acquisition, analysis, or interpretation of data, or the creation of new software used in the work, or have drafted the work or substantively revised it.

Please use Surname and Initial of Forename to refer to an author's contribution. For example: made substantial contributions to conception and design of the study and performed data analysis and interpretation: Salas H, Castaneda WV; performed data acquisition, as well as provided administrative, technical, and material support: Castillo N, Young V.

If an article is single-authored, please include "The author contributed solely to the article." in this section.

2.3.3.3 Availability of Data and Materials

In order to maintain the integrity, transparency and reproducibility of research records, authors should include this section in their manuscripts, detailing where the data supporting their findings can be found. Data can be deposited into data repositories or published as supplementary information in the journal. Authors who cannot share their data should state that the data will not be shared and explain it. If a manuscript does not involve such issue, please state "Not applicable." in this section.

2.3.3.4 Financial Support and Sponsorship

All sources of funding for the study reported should be declared. The role of the funding body in the experiment design, collection, analysis and interpretation of data, and writing of the manuscript should be declared. Any relevant grant numbers and the link of funder's website should be provided if any. If the study is not involved with this issue, state "None." in this section.

2.3.3.5 Conflicts of Interest

Authors must declare any potential conflicts of interest that may be perceived as inappropriately influencing the representation or interpretation of reported research results. If there are no conflicts of interest, please state "All authors declared that there are no conflicts of interest." in this section. Some authors may be bound by confidentiality agreements. In such cases, in place of itemized disclosures, we will require authors to state "All authors declare that they are bound by confidentiality agreements that prevent them from disclosing their conflicts of interest in this work." If authors are unsure whether conflicts of interest exist, please refer to the "Conflicts of Interest" of *EVCNA* Editorial Policies for a full explanation.

2.3.3.6 Ethical Approval and Consent to Participate

Research involving human subjects, human material or human data must be performed in accordance with the Declaration of Helsinki and approved by an appropriate ethics committee. An informed consent to participate in the study should also be obtained from participants, or their parents or legal guardians for children under 16. A statement detailing the name of the ethics committee (including the reference number where appropriate) and the informed consent obtained must appear in the manuscripts reporting such research.

Studies involving animals and cell lines must include a statement on ethical approval. More information is available at Editorial Policies.

If the manuscript does not involve such issue, please state "Not applicable." in this section.

2.3.3.7 Consent for Publication

Manuscripts containing individual details, images or videos, must obtain consent for publication from that person, or in the case of children, their parents or legal guardians. If the person has died, consent for publication must be obtained from the next of kin of the participant. Manuscripts must include a statement that a written informed consent for publication was obtained. Authors do not have to submit such content accompanying the manuscript. However, these documents must be available if requested. If the manuscript does not involve this issue, state "Not applicable." in this section.

2.3.3.8 Copyright

Authors retain copyright of their works through a Creative Commons Attribution 4.0 International License that clearly states how readers can copy, distribute, and use their attributed research, free of charge. A declaration "© The Author(s) 2022." will be added to each article. Authors are required to sign License to Publish before formal publication.

2.3.3.9 References

Preferably original research articles that directly support the statements should be cited. Review articles could be cited when they specifically address the statement made in the manuscript. An abstract should not be used as a reference. Non-specific citations should be avoided.

References should be numbered in order of appearance at the end of manuscripts. In the text, reference numbers should be placed in square brackets and the corresponding references are cited thereafter. If the number of authors is less than or equal to six, we require to list all authors' names. If the number of authors is more than six, only the first three authors' names are required to be listed in the references, other authors' names should be omitted and replaced with "et al.". Abbreviations of the journals should be provided on the basis of Index Medicus. Information from manuscripts accepted but not published

should be cited in the text as “Unpublished material” with written permission from the source.

Types	Examples
Journal articles by individual authors	Weaver DL, Ashikaga T, Krag DN, et al. Effect of occult metastases on survival in node-negative breast cancer. <i>N Engl J Med</i> 2011;364:412-21. [PMID: 21247310 DOI: 10.1056/NEJMoa1008108]
Organization as author	Diabetes Prevention Program Research Group. Hypertension, insulin, and proinsulin in participants with impaired glucose tolerance. <i>Hypertension</i> 2002;40:679-86. [PMID: 12411462]
Both personal authors and organization as author	Vallancien G, Emberton M, Harving N, van Moorselaar RJ, Alf-One Study Group. Sexual dysfunction in 1,274 European men suffering from lower urinary tract symptoms. <i>J Urol</i> 2003;169:2257-61. [PMID: 12771764 DOI: 10.1097/01.ju.0000067940.76090.73]
Journal articles not in English	Zhang X, Xiong H, Ji TY, Zhang YH, Wang Y. Case report of anti-N-methyl-D-aspartate receptor encephalitis in child. <i>J Appl Clin Pediatr</i> 2012;27:1903-7. (in Chinese)
Journal articles ahead of print	Odibo AO. Falling stillbirth and neonatal mortality rates in twin gestation: not a reason for complacency. <i>BJOG</i> 2018; Epub ahead of print [PMID: 30461178 DOI: 10.1111/1471-0528.15541]
Books	Sherlock S, Dooley J. Diseases of the liver and biliary system. 9th ed. Oxford: Blackwell Sci Pub; 1993. pp. 258-96.
Book chapters	Meltzer PS, Kallioniemi A, Trent JM. Chromosome alterations in human solid tumors. In: Vogelstein B, Kinzler KW, editors. The genetic basis of human cancer. New York: McGraw-Hill; 2002. pp. 93-113.
Online resource	FDA News Release. FDA approval brings first gene therapy to the United States. Available from: https://www.fda.gov/NewsEvents/Newsroom/PressAnnouncements/ucm574058.htm . [Last accessed on 30 Oct 2017]
Conference proceedings	Harnden P, Joffe JK, Jones WG, editors. Germ cell tumours V. Proceedings of the 5th Germ Cell Tumour Conference; 2001 Sep 13-15; Leeds, UK. New York: Springer; 2002.
Conference paper	Christensen S, Oppacher F. An analysis of Koza's computational effort statistic for genetic programming. In: Foster JA, Lutton E, Miller J, Ryan C, Tettamanzi AG, editors. Genetic programming. EuroGP 2002: Proceedings of the 5th European Conference on Genetic Programming; 2002 Apr 3-5; Kinsdale, Ireland. Berlin: Springer; 2002. pp. 182-91.
Unpublished material	Tian D, Araki H, Stahl E, Bergelson J, Kreitman M. Signature of balancing selection in Arabidopsis. <i>Proc Natl Acad Sci U S A</i> . Forthcoming 2002.

For other types of references, please refer to U.S. National Library of Medicine.

The journal also recommends that authors prepare references with a bibliography software package, such as EndNote to avoid typing mistakes and duplicated references.

2.3.3.10 Supplementary Materials

Additional data and information can be uploaded as Supplementary Materials to accompany the manuscripts. The supplementary materials will also be available to the referees as part of the peer-review process. Any file format is acceptable, such as data sheet (word, excel, csv, cdx, fasta, pdf or zip files), presentation (powerpoint, pdf or zip files), image (cdx, eps, jpeg, pdf, png or tiff), table (word, excel, csv or pdf), audio (mp3, wav or wma) or video (avi, divx, flv, mov, mp4, mpeg, mpg or wmv). All information should be clearly presented. Supplementary materials should be cited in the main text in numeric order (e.g., Supplementary Figure 1, Supplementary Figure 2, Supplementary Table 1, Supplementary Table 2, etc.). The style of supplementary figures or tables complies with the same requirements on figures or tables in main text. Videos and audios should be prepared in English and limited to a size of 500 MB.

2.4 Manuscript Format

2.4.1 File Format

Manuscript files can be in DOC and DOCX formats and should not be locked or protected.

2.4.2 Length

There are no restrictions on paper length, number of figures, or amount of supporting documents. Authors are encouraged to present and discuss their findings concisely.

2.4.3 Language

Manuscripts must be written in English.

2.4.4 Multimedia Files

The journal supports manuscripts with multimedia files. The requirements are listed as follows:

Videos or audio files are only acceptable in English. The presentation and introduction should be easy to understand. The frames should be clear, and the speech speed should be moderate.

A brief overview of the video or audio files should be given in the manuscript text.

The video or audio files should be limited to a size of up to 500 MB.

Please use professional software to produce high-quality video files, to facilitate acceptance and publication along with the

submitted article. Upload the videos in mp4, wmv, or rm format (preferably mp4) and audio files in mp3 or wav format.

2.4.5 Figures

Figures should be cited in numeric order (e.g., Figure 1, Figure 2) and placed after the paragraph where it is first cited; Figures can be submitted in format of tiff, psd, AI or jpeg, with resolution of 300-600 dpi;

Figure caption is placed under the Figure;

Diagrams with describing words (including, flow chart, coordinate diagram, bar chart, line chart, and scatter diagram, *etc.*) should be editable in word, excel or powerpoint format. Non-English information should be avoided;

Labels, numbers, letters, arrows, and symbols in figure should be clear, of uniform size, and contrast with the background; Symbols, arrows, numbers, or letters used to identify parts of the illustrations must be identified and explained in the legend;

Internal scale (magnification) should be explained and the staining method in photomicrographs should be identified;

All non-standard abbreviations should be explained in the legend;

Permission for use of copyrighted materials from other sources, including re-published, adapted, modified, or partial figures and images from the internet, must be obtained. It is authors' responsibility to acquire the licenses, to follow any citation instruction requested by third-party rights holders, and cover any supplementary charges.

2.4.6 Tables

Tables should be cited in numeric order and placed after the paragraph where it is first cited;

The table caption should be placed above the table and labeled sequentially (e.g., Table 1, Table 2);

Tables should be provided in editable form like DOC or DOCX format (picture is not allowed);

Abbreviations and symbols used in table should be explained in footnote;

Explanatory matter should also be placed in footnotes;

Permission for use of copyrighted materials from other sources, including re-published, adapted, modified, or partial tables from the internet, must be obtained. It is authors' responsibility to acquire the licenses, to follow any citation instruction requested by third-party rights holders, and cover any supplementary charges.

2.4.7 Abbreviations

Abbreviations should be defined upon first appearance in the abstract, main text, and in figure or table captions and used consistently thereafter. Non-standard abbreviations are not allowed unless they appear at least three times in the text. Commonly-used abbreviations, such as DNA, RNA, ATP, *etc.*, can be used directly without definition. Abbreviations in titles and keywords should be avoided, except for the ones which are widely used.

2.4.8 Italics

General italic words like *vs.*, *et al.*, *etc.*, *in vivo*, *in vitro*; *t* test, *F* test, *U* test; related coefficient as *r*, sample number as *n*, and probability as *P*; names of genes; names of bacteria and biology species in Latin.

2.4.9 Units

SI Units should be used. Imperial, US customary and other units should be converted to SI units whenever possible. There is a space between the number and the unit (i.e., 23 mL). Hour, minute, second should be written as h, min, s.

2.4.10 Numbers

Numbers appearing at the beginning of sentences should be expressed in English. When there are two or more numbers in a paragraph, they should be expressed as Arabic numerals; when there is only one number in a paragraph, number < 10 should be expressed in English and number > 10 should be expressed as Arabic numerals. 12345678 should be written as 12,345,678.

2.4.11 Equations

Equations should be editable and not appear in a picture format. Authors are advised to use either the Microsoft Equation Editor or the MathType for display and inline equations.

2.5 Submission Link

Submit an article via <https://oaemesas.com/login?JournalId=evcna>.



www.oaepublish.com

Extracellular Vesicles and Circulating Nucleic Acids
(EVCNA)

Los Angeles Office

245 E Main Street ste122, Alhambra,

CA 91801, USA

E-mail: editorial@evcna.com

Website: <https://evcna.com>

